



**HAL**  
open science

# Study of the structure-properties relationship of polymeric materials using coupled techniques

Daniel Hermida Merino

► **To cite this version:**

Daniel Hermida Merino. Study of the structure-properties relationship of polymeric materials using coupled techniques. Physics [physics]. Université de Lorraine, 2020. tel-03092454

**HAL Id: tel-03092454**

**<https://hal.univ-lorraine.fr/tel-03092454>**

Submitted on 2 Jan 2021

**HAL** is a multi-disciplinary open access archive for the deposit and dissemination of scientific research documents, whether they are published or not. The documents may come from teaching and research institutions in France or abroad, or from public or private research centers.

L'archive ouverte pluridisciplinaire **HAL**, est destinée au dépôt et à la diffusion de documents scientifiques de niveau recherche, publiés ou non, émanant des établissements d'enseignement et de recherche français ou étrangers, des laboratoires publics ou privés.

Public Domain

**Ecole Doctorale C2 MP  
(Chimie Mécanique Matériaux Physique)**

DE L'UNIVERSITÉ DE LORRAINE

LABORATOIRE LMOPS

Présentée et soutenue publiquement pour l'obtention du titre de

**Habilitation à diriger des recherches**

par

**Daniel Hermida Mérimo**

**Etude de la relation structure-propriétés des matériaux polymères  
par techniques couplées**

**Study of the structure-properties relationship of polymeric  
materials using coupled techniques.**

Soutenue le 14 décembre 2020

**Membres du jury :**

Pr Corine BAS, Université Savoie Mont Blanc LEPMI UMR 5279	Rapportrice
Pr Noëlle BILLON, CEMEF, Sophia Antipolis	Rapportrice
Pr Manuel Martínez Piñeiro, Universidade de Vigo, Vigo	Rapporteur
Pr Valérie GAUCHER, UMET, Université Lille1	Examinatrice
Pr Isabelle ROYAUD, IJL, Université de Lorraine, Nancy	Examinatrice
Dr Carlos ALONSO MORENO, Université de Castilla-La Mancha, Albacete. Espagne	Invité
Dr Guiseppe PORTALE, Université de Groningen, Pays-Bas	Invité
Pr Patrice BOURSON, LMOPS, Université de Lorraine, Metz	Parrain scientifique

## Sommaire

Resumé .....	4
Abstract.....	4
Introduction .....	5
Etat Civil .....	8
Indicateurs de la qualité de la production scientifique .....	8
Formation académique universitaire.....	9
Licences, maîtrises et diplômes d'ingénieur .....	9
Doctorats.....	9
Expérience pédagogique.....	9
Direction de thèse de doctorat ou de projets de fin d'études.....	9
Projet scientifique.....	11
1-Understanding of the structural development of polymeric materials upon extreme conditions that mimic the industrial environment.....	12
2-Investigation of the internal nanostructural development of block copolymers polymerization under polymeric sc-CO <sub>2</sub> .....	14
3- Co-proposer PhD Thesis project awarded; "Etude multi-échelle de l'impact de l'ajout de fluoroélastomère sur la structure du PVDF par des mesures in situ couplées", Université de Lorraine. ....	16
4-Controlling of fibrillization for drug delivery. ....	32
5-Caroline Grant (from Oct 1 <sup>st</sup> 2017 to Nov. 30 <sup>th</sup> 2020) in the project "NODENS" which is a Caroline Fellowship program co-founded by European Union Horizon 2020 Marie Skłodowska-Curie actions and Irish Research Council. ....	50
6-Scientific granted project by Fapesp (Sao Paulo Federal Research Council) for the investigation of 'In situ studies of nanoparticles nucleation and growth assisted by simultaneous SAXS and WAXS and XAS in combination with UV-visible spectroscopy', 2017, .....	52
7- Co-proposer PhD Thesis project awarded ; 'Nouvelle génération de biopolymères nanostructurés pour la fabrication additive et l'électrofilage, Université de Lorraine. ....	57
8- Study of the nanostructure of the fish gelatin hydrogels for drug delivery applications .	65
9- Main applicant as well as co-applicant of a series of synchrotron proposals as well as other polymer research projects. ....	71
10- Part of the scientific panel of bl11 NCD in Alba sincrotrón. ....	71
11-Beamline scientist responsible of bm26/ DUBBLE at ESRF from July 2015.....	72
Conclusions.....	75
PROJETS ET PRODUCTIONS SCIENTIFIQUES.....	76
Cours et séminaires de formation pédagogique universitaire.....	76
Expérience scientifique et technologique .....	76

Activité scientifique ou technologique.....	76
Participation à des projets de R&D&I financés à travers des procédures concurrentielles d'organismes publics ou privés .....	76
Participation à des contrats, conventions ou projets de R&D&I ne résultant pas de procédures concurrentielles, avec des entreprises (ou dans le cadre d'entreprises) et/ou des administrations .....	95
Publications, documents scientifiques et techniques ou technologiques ou autre publication .....	96
Travaux présentés lors de congrès nationaux ou internationaux .....	105
Comités consultatifs scientifiques, sociétés scientifiques .....	106
Expérience de gestion de R&D&I .....	107
Séjour dans des centres de R&D&I ou bien des entreprises nationales ou internationales .....	108
Aides et bourses obtenues .....	110
Résumé des autres titres .....	110

# Resumé

Mes recherches portent principalement sur l'étude des relations structure-propriété dans le domaine de la matière molle dans différents milieux tels que le massif, la solution ainsi que les films minces. En particulier, j'ai développé mon activité de recherche scientifique en interne, en menant des expériences de diffusion de la lumière à la fois en mode transmission et en mode angle rasant, en combinaison avec plusieurs spectroscopies et techniques mécaniques dans le domaine des polymères comme la cristallisation des polymères, les polymères supramoléculaires auto-assemblés, les systèmes polymères fonctionnels avancés et les systèmes hybrides métal-organiques. En tant que chercheur travaillant sur une infrastructure scientifique de pointe (ESRF), j'ai acquis des connaissances exceptionnelles à la pointe de l'instrumentation des rayons X et j'ai ainsi bénéficié d'une interaction étroite avec les groupes de recherche les plus éminents en science des matériaux, en particulier la matière condensée molle, aux Pays-Bas et en Europe. Cela m'a encouragé à développer de nouveaux environnements d'échantillonnage et à réaliser des expériences de pointe en matière de rayons X en combinaison avec plusieurs autres techniques dans le domaine de la matière molle, telles que la microscopie, la calorimétrie, la spectroscopie et la rhéologie. Actuellement, j'ai concentré mes recherches sur le développement et la caractérisation de nouveaux copolymères blocs de biosourcés avec des blocs biocompatibles. Les nouveaux biopolymères avancés sont des candidats idéaux pour des applications dans des domaines vitaux du domaine biomédical ou pharmaceutique lorsqu'ils sont associés à des médicaments et à des nanoparticules métalliques clés.

# Abstract

The main focus of my research is the study of the structure-property relationships in the soft matter area in different medium such as bulk, solution as well as thin films. Particularly, I have developed my scientific in-house research activity, conducting scattering experiments both in transmission and grazing angle mode, in combination with several spectroscopies and mechanical techniques in the polymeric field such as polymer crystallization, self-assembled supramolecular polymers, advanced functional polymeric systems and metal-organic hybrid systems.

As a researcher working on a leading scientific infrastructure (ESRF), I have acquired an outstanding knowledge at the forefront of X-ray instrumentation and thus, I have benefited from close interaction with the most prominent research groups in materials science, specifically soft condensed matter, in the Netherlands and Europe. This has encouraged me to develop novel sample environments and performed cutting edge X-ray experiments in combination with several other leading techniques in a soft matter such as microscopy, calorimetry, spectroscopy, rheology. Currently, I have focused my research on the development and characterization of novel biosource block-copolymers with biocompatible blocks. Novel advanced biopolymers are ideal candidates with applications in vital areas of the biomedical or pharmaceutical field when coupled with drugs and key metallic nanoparticles.

# Introduction

The main focus of my research is the study of the structure-property relationships in the soft matter area in different medium such as bulk, solution as well as thin films. Particularly, I have developed my scientific in-house research activity, conducting scattering experiments both in transmission and grazing angle mode, in combination with other techniques in the polymeric field such as polymer crystallization, self-assembled supramolecular polymers, advanced functional polymeric systems and metal-organic hybrid systems.

I am currently the scientist responsible for the SAXS-WAXS station in DUBBLE at the ESRF, Grenoble as an NWO employee. As a beamline scientist of bm26, I have benefited from the long-standing and extensive investigation of polymer crystallization studies in quiescent and industrial processing conditions conducted at the beamline. A wide range of polyolefins, polyamides, have been investigated at extreme conditions to understand the mechanism of crystallization and the kinetics of expected mesophases and oriented structures formations.

I have promoted further the in-situ monitoring of nanostructure development by simultaneous SAXS/WAXS under external thermal and mechanical fields by enlarging the length scale in combination with spectroscopies techniques and additional multivariate analysis due to the increase of acquired metadata per experiment. Likewise, I have successfully applied for several scientific projects in collaboration with European partners in the soft matter field to advance in the design of novel functional polymeric materials with tailored properties with particular emphasis, in the use of green approaches as well as biocompatible application due to increase by the society demands for bioenvironmental policies.

I have investigated the nanostructure formation during the synthesis of structured block copolymer under extreme conditions such as the formation of polymeric microparticles in sc-CO<sub>2</sub> in collaboration with Professor Steven Howdle at University of Nottingham. Firstly, a novel X-ray reactor was designed that then permitted to probe in-situ the influence of sc-CO<sub>2</sub>-philicity of the different blocks in the internal structural development of polymeric block-copolymer microparticles.

In addition, I have participated to advance the polymer science research at processing conditions at the beamline particularly at relevant industrial conditions as a co-proposer of the successful DPI (Dutch Polymer Institute) project "Online Polyolefin structuring during Cast Film Extrusion" granted on June the 1st of 2018 by Dr. Portale at University of Groningen. The cast film extrusion has lately been adopted in the packing industry due to the beneficial optical properties and film thickness distribution in the cross direction obtained compare to typically blow film process. Furthermore, I have also investigated together with Dr. Portale the main parameters that defined the polymeric film formation by performing in-situ GISAXS/GIWAXS experiments that allows to describe the crystallinity and microphase separation of block copolymers as well as polymer blends. The assessment of the role of as several phenomena such as macrophase separation, nanostructure development and film percolation, occur concomitantly is crucial to control the film formation.

Moreover, I gained visiting grants as both junior and senior researcher at the "Universidad de Castilla la Mancha" to endorse the understanding of the key structural parameters to design novel molecular organic and polymeric systems with sensing applications and specially for delivery drug delivery systems.

Consequently, I have then participated as a co-applicant of the successful synthetic project "Procesos cataliticos para la conversion de CO<sub>2</sub> en productos de interest industrial" of the science ministry of Spain in collaboration with the "Universidad de Castilla la Mancha". Particularly, the synthesis of biodegradable as well as biocompatible novel polyester by

organometallic catalysis was aimed to attain both control on the Mw and stereoregularity as well as narrow polydispersity that in turn, were evaluated as drug nanocarriers. The manuscript published with the preliminary results has been reproduced in the press for being selected for its importance in fundamental research and in the application of X-rays by the ALBA synchrotron.

<https://www.sincrotronalba.es/es/actualidad/noticias/nuevas-nanoparticulas> biocompatibles-  
contra-el-cancer-demama

Furthermore, I have studied metal-organic hybrid systems that provide a novel approach to combine the mechanical support that offers the polymeric material with the improvement of targeted properties. Likewise, I have successfully applied together with associate Professor José Fernando Queiruga to the FAPESP scientific council the support of the structural investigation by combined techniques of hybrid systems with the research project: "In situ studies of nanoparticles nucleation and growth assisted by simultaneous SAXS and WAXS and XAS in combination with UV-visible spectroscopy".

I have studied the nanostructure of Nafion-Cs nanoparticles (N-CSP) composites by simultaneous SAXS/XAS as well as SAXS/WAXS experiments in order to enhance the proton conductivity at working conditions. Hybrid metal-polymeric membranes promote the maintenance of high protonic conductivity at low humidity conditions. The Nafion-Cs nanoparticles composites nanostructural has been investigated at high temperatures to understand the increased protonic conductivity in relation to Nafion under anhydrous conditions. Moreover, I have designed a novel X-ray flow cell to probe the growth of the gold nanoparticles in mild conditions by simultaneous SAXS- UV-vis spectroscopy to correlate the changes on the plasmon with the morphological evolution minimizing the X-rays detrimental effect on the nanoparticle formation. In the next future, the nanoparticles growth will be integrated in supramolecular hydrogels to attain the desired mechanical characteristics for biomedical applications as drug nanocarriers that feature sensing capabilities.

Since the research I have developed during my PhD, I have enthusiastically involved in the design proviso of novel supramolecular polymers with responsive specific functionalities that harnessed from the dynamic and specificity of the non-covalent interactions nature. Furthermore, the hierarchical self-organization that defines the supramolecular nanostructure is commonly employed by conventional polymeric systems and thus, the understanding of key parameters that govern their self-assembly is beneficial to advance in the development of polymeric systems.

As with conventional, covalently bonded polymers, the macroscopic properties of supramolecular polymers (such as viscosity and tensile strength) are intimately related to its nanostructure. The versatility of the supramolecular architectures offers the possibility of constructing chemical architectures displaying notable structural complexity, from linear polymeric chains to networks and hyperbranched systems. Supramolecular entities can, in turn, enable the production of new thermoplastic elastomers and tuneable polymer materials. A systematic study of the effect of supramolecular interactions of both the end group and linkers on the nanostructure of self-assembled polymers has been the aim of my research on the supramolecular field.

Furthermore, I have investigated the gelation mechanism of mainly supramolecular systems, particularly, in combination with the presence of therapeutic agents, to design drug nanocarriers for the pharmaceutical administration in corporal areas with targeted barriers. The structure-activity relationship and the gelation process that drives the self-assembly of potential supramolecular gelators into gels is not fully understood and the majority of gels are

found serendipitously. However, it has been established that gelation is mainly controlled by the gelator architecture, gelator concentration, gelation conditions and solvent effects. Attempts to understand the molecular assembly of a low molecular hydrogelator into molecular-scale fibrils and the subsequent hierarchical organization of the fibrils into spanning network that percolates the solution by fibril-fibril interaction has been investigated. The mechanism development of a molecular solution into insoluble fibrillar gel network is a phase separation process driven thermodynamically by solution saturation. Moreover, the acquired understanding of the hydrogelator fibrillization, as well as their self-recognition mechanism, has been applied to design responsive nanocarriers for targeted pharmaceutical agents that will be encapsulated and released in a controlled fashion. Subsequently, the passive upload of an antitumoral (Doxorubicin) and the posterior release from the hydrogelator network has been evaluated in vitro glioblastoma cells in collaboration with the “Universidad de Castilla la Mancha” as part of previous mentioned partnership.

In order to continue the investigation on the gelation mechanism, I successfully obtained a joint application for Caroline Grant with Bing Wu, to spend 36 months (from Dec. 1st 2017 to Nov. 30th 2020) working as a guest researcher in the project "NODENS" which is a Caroline Fellowship program cofounded by European Union Horizon 2020 Marie Skłodowska-Curie actions and Irish Research Council.

Furthermore, I have co-applied successfully to the regional Lorraine research program to cofinance a PhD project in collaboration with Arkema and the LMOPS titled “Etude multi-échelle de l’impact de l’ajout de fluoroélastomère sur la structure du PVDF par des mesures in situ couplées”. In addition, I have been selected in the fellowship program of the “Université de Lorraine” as a scientific visitor for 2018, 2019 and 2020 courses. During my scientific stay, I have gained experience in Raman spectroscopy, which offer great complementary opportunities to be coupled with scattering techniques as well as to advance on the application of Multivariate data analysis (MVA) for SAXS-WAXS data acquired together with Raman spectroscopy in order to correlate complementary structural information.

Currently, I have focused my research on the development and characterization of novel biosourced block-copolymers with biocompatible blocks. Novel advanced biopolymers are ideal candidates with applications in vital areas of the biomedical or pharmaceutical field when coupled with drugs and key metallic nanoparticles. I have participated together with Professor Patrice Bourson at “Université de Lorraine” to finance a PhD project at LMOPS titled “New generation of nanostructured biopolymers for additive manufacturing and electrospinning”, to synthesise novel block copolymer PLA stereo-complexes of high  $M_w$  for potential nanomedicine applications in collaboration with “Universidad de Castilla la Mancha”.

Moreover, I have initiated the study of gelatin from fish sources to develop pharmaceutical drug delivery systems as well as promoting the valorization of value-added products derived from fisheries waste sources to enhance the environmental sustainability and as a contribution to the circular economy. The research is conducted in collaboration with both “Universidade de Vigo” and “Instituto de investigacions mariñas” at the CSIC (Spanish scientific council). Furthermore, the mechanical properties of the generated gelatin hydrogels were enhanced by the formation of double network gel using a cohydrogelator as ionic liquids (ILs) that are considered green solvents due to their biodegradability and low toxicity.

# Etat Civil

Nom:	<b>Hermida Merino</b>
Prénoms:	Daniel
DNI:	36157638M
ORCID:	0000-0002-8181-158X
Sexe:	Homme
Nationalité:	Espagne
Pays de naissance:	Espagne
Communauté autonome ou région de naissance:	Galice
Ville de naissance:	Vigo
Adresse de contact:	8a Rue du Jura
Code postal:	74160
Pays :	France
Ville:	St Julien en Genevois
Téléphone fixe:	(0033) 0476882375
Adresse électronique:	d.hermida@gmail.com
Téléphone portable:	(0033) 0601794459

Situation professionnelle actuelle uniquement si vous travaillez (pas si vous êtes au chômage)

Nom de l'établissement: DUBBLE                      Type d'établissement: Centre de R&D  
Département, service,...: ESRF  
Catégorie / fonction ou poste: Scientifique Senior Beamline en DUBBLE à E.S.R.F / Responsable bm26  
Date de début: 01/01/2015  
Modalité de contrat: Contrat professionnel à durée indéterminée

## Indicateurs de la qualité de la production scientifique

---

**H index 20**

i-10 index 43

Près de 1950 citations

>74 proposals in synchrotrons across Europe such as ESRF, ILL, Diamond,Alba, Daresbury, PETRA III, ISIS y Hasylab

**> 90 publications**

34% D1

39% Q1

73% D1+Q1

## Formation académique universitaire

---

### Licences, maîtrises et diplômes d'ingénieur

Titulaire d'une maîtrise dans Sciences Chimiques Modalité Chimique Physique

Université Universidade de Vigo (Espagne)

Date d'obtention du diplôme: 21/06/2003

### Doctorats

Doctor of Philosophy/Programme officiel de doctorat en nanoscience et nanotechnologie

PhD Thermo-responsive reversible supramolecular polymers

Jury : Professeur Anthony J. Ryan et Professeur Howard Colquhoun

Université de Reading (UK)

Date d'obtention du diplôme: 12/2010

## Expérience pédagogique

---

Type d'enseignement: Enseignement officiel dans le cadre de ma thèse (environ 100 h/an, donc 300h d'enseignement)

Nom de la matière/intitulé du cours: Cours TD TP de pratique de laboratoire en physico-chimie

Type de programme: Maîtrise

Diplôme: University of Reading

Date de début: 05/02/2007

Date de fin: 01/06/2009

Date du dernier cours: 01/06/2009

University of Reading, Faculté, institut, centre: School of Chemistry

Département: School of Chemistry

Ville: Reading, Royaume-Uni

Langue d'enseignement: Anglais

## Direction de thèse de doctorat ou de projets de fin d'études

---

1. Thèse de doctorat : **Carmen Moya López-Peláez**

Titre "New generation of nanostructured biopolymers for additive manufacturing and electrospinning",

Co-directeur de thèse: Patrice Bourson; Daniel Hermida Merino (33%); David Chapron

Université: Université de Lorraine, Laboratoire LMOPS Metz

Date de soutenance: 01/09/2022

2. Thèse de doctorat : **Federico Di Sacco**

Titre "Polyolefin structuring during Cast Film Extrusion Polyolefin structuring during Cast Film Extrusion"

Co-encadrant des expériences synchrotron Online Polyolefin structuring during Cast Film Extrusion"

Co-encadrant de thèse sur le meausures de synchrotron: G. Portale

Université: Université de Groningen

Date de soutenance: 30/09/2021

3. Master : **Murillo Donizeti dos Santos Rosa**

Titre "Nucleação e crescimento de nanopartículas de ouro incorporado em hidrogel/ Trabajo para tener obtención del master"

Co-directeur de thèse: Jose Fernando Queiruga Rey; Daniel Hermida Merino

Université: Universidade Federal do ABC, Santo André, Brésil

Date de soutenance: 01/06/2021

4. Master : **Victor Cruz de Souza**

Titre " SAXS-WAXS/ EXAFS in situ studies of thermal activated nucleation and growth process of CsHSO<sub>4</sub> in Nafion "

Co-directeur de thèse: Jose Fernando Queiruga Rey; Daniel Hermida Merino

Université: Universidade Federal do ABC, Santo André , Brésil

Date de soutenance: 01/02/2021

5. Thèse de doctorat : **Sarah Saidi**

Titre "Etude multi-échelle de l'impact de l'ajout de fluoroélastomère sur la structure du PVDF par des mesures in situ couplées"

Co-directeur de thèse: Patrice Bourson; David Chapron;

Coencadrants : Daniel Hermida Merino

Université de Lorraine LMOPS Metz

Date de soutenance: 01/11/2020

6. Post-doc : **Bing Wu**

Titre: "Novel pOlymeric materials DEsigNed for drug delivery System (NODENS)/CAROLINE"

Université: Royal College of Science for Ireland

Co-encadrant Andreas Heise; Bing Wu; Daniel Hermida Merino; Kay Saalwaechter

Fin du projet: 30/09/2020

7. Post-Doc : **Carolina Hermida Merino**

titre "Etude de gels de sources biologiques en combinaison avec des liquides ioniques"

Université de Vigo

Co-encadrant : Daniel Hermida Merino, Ana B Pereiro

Fin du projet: 31/12/2020

# Projet scientifique

I have started by scientific career by completing a Ph.D. in supramolecular polymers under the supervision of Prof. Ian Hamley and Prof. Wayne Hayes at Reading University, entitled “Thermo-responsive reversible supramolecular polymers”. My Ph.D. was focussed on the synthesis and characterization of novel thermo-responsive self-assembled supramolecular polymers. In particular, the main aim was the study of the dynamic mechanism of the self-assembly mechanism in supramolecular polymers under thermal stimuli understanding the interplay between mechanical properties and the nanostructure of these smart tuneable materials.

I then joined the DUBBLE beamline (SAXS/WAXS) at ESRF as a post-doctoral fellow from Eindhoven Technical University first and then from the Dutch Polymer Institute (DPI) to promote the research of polymer materials structure under processing conditions. I was responsible for scientific contact between the Dutch polymer groups and DUBBLE for the application of X-rays in combination with other techniques for the study of structural and morphological changes during polymerization and polymer processing.

The role involved:

- The development of new experiments to study polymer structure and dynamics with X-rays.
- Attract new DPI groups to the beamline and apply for beamtime for novel experiments.
- Local contact during the experiments at DUBBLE.
- Development of sample environment for the specific requirements of combining different techniques in combination with X-rays techniques.
- Modeling of polymer morphology.

Currently, I am employed by the Netherlands Council for Scientific Research (NWO) as the beamline scientist responsible for the Dutch-Belgium SAXS/WAXS beamline at ESRF. I am responsible for leading and coordinating beamline BM26 staff in order to design and validate new experiments. I manage the beamtime schedule. Moreover, I advise visitor scientists on experimental strategy, including support on data collection and interpretation. I ensure continuous development of novel sample environments by performing cutting edge X-rays experiments in combination with other techniques, developing my research on the structure-property relationship of novel materials of soft matter by SAXS-WAXS, GISAXS, and GIWAXS techniques.

During my scientific career, I have applied for projects to industrial and governmental grants in order to develop my research.

The fund-raising was essential to strengthen and enlarge my research activities in the different areas of the knowledge process. Through my research, I have obtained financial support to design and manufacture novel samples environments. I have been actively applying for beamtime in different synchrotrons across Europe to perform cutting edge experiments. Moreover, I have collaborated closely with leading groups in the soft matter area to successfully applied to national and international grants to fund long term research projects and thus, to fulfill independently the research responsibilities.

I will list my scientific achievements in different areas of my research activities. Particularly, herein, I will focus on the research conducted recently in my scientific career. I have selected a series of my current research projects that are presented briefly along with a significant manuscript according to the subject matter. Particularly, I expanded the updated scientific projects in collaboration with the “Université de Lorraine” as well as biomaterials with nanomedicine applications.

## 1-Understanding of the structural development of polymeric materials upon extreme conditions that mimic the industrial environment.

---

My main scientific aim during the postdoc period in DUBBLE was the application of time-resolved X-ray diffraction techniques for studying structural and morphological changes during polymerization and processing. Polymers undergo extreme thermal quenching and high shear rates, during processing that affects the nanostructure and thus, the mechanical properties of the final polymeric materials. The high flux and collimated beam together with the new detector technology have enabled us to perform in situ simultaneous SAXS/WAXS experiments during polymer processing to understand the parameters that govern the structural evolution upon industrial conditions (Figure 1.1). I have spent 3 months in the Department of Chemical Engineering and Chemistry of the Eindhoven University of Technology to identify scientific projects that could be benefited from X-ray characterization.

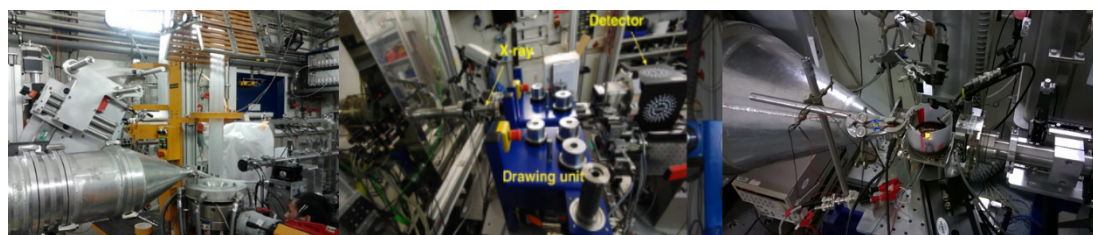


*Figure 1.1. Pictures of in situ time-resolved scattering experiments in combination with other relevant techniques to monitor the polymer nanostructuration at extreme conditions that mimic real industrial environments*

I have participated in the investigation of both commodity polymers, as well as specialty polymers at different thermal and/or shear conditions that lead us to tens of publications in the field. Particularly, we have published a series of reviews on the area to summarize the advances on the structure-property relationship of polymeric materials under extreme conditions:

1. Giuseppe Portale, **Daniel Hermida-Merino** and Wim Bras, “*Polymer research and synchrotron radiation perspectives*”; European Polymer Journal (2016) (online) DOI: 10.1016/j.eurpolymj.2016.04.015
2. Anthony J. Ryan, Wim Bras, **Daniel Hermida-Merino**, Dario Cavallo; “*The interaction between fundamental and industrial research and experimental developments in the field of polymer crystallization*”; Journal of Non-Crystalline Solids (in press) (2016) <http://dx.doi.org/10.1016/j.jnoncrysol.2016.07.039>

3. Benny Luijsterburg, Peter Jobse, **Daniel Hermida Merino**, Ton Peijs, Han Goossens; *Solid-state Drawing of  $\beta$ -nucleated Polypropylene: Effect of Additives on Drawability and Mechanical Properties*; J. Polym. Sci. B Polym. Phys., 52: 1071–1082. doi: 10.1002/polb.23533
4. Giuseppe Portale, Dario Cavallo, Giovanni Carlo Alfonso, **Daniel Hermida-Merino**, Martin van Drongelen, Luigi Balzano, G. W. M. Peters, J. G. P. Goossens and Wim Bras, *Polymer crystallization studies under processing-relevant conditions at the SAXS/WAXS DUBBLE beamline at the ESRF*, J. Appl. Cryst. (2013). 46, 1681–1689



## Feature Article

## Polymer research and synchrotron radiation perspectives

Giuseppe Portale<sup>a</sup>, Daniel Hermida-Merino<sup>b</sup>, Wim Bras<sup>b,\*</sup><sup>a</sup> Univ Groningen, Zernike Inst. Adv. Mat., Macromol Chem & New Polymer Mat, Nijenborgh 4, NL-9747 AG Groningen, The Netherlands<sup>b</sup> Netherlands Organisation for Scientific Research (NWO), DUBBLE@ESRF BP CS40220, 38043 Grenoble, France

## ARTICLE INFO

## Article history:

Received 18 January 2016

Received in revised form 8 April 2016

Accepted 14 April 2016

Available online 26 April 2016

## Keywords:

Synchrotron radiation

On-line processing

Polymers

X-ray scattering

## ABSTRACT

The developments in synchrotron radiation based polymer research have been profound over the last two decades. Not only have many more beamlines suitable for soft condensed matter research become available since the pioneering days but also the technical developments with respect to X-ray beam quality and position sensitive X-ray detectors have been very substantial. This has allowed to increase the degree of experimental sophistication considerably by introducing sample environments which not only allow the materials to be studied outside of equilibrium conditions but in fact in conditions which closely start to resemble realistic processing conditions. These developments now allow polymer researchers to bring synchrotron radiation based tools to the whole spectrum from academic relevant characterisations to trying to understand the effects that desired processing parameters have on the final materials.

In this manuscript, which is not intended as a comprehensive history, it is described how the historic interplay between technical developments and the experimental desires has generated the soft condensed matter synchrotron radiation toolbox that is at present available by following some of the major areas that have been the subject of polymers in the last two decades.

© 2016 Elsevier Ltd. All rights reserved.

## Contents

1. Introduction	416
1.1. Combinations of techniques	416
1.2. Sample environments	417
2. Commodity polymers	418
2.1. Quiescent crystallization studies	420
2.2. Crystallisation studies under processing conditions	420
2.3. On-line chemistry	422
3. Specialty polymers	423
3.1. Conventional block copolymers	423
3.2. Conductive polymers	424
4. Developments in synchrotron sources and beamline equipment	426
4.1. SR sources	426
4.2. Developments in data handling	428

\* Corresponding author.

E-mail address: [wim.bras@esrf.eu](mailto:wim.bras@esrf.eu) (W. Bras).

5. Conclusions . . . . .	428
Acknowledgements . . . . .	428
References . . . . .	428

## 1. Introduction

Polymer research using synchrotron radiation based X-ray scattering beam lines has an extended history which is characterized by an ever increasing level of experimental sophistication. Where in the early day's synchrotron sources were still required to obtain simple data required for morphological and phase determination of bulk polymers we now see that this role has been taken over by home laboratory based sources which have benefitted from the improvements in X-ray generator, X-ray optics and detector technology. The polymer research area where the more powerful and well collimated X-ray beams of synchrotron sources are still a requirement for successful experiments has therefore shifted. In this we can discern two main directions in which the experiments have developed. In the first place the development of time-resolved experiments with second and sub-second time resolution and in the second place the increased spatial resolution achieved by drastically reducing the beam size from hundreds of micros to few tens of nanometers without the detrimental lack of intensity to map the structure of polymeric samples (i.e. thin films and fibers).

The commodity polymers like for instance the different polyolefins have formed an important part of polymer based synchrotron radiation (SR) research since the start. Initially this was mainly a matter of semi static characterisations where the main sophistication was that slow thermally induced structural changes could be followed with data framing rates in the minutes. The limitations here were mainly due to the available detectors which were lacking in detection efficiency, could only handle limited count rates and had rather long read-out times. Over the years this gradually improved and time framing on the order of seconds per frame became feasible [1,2].

However, the field really took off when combined small and wide angle X-ray scattering experiments (SAXS/WAXS) became routinely available. In the early years these instrumentation combinations were mainly used for determinations of phase diagrams and slow crystallization kinetics. This is to some degree still an important subject due to the better control over materials manufacturing which allows for instance to create blends from the same mother material but with a sharp bimodal distribution in the molecular weights. The improved control over tacticity and molecular weight now allows for enhanced processing pathways which can be studied on the beamlines. This requires the more specialised sample environments which can mimic the processing conditions generally encountered in the industrial context. This is not only a matter of controlling pressure, volume and temperature ( $P, V, T$ ) but in general the appropriate combinations of these parameters. Although this falls outside of the traditionally named 'extreme conditions' experiments, like high pressure, magnetic field or temperature, the combined set of parameters and the time scale over which such experiments can be carried out should also qualify for the category of 'extreme conditions'. This type of experiment can now also be used to validate the simulation code of which the development has also progressed considerably over the years.

Specialty polymers only have a limited commercial market share but a disproportional large amount of experiments in soft condensed matter are dedicated to this category of materials. Whereas the emphasis of the commodity experiments has shifted towards what to do with the materials for the specialty materials a large proportion of the research is still mainly dedicated to characterisation studies. However, thanks to the earlier experimental developments in commodity polymer research, and the communal expertise build up over the years on how to perform more complicated experiments, the transition from pure academic research of specialty polymers towards actual processing can be foreseen to be much faster compared to the commodity materials. The developments in beamlines and detector technology allow the implementation of experiments with the sample environments that are required for these materials. This can range from on-line thin layer coating to fuel cells or batteries, where the operating cycle of the devices for which these polymers are intended, can be simulated.

### 1.1. Combinations of techniques

The low electron density contrast in polymeric materials was in the early years of synchrotron radiation scattering beamlines one of the main motivations to leave the home laboratory, with its Kratky camera, and make the travel to a central facility where the same static experiments could be done faster and with a higher data quality. Soon, however, it was realised that the several orders higher flux also allowed to follow the evolution of samples in time as function of external parameters [3,4].

Several years later the first successful combinations of X-ray scattering with other techniques were pioneered. In the first place the logical combination of SAXS with WAXS but at later times also with non X-ray based techniques like Differential Scanning Calorimetry (DSC) and a variety of spectroscopic methods. This was combined with an ever increasing sophistication in the sample handling. The developments in this have been reviewed several times in the past [5,6] and we therefore will not dwell on this subject for too long.

Important to realise, however, is that in contrast to the general perception the increase in available X-ray flux has not been the main stimulus for the developments described above. Although not irrelevant, once the flux has reached a threshold, increases are less relevant but the collimation of the beam becomes the more important parameter. For instance in the early days of SAXS/WAXS combinations one could not place two separate detectors at more than 2–3 m from each other

since otherwise the over-underfocus of the optics would render heavily distorted scattering patterns on one or both detectors. With the increase in collimation the focal depth of field has increased that much that it is now possible to place the SAXS and WAXS detector 20–30 m apart and place several detectors in between which allows to cover a very large scattering vector range [7]. Similar considerations can be made for the installation of more complex sample environments where the use of a small, less divergent, beam simplifies the installation considerably.

In fact the ever increasing flux densities that beamlines can generate could be seen as an inconvenience for a large body of experiments. The onset of radiation damage is in general recognisable and acknowledged but rarely reported in the literature. Therefore a comprehensive understanding of the damaging effects of X-rays, and the solutions to the problems that are caused by the interactions of X-rays with polymeric materials, is at the moment still elusive. The same is true for radiation induced modifications of materials which one maybe cannot strictly classify as 'damage'. These effects are less common and not always recognised but do occur over a large range of materials with a tendency to be more pronounced in samples containing solvents [8] or which are amorphous [9] and might play a role in crystallization experiments where crystallization nuclei could potentially be formed due to the interaction of the X-rays with the material. It is clear, however, that the tendency of X-ray beams to get brighter and smaller through the years should be handled with care for conventional polymer research.

## 1.2. Sample environments

At present there are not many valid reasons anymore for performing static polymer experiments on a synchrotron radiation source. Even though heating/cooling cycles, in time/temperature resolved experiments, are still probably the most commonly carried out experiments, the tendency has become to introduce more complicated sample environments which can bring the materials in a variety of ways out of their equilibrium. What is becoming even more common is that there is not a single parameter which is varied but that a combination of parameters is changed. One can think for instance of the multitude of shear induced crystallization experiments where during the cooling a brief shear pulse is applied and subsequently the crystallization kinetics is investigated.

Taking this a step further are the environments where one either tries to mimic industrial processing conditions, where cooling/deformation and shear are often applied partially in sequence or simultaneous, or very highly controlled experiments where accurate control is maintained over pressure, volume and temperature. Similar steps have been seen in the developments of environments for reactive processing.

With improved synthesis techniques more well defined block copolymer systems have started to being used. The fascinating self assembly properties of these molecules initially saw many studies into the fundamentals of phase diagrams as function of temperature and composition [10–12]. The time for the shift between fundamental research and more applied work [13], around 10 years, has been much shorter than the comparable time in the case of the commodity style polymers which was around 20 years. We can attribute this to both the technical developments on the beamlines, the increase in expertise how to conduct more complicated experiments and the improvements in polymer synthesis.

A similar story can probably be told for the development of organic photovoltaic cells and other organic electronics. By the nature of the applications which mainly is in the field of thin films there has been a further shift towards techniques suitable for investigating these thin layers like grazing incidence X-ray scattering. Between the advent of this field, around 2000, and present one has progressed from phase determinations to on-line roll-roll processing.

In the remainder of this text we will mainly concentrate on experiments done in the transmission geometry. This is not because the grazing incidence configuration is deemed to be less important but due to the fact that this has become field in

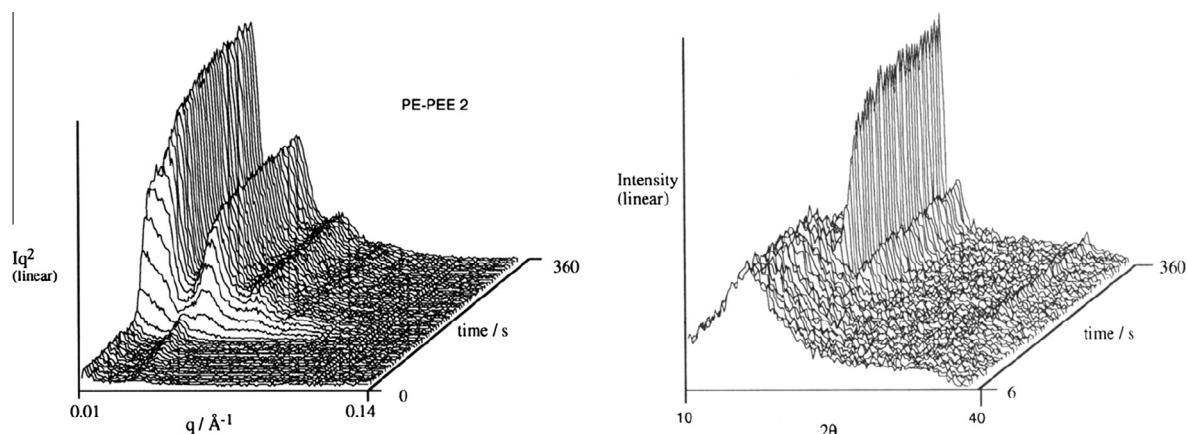


**Fig. 1.** Time-resolved SAXS (left panel) and WAXS (right panel) patterns obtained in a combined experiment where the PE-PEE diblock copolymers were cooled from the melt [14]. Even though the detectors and X-ray intensity in this experiment from 1995 were not of the same quality/intensity as is available at present high data quality could be achieved in time frames of 1–5 s/frame (reproduced with permission).

itself and deserves to be treated separately. However, many research issues are tackled by a combination of both experimental configurations and where appropriate we will indicate where this is the case.

## 2. Commodity polymers

The crystallization behaviour of polyolefins and blends of different polyolefins has long been an important research area not only because of the fundamental interest in how some of these long molecules still manage to escape the disordered spaghetti state they form in the melt towards a much more ordered phase, but also because of the industrial background.

The kinetics of crystallization could be followed with reasonable accuracy by either WAXS or SAXS experiments. In the case of WAXS one could use the peak intensities and follow how these grew from the disordered melt. By using SAXS one could follow the increase of electron density and use this as a probe for the increase in degree of crystallinity. However, with these independent methods the details of what occurred at the very early stages, where the crystallization was initiated, remained elusive. One of the most important steps in these studies was the introduction of combined SAXS/WAXS experiments. This enabled for the first time to observe the events taking place at the different length scales that were involved.

An example of early SAXS/WAXS results is a study [14] of structure development in semicrystalline poly(ethylene)-poly(ethylene) and poly-(ethylene)-poly(ethylene-propylene) diblock copolymers when crystallizing from the ordered melt. Representative SAXS and WAXS data are shown in Fig. 1.

For these experiments a nominal cooling rate of  $40\text{ }^{\circ}\text{C min}^{-1}$  was used. The main limitation with respect to the cooling rate was the thermal control of the sample and was not due to the X-ray experimental equipment. Even with the rather low count rate proportional gas detectors sufficient statistics could be accumulated in time-frame lengths of 1–5 s/frame. The derived parameters, like the scattering invariant,  $Q = \int_0^{\infty} q^2 I(q) dq$ , from the SAXS data and the integrated intensity of the most intense WAXS peak (1 1 0),  $Q = \int_{q_1}^{q_2} I(q) dq$ , are shown in Fig. 2.

When comparing the combined SAXS/WAXS data as obtained in the 90's with a similar experiment carried out 15 years before we can see the improvement in data quality. For the X-ray based experiments this can mainly be attributed to the improvements in detector quality in that period. Where once limited count rate gas wire chambers or high background noise level CCD detectors with a limited dynamic range were used, we nowadays can benefit from photon counting pixel detectors which combine the single photon counting capability of the gas wire chambers with the high count rate capacities of CCD detectors but with a much improved dynamic range with respect to counting statistics.

An example of this much improved data quality is shown in Fig. 3. This shows results from a combined SAXS/WAXS/DSC/conductivity experiment on poly(epsilon-caprolactone) to which multiwalled carbon nanotubes were added in order to form a nanocomposite [15]. Where in the data shown in Fig. 2 certainly the WAXS data obtained in 1995 was still rather noisy, for the experiment similar in time evolution and X-ray scattering power performed in 2014, the noise level has fallen to insignificant levels.

What is maybe less noticeable at first sight, but certainly true in the experience of the researchers working on the beam-lines, is the much reduced time and effort required to reduce the data and to perform the type of analysis that one requires. Although it is deplorable that still no wide spread data package exists that is recognised to be a kind of standard, software packages like Matlab etc. allow even less software oriented researchers to be able to extract the parameters that one wants to obtain from a data set many times faster than was possible only a decade ago.

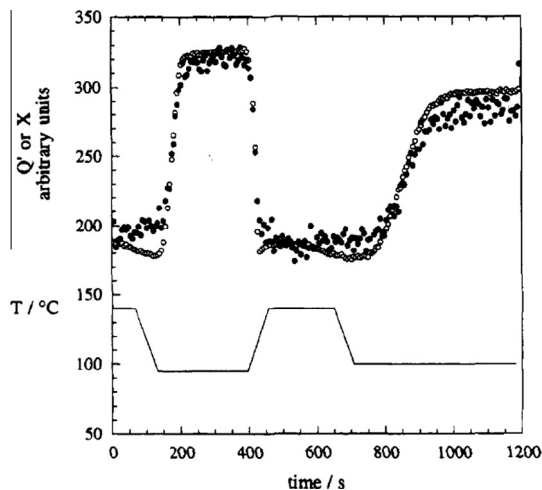


**Fig. 2.** The derived data obtained from the SAXS and WAXS raw data shown in Fig. 1. The scattering invariant  $Q = \int_0^{\infty} q^2 I(q) dq$  (open symbols) and the integrated intensity of the WAXS (1 1 0) peak (closed symbols) are given as function of time and temperature. The data quality is remarkably good even though the WAXS data is intrinsically more noisy than the SAXS data.

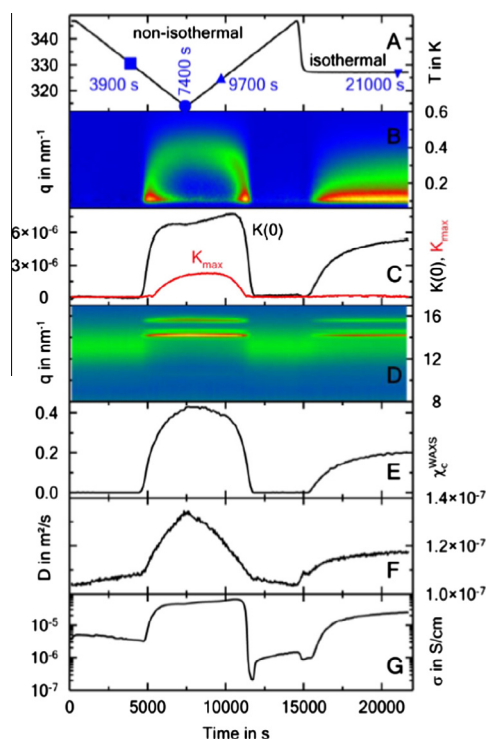


**Fig. 3.** Derived parameters from a SAXS/WAXS/DSC/calometric/conductivity experiment [15] obtained during thermal treatments of a polymer sample doped with Multi Walled Carbon Nano Tubes. (A) Thermal profile, (B) raw data, (C) derived electron density data (SAXS), (D) Raw WAXS data, (E) degree of crystallinity derived from WAXS data, (F) thermal diffusivity, (G) electrical conductivity. Data obtained with modern detectors and sample environments.

The improvement in data quality between combinations of X-ray based experiments and non X-ray based experiments, like for instance SAXS in combination with Thermal Analysis methods, e.g. DSC, has in some areas also made great strides. DSC was one of the first sample environments/technique combinations that was utilised on line [16–18]. One of the major problems with DSC is that in order to obtain the highest quality data one requires the sample to be thermally shielded. Experimentally this is in disagreement with the requirement to have X-ray access. The higher X-ray intensity and the introduction of flash DSC type of instruments has allowed more accurate and faster experiments [15,19,20]. In Fig. 4 the right hand panel describes one of the earlier SAXS/DSC experiments with a conventional heating rate of several 10's of

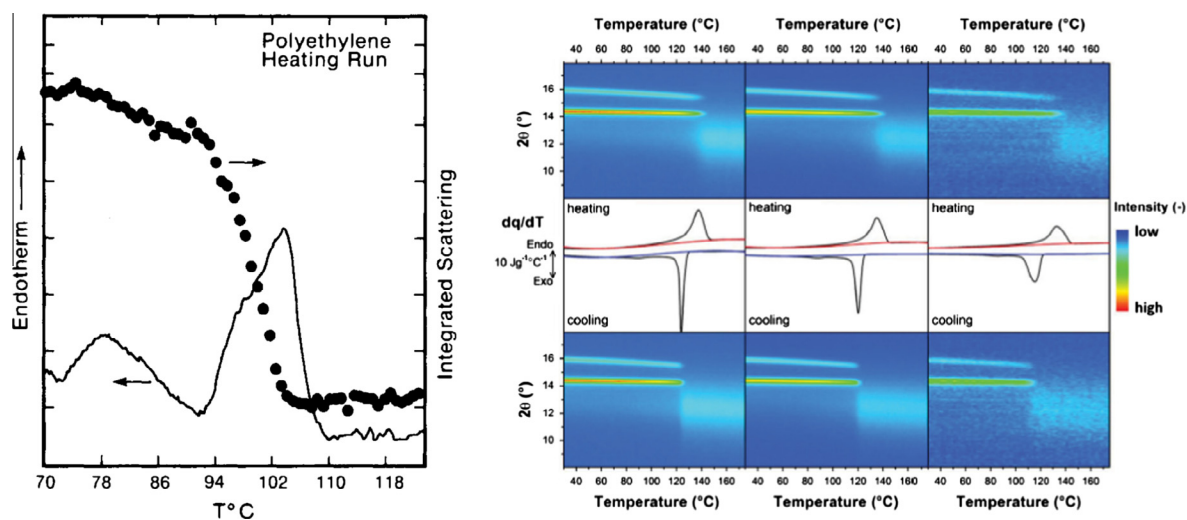


**Fig. 4.** Combined X-ray scattering and thermal analysis data. The left hand panel shows the slow cooling and crystallization from a polyethylene sample [16] obtained around 1985. The right hand panel shows a similar experiment [20] using a flash DSC, well collimated beamline and efficient photon counting detectors performed in 2015. The differences in data quality are clearly visible.

degrees/minute. In the right hand panel WAXS/flash DSC data are shown. If we keep in mind that to obtain good quality WAXS data is more difficult than to obtain a good quality SAXS invariant, a theme which we will explore in more detail, then we can see a remarkable improvement in data quality.

Many other examples of improvements, over the last decades, in experimental results on commodity polymers can be found in the literature. The main reason why this has become possible is the fact that the quality of X-ray position sensitive detector has finally come up to the level that one can fully benefit from the available synchrotron beams. The limiting step at present has become the X-ray dose that materials can handle before their physical structure and their physical/chemical interactions are being changed by the X-ray doses.

### 2.1. Quiescent crystallization studies

The development of crystallinity when pure semi-crystalline polymers are quenched below their melting temperature has long been an important subject not only because of the pure scientific interest how long chain molecules behave in such conditions but also because of the potential industrial interest. In the case of quiescent crystallization where the only parameter is the degree of under-cooling the interest is mainly fundamental since this is hardly a condition that will be encountered in an industrial processing environment where other factors like shear and the addition of different crystallization enhancers and clearing agents also have to be considered. However, the fundamental data that can be obtained is still interesting.

In this area we encounter an issue which highlights the limits to which X-ray scattering and diffraction can play a role. In the extended debate about the initial stages of polymer crystallization it was postulated that one could distinguish between a nucleation and growth model and a model by which density fluctuations would precede the crystallization event which would be some kind of spinodal decomposition process. The arguments used were that the density fluctuations would generate a SAXS intensity and this would precede the occurrence of diffraction peaks, evidencing the formation of crystalline regions, if a spinodal type of crystallization would take place. If the more conventional model of nucleation and growth would be true the SAXS intensity due to the formation of lamellae containing crystalline regions, and the diffraction peaks, would start to grow at the same time [21–24]. The early results were probably hampered by detector issues where sensitivity, efficiency and electronic noise levels all played a role. It would be a mistake, however, to assume that with the present generation of highly effective photon counting detectors [25] this issue could be settled by relying on scattering data alone. One should realise that crystallinity can exist even though it is not detected by WAXS. Very small and/or disordered crystallites with a low volume fraction will not render diffraction peaks that will be noticeable in the experimental noise. However, these will constitute volumes with a slightly different density with length scales detectable with SAXS. This will not be distinguishable from the intensity generated by fluctuations. In other words, even with the best detectors, one will always find that the SAXS intensity increases before the WAXS intensity.

It is at times puzzling to notice that one is willing to accept the fact that there are different sensitivities to crystallization effects between for instance DSC, Raman or dielectric spectroscopy [26] but that when comparing two techniques based upon X-ray interactions one immediately assumes that the sensitivities between the techniques will be identical. This also should not be interpreted as a statement that X-rays cannot play a role here since by utilising the crystallization kinetics data one can compare this with the theoretical studies and simulations [22,27,28].

An issue that has not been thoroughly investigated in this context is if the interaction of the samples with the intense synchrotron X-ray beams does not have an effect on the crystallization kinetics. In general one associates synchrotron beams with radiation damage but there is growing evidence that in disordered materials the absorption of the photons can cause unexpected effects due to the creation of electronic defects in glassy matter [9,29], hydrolysis products in solutions [8], etc. It is not unthinkable that free radical created by X-ray absorption induce cross linking between the polymer molecules and thus alter the crystallization rate.

### 2.2. Crystallisation studies under processing conditions

The introduction of large scale equipment on beamlines that could mimic some aspects of polymer processing has a long history [22,30,31]. Initially the main problem was to have the infrastructure in a SAXS/WAXS experimental hutch that allowed to install these sometimes rather voluminous sample environments on a beamline. Issues with lack of space, inflexible optical benches and lack of pressure lines and exhausts were numerous. Once these problems were sorted [22,32,33] to some degree, the main problem, in contrast to the popular belief, was not the lack of X-ray flux but the lack of suitable detectors that could handle the data at framing rates and with low enough noise levels. This had as a consequence that even though industrial inspired sample environments were used the cooling/extension rates etc. were mainly of academic interest. There they've played an important part in the rekindling of the fundamentals of the polymer crystallization debate [21–23,34].

In real industrial life, the crystallizing polymer melt is subjected to a combination of high cooling rates and shear forces during the most common production processes such as injection molding, film blowing and fiber spinning. These conditions are often extreme and cooling rates as high as 100–1000 °C/s and shear rates ranging from 1 to 1000 s<sup>-1</sup> can be attained. The most illustrative example is injection molding. During injection molding, the polymer is melted in an extruder and subsequently injected, into a cold mold where it solidifies acquiring the mold shape. The thermo-mechanical history to which

the polymer melt is subjected determines the formation of complex skin-core morphologies, where the formation of mesomorphic, highly oriented/highly crystalline and isotropic structures occurs simultaneously.

Due to the high cooling rates and to the enhancing of crystallization rate due to shear, the structural evolution of semicrystalline polymers in processing conditions can last few seconds. High brilliance X-ray synchrotron sources are thus a unique tool to study on-line and in-situ polymer crystallization in relevant industrial conditions, offering the possibility to perform measurements with micro and millisecond resolution. Among the other techniques, microscopy techniques are certainly valuable for visualizing in real space the final structure, but they are destructive and cannot be applied for in-situ studies. On the other hand, fast chip calorimetry can study melting and crystallization events at cooling rates well comparable to the ones found in industrial processing, however the sample quantity required for fast chip calorimetry (nanograms) is far too small to be comparable with real specimen. FTIR and laser scattering can also be performed with millisecond time resolution, however they require samples much thinner than the ones used in reality. On the contrary, synchrotron X-ray scattering techniques such as SAXS and WAXD can be performed with micro and milliseconds resolution on samples with thickness ranging from microns to some millimetres. Moreover, complex sample environment mimicking real processing machines can be used.

The effect of fast cooling on polymer structure has been long studied in literature. Semicrystalline polymers are generally characterized by a certain amount of defects such as variation in chemical composition, different configuration of neighbouring repeating units and different conformation of portions of the chains. These defects hinder chain packing and a large amount of structural disorder is generated when melt is rapidly cooled below its melting temperature. The highly defective structures generated in these conditions are intermediate between the crystalline and amorphous ones and are usually called mesomorphic phases, or simply mesophases. Mesomorphic phases have been observed for a large number of homopolymers such as iPP [35–37] polyamides [38] and polyesters [39,40]. Due to its industrial relevance, iPP mesophase is one of the most studied and well characterized. Though the observation of mesophase occurrence can be achieved by off-line X-ray diffraction of a polymer quenched from the melt, observation of mesophase development in real time is a more challenging task. Traditionally, mesomorphic structuring from the melt has been studied by calorimetric techniques. Wunderlich et al. [41] showed first the occurrence of the mesophase between 60 and 0 °C in iPP when cooled at 70 °C/s. For polymers characterized by high crystallization rates and low degree of defects, it is however difficult to obtain pure mesophase using conventional calorimetry. Cooling rates as high as  $-4000$  °C/s can currently be achieved by using the so-called fast chip calorimetry [42,43]. However, calorimetric techniques cannot provide directly information about what phases develop and off-line spectroscopic or diffraction measurements are required. Moreover, quantitative analysis always requires the knowledge of thermal data from pure phases. On the other hand, X-ray diffraction experiments during fast cooling would provide quantitative and exhaustive information on phase formation.

With the very high cooling rates mentioned above, and realising that, in the industrial context, this also will be accompanied by preceding shear and rapid volume changes we remind the reader here about the statement in the introduction regarding the study of extreme conditions. Not a single parameter is changed very rapidly here but a combination of several.

It is only in the last 5 years that real time X-ray diffraction during ultrafast cooling became feasible thanks to the development of ultrasensitive noiseless X-ray detectors for synchrotron radiation and thanks to the development of novel sample environments [44]. The first real time detection of iPP mesophase using WAXD has been reported by Cavallo et al. in 2010 [45] using a simple and effective apparatus to produce ballistic cooling with cooling rates from 20 °C/s to 300 °C/s. This simple approach allowed the authors to follow the polymer structuring process during fast cooling by simultaneous thermal and X-ray analysis. Moreover, by using the so-called continuous cooling curve (CCC) diagrams, the time and temperature coordinates for the formation of the mesophase with respect to the most stable phase can be identified clearly [45]. Fig. 5a shows the temperature directly measured inside the sample together with the evolution of the crystallinity calculated from WAXD during a ballistic non isothermal cooling experiment. Deviation of the sample temperature from the natural cooling curve reveals sample crystallization. Thus the derivative of the sample temperature, i.e. the instantaneous sample cooling rate, shows a peak at the crystallization temperature. Comparing the instantaneous cooling rate with the crystallinity evolution as a function of time or temperature demonstrate that the peak in the thermal analysis curve occurs at the maximum rate of phase formation (Fig. 5b). By cooling at different rates iPP and propene/ethylene random copolymers with increasing

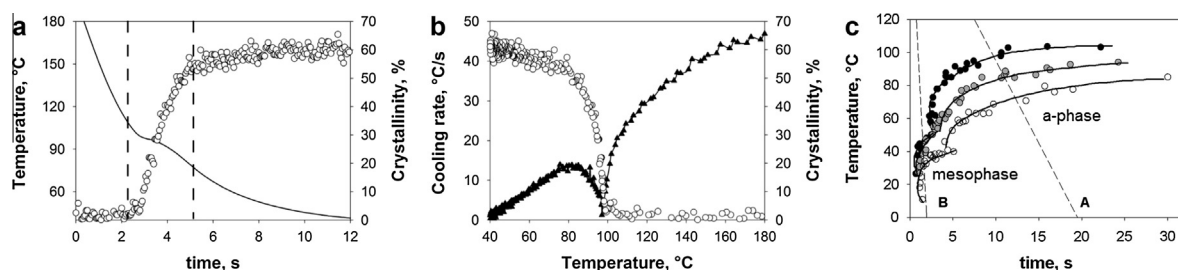


**Fig. 5.** (a) Comparison of the instantaneous sample temperature and the X-ray crystallinity developed during cooling at 30 °C/s as a function of time. (b) Comparison of the instantaneous sample cooling rate and the X-ray crystallinity developed during cooling at 30 °C/s as a function of sample temperature. (c) CCC diagrams for propene-ethylene random copolymers. (black circles) pure iPP, (grey circles) 3.4% of ethylene counts, (open circles) 7.3% of ethylene counts. (a) and (b) are reprinted with permission from [45] and (c) is adapted with permission from [46].

ethylene co-unit content and plotting the temperature when the maximum rate of phase formation is attained versus time CCC diagrams can be constructed (Fig. 5c). The CCC diagrams in Fig. 5c have a double “nose” shape, with the top region related to the formation of the most stable alpha form and the bottom region related to the mesophase formation. Given a certain cooling history, the prevailing structure that will form can be predicted from the CCC diagrams.

This approach has been successfully applied also to polyamides [47] and polyesters [48].

Most recently, simultaneous fast chip calorimetry (flash DSC) and WAXD measurements also became feasible making possible quantitative analysis of polymer structuring at even higher cooling rates and also isothermal experiments after rapid quenching that could not be performed using ballistic devices [20].

The other important parameter in industrial polymer processing is flow. The effect of flow on polymer crystallization during polymer processing is dramatic and flow-induced crystallization is a complex phenomenon that is still extensively studied nowadays. Application of flow to a polymer melt can cause substantial transitions in kinetics and morphology of the polymers. The well-known shish-kebab morphology is often formed during flow-induced crystallization where long crystalline fibers (shish) serve as nuclei for further crystallization of lamellae growing perpendicularly to the fibrils (kebab).

Shearing apparatus using slit flow geometry have been recently developed in order to elucidate the mechanism of formation of thread-like precursors, shish and kebabs in real time [49,50]. These machines allow to reach the high stress regime with well-defined flow conditions and closely mimic industrial conditions. In-situ WAXD and SAXS measurements during and after flow in the high flow regime showed that not only thread-like precursors but even elongated crystalline fibers can be formed during quite short flow pulses, resulting in a dramatic viscosity change [51]. Due to the pressure that builds up during the injection phase in injection molding, polymer structuring is also expected to be influenced by pressure. This has been recently demonstrated experimentally for linear low-density polyethylene (LLDPE) [52].

Thanks to the possibility to host large apparatus in a synchrotron beamline, extruders, fiber spinning apparatus and even very large film blower can be used to collect online data during a polymer processing experiment with conditions virtually equal to the ones encountered in industry. For instance, the structural evolution during melt spinning of polyethylene, nylon and PVDF has been extensively studied in the past using both SAXS and WAXS [31,53]. Recently, systematic data on the LLDPE structural evolution during film blowing have been produced by SAXS and WAXD [54,55]. See Fig. 6.

In order to be able to install large scale sample environments like the film blowing unit shown in Fig. 6 the experimental infrastructure to handle this should be available. There are only a few SAXS/WAXS beamlines where this is the case and for future generations of beamlines, when one intends to carry out a program in polymer processing, one is well advised to make this infrastructure part of the initial design. The experimental hutch should for instance be large enough to accommodate encumbering machinery as well as possess motorised dispositives such as cranes, linear stages, goniometers and cradle motors that are able to handle heavy instruments. Moreover, exhausting systems are required to conduct safely synthesis in situ involving gases. For SAXS experiments, extra care should be taken to reduce the air absorption/scattering and specially customized exit/entrance windows should be designed to limit the air gap, whilst still hosting large equipment around the sample (see the shallow 60 cm long cone of the SAXS vacuum line in Fig. 6).

### 2.3. On-line chemistry

The synthesis of novel materials is commonly hampered by the lack of knowledge on the fine control of complex synthetic steps. A chemical synthesis is a thermodynamic system that involves generally several chemical reactions of reagents

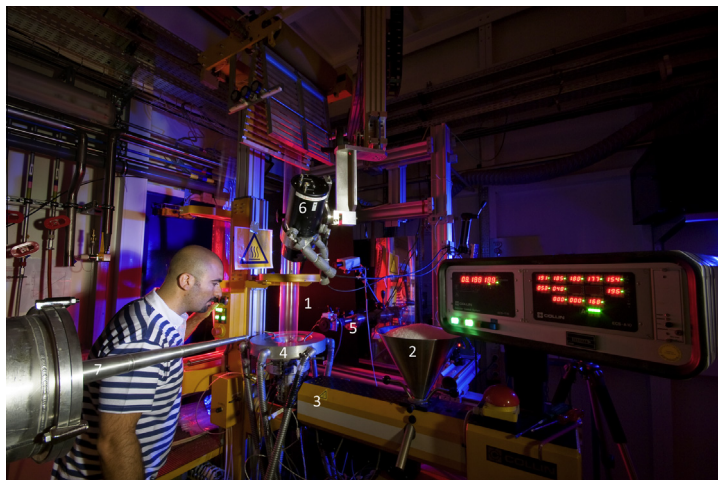


**Fig. 6.** Film blowing unit installed on beamline BM26A at the ESRF [56]. 1-blown film, 2-feeding hopper, 3-extruder, 4-film blow die, 5-X-ray beam, 6-WAXS detector, 7-SAXS detector. This set-up was used to collect data on the structural evolution of LLDPE [55,57]. With the appropriate infrastructure in place this type of sample environment can be installed in a couple of hours.

with subsequent intermediates as well as their different relationship with the synthetic medium. Commonly, the monitoring of the chemical synthesis is predominantly followed by sampling aliquots and offline spectroscopic techniques and frequently focused on kinetic studies. However, online structural investigations are crucial in order to understand the dependence of the final product on the mechanism of formation.

Great efforts have been carried out to develop novel X-ray cells that permit the monitoring in situ by simultaneous SAXS-WAXS experiments in combination with other techniques such as FT-IR spectroscopy to elucidate the dependency of the phase separation onset and the reaction kinetics [58].

Particularly, polymer science has significantly advanced along with the development of the X-rays cells for synchrotron studies as provides time resolved structural information during that mimic real polymer processing extreme conditions.

Hydrogen bonding was considered to drive the phase separation in segmented polyurethanes as studied by FT-IR. However, in situ SAXS experiments in combination with FT-IR of a series of polyurethane reactions have been shown that free energy of mixing as the molecular weight increased led to the microphase separation morphology that preceded the kinetics of hydrogen bonding formation [58].

Reaction injection molding (RIM) [59] is a widely employed operating method in the industry of a wide broad of segmented block copolymers such as copolyurethanes [60], copoly(urethane-urea)s [61,62], copolyureas [63–65] and copoly(ether-amide)s to generate complex polymer elements in a fast and malleable processing routine. The polymer reaction by RIM comprises concomitantly phase separation, crystallization and cross-linking of the copolymer obtained as a kinetic competition that defined the development of the final structure [66]. The initial low viscosity monomers mixture reacts instantly that subsequently develops from a glassy solution during the mold filling as a result of the cross-linking of the ongoing copolymerization to a highly cross-linked stiff polymer material. In situ structural investigations of the morphology development of a RIM copoly(isocyanate-urea) reaction by SAXS have shown that at a critical isocyanate conversion a microphase separation transition occurred [67]. The growth of the microphase separation has been found to progress by a spinodal decomposition and deterred by the glassy polyisocyanurate phase. Similarly, the polymerization of water-flown flexible polyurethane foams have been investigated by in situ SAXS experiments as well as by FT-IR spectroscopy and rheology [68]. The concomitant synthesis of a polyether polyol and water with diisocyanate lead to a homogenous solution of reagents, homopolymer, hard segment segments and water reacted isocyanate mixture [69]. The complex system was simultaneously blown by the release of CO<sub>2</sub> of the water-diiisocyanate into a foam and thus, maintaining the core of the foam in quasi-adiabatic state. The microphase separated morphology evolved through a spinodal decomposition following a time dependent Ginzburg-Landau model that was detained at a glassy state when the T<sub>g</sub> of the complex system attained the reaction temperature, the so-called Berghmans point. As a result, the vitrification of the reaction system deterred the foam expansion [69].

Recently, supercritical CO<sub>2</sub> (sc-CO<sub>2</sub>) has largely been employed as a green reacting medium that offers advantages to traditional organic solvents. Sc-CO<sub>2</sub> is inexpensive and recoverable after use that eliminate the need for tedious drying steps and it is also inert to free radical reactions. However, the lack of solubility of most of the block copolymer in sc-CO<sub>2</sub> has prevented the applicability in industrial polymer applications. Dispersion polymerization of block copolymers in one pot synthesis in sc-CO<sub>2</sub> by reversible addition-fragmentation chain-transfer (RAFT) have shown to be an easy alternative method to produce microparticules with a wide array of internal well-defined structures [70]. However, the nature of the reacting medium (high pressure) have limited the understanding of polymerization kinetics, morphological development mechanism as well as phase behaviour of the block copolymer obtained in sc-CO<sub>2</sub>.

Several block copolymers synthesised by dispersion polymerization in sc-CO<sub>2</sub> in which one of the blocks was consistently poly(methyl methacrylate) (PMMA) whilst the second block differed in CO<sub>2</sub>-philicity have monitored by SAXS experiments [71]. The obtained morphology has been found to shift on the predicted phase diagram depending on the CO<sub>2</sub>-philicity of the second block. The difference in CO<sub>2</sub>-philicity defined the absorption of CO<sub>2</sub> by the different blocks that leads to the formation of kinetically-trapped morphologies.

Obviously also in the study of structure formation by on-line chemistry one will look for the opportunities to push the boundaries farther. For very fast reactions one probably has to revert to microfocus techniques and stop flow or ballistic coalescence of bubbles containing the reagents [72–74]. However, there are two issues that one should take into consideration here. The first one is the possibility that too high a local radiation dose can influence the chemical reactions. The second issue is that the reduction in size might render results that might be less relevant in an industrial context. The first issue requires conscientious cross checks to eliminate artefacts. The second should be assessed on a case to case basis and definitely should not stop one performing experiments which have mainly academic interest.

### 3. Specialty polymers

#### 3.1. Conventional block copolymers

The morphological richness which is displayed by block copolymers is by now well established. Where in the 90's synchrotron radiation SAXS/WAXS was an excellent tool for the determination of phase diagrams [10,11] the developments in beamline instrumentation pioneered with the polymer processing experiments, in combination with improved synthesis control, have created the know-how and materials that allows the transition from characterisation to processing to be

speeded up manifold for this class of materials. As an example of this recent developments in polymeric organic conductors and semiconductors in combination with synchrotron radiation beamlines will be discussed more extensively in the next section. However, the developments discussed in the next section are not limited to conducting systems but parallel developments on specialised processing to other specialty polymers start to appear more abundantly [75,76].

Another important development, due to the area in which these organic materials might be used, like electronic components, but above all like cheap devices for energy generation, the emphasis in this area is also shifting from the bulk characterisation and processing, to more thin films. The developments in grazing incidence scattering, both technical as well as in data analysis, which in the early years were quite slow [77] have in recent years been very fast [78].

### 3.2. Conductive polymers

The global need for energy stimulates the development of new technology to extract more efficiently energy from renewable sources. Among the different renewable sources, solar energy represent a fabulous opportunity with its estimated energy potential of 23,000 TW/year. Solar energy can be converted into electricity using photovoltaic devices. Despite the higher efficiency of silicon based photovoltaic devices, organic photovoltaic devices (OPVs) represent an interesting alternative due to their low cost and easy processing and have received massive attention in the last years. Among the OPVs, polymer based OPVs are particularly interesting as they allow easy fabrication and integration of the photoactive polymer layer into light-weight and flexible substrates, also made out from polymers like PET.

The most classical polymer based OPV, is the bulk heterojunction (BHJ) OPV device. Here, the active layer is composed by a blend of a semiconducting polymer that acts as electron donor and a small molecule with function of electron acceptor. The fullerene derivative [6,6]-phenyl-C61-butyric acid methyl ester known as PCBM is usually used as electron acceptor, whilst poly(3-hexyl thiophene) known as P3HT is the mostly used electron donor polymer. Other polymers are also used such as poly(diketopyrrolopyrrole) (DPP) [79] or poly(benzothiadiazole) [80] based derivatives an efficiency of the order of 10% have been reported [81].

In order to achieve high efficiency, two aspects of the active layer have to be considered: (i) the chemical structure of the acceptor and donor materials and (ii) the characteristic length scale of the local morphology. The chemical structure has to be fine-tuned such that the highest-occupied molecular orbital (HOMO) and lowest-unoccupied molecular orbital (LUMO) levels allows the material to achieve a high open-circuit voltage with a small energy bandgap, whilst maintaining a LUMO level high enough for efficient charge separation [82]. On the other hand, due to the very limited diffusion length of the exciton (about 10 nm), a local morphology with characteristic length scale of the order of 10–20 nm and with a large interface between the donor and acceptor materials is desirable. Thus, the study of the nanostructure of the active materials is crucial to understand and establish the structure-property relationship in OPVs.

Several microscopy techniques have been employed to visualize in real space the structure of OPV materials. In particular bright-field TEM [83] and 3D electron tomography have showed the network nature of the active material composed by PCBM and crystalline P3HT interpenetrated domains [84]. On the other hand, scattering techniques can be successfully used to investigate the morphology in OPV in the range of 0.1–100 nm. Due to the thin film nature of the OPV active layer (typically 100–200 nm), the use of transmission SAXS remains quite limited [85] and surface sensitive scattering techniques such as GISAXS and GIWAXS have proven to be the best techniques to investigate the active layer morphology [86]. Moreover, GISAXS/ GIWAXS data acquired using 2D detectors offer the possibility to extract from one single image information about the structure of the conjugated polymer (i.e. lamellar), the size of crystallites, the degree of crystallinity and the orientation of the crystalline domains [86,87]. Static GISAXS/GIWAXS are nowadays routine techniques to study the structure of the OPV active layer. Fig. 7 shows the connection between the structure and the GIWAXS patterns for a typical pi-conjugated polymer with lamellar-like structure. It is clear how sensitive is a GIWAXS measurement to the mosaicity of the thin polymer film. From the orientation of the diffraction peaks, especially the 100 reflection for the P3HT lamellar structure, the average orientation of the P3HT crystals in the thin film can be extracted (edge-on or flat-on configuration).

Advanced methods to measure with extract the full pole figure for the conjugated polymer crystals in grazing incidence geometry has been developed [89]. When performed at synchrotrons, GISAXS/GIWAXS can be used to study in real time the process of structuring of the active layer.

Initial real time studies of the structure development of the active layer morphology have been conducted during film drying of P3HT/PCBM (reference of Docsh group) as well as pDPP/PC<sub>71</sub>BM (where pDPP is a copolymer of diketopyrrolopyrrole and quaterthiophene) by the group of Russell [90] and during a roll-to-roll coating prototype process of P3HT/PCBM [91,92].

The final structure of the polymeric materials during the formation of thin layers from solution is a complex multistage mechanism that involves concomitant physical and chemical processes.

During solvent casting of pDPP/PC<sub>71</sub>BM from a 1,2-dichlorobenzene: chloroform (DCB:CF) 1:4 w/w solution, four different stages have been observed [90] (see Fig. 8c). Firstly, The onset of pDPP precipitation/crystallization during CF evaporation occurs whilst PCBM is still completely dissolved (appearance of the 100 diffraction signal). Further crystallization of pDPP into a better defined semicrystalline fibrillar network (increase in the scattered GIWAXS and GISAXS intensity, see Figure). pDPP crystallization forces segregation of PCBM to form a phase segregated structure with better defined scattering entities. Finally the phase separation becomes more and more enhanced and the crystalline structure more perfect. Similar multistage process for the phase separation are believed to occur during spin coating [93]. The evolution of the structural

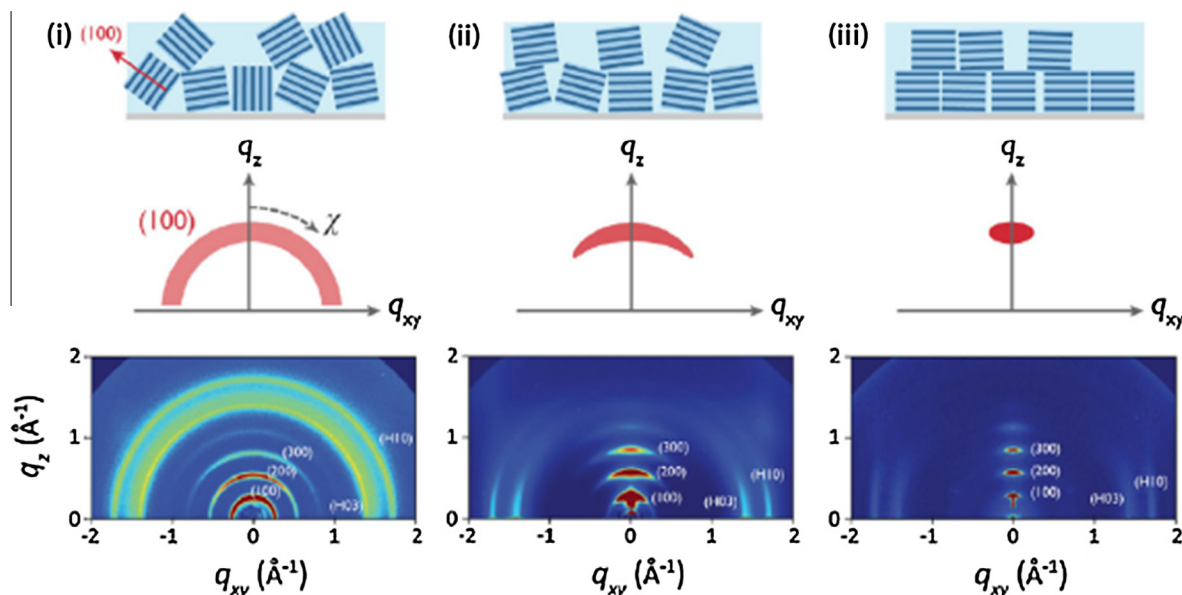


**Fig. 7.** Overview of the structural information that can be extracted from GIWAXS images. (i) Random crystallites orientation; (ii) crystallites with partial orientation; (iii) crystallites highly oriented with the (001) plane parallel to the substrate. Reprint with permission from [88].

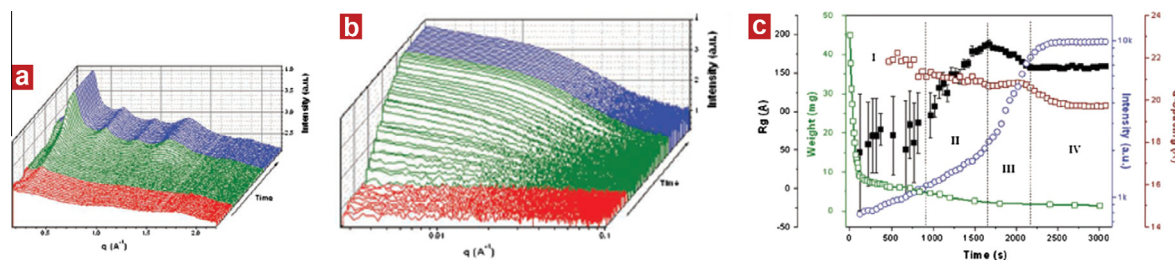


**Fig. 8.** In situ GIWAXS (a) and GISAXS (b) of pDPP and PC<sub>71</sub>BM blends processed from a DCB:CF solvent mixture. (c) Summary of the in-situ GIWAXS and GISAXS results during solvent evaporation. Adapted with permission from [90].

parameters, the extent of phase separation and the final morphology are strongly influenced by the presence of co-solvent [94], composition of the starting solution [93] and processing conditions [95].

GIWAXS data acquired during a fast combinatorial study on a pre-coated tape produced using a roll-to-roll process showed that a critical concentration of P3HT in the drying film has to be reached before P3HT crystallization sets in (see Figs. 9 and 10) [91].

Representative results obtained with the experimental set-up depicted in Fig. 9 are shown in Fig. 10. The effect of adding a high boiling point co-solvent such as orthodichlorobenzene (ODCB) to a drying P3HT/chloroform solution during roll-to-roll processing has been elucidated (see Fig. 10a and b). As expected, the drying process is slowed down significantly as a result of the ODCB addition and P3HT crystallization is significantly delayed and higher P3HT crystalline degree could be attained at the end of the drying (Fig. 10b). The onset of P3HT crystallization changes from 0.6 s to 18 s due to the ODCB presence. PCBM addition further delays the P3HT crystallization, as the time for the P3HT to reach the critical concentration for its crystallization is delayed [92] At the same time, PCBM has a negative effect on the P3HT crystallization and lower crystallinity is obtained (Fig. 10c).

Other in-situ GISAXS/GIWAXS works have been conducted during in-situ GISAXS/GIWAXS works during spin coating [93], blade-coating [96] slot-die coating [97] and during printing [98].

In-situ synchrotron GISAXS and GIWAXS investigation have helped researchers to understand what the mechanism of structuring during film formation is and provided crucial information on what is the best formulation of the starting solution and how to control solvent evaporation to achieve the optimized morphology for the best power conversion performances.

Whilst all the above cited works have showed the feasibility of synchrotron GISAXS/GIWAXS experiments during processing, structural investigation during real processing conditions (namely industrial roll-to-roll process) is still a challenge. The feasibility of these studies has been showed already [91,92] and, soon, structuring of the OPV active layer in real processing conditions will be unveiled. GISAXS and GIWAXS remain probably the most versatile and powerful techniques to study organic semiconductors in thin films.

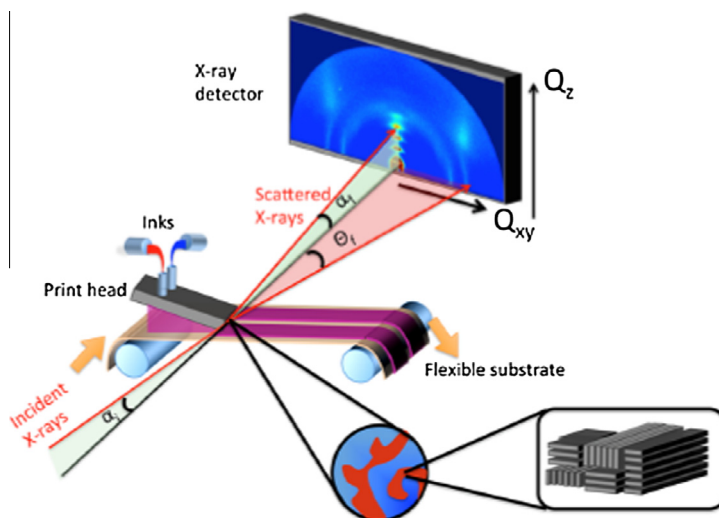


**Fig. 9.** Panel (a) shows the physical set up for a roll to roll printer installed on beamline 7.3.3. at the Advanced Light Source (ALS, Berkeley) [119]. Panel (b) shows the overall lay-out for in-situ GISAXS/GIWAXS investigation of the experiment with respect to the X-ray storage ring.

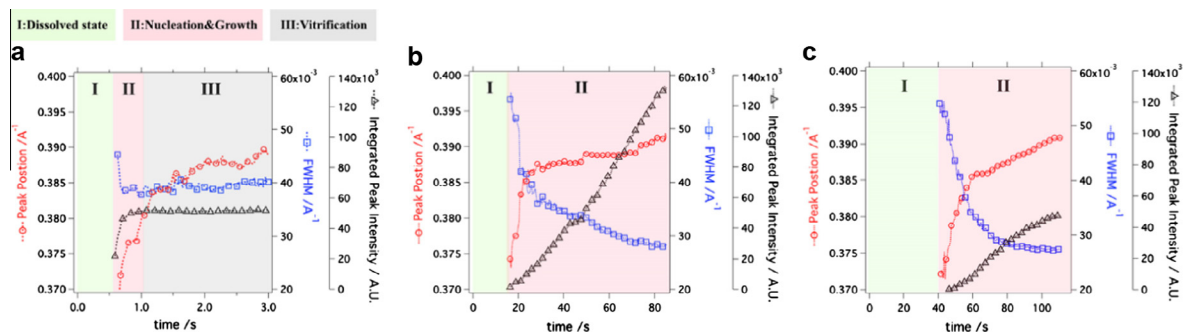


**Fig. 10.** Summary of the in-situ GIWAXS results during drying in a roll-to-roll processing express in terms of relative P3HT concentration. The top panel shows the integrated intensity of the (1 0 0) WAXS diffraction peak. The middle panel shows the coherence length derived from the WAXS data. The bottom panel shows the shift of the (1 0 0) diffraction peak as function of concentration. Adapted with permission from [91].

## 4. Developments in synchrotron sources and beamline equipment

### 4.1. SR sources

One of the questions that one can ask is if there is still a future for synchrotron radiation based polymer research? The developments in conventional X-ray sources, for instance using liquid metal targets [99] and focussing optics [100] have brought very highly performing systems to the home laboratory. Although not at the level yet of what SR sources can do this has reduced the number of required visits for routine experiments to SR beamlines considerably. Alternative X-ray sources based upon strong pulsed laser systems have seen developments in recent years as well. There are several different schemes which can be used but these are for the moment still lacking in the required low beam divergence required for scattering and diffraction although for imaging purposes some of these methods are already well suitable [101,102]. Since the underlying physics of these X-ray generation techniques has been worked out it probably will become an engineering effort to increase the beam quality. This, in combination with the requirement to develop user models instead of prototypes, set up a sales and after sales organisation and bring down the price to a level that it is affordable for a university department or industrial laboratory will require probably around 10–15 years. The beam quality, with respect to intensity and divergence, that probably will be achievable, will be comparable to a second generation synchrotron radiation source [32,103,104].

Another perceived ‘threat’ is the development of Free Electron Lasers (FEL’s). For some these are seen as the snake oil for every experiment but in reality these facilities are unlikely to play a role in the present materials science research setting due to the too high temporal flux which will make time-resolved experiments slower than the nanosecond level impossible since the samples will be destroyed in that time scale. The fact that we can study a chemical reaction on the nano-femto second time scale is very interesting as such but hardly relevant for, among else, polymer crystallization and deformation.

The developments in detector technology in recent years are nearly as astounding as the progress made with the X-ray sources. Where efficient high count rate position sensitive detectors were less than a decade either Charge Coupled Devices which suffered from read out noise [105] or gas based chambers which required elaborate gas handling systems [106], these have virtually now all been superseded by the hybrid pixel detectors [107,108] which offer both high count rate as well as single photon counting. Even though the pixel sizes are still relatively large one can expect this issue to be tackled by the manufacturers in the near future and then these detectors will also be usable for microfocus experiments. Although these developments have also been useful for conventional lab set ups, the synchrotron beamlines have benefitted most from the increased detector efficiency and count rate due to the fact that the disparity between the number of to be detected photons and maximum detector count rates was higher on SR beamlines than in home laboratory set ups.

In the meantime the introduction of more complex sample environments increased the demand for access by a larger number of research groups which are still benefitting from the higher flux and better collimation of even the best conventional X-ray sources.

Further developments of the X-ray sources with respect to photon flux can be made possible by the SR machine and beamline developers but it becomes questionable if this should be the main driving force for developments. During a materials science experiment lasting beyond several minutes the radiation load on samples can easily exceed the maximum dose rate during beyond which the samples either are damaged to a sufficiently large degree that the experimental results are not representative of the samples any more or that structure formation is influenced by the creation of a larger number of crystallization nucleation sites [8,29] or by cross linking which even becomes apparent when measuring thermodynamic data [109].

If we take the above considerations into account it appears that for the foreseeable future (i.e. 8–10 years) the difference in beam quality between SR beamlines and home laboratory sources will ensure the need for synchrotron beam lines for X-ray scattering and diffraction of soft condensed matter systems even though the quality of both home sources as well as SR sources have increased over the years. The X-ray flux threshold required to be able to do time-resolved experiments, which is a combination of X-ray flux, X-ray contrast and required time resolution and statistical data quality, is for some slow experiments and with specific samples reached even with home sources. For fast experiments, weak scatterers and when using complicated sample environments this is not reached yet and maybe will remain elusive even in the coming years.

Since sample preparation methods have become more elaborate there is a tendency not only to take a look at the finished materials and the processing but move research forwards in the production time line where the materials are being synthesized. Since this synthesis often entails catalysts with active metallic sites it can be foreseen that techniques like X-ray Absorption Spectroscopy (XAS) which can shed light on the changing electronic environment around these metallic sites, will gain in popularity as well. This might be in combination with the scattering techniques which can simultaneously render more structural information [110]. XAS experiments, which in soft condensed matter research took many hours for each scan years ago [111,112], can now be done in minutes. This offers promises in for instance the area of supramolecular chemistry. See Fig. 11.

Especially when such spectroscopic techniques can be combined with techniques that can render structural information like SAXS and WAXS, or other non X-ray based experimental approaches, this has the promise to become a new area in polymer and soft condensed matter research [110,112,113].

X-ray spectroscopy using soft- or tender X-rays, with photon energies <5 keV, are benefitting at present from the development of some new beamlines and are very useful in the elucidation of more complicated structural issues in block-copolymers [114]. Developments in this area are unfortunately limited to the synchrotron radiation laboratories specialised in soft X-ray generation which are much less in number than the storage rings generating hard X-rays.

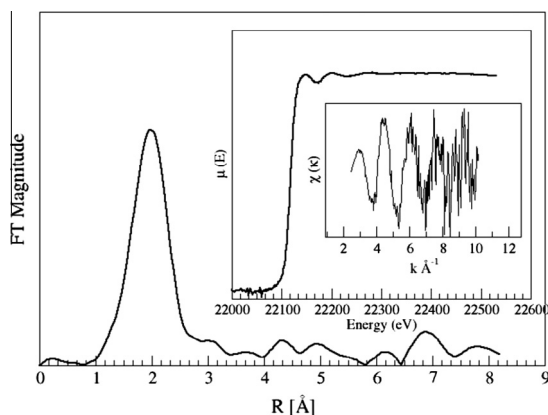


**Fig. 11.** An X-ray Absorption Spectroscopy scan from a Ruthenium containing soft condensed matter sample. This kind of data can be used to shine light on the coordination of metallic complexes with the surrounding organic medium. The graph shows the data and the inset the derived data. These experiments using reasonable time scales and X-ray doses were hardly feasible 10 years ago but have moved into the realm of reality in the last number of years.

## 4.2. Developments in data handling

An emerging trend in the handling of data is to combine experiments, both as a post experiment analysis technique as well as in real time, with numerical simulations. The tremendous increase in available computing power in the last decade has enabled this [115]. Although such attempts are tempting, and this path should definitely be investigated, there are also risks inherent to this approach in that it is most unlikely that this can be done in a completely model independent fashion.

Other promising approaches, which are still on the primary data side, are attempts to co-analyse the data obtained from different techniques instead of considering these data sets as independent data sets and only combine them after the full analysis on both techniques is done [116,117].

Inspired by experiments that can be performed on Free Electron Lasers one can also imagine some progress using fluctuation scattering [118]. Such approaches, just like protein solution scattering however, should be developed with a clear understanding of the theoretical limitations of the information contents of the scattering data as well as how the convolution of the theoretical mathematical world intersects with the real data world where data points have error bars, background subtraction issues and non ideal detector systems.

## 5. Conclusions

With respect to the commodity polymers one can draw the conclusion that over the last twenty years the emphasis of research has shifted from the more academic studies towards experiments which are more application directed. In this we can think of the approaches where very controlled, with respect to molecular weight, or molecular weight distributions, and well characterized samples are brought into environments where the parameters like pressure, shear, thermal quenches and volume can be set in such a fashion that industrial conditions are mimicked.

For the non-commodity polymers the time-line between the initial characterisations and phase diagram determinations towards these materials under operando, in devices, or in processing conditions, can be much shorter. The available instrumentation has much improved in recent years but also the collective experience of performing SR based experiments among polymer researchers has grown thanks to more beamlines becoming available and the passing on of the expertise from the pioneers towards new generations of students.

Grazing incidence scattering has shown to be a powerful tool in the studies of block copolymer films. Where in the early years [77] both the technical as well as software developments in this area were rather slow in the last decade this has accelerated considerably [78]. With the ever increasing world energy consumption and the high interest there is in energy generation in which these OPV blockcopolymers potentially it looks like two developments have come together at the right time. It might be interesting to see for future students of the history of technological development whether these were indeed separate developments or if the interplay between X-ray scattering technology and specialty polymer processing needs had been the main driving force.

## Acknowledgements

Although the emphasis of the examples given in this manuscript are centered around examples from the beamlines that we are best acquainted with we would like to acknowledge the fact that the communal expertise both in the international polymer community as well as in the synchrotron instrumentation community has grown at a very fast pace in the last decades. We gratefully acknowledge collaborations and inspirations regarding instrumentation developments with Gerrit Peters, Han Goossens, Han Meijer, Dario Cavallo, Alex Hexemer, Cheng Wang, Nick Terrill, Tony Ryan, Patrick Fairclough, Oleg Mykhaylyk and many others. The Dutch Polymer Institute is gratefully acknowledged for the financial support for DHM in specific and the long term support in general.

## References

- [1] A. Gabriel, F. Dauvergne, G. Rosenbaum, Linear, circular and 2 dimensional position-sensitive detectors, *Nucl. Instrum. Methods* 152 (1) (1978) 191–194.
- [2] C.J. Boulin, R. Kempf, A. Gabriel, M.H.J. Koch, Data acquisition-systems for linear and area X-ray-detectors using delay-line readout, *Nucl. Instrum. Methods Phys. Res. Sect. A – Accel. Spectrometers Detectors Assoc. Equip.* 269 (1) (1988) 312–320.
- [3] A.J. Ryan, W. Bras, G.R. Mant, G.E. Derbyshire, A direct method to determine the degree of crystallinity and lamellar thickness of polymers – application to polyethylene, *Polymer* 35 (21) (1994) 4537–4544.
- [4] S. Buchner, D. Wiswe, H.G. Zachmann, Kinetics of crystallization and melting behavior of poly(ethylene naphthalene-2,6-dicarboxylate), *Polymer* 30 (3) (1989) 480–488.
- [5] W. Bras, A.J. Ryan, Sample environments and techniques combined with Small Angle X-ray Scattering, *Adv. Colloid Interface Sci.* 75 (1) (1998) 1–43.
- [6] W. Bras, S. Koizumi, N.J. Terrill, Beyond simple small-angle X-ray scattering: developments in online complementary techniques and sample environments, *IUCr* 1 (6) (2014).
- [7] S.J. Weigand, D.T. Keane, DND-CAT's new triple area detector system for simultaneous data collection at multiple length scales, *Nucl. Instrum. Methods Phys. Res. Sect. A – Accel. Spectrometers Detectors Assoc. Equip.* 649 (1) (2011) 61–63.
- [8] H.G. Cui, E.T. Pashuck, Y.S. Velichko, S.J. Weigand, A.G. Cheetham, C.J. Newcomb, S.I. Stupp, Spontaneous and X-ray-triggered crystallization at long range in self-assembling filament networks, *Science* 327 (5965) (2010) 555–559.
- [9] H.B. Stanley, D. Banerjee, L. van Breemen, J. Ciston, C.H. Liebscher, V. Martis, D.H. Merino, A. Longo, P. Pattison, G.W.M. Peters, G. Portale, S. Sen, W. Bras, X-ray irradiation induced reduction and nanoclustering of lead in borosilicate glass, *CrystEngComm* 16 (39) (2014) 9331–9339.

- [10] S. Forster, A.K. Khandpur, J. Zhao, F.S. Bates, I.W. Hamley, A.J. Ryan, W. Bras, Complex phase-behavior of polyisoprene-polystyrene diblock copolymers near the order-disorder transition, *Macromolecules* 27 (23) (1994) 6922–6935.
- [11] A.K. Khandpur, S. Forster, F.S. Bates, I.W. Hamley, A.J. Ryan, W. Bras, K. Almdal, K. Mortensen, Polyisoprene-polystyrene diblock copolymer phase diagram near the order-disorder transition, *Macromolecules* 28 (26) (1995) 8796–8806.
- [12] N.P. Balsara, M. Tirrell, T.P. Lodge, Micelle formation of BAB triblock copolymers in solvents that preferentially dissolve the A-block, *Macromolecules* 24 (8) (1991) 1975–1986.
- [13] N.S. Wanakule, A. Panday, S.A. Mullin, E. Gann, A. Hexemer, N.P. Balsara, Ionic conductivity of block copolymer electrolytes in the vicinity of order-disorder and order-order transitions, *Macromolecules* 42 (15) (2009) 5642–5651.
- [14] A.J. Ryan, I.W. Hamley, W. Bras, F.S. Bates, Structure development in semicrystalline diblock copolymers crystallizing from the ordered melt, *Macromolecules* 28 (11) (1995) 3860–3868.
- [15] A. Wurm, D. Lellinger, A.A. Minakov, T. Skipa, P. Poetschke, R. Nicula, I. Alig, C. Schick, Crystallization of poly(epsilon-caprolactone)/MWCNT composites: a combined SAXS/WAXS, electrical and thermal conductivity study, *Polymer* 55 (9) (2014) 2220–2232.
- [16] T.P. Russell, J.T. Koberstein, Simultaneous differential scanning calorimetry and small-angle X-ray-scattering, *J. Polym. Sci. Part B – Polym. Phys.* 23 (6) (1985) 1109–1115.
- [17] M. Kellens, W. Meeussen, R. Gehrke, H. Reynaers, Synchrotron radiation investigations of the polymorphic transitions of saturated monoacid triglycerides.1. Tripalmitin and tristearin, *Chem. Phys. Lipids* 58 (1–2) (1991) 131–144.
- [18] W. Bras, G.E. Derbyshire, A. Devine, S.M. Clark, J. Cooke, B.E. Komanschek, A.J. Ryan, The combination of thermal-analysis and time-resolved X-ray techniques – a powerful method for materials characterization, *J. Appl. Crystallogr.* 28 (1995) 26–32.
- [19] M. Rosenthal, D. Doblas, J.J. Hernandez, Y.I. Odarchenko, M. Burghammer, E. Di Cola, D. Spitzer, A.E. Antipov, L.S. Aldoshin, D.A. Ivanov, High-resolution thermal imaging with a combination of nano-focus X-ray diffraction and ultra-fast chip calorimetry, *J. Synchrotron Radiat.* 21 (2014) 223–228.
- [20] D. Baeten, V.B.F. Mathot, T.F.J. Pijpers, O. Verkinderen, G. Portale, P. Van Puyvelde, B. Goderis, Simultaneous synchrotron WAXD and fast scanning (Chip) calorimetry: on the (isothermal) crystallization of HDPE and PA11 at high supercoolings and cooling rates up to 200 °C s<sup>-1</sup>, *Macromol. Rapid Commun.* 36 (12) (2015) 1184–1191.
- [21] P.D. Olmsted, W.C.K. Poon, T.C.B. McLeish, N.J. Terrill, A.J. Ryan, Spinodal-assisted crystallization in polymer melts, *Phys. Rev. Lett.* 81 (2) (1998) 373–376.
- [22] N.J. Terrill, P.A. Fairclough, E. Towns-Andrews, B.U. Komanschek, R.J. Young, A.J. Ryan, Density fluctuations: the nucleation event in isotactic polypropylene crystallization, *Polymer* 39 (11) (1998) 2381–2385.
- [23] G. Strobl, From the melt via mesomorphic and granular crystalline layers to lamellar crystallites: a major route followed in polymer crystallization?, *Eur Phys. J. E* 3 (2) (2000) 165–183.
- [24] Z.G. Wang, B.S. Hsiao, E.B. Sirota, S. Srinivas, A simultaneous small- and wide-angle X-ray scattering study of the early stages of melt crystallization in polyethylene, *Polymer* 41 (25) (2000) 8825
- [25] T. Donath, S. Brandstetter, L. Cibik, S. Commichau, P. Hofer, M. Krumrey, B. Luthi, S. Marggraf, P. Muller, M. Schneebeli, C. Schulze-Briese, J. Wernecke, Characterization of the PILATUS photon-counting pixel detector for X-ray energies from 1.75 keV to 60 keV, 11th International Conference on Synchrotron Radiation Instrumentation (Sri 2012), vol. 425, 2013.
- [26] I. Sics, A. Nogales, T.A. Ezquerro, Z. Denchev, F.J. Balta-Calleja, A. Meyer, R. Dohrmann, Simultaneous measurements of small angle X-ray scattering, wide angle X-ray scattering, and dielectric spectroscopy during crystallization of polymers, *Rev. Sci. Instrum.* 71 (4) (2000) 1733–1736.
- [27] E.L. Heeley, C.K. Poh, W. Li, A. Maidens, W. Bras, I.P. Dolbnya, A.J. Gleeson, N.J. Terrill, J.P.A. Fairclough, P.D. Olmsted, R.I. Ristic, M.J. Hounslow, A.J. Ryan, Are metastable, precrystallisation, density-fluctuations a universal phenomena?, *Faraday Discuss* 122 (2003) 343–361.
- [28] E.L. Heeley, T. Gough, D.J. Hughes, W. Bras, J. Rieger, A.J. Ryan, Effect of processing parameters on the morphology development during extrusion of polyethylene tape: an in-line small-angle X-ray scattering (SAXS) study, *Polymer* 54 (24) (2013) 6580–6588
- [29] V. Martis, S. Nikitenko, S. Sen, G. Sankar, W. van Beek, Y. Filinchuk, I. Snigireva, W. Bras, Effects of X-rays on crystal nucleation in lithium disilicate, *Cryst. Growth Des.* 11 (7) (2011) 2858–2865.
- [30] M.J. Elwell, S. Mortimer, A.J. Ryan, W. Bras, A synchrotron SAXS study of the structure development kinetics during the reactive processing of flexible polyurethane foam, *Nucl. Instrum. Methods Phys. Res. Sect. B – Beam Interactions Mater. Atoms* 97 (1–4) (1995) 261–264.
- [31] M. Cakmak, A. Teitge, H. Zachmann, J. White, On-line small-angle and wide-angle X-ray scattering studies on melt-spinning poly (vinylidene fluoride) tape using synchrotron radiation, *J. Polym. Sci., Part B: Polym. Phys.* 31 (3) (1993) 371–381.
- [32] W. Bras, G.E. Derbyshire, A.J. Ryan, G.R. Mant, A. Felton, R.A. Lewis, C.J. Hall, G.N. Greaves, Simultaneous time resolved SAXS and WAXS experiments using synchrotron radiation, *Nucl. Instrum. Methods Phys. Res. Sect. A – Accel. Spectrometers Detectors Assoc. Equip.* 326 (3) (1993) 587–591.
- [33] N. Bliss, J. Bordas, B. Fell, N. Harris, W. Helsby, G.R. Mant, W. Smith, E. Towns-Andrews, W16. 1: a new fixed wavelength diffraction station at the SRS Daresbury, *Rev. Sci. Instrum.* 66 (2) (1995) 1311–1313.
- [34] Z.G. Wang, B.S. Hsiao, E.B. Sirota, S. Srinivas, A simultaneous small- and wide-angle X-ray scattering study of the early stages of melt crystallization in polyethylene, *Polymer* 41 (25) (2000) 8825–8832.
- [35] G. Natta, M. Peraldo, P. Corradini, Smectic mesomorphic form of isotactic polypropylene, *Rend Accad Naz Lincei* 26 (1959) 14–17.
- [36] P. Corradini, V. Petraccone, C. De Rosa, G. Guerra, On the structure of the quenched mesomorphic phase of isotactic polypropylene, *Macromolecules* 19 (11) (1986) 2699–2703.
- [37] S. Piccarolo, M. Saiu, V. Brucato, G. Titomanlio, Crystallization of polymer melts under fast cooling. II. High-purity iPP, *J. Appl. Polym. Sci.* 46 (4) (1992) 625–634.
- [38] L. Penel-Pierron, C. Depecker, R. Seguela, J.M. Lefebvre, Structural and mechanical behavior of nylon 6 films part I. the crystalline phases, *J. Polym. Sci., Part B: Polym. Phys.* 39 (5) (2001) 484–495.
- [39] J. Watanabe, M. Hayashi, Thermotropic liquid crystals of polyesters having a mesogenic p, p'-biphenyl unit. 1. Smectic A mesophase properties of polyesters composed of p, p'-biphenyl acid and alkylene glycols, *Macromolecules* 21 (1) (1988) 278–280.
- [40] J. Watanabe, M. Hayashi, Thermotropic liquid crystals of polyesters having a mesogenic p, p'-biphenyl unit. 2. X-ray study on smectic mesophase structures of BB-5 and BB-6, *Macromolecules* 22 (10) (1989) 4083–4088.
- [41] Z.Q. Wu, V. Dann, S. Cheng, B. Wunderlich, Fast DSC applied to the crystallization of polypropylene, *J. Therm. Anal. Calorim.* 34 (1) (1988) 105–114.
- [42] E. Zhuravlev, C. Schick, Fast scanning power compensated differential scanning nano-calorimeter: 1. The device, *Thermochim. Acta* 505 (1) (2010) 1–13.
- [43] E. Zhuravlev, C. Schick, Fast scanning power compensated differential scanning nano-calorimeter: 2. Heat capacity analysis, *Thermochim. Acta* 505 (1) (2010) 14–21.
- [44] G. Portale, D. Cavallo, G.C. Alfonso, D. Hermida-Merino, M. van Drongelen, L. Balzano, G.W.M. Peters, J.G.P. Goossens, W. Bras, Polymer crystallization studies under processing-relevant conditions at the SAXS/WAXS DUBBLE beamline at the ESRF, *J. Appl. Crystallogr.* 46 (2013) 1681–1689.
- [45] D. Cavallo, G. Portale, L. Balzano, F. Azzurri, W. Bras, G.W. Peters, G.C. Alfonso, Real-time WAXD detection of mesophase development during quenching of propene/ethylene copolymers, *Macromolecules* 43 (24) (2010) 10208–10212.
- [46] D. Cavallo, F. Azzurri, R. Floris, G.C. Alfonso, L. Balzano, G.W. Peters, Continuous cooling curves diagrams of propene/ethylene random copolymers. The role of ethylene counts in mesophase development, *Macromolecules* 43 (6) (2010) 2890–2896.
- [47] D. Cavallo, L. Gardella, G.C. Alfonso, G. Portale, L. Balzano, R. Androsch, Effect of cooling rate on the crystal/mesophase polymorphism of polyamide 6, *Colloid Polym. Sci.* 289 (9) (2011) 1073–1079.
- [48] D. Cavallo, D. Mileva, G. Portale, L. Zhang, L. Balzano, G.C. Alfonso, R. Androsch, Mesophase-mediated crystallization of poly (butylene-2, 6-naphthalate): an example of Ostwald's rule of stages, *ACS Macro Lett.* 1 (8) (2012) 1051–1055.

- [49] L. Fernandez-Ballester, T. Gough, F. Meneau, W. Bras, F. Ania, F.J. Balta-Calleja, J.A. Kornfield, Simultaneous birefringence, small- and wide-angle X-ray scattering to detect precursors and characterize morphology development during flow-induced crystallization of polymers, *J. Synchrotron Radiat.* 15 (2) (2008) 185–190.
- [50] J.-W. Housmans, L. Balzano, D. Santoro, G. Peters, H. Meijer, A design to study flow induced crystallization in a multipass rheometer, *Int. Polym. Proc.* 24 (2) (2009) 185–197.
- [51] Z. Ma, L. Balzano, T. van Erp, G. Portale, G.W. Peters, Short-term flow induced crystallization in isotactic polypropylene: How short is short?, *Macromolecules* 46 (23) (2013) 9249–9258.
- [52] E. Troisi, G. Portale, Z. Ma, M. van Dronghelen, D. Hermida-Merino, G. Peters, Unusual melting behavior in flow induced crystallization of LLDPE: effect of pressure, *Macromolecules* 48 (8) (2015) 2551–2560.
- [53] J. Schultz, B.S. Hsiao, J. Samon, Structural development during the early stages of polymer melt spinning by in-situ synchrotron X-ray techniques, *Polymer* 41 (25) (2000) 8887–8895.
- [54] M. van Dronghelen, D. Cavallo, L. Balzano, G. Portale, I. Vittorias, W. Bras, G.C. Alfonso, G.W.M. Peters, Structure development of low-density polyethylenes during film blowing: a real-time wide-angle X-ray diffraction study, *Macromol. Mater. Eng.* 299 (12) (2014) 1494–1512.
- [55] E. Troisi, M. van Dronghelen, H. Caelers, G. Portale, G. Peters, Structure evolution during film blowing: an experimental study using in-situ small angle X-ray scattering, *Eur. Polym. J.* 74 (2016) 190–208.
- [56] W. Bras, I.P. Dolbnya, D. Detollenaere, R. van Tol, M. Malfois, G.N. Greaves, A.J. Ryan, E. Heeley, Recent experiments on a combined small-angle/wide-angle X-ray scattering beam line at the ESRF, *J. Appl. Crystallogr.* 36 (2003) 791–794.
- [57] M. van Dronghelen, D. Cavallo, L. Balzano, G. Portale, I. Vittorias, W. Bras, G.C. Alfonso, G.W. Peters, Structure development of low-density polyethylenes during film blowing: a real-time wide-angle X-ray diffraction study, *Macromol. Mater. Eng.* 299 (12) (2014) 1494–1512.
- [58] W. Bras, G.E. Derbyshire, D. Bogg, J. Cooke, M.J. Elwell, B.U. Komanschek, S. Naylor, A.J. Ryan, Simultaneous studies of reaction kinetics and structure development in polymer processing, *Science* 267 (5200) (1995) 996–999.
- [59] A.J. Ryan, Spinodal decomposition during bulk copolymerization: reaction injection moulding, *Polymer* 31 (4) (1990) 707–712.
- [60] R. Camargo, C. Macosko, M. Tirrell, S. Wellinghoff, Phase separation studies in RIM polyurethanes catalyst and hard segment crystallinity effects, *Polymer* 26 (8) (1985) 1145–1154.
- [61] D. Nissen, R. Markovs, Aromatic diamines as chain extenders in RIM urethane elastomers, *J. Elastomers Plast.* 15 (2) (1983) 96–112.
- [62] R. Turner, Stress relaxation properties of some reaction injection molded (RIM) and reinforced RIM systems, *Polym. Compos.* 5 (2) (1984) 151–154.
- [63] R. Dominguez, Amine-terminated polyether resins in RIM, *J. Cell Plast.* 20 (6) (1984) 433–436.
- [64] W.R. Willkomm, Z. Chen, C. Macosko, D.A. Gobran, E.L. Thomas, Properties and phase separation of reaction injection molded and solution polymerized polyureas as a function of hard block content, *Polym. Eng. Sci.* 28 (14) (1988) 888–900.
- [65] A. Ryan, J. Stanford, A. Wilkinson, Structure-property relations in non-linear, segmented copolyureas formed by reaction injection moulding, *RIM, Polym. Bull.* 18 (6) (1987) 517–523.
- [66] A.J. Ryan, W.R. Willkomm, T.B. Bergstrom, C.W. Macosko, J.T. Koberstein, C.C. Yu, T.P. Russell, *Macromolecules* 24 (1991) 2883.
- [67] A.N. Wilkinson, S. Naylor, M.J. Elwell, P. Draper, B.U. Komanschek, J.L. Stanford, A.J. Ryan, A synchrotron SAXS study of structure development in a copoly(isocyanurate-urea) formed by RIM, *Polymer* 37 (10) (1996) 2021–2024.
- [68] M.J. Elwell, A.J. Ryan, H.J.M. Grünbauer, H.C. Van Lieshout, In-situ studies of structure development during the reactive processing of model flexible polyurethane foam systems using FT-IR spectroscopy, synchrotron SAXS, and rheology, *Macromolecules* 29 (8) (1996) 2960–2968.
- [69] M.J.A. Elwell, A.J. Ryan, S. Mortimer, *Macromolecules* 27 (1994) 5428.
- [70] J. Jennings, M. Beija, A.P. Richez, S.D. Cooper, P.E. Mignot, K.J. Thurecht, K.S. Jack, S.M. Howdle, One-pot synthesis of block copolymers in supercritical carbon dioxide: a simple versatile route to nanostructured microparticles, *J. Am. Chem. Soc.* 134 (10) (2012) 4772–4781.
- [71] D. Hermida-Merino, G. Portale, P. Fields, R. Wilson, S.P. Bassett, J. Jennings, M. Dellar, C. Gommès, S.M. Howdle, B.C. Vrolijk, A high pressure cell for supercritical CO<sub>2</sub> on-line chemical reactions studied with X-ray techniques, *Rev. Sci. Instrum.* 85 (9) (2014) 093905.
- [72] R. Graceffa, M. Burghammer, R.J. Davies, C. Riekel, Probing ballistic microdrop coalescence by stroboscopic small-angle X-ray scattering, *Appl. Phys. Lett.* 101 (25) (2012).
- [73] R. Graceffa, R.P. Nobrega, R.A. Barrea, S.V. Kathuria, S. Chakravarthy, O. Bilsel, T.C. Irving, Sub-millisecond time-resolved SAXS using a continuous-flow mixer and X-ray microbeam, *J. Synchrotron Radiat.* 20 (2013) 820–825.
- [74] S.V. Kathuria, A. Chan, R. Graceffa, R.P. Nobrega, C.R. Matthews, T.C. Irving, B. Perot, O. Bilsel, Advances in turbulent mixing techniques to study microsecond protein folding reactions, *Biopolymers* 99 (11) (2013) 888–896.
- [75] E. Rebollar, M. Castillejo, T.A. Ezquerro, Laser induced periodic surface structures on polymer films: from fundamentals to applications, *Eur. Polym. J.* 73 (2015) 162–174.
- [76] Z. Di, D. Posselt, D.-M. Smilgies, C.M. Papadakis, Structural rearrangements in a lamellar diblock copolymer thin film during treatment with saturated solvent vapor, *Macromolecules* 43 (1) (2009) 418–427.
- [77] A. Naudon, D. Thiaudiere, Grazing-incidence small-angle scattering. thin films, *J. Appl. Crystallogr.* 30 (2) (1997) 822–827.
- [78] A. Hexemer, P. Müller-Buschbaum, Advanced grazing-incidence techniques for modern soft-matter materials analysis, *IUCr* 2 (1) (2015) 106–125.
- [79] J.J. van Franeker, G.H. Heintges, C. Schaefer, G. Portale, W. Li, M.M. Wienk, P. van der Schoot, R.A. Janssen, Polymer solar cells: solubility controls fiber network formation, *J. Am. Chem. Soc.* 137 (36) (2015) 11783–11794.
- [80] S. Beaupré, M. Leclerc, PCDTBT: en route for low cost plastic solar cells, *J. Mater. Chem. A* 1 (37) (2013) 11097–11105.
- [81] J. You, L. Dou, K. Yoshimura, T. Kato, K. Ohya, T. Moriarty, K. Emery, C.-C. Chen, J. Gao, G. Li, Y. Yang, A polymer tandem solar cell with 10.6% power conversion efficiency, *Nat. Commun.* 4 (2013).
- [82] M.C. Scharber, D. Wuhlbacher, M. Koppe, P. Denk, C. Waldauf, A.J. Heeger, C.L. Brabec, Design rules for donors in bulk-heterojunction solar cells – towards 10% energy-conversion efficiency, *Adv. Mater.* 18 (6) (2006) 789–.
- [83] X.N. Yang, J. Loos, S.C. Veenstra, W.J.H. Verhees, M.M. Wienk, J.M. Kroon, M.A.J. Michels, R.A.J. Janssen, Nanoscale morphology of high-performance polymer solar cells, *Nano Lett.* 5 (4) (2005) 579–583.
- [84] S.S. van Bavel, E. Sourty, G. de With, J. Loos, Three-dimensional nanoscale organization of bulk heterojunction polymer solar cells, *Nano Lett.* 9 (2) (2009) 507–513.
- [85] A.J. Parnell, A.J. Cadby, O.O. Mykhaylyk, A.D.F. Dunbar, P.E. Hopkinson, A.M. Donald, R.A.L. Jones, Nanoscale phase separation of P3HT PCBM thick films as measured by small-angle X-ray scattering, *Macromolecules* 44 (16) (2011) 6503–6508.
- [86] P. Müller-Buschbaum, The active layer morphology of organic solar cells probed with grazing incidence scattering techniques, *Adv. Mater.* 26 (46) (2014) 7692–7709.
- [87] P. Müller-Buschbaum, The active layer morphology of organic solar cells probed with grazing incidence scattering techniques, *Adv. Mater.* 26 (46) (2014) 7692–7709.
- [88] F. Liu, Y. Gu, X. Shen, S. Ferdous, H.-W. Wang, T.P. Russell, Characterization of the morphology of solution-processed bulk heterojunction organic photovoltaics, *Prog. Polym. Sci.* 38 (12) (2013) 1990–2052.
- [89] J.L. Baker, L.H. Jimison, S. Mannsfeld, S. Volkman, S. Yin, V. Subramanian, A. Salleo, A.P. Alivisatos, M.F. Toney, Quantification of thin film crystallographic orientation using X-ray diffraction with an area detector, *Langmuir* 26 (11) (2010) 9146–9151.
- [90] F. Liu, Y. Gu, C. Wang, W. Zhao, D. Chen, A.L. Briseno, T.P. Russell, Efficient polymer solar cells based on a low bandgap semi-crystalline DPP polymer-PCBM blends, *Adv. Mater.* 24 (29) (2012) 3947–3951.
- [91] A.P.L. Bottiger, M. Jorgensen, A. Menzel, F.C. Krebs, J.W. Andreasen, High-throughput roll-to-roll X-ray characterization of polymer solar cell active layers, *J. Mater. Chem.* 22 (42) (2012) 22501–22509.

- [92] X. Gu, J. Reinspach, B.J. Worfolk, Y. Diao, Y. Zhou, H. Yan, K. Gu, S. Mannsfeld, M.F. Toney, Z. Bao, Compact roll-to-roll coater for in situ X-ray diffraction characterization of organic electronics printing, *Acs Appl. Mater. Interfaces* 8 (3) (2016) 1687–1694.
- [93] K.W. Chou, B. Yan, R. Li, E.Q. Li, K. Zhao, D.H. Anjum, S. Alvarez, R. Gassaway, A. Biocca, S.T. Thoroddsen, A. Hexemer, A. Amassian, Spin-cast bulk heterojunction solar cells: a dynamical investigation, *Adv. Mater.* 25 (13) (2013) 1923–1929.
- [94] J.J. van Franeker, M. Turbiez, W. Li, M.M. Wienk, R.A.J. Janssen, A real-time study of the benefits of co-solvents in polymer solar cell processing, *Nat. Commun.* 6 (2015).
- [95] Y. Yao, J.H. Hou, Z. Xu, G. Li, Y. Yang, Effect of solvent mixture on the nanoscale phase separation in polymer solar cells, *Adv. Funct. Mater.* 18 (12) (2008) 1783–1789.
- [96] L.J. Richter, D.M. DeLongchamp, F.A. Bokel, S. Engmann, K.W. Chou, A. Amassian, E. Schaible, A. Hexemer, In situ morphology studies of the mechanism for solution additive effects on the formation of bulk heterojunction films, *Adv. Energy Mater.* 5 (3) (2015).
- [97] F. Liu, S. Ferdous, E. Schaible, A. Hexemer, M. Church, X. Ding, C. Wang, T.P. Russell, Fast printing and in situ morphology observation of organic photovoltaics using slot-die coating, *Adv. Mater.* 27 (5) (2015) 886–891.
- [98] C.M. Palumbiny, F. Liu, T.P. Russell, A. Hexemer, C. Wang, P. Mueller-Buschbaum, The crystallization of PEDOT:PSS polymeric electrodes probed in situ during printing, *Adv. Mater.* 27 (22) (2015) 3391–3397.
- [99] O. Hemberg, M. Otendal, H.M. Hertz, Liquid-metal-jet anode electron-impact X-ray source, *Appl. Phys. Lett.* 83 (7) (2003) 1483–1485.
- [100] M. Schuster, H. Gobel, Application of graded multilayer optics in X-ray diffraction, *Adv. X-ray Anal.* 39 (1998) 57–72.
- [101] L.T. Hudson, J.F. Seely, Laser-produced X-ray sources, *Radiat. Phys. Chem.* 79 (2) (2010) 132–138.
- [102] M. Bech, O. Bunk, C. David, R. Ruth, J. Rifkin, R. Loewen, R. Feidenhans'l, F. Pfeiffer, Hard X-ray phase-contrast imaging with the compact light source based on inverse Compton X-rays, *J. Synchrotron Radiat.* 16 (2009) 43–47.
- [103] J. Bordas, M.H.J. Koch, P.N. Clout, E. Dorrington, C. Boulin, A. Gabriel, A synchrotron radiation camera and data acquisition-system for time resolved X-ray-scattering studies, *J. Phys. E-Sci. Instrum.* 13 (9) (1980) 938–944.
- [104] H.G. Zachmann, D. Wiswe, R. Gehrke, C. Riekel, Characterization of polymers with specific properties by means of synchrotron radiation, *Makromol. Chem.-Macromol. Chem. Phys.* (1985) 175–188.
- [105] S.M. Gruner, M.W. Tate, E.F. Eikenberry, Charge-coupled device area X-ray detectors, *Rev. Sci. Instrum.* 73 (8) (2002) 2815–2842.
- [106] I.P. Dolbnya, H. Alberda, F.G. Hartjes, F. Udo, R.E. Bakker, M. Konijnenburg, E. Homan, I. Cerjak, P. Goettkindt, W. Bras, A fast position sensitive microstrip-gas-chamber detector at high count rate operation, *Rev. Sci. Instrum.* 73 (11) (2002) 3754–3758.
- [107] C. Broennimann, E.F. Eikenberry, B. Henrich, R. Horisberger, G. Huelsen, E. Pohl, B. Schmitt, C. Schulze-Briese, M. Suzuki, T. Tomizaki, H. Toyokawa, A. Wagner, The PILATUS 1M detector, *J. Synchrotron Radiat.* 13 (2006) 120–130.
- [108] V. Radicci, A. Bergamaschi, R. Dinapoli, D. Greiffenberg, B. Henrich, I. Johnson, A. Mozzanica, B. Schmitt, X. Shi, EIGER a new single photon counting detector for X-ray applications: performance of the chip, *J. Instrum.* 7 (2012) 11.
- [109] W. Bras, H. Goossens, B. Goderis, Hard X-ray techniques suitable for polymer experiments, *IOP Conf. Ser.: Mater. Sci. Eng.* 14 (2010) 012001.
- [110] S. Nikitenko, A.M. Beale, A.M.J. van der Eerden, S.D.M. Jacques, O. Leynaud, M.G. O'Brien, D. Detollenaere, R. Kaptein, B.M. Weckhuysen, W. Bras, Implementation of a combined SAXS/WAXS/QEXAFS set-up for time-resolved in situ experiments, *J. Synchrotron Radiat.* 15 (2008) 632–640.
- [111] B.P. Grady, J.A. Floyd, W.B. Genetti, P. Vanhoorne, R.A. Register, X-ray absorption spectroscopy studies of zinc-neutralized ethylene methacrylic acid ionomers, *Polymer* 40 (2) (1999) 283–288.
- [112] Y.S. Ding, S.R. Hubbard, K.O. Hodgson, R.A. Register, S.L. Cooper, Anomalous small-angle X-ray-scattering from a sulfonated polystyrene ionomer, *Macromolecules* 21 (6) (1988) 1698–1703.
- [113] A. Longo, F. Giordano, F. Giannici, A. Martorana, G. Portale, A. Ruggirello, V.T. Liveri, Combined small-angle X-ray scattering/extended X-ray absorption fine structure study of coated Co nanoclusters in bis(2-ethylhexyl)sulfosuccinate, *J. Appl. Phys.* 105 (11) (2009).
- [114] E. Gann, A. Young, B. Collins, H. Yan, J. Nasiatka, H. Padmore, H. Ade, A. Hexemer, C. Wang, Soft X-ray scattering facility at the Advanced Light Source with real-time data processing and analysis, *Rev. Sci. Instrum.* 83 (4) (2012) 045110.
- [115] A. Sarje, X.S. Li, A. Hexemer, High-performance inverse modeling with reverse Monte Carlo simulations, in: 2014 43rd International Conference on Parallel Processing (ICPP). Proceedings, 2014, pp. 201–210.
- [116] S. Haas, T.S. Plivelic, C. Dicko, Combined SAXS/UV-vis/Raman as a diagnostic and structure resolving tool in materials and life sciences applications, *J. Phys. Chem. B* 118 (8) (2014) 2264–2273.
- [117] D.S. Smirnova, J.A. Kornfield, D.J. Lohse, Morphology development in model polyethylene via two-dimensional correlation analysis, *Macromolecules* 44 (17) (2011) 6836–6848.
- [118] J.J. Donatelli, P.H. Zwart, J.A. Sethian, Iterative phasing for fluctuation X-ray scattering, *Proc. Natl. Acad. Sci. USA* 112 (33) (2015) 10286–10291.
- [119] A. Hexemer, W. Bras, J. Glossinger, E. Schaible, E. Gann, R. Kirian, A. MacDowell, M. Church, B. Rude, H. Padmore, A SAXS/WAXS/GISAXS beamline with multilayer monochromator, *J. Phys.: Conf. Ser.* 247 (2010) 012007.



**Giuseppe Portale** graduated and received his PhD in chemistry from the University of Rome “La Sapienza”. After a PhD in polymer physics using synchrotron radiation, he moved to the ESRF for a post-doc funded by the Dutch Polymer Institute (DPI) in 2006 to develop new experiments to study polymer structure and dynamics with X-rays. In 2009 he became beam line scientist for the Netherlands Organization for Scientific Research at the ESRF, where he was the responsible for the SAXS/WAXS BM26B beam line. From 2015, he is Assistant Professor at the Zernike Institute for Advanced Materials in Groningen where he leads the group of polymer physics with focus on the structure-property relationships in polymers for energy applications and in organic/inorganic hybrid systems.



**Daniel Hermida-Merino** received his Master of Science in Chemistry at the University of Vigo. He completed a PhD in supramolecular polymers under the supervision of Prof. Ian Hamley and Prof. Wayne Hayes at Reading University. He then joined the ESRF as a post-doctoral fellow from Eindhoven Technical University first and then from Dutch Polymer Institute (DPI) to promote the research of polymer materials under processing conditions. Currently, He is employed by the Netherlands Council for Scientific Research (NWO) as the beamline scientist responsible of the Dutch-Belgium SAXS/WAXS beamline (BM26b) at ESRF.



**Wim Bras** is a physics graduate from Groningen University (Netherlands). After graduation he was employed by the Netherlands Council for Scientific Research (NWO) to work as a beam line scientist in Daresbury Laboratory (UK). Based on his work there he obtained a PhD from Liverpool John Moores University. In close collaboration with the polymer groups from Tony (AJ) Ryan an extensive portfolio of experimental possibilities for soft condensed matter and X-ray scattering was created. After 7 years he was transferred by NWO to the ESRF in Grenoble to construct a new beamline for the DUBBLE project and then appointed as project leader. For the last 10 years he also has spend two months per year in Lawrence Berkeley Lab as advisor and visiting scientist with the X-ray scattering beamlines.

## 2-Investigation of the internal nanostructural development of block copolymers polymerization under polymeric sc-CO<sub>2</sub>.

The investigation of novel block polymers possesses great interest to enlarge the number of tuneable applications arising from the nature of their self-assembly. Block copolymer synthesis has become simpler in recent years as a result of the advent of controlled radical polymerizations. Simple methodology, combined with industrially relevant conditions, lead to more widespread applications. Supercritical carbon dioxide (sc-CO<sub>2</sub>) is an environmentally “Green” solvent with unique properties such as considerable changes in solvent density achieved by changing the temperature and pressure. The medium has been exploited extensively for a wide range of polymerizations, but especially for dispersion polymerization.

The nature of sc-CO<sub>2</sub>, its low dielectric constant and low polarizability per unit volume, results in low solubility potential of many polymers which can be exploited for dispersion polymerization. A new route to block copolymers by reversible addition-fragmentation chain transfer (RAFT) polymerization in a dispersion polymerization in supercritical CO<sub>2</sub> has been developed in order to afford the growth of the microparticles with internal structure in sc-CO<sub>2</sub>. will be able to resolve the incipient morphology of the microparticle system, especially the internal structure, as a result of the contrast matching. Also, I have gained an insight into the structural changes that occur upon temperature and pressure modification. Understanding complex systems in sc-CO<sub>2</sub> is crucial for its employment as an alternative green solvent. Polymer synthesis with blocks with different CO<sub>2</sub>phocity has been carried out to understand the effect of the different affinities to sc-CO<sub>2</sub> has an impact on the phase diagram of the block copolymers during the polymerization. However, there was a lack of knowledge on the morphological evolution during the polymerizations as a result of the synthetic conditions that deter the understanding of the parameters that affect the final morphology. I have firstly designed a novel X-ray vessel to allow the study of chemical reactions upon sc-CO<sub>2</sub> together with the group of prof. Steven M. Howdle at Nottingham University (see Figure 2.1). Consequently, I have been a visiting scientist in Howdle’s groups in order to gain a deep understanding on the polymerizations in sc-CO<sub>2</sub> as well as sharing my expertise in X-ray experiments to manufacture the X-ray vessel. Moreover, I have spent a month in the Physical Chemistry and Soft Matter department of Wageningen University under the supervision of prof. Martien Cohen Stuart in order to prepare offline future experiments at the synchrotron.

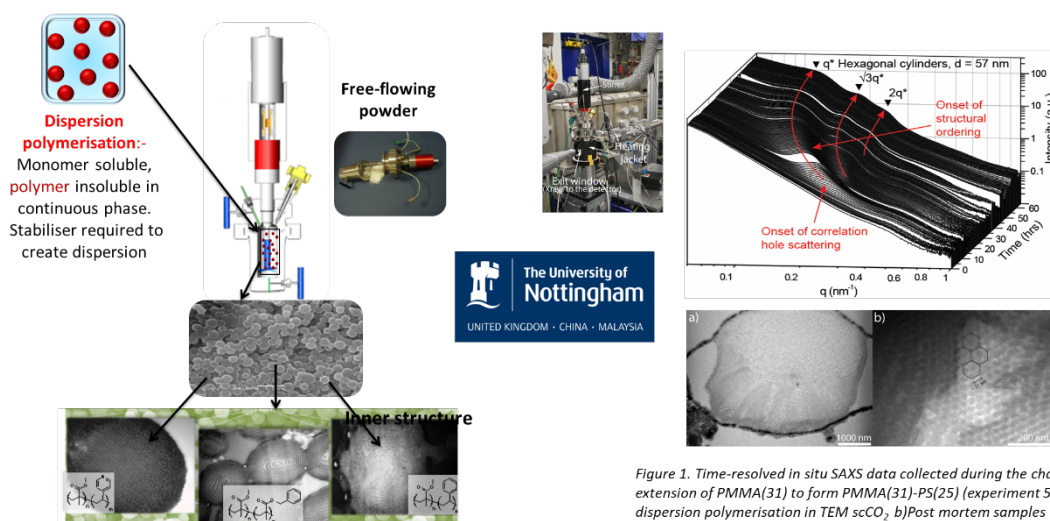


Figure 1.2. Summary of the polymerization of block copolymers under sc-CO<sub>2</sub> in a novel X-ray vessel.

High impact papers were published to follow the technical manuscript about the design and manufacturing of the X-ray vessel designed for conducting the polymerizations in situ.

Publications of the Project :

1. **Daniel Hermida-Merino**, Giuseppe Portale, Peter Fields, Richard Wilson, Simon P. Bassett, James Jennings, Martin Dellar, Cedric Gommès, Steven M. Howdle, Benno C. M. Vrolijk, and Wim Bras; "A high pressure cell for supercritical CO<sub>2</sub> on-line chemical reactions studied with x-ray techniques"; Review of Scientific Instruments, **85**, 093905 (2014), DOI: <http://dx.doi.org/10.1063/1.4895717>.
2. David Alaimo, **Daniel Hermida Merino**, Bruno Grignard, Wim Bras, Christine Jérôme, Antoine Debuigne, Cedric J Gommès: Small-Angle X-ray Scattering Insights into the Architecture-dependent Emulsifying Properties of Amphiphilic Copolymers in Supercritical CO<sub>2</sub>. The Journal of Physical Chemistry B 12/2014; 119(4), DOI:10.1021/jp5086558
3. J. Jennings, S. P. Bassett, **D. Hermida-Merino**, G. Portale, W. Bras, L. Knight, J. J. Titman, T. Higuchi, H. Jinnai and S. M. Howdle; "How does dense phase CO<sub>2</sub> influence the phase behaviour of block copolymers synthesised by dispersion polymerisation?"; Polym. Chem., (2016) 7, 905-916; DOI: 10.1039/C5PY01823.
4. Mohammad Alauhdin, Thomas M Bennett, Guping He, Simon P. Bassett, Giuseppe Portale, Wim Bras, **Daniel Hermida-Merino\***, Steven M Howdle: *Monitoring Morphology Evolution within Block Copolymer Microparticles during Dispersion Polymerisation in Supercritical Carbon Dioxide: A High Pressure SAXS Study*. Polymer Chemistry 12/2018; 10(7), DOI:10.1039/C8PY01578C.



Cite this: *Polym. Chem.*, 2019, **10**, 860

# Monitoring morphology evolution within block copolymer microparticles during dispersion polymerisation in supercritical carbon dioxide: a high pressure SAXS study†

Mohammad Alauhdin,<sup>‡a</sup> Thomas M. Bennett,<sup>‡a</sup> Guping He,<sup>a</sup> Simon P. Bassett,<sup>a</sup> Giuseppe Portale,<sup>c</sup> Wim Bras,<sup>d</sup> Daniel Hermida-Merino<sup>\*b</sup> and Steven M. Howdle<sup>‡\*a</sup>

Reversible addition–fragmentation chain transfer (RAFT) dispersion polymerisation in supercritical carbon dioxide is an effective process for creating block copolymer microparticles with internal nanostructures. Here we report an alternative synthesis route involving completely independent steps by exploiting the livingness of RAFT-terminated PMMA microparticles and their unique ability to be redispersed in scCO<sub>2</sub>. This not only enables a series of block copolymers to be created from a single RAFT dispersion synthesised PMMA homopolymer batch, thus improving reproducibility, but also adds flexibility by allowing the time and concentration requirements for each stage to be decoupled. The internal morphology development and evolution for a series of poly(methyl methacrylate-*block*-styrene) (PMMA-*b*-PS) block copolymer microparticles synthesised *via* this route was monitored *via in situ* small-angle X-ray scattering (SAXS) using an autoclave with diamond windows. Together with offline kinetics experiments and post-mortem transmission electron microscopy imaging, this study provides remarkably detailed insights into block copolymer self-organisation phenomena in scCO<sub>2</sub>. Specifically, the time period over which this block copolymer undergoes phase separation before progressing from an arrangement of spheres to lamellae *via* the hexagonal cylinder phase is elucidated, and the data are used to plot a detailed empirical phase diagram for this block copolymer system in scCO<sub>2</sub>.

Received 6th November 2018,  
Accepted 21st December 2018

DOI: 10.1039/c8py01578c

rs.c.li/polymers

## Introduction

Block copolymers are a remarkable class of materials because of their ability to spontaneously self-organise into a variety of ordered mesoscopic morphologies. It is well understood that three parameters dictate this process: the volume fraction of each block ( $f$ ), the Flory–Huggins polymer–polymer interaction parameter ( $\chi$ ) and the degree of polymerisation ( $N$ ).<sup>1,2</sup> For a linear A–B diblock copolymer the various morphologies that can be formed in this way include lamellae (LAM), cylin-

ders (CYL), gyroids (GYR) and spheres (SPH), each of which can influence the physical properties of the overall material.<sup>3–5</sup> This has given rise to numerous studies aiming to exploit these structures for a diverse range of applications including drug delivery,<sup>6</sup> polyelectrolytes,<sup>7,8</sup> nanoporous membranes,<sup>9</sup> photonics,<sup>10,11</sup> thin film nanolithography,<sup>12–14</sup> organic photovoltaics<sup>15</sup> and as templates for inorganic materials.<sup>16–18</sup>

In more recent years the concept of confining self-assembled block copolymers within three dimensional micron-size structures such as spheres or worms has received considerable interest.<sup>19</sup> This is because the resulting hierarchically structured materials exhibit multiple levels of structural organisation simultaneously over disparate length scales, thus providing synergies between mechanical properties, transport properties and enhanced surface area.<sup>20,21</sup> A variety of novel approaches towards the synthesis of such materials have been actively investigated in the literature to date. The most common of these exploit solvent evaporation processes, typically from block copolymer solutions in solvent/nonsolvent mixtures such as the self-organised reprecipitation (SORP)<sup>22–24</sup> and evaporation-induced self-assembly (EISA)<sup>25–27</sup> methods, or dispersed

<sup>a</sup>School of Chemistry, The University of Nottingham, University Park, Nottingham, NG7 2RD, UK. E-mail: steve.howdle@nottingham.ac.uk

<sup>b</sup>Netherlands Organisation for Scientific Research (N.W.O), DUBBLE@ESRF, CS40220, 38043 Grenoble Cedex 9, France

<sup>c</sup>Zernike Institute for Advanced Materials, University of Groningen, Nijenborg 4, 9747 AG, The Netherlands

<sup>d</sup>Oak Ridge National Laboratory, Chemical Sciences Division, One Bethel Valley Road, Oak Ridge, Tennessee 37831, USA

†Electronic supplementary information (ESI) available. See DOI: 10.1039/c8py01578c

‡These authors contributed equally to this work.

in particles<sup>28</sup> or aerosols.<sup>29</sup> However, the drawbacks of these methods include the requirement for multiple steps, the use of volatile organic solvents and unrealistic reaction conditions (nano-object concentration typically <1 wt%) for scaled-up use.

An alternative route is the use of emulsion, miniemulsion or dispersion polymerisation, in which self-organisation occurs within a particle as the block copolymers are synthesised, typically using controlled/living radical polymerisation (CLRP) techniques. CLRP in dispersed systems can advantageously be prepared at high concentration or solid content (up to 40 wt%) and overall presents a simpler and potentially commercial route to block copolymer particles because the synthesis and self-organisation steps take place simultaneously.<sup>19</sup> RAFT polymerisation is one of the CLRP techniques that has received considerable attention in the preparation of functional block copolymers in this way.<sup>30</sup> In particular, RAFT dispersion polymerisation has been successfully applied in producing amphiphilic block copolymer nano-objects of controlled size and morphology through the robust and efficient polymerisation-induced self-assembly (PISA) route.<sup>31–33</sup> Recently, our group has reported a block copolymer synthesis route *via* RAFT dispersion polymerisation in supercritical carbon dioxide (scCO<sub>2</sub>) which allowed the one-pot fabrication of unique nanostructured-block copolymer microparticles that would not normally be obtained in conventional media.<sup>34–37</sup>

Dispersion polymerisation in scCO<sub>2</sub> is an effective technique in this regard because scCO<sub>2</sub> is a good solvent for most common vinyl monomers and a non-solvent for their polymers. This process also allows the size and morphology of the resulting polymer particles to be readily tuned.<sup>38</sup> Moreover, scCO<sub>2</sub> as a polymerisation medium is not only beneficial as an alternative 'green' solvent, but also provides additional advantages such as simplified product recovery, lower processing temperature, and the absence of solvent residue.<sup>39–42</sup> These advantages arise from the ability of scCO<sub>2</sub> to swell and plasticise various polymers as a function of pressure.<sup>39,43,44</sup> This allows the block copolymers to self-organise during the polymerisation process, even at moderate temperatures, thereby circumventing the need for time consuming post polymerisation annealing and/or mixing steps. It has also been observed that blocking efficiencies obtained in scCO<sub>2</sub> are comparable with, and often favourable to, those observed in other CRP reactions in heterogeneous media. This was attributed to the high diffusivity of scCO<sub>2</sub> improving access of the second monomer to the polymerization *loci*.<sup>35</sup> However, one potential consequence of this phenomenon is a deviation of the internal morphology of the block copolymer systems investigated from that expected for a block copolymer of equivalent  $f_A$  in the melt state. This has been attributed to changes in the apparent volume fraction of the segments in a scCO<sub>2</sub> environment due to variations in the CO<sub>2</sub>-philicity of each block, thus altering and even inducing morphological transitions.<sup>36,45,46</sup> This effect was clearly evident after dissolving and solvent casting the as-synthesised block copolymer microparticles into bulk films, which after annealing returned to their predicted equilibrium morphologies.<sup>34</sup>

The phase separation behaviour of block copolymers is often studied using small angle X-ray scattering (SAXS) because it is a relatively non-destructive and high-throughput technique that can probe structural features on the nano-scale and also permits *in situ* measurements.<sup>33,47–49</sup> SAXS is commonly used in corroboration with other techniques, such as electron microscopy, because although it provides more representative information of the structural properties of a sample, the data can often be ambiguous when considering samples with unconventional and/or intermixed morphologies. A combination of transmission electron microscopy (TEM) and SAXS analysis has been utilised previously to fully characterise the microphase separation within block copolymer microparticles prepared in scCO<sub>2</sub> and confirm the persistence of the observed morphology throughout an entire sample.<sup>34,36</sup> Recently, synchrotron radiation SAXS studies were undertaken for the first time to investigate the morphological transitions that occur *in situ* during the non-aqueous PISA synthesis of poly(stearyl methacrylate)-*b*-poly(benzyl methacrylate) (PSMA-*b*-PBzMA) diblock copolymers.<sup>50</sup> An *in situ* SAXS kinetics study has also demonstrated that morphology changes during the synthesis of a PMMA-*b*-PBzMA block copolymer microparticle sample *via* RAFT dispersion polymerisation in scCO<sub>2</sub> could be detected, but no interpretation of the order development and thermodynamics of the system were discussed.<sup>51</sup>

Given that many of the desirable properties of block copolymers originate from their well-defined nanostructures, the ability to precisely predict when an ordered morphology will form and what structure it will take are crucial pieces of information. This article describes several advances in the synthesis of block copolymer microparticles *via* dispersion polymerisation in scCO<sub>2</sub> and the characterisation of their internal structures. Most importantly, we demonstrate that the synthesis of nanostructured block copolymer microparticles can be separated into two completely independent steps. We exploit the livingness of RAFT-terminated macro chain transfer agent (macroCTA) PMMA microparticles, which retain activity even after storage for several months, and their ability to be redispersed in scCO<sub>2</sub>. This enables a series of block copolymers to be created from a single RAFT dispersion synthesised PMMA homopolymer batch, thus improving reproducibility and also increasing flexibility by allowing the time and concentration requirements for each stage to be decoupled. We then monitored the internal morphology development and subsequent evolution for a series of PMMA-*b*-PS block copolymer microparticles synthesised using this route *via in situ* SAXS. Together with offline kinetics experiments and TEM characterisation this approach provides remarkably detailed insights of the self-organisation process occurring within block copolymer microparticles in scCO<sub>2</sub>.

## Experimental

### Materials

S-Dodecyl-S'-( $\alpha,\alpha'$ -dimethyl- $\alpha''$ -acetic acid) trithiocarbonate (DATC) was synthesised following literature procedures.<sup>52</sup>

$\alpha$ -Azobisisobutyronitrile (AIBN, Wako, 97%) was purified by recrystallising twice from methanol. Methyl methacrylate (MMA, Fisher, >99%) and styrene (Alfa Aesar, 99%) were purified by eluting through a column of basic alumina prior to use. Poly(dimethylsiloxane monomethyl methacrylate) (PDMS-MA, ABCR, number-average molecular weight ( $M_n$ ) = 10 000 g mol<sup>-1</sup>) and ruthenium tetroxide (RuO<sub>4</sub>, Acros, 0.5% solution in water) was used as received. Dry CO<sub>2</sub> (SFC grade, 99.99%) was purchased from BOC or Air Liquide. HPLC grade THF (Fisher) and HPLC grade chloroform (Aldrich) were used without further purification. For TEM, Agar 100 epoxy resin (Agar Scientific) was used as received, and mixed to target a formulation of medium hardness for embedding samples before being allowed to set at 50 °C for 48 hours.

### RAFT dispersion polymerisation of MMA in scCO<sub>2</sub>

The RAFT dispersion polymerisation of PMMA has been reported previously.<sup>53</sup> In a typical procedure targeting PMMA with a molecular weight of 25 kDa, RAFT agent (DATC, 165 mg, 0.45 mmol), AIBN (73 mg, 0.23 mmol) and macro-monomer stabiliser (PDMS-MA, 5 wt% relative to MMA) were added to a standard 60 mL autoclave. The autoclave was purged with CO<sub>2</sub> for 30 minutes, during which time MMA (11.3 g, 112.7 mmol) was degassed by bubbling with argon at 0 °C before being charged into the autoclave under a positive flow of CO<sub>2</sub>. The autoclave was then sealed and pressurised to 50 bar, heated to 65 °C and then the pressure was topped up to 275 bar. The reaction was stirred at 300 rpm for 18 hours, after which time the heating jacket was switched off and the autoclave was vented over a period of 15 minutes upon cooling to ambient temperature. In all cases the PMMA product was collected as a fine, pale yellow powder with gravimetric conversions >95%.

### X-ray autoclave characteristics

An improved version of the X-ray autoclave previously developed by the Howdle group<sup>51</sup> was constructed in-house at the University of Nottingham and used for all of the SAXS monitored reactions (see ESI Fig. S1†). The features of this design are a 60 mL capacity and working pressure and temperature limits of 300 bar and 120 °C, respectively. In addition, the X-ray windows are mounted in a small, independent holder that facilitates efficient stirring throughout the vessel, crucial for *in situ* polymerisation studies, and also aids product collection and cleaning when removed post reaction.

### Small-angle X-ray scattering setup

Time-resolved SAXS experiments were conducted at the Dutch-Belgian Beamline (DUBBLE) station BM26-B of the European Synchrotron and Radiation Facility (ESRF) in Grenoble, France.<sup>54</sup> Experiments were performed using a wavelength ( $\lambda$ ) of 0.6526 Å (15 KeV) and a sample-to-detector distance of 3000 m. A Dectris-Pilatus 1 M detector with a resolution of 981 × 1043 pixels and a pixel size of 172 × 172 μm was employed to record the 2D scattering profiles, covering a scattering angle range  $q = 0.07$ – $3.65$  nm<sup>-1</sup>, where the modulus of the scattering

vector  $q$  is defined as  $q = 4\pi/\lambda \sin \theta$ , with  $2\theta$  being the scattering angle. SAXS profiles of the reaction mixtures were collected every 2.5 minutes, with an exposure time of 30 seconds. The diffraction rings from a Silver Behenate powder standard were used to calibrate the scattering angle scale. The SAXS images were normalised with respect to the incident beam intensity and were corrected for absorption and background scattering from the diamond windows and scCO<sub>2</sub> within the autoclave. After correction, radial averaging around the beam centre was conducted in order to convert the SAXS images into the  $I(q)$  vs.  $q$  curves.

### Chain extension of PMMA microparticles with styrene monitored *via in situ* small-angle X-ray scattering in scCO<sub>2</sub>

The polymers described here are designated with the generalized label PMMA( $X$ ) and PS( $X$ ), where  $X$  denotes the  $M_n$  values in kDa. In a typical reaction, the chain extension of PMMA(31) with PS(25) was monitored *in situ via* time resolved SAXS. MacroCTA PMMA microparticles (5.94 g, 0.192 mmol), synthesised as described above, were added to the X-ray autoclave along with the PDMS-MA (5 wt% relative to styrene monomer) stabiliser. After gently purging the X-ray autoclave with CO<sub>2</sub> for 30 minutes, the vessel was sealed, pressurised to 50 bar and then heated to 65 °C before finally topping up the pressure to 275 bar. After stirring for at least 2 hours at 300 rpm under these conditions, the pressure inside the X-ray autoclave was reduced to 200 bar and styrene (5.45 g, 52.3 mmol) containing AIBN (30 mg, 0.093 mmol), which had been degassed by bubbling with argon for 30 minutes, was injected through the head of the autoclave at a rate of 1 mL min<sup>-1</sup> using a HPLC pump (Jasco). The styrene was allowed to polymerise for 64 hours, during which time SAXS profiles of the reaction mixture were collected every 2.5 minutes with an exposure time of 30 seconds. On completion, the temperature was reduced to ambient over a period of approximately 1 hour, and the X-ray autoclave was vented over an additional period of approximately 15 minutes. In each case involving styrene monomer the products were collected as pale yellow and slightly clumped powders due to microparticle surface dissolution and partial fusion by the residual monomer. For the reaction involving the synthesis of PMMA-*b*-PMMA a homogeneous fine pale yellow powder was obtained instead.

### Offline kinetics investigation of the chain extension of macroCTA PMMA microparticles with styrene *via* reaction sampling

The representative chain extension of PMMA(25) (3.34 g, 0.134 mmol) with styrene (10 g, 96.0 mmol) was repeated offline in a 60 mL stainless steel autoclave with a sampling tap on the base to collect the polymer product at various times throughout the polymerisation. This was performed as described above for the *in situ* experiments using AIBN (25 mg, 0.077 mmol), with the exception that at time periods of 21, 37, 53, 60 and 84 hours, a ~1 mL closed sampling pipe was screwed onto the bottom of the reactor and the sampling tap was opened to the reaction for 5 seconds.

## Polymer characterisation

PMMA-*b*-PS block copolymers were analysed by  $^1\text{H}$  NMR in  $\text{CDCl}_3$  on a Bruker DPX 400 MHz spectrometer in order to determine the molecular weight of the polystyrene blocks ( $M_n$ ,  $^1\text{H}$  NMR) and the overall mass fraction of the block copolymers. This was converted to the PMMA volume fraction ( $f_{\text{PMMA}}$ ) using the reported melt densities of the individual homopolymers: PMMA =  $1.17\text{ g cm}^{-3}$  and PS =  $1.05\text{ g cm}^{-3}$ .<sup>55</sup> The molecular weight ( $M_n$ , GPC) and the dispersity ( $\mathcal{D}$ ) of the homo and block copolymers were also determined by GPC using either an Agilent PL GPC 120 in THF or a PL GPC 50 in chloroform. Analyses were run at  $40\text{ }^\circ\text{C}$  with flow rates of  $1\text{ mL min}^{-1}$  and  $0.5\text{ mL min}^{-1}$ , respectively, and the columns were calibrated with narrow dispersity PMMA standards.

## Transmission electron microscopy (TEM)

Block copolymer particles were embedded in epoxy resin (Agar 100) and set at  $50\text{ }^\circ\text{C}$  for 48 hours before being ultramicrotomed at room temperature to  $\sim 100\text{ nm}$  slices with a diamond knife (Leica Diatome Ultra 45 $^\circ$ ) and collected on copper grids. Where specified, the PMMA-*b*-PS particle sections were stained prior to imaging with  $\text{RuO}_4$  for 2 hours, which adsorbs selectively to PS. Imaging of particle samples was completed using a FEI Tecnai TEM operating at an accelerating voltage of  $100\text{ kV}$ .

## Results and discussion

### Synthesis and characterisation of PMMA microparticles in $\text{scCO}_2$

In previous publications we reported on the one pot RAFT dispersion synthesis of structured block copolymer microparticles in  $\text{scCO}_2$ . In this scenario the second monomer was injected under pressure once the MMA polymerisation had reached high conversion.<sup>35,36</sup> Here we explore a much improved “two-pot” route that separates the block copolymer synthesis into two independent pressurisation/polymerisation/depressurisation stages. The success of this approach hinges on retaining the “livingness” of the PMMA seed particles and successfully redispersing them in  $\text{scCO}_2$  prior to adding the second monomer. Such redispersion can be achieved by incorporating additional PDMS-MA stabiliser into the vessel to account for the volume increase of the particles as  $M_n$  increases, allowing a series of previously synthesised PMMA particles to be chain extended.<sup>53</sup> The role of the additional PDMS-MA stabiliser in improving the redispersion process was determined through a series of test polymerisations undertaken prior to the reactions described here. In these cases, chain extension of the macroCTA PMMA microparticles was still observed, but the block copolymer microparticle products were very poorly defined (ESI Fig. S2 $\dagger$ ).

In the first stage of the process, a series of PMMA microparticle batches with varying  $M_n$  values (Table 1) were synthesised *via* RAFT dispersion polymerisation in  $\text{scCO}_2$ , and then used for chain extension experiments monitored *via in situ* SAXS

**Table 1** Characteristics of the PMMA particles prepared *via* dispersion polymerisation in  $\text{scCO}_2$

Exp.	Name	$M_n$ , theo. <sup>a</sup> (kDa)	$M_n$ , exp. <sup>b</sup> (kDa)	$\mathcal{D}$ <sup>b</sup>	Conv. <sup>c</sup> (%)
1	PMMA(31)	30	31	1.16	96
2	PMMA(25)	25	25	1.19	95
3	PMMA(58)	50	58	1.39	98
4	PMMA(54)	50	54	1.19	98

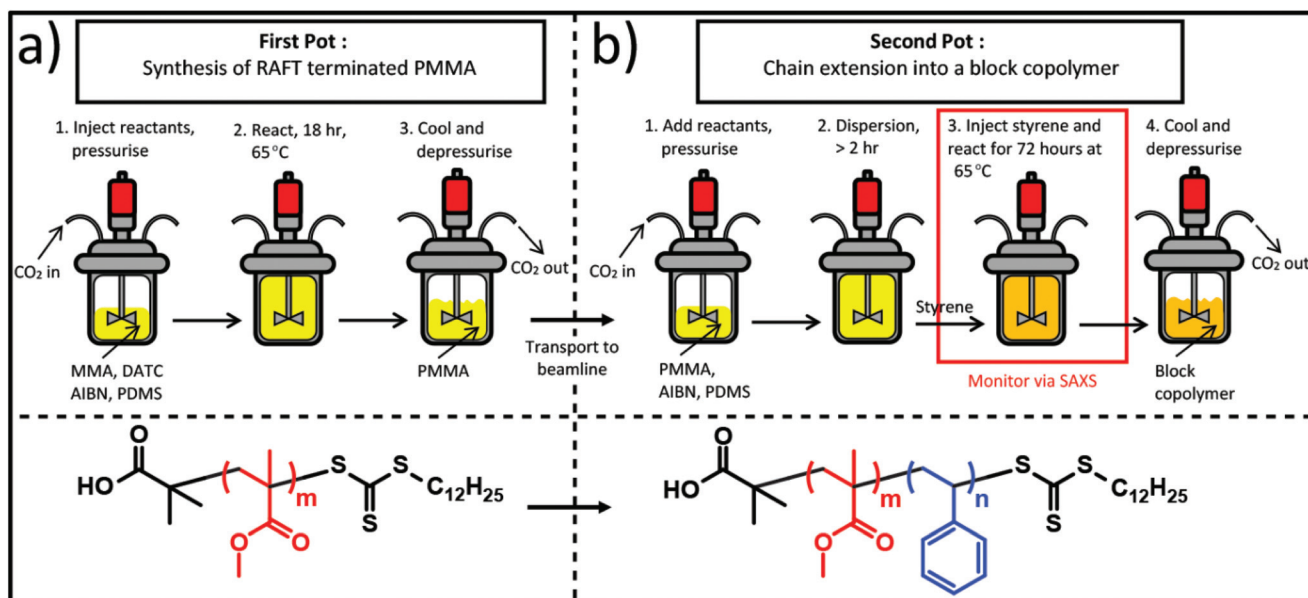
<sup>a</sup>  $M_{n,\text{theo}}$  was calculated by:  $[\text{MMA}]/[\text{RAFT}] \times 100.11$ . <sup>b</sup> Determined by GPC in THF against PMMA standards. <sup>c</sup> Determined gravimetrically.

(Scheme 1a).<sup>53</sup> In each case excellent molecular weight control and narrow dispersity values were achieved as confirmed by the GPC traces (ESI Fig. S3 $\dagger$ ), demonstrating that the DATC RAFT agent in the seed particles was active and able to control the polymerisations effectively. Analysis of each product with SEM revealed that discrete spherical particles were formed in all cases with sizes ranging between  $1.7\text{--}2.2\text{ }\mu\text{m}$  (ESI Fig. S4 $\dagger$ ).

### PMMA microparticle chain extensions in $\text{scCO}_2$ monitored *via in situ* SAXS

Four different chain extension reactions were monitored *via* time-resolved SAXS *in situ*. The characteristics of the final products (GPC,  $^1\text{H}$  NMR, DSC and TEM analysis of the morphology) are listed in Table 2 (see ESI Fig. S3 and S5 $\dagger$  for the GPC and DSC traces for each sample, respectively). Here the experiment numbers 5–8 correspond respectively with chain extension reactions of PMMA homopolymers 1–4 (Table 1). Styrene was selected as the second monomer because (a) PMMA and PS domains have high X-ray contrast, (b) the Flory–Huggins polymer–polymer interaction parameter ( $\chi$ ) of this diblock copolymer is known,<sup>56</sup> and (c) the phase behaviour has been widely investigated both in the bulk<sup>12,57</sup> and solution states,<sup>58,59</sup> including in  $\text{scCO}_2$ .<sup>34</sup> Furthermore, PMMA and PS have considerably different  $\text{CO}_2$ -affinities,<sup>60</sup> and the small  $k_p$  for styrene means the polymerisation proceeds over a greater time period,<sup>61</sup> allowing subtle or slow changes in the phase behaviour due to molecular weight or  $\text{scCO}_2$  swelling to be tracked and potentially decoupled more effectively using the SAXS profiles.

For each polymerisation, a constant PMMA loading of 5 grams was used along with 5 wt% of PDMS-MA stabiliser, which were stirred together at the reaction temperature and pressure ( $65\text{ }^\circ\text{C}$  and 275 bar) for a minimum of 2 hours in order to redisperse the microparticles prior to adding the styrene monomer (Scheme 1b). The styrene polymerization kinetics were studied for experiments 5 and 6 in a standard 60 mL sampling autoclave, as described further in the ESI (see also ESI Fig. S6 and S7 $\dagger$ ). These reactions revealed that the styrene polymerisation ultimately takes  $>72$  hours to reach high conversion ( $>90\%$ ), meaning that achieving full conversion at the beamline was not possible in the time frame available. This explains the discrepancy between the targeted and obtained  $M_n$  values for each polymer synthesised during *in situ*



**Scheme 1** The “two pot” synthesis method used to prepare the block copolymers monitored *via* time resolved SAXS. (a) Preparation of PMMA particles *via* dispersion polymerisation and (b) PMMA particle redispersion with additional PDMS-MA stabiliser and subsequent chain extension with styrene at the beamline.

**Table 2** Characteristics of the PMMA-*b*-PS products synthesised during the *in situ* SAXS characterisation

Exp.	Name	Block 2 reaction time (h)	$M_n$ theo (BCP, kDa) <sup>a</sup>	$M_n$ exp. (BCP, kDa) <sup>c</sup>	$f_{\text{PMMA}}$ <sup>c</sup>	$D^b$	Morph. <sup>d</sup>	$T_{g,\text{PMMA}}^e$ (°C)	$T_{g,\text{PS}}^e$ (°C)	Conv. <sup>f</sup> (%)
5	PMMA(31)-PS(25)	64	70	55.7	0.53	1.5	CYL	118.4	95.5	79
6	PMMA(25)-PS(50)	63	100	75	0.31	1.84	CYL/LAM	118.2	95.1	80
7	PMMA(58)-PS(12)	71	80	70.2	0.81	1.51	DIS	122.5	N/O	76
8	PMMA(54)-PMMA(44)	23	100	95.4	1.00	1.45	DIS	123.0	N/A	97

<sup>a</sup>  $M_{n,\text{theo}}$  was calculated by:  $[\text{Monomer}]/[\text{PMMA macroCTA}] \times \text{MW monomer}$ . <sup>b</sup> Determined by GPC in THF against PMMA standards. <sup>c</sup> From <sup>1</sup>H NMR. <sup>d</sup> From TEM images. <sup>e</sup> Measured by DSC, N/O = not observed due to a lack of phase separation. <sup>f</sup> Determined gravimetrically, residual monomer present.

SAXS monitoring (Table 2). We also note here that the molar mass dispersity values for the block copolymers synthesised here are typically higher than for analogous homogeneous solution based syntheses. However, these values are comparable to results reported previously for this block copolymer system by our group using the one-pot approach,<sup>35</sup> as well as other examples of heterogeneous syntheses in the literature. This is attributed to the higher tendency of styrenic monomers to terminate by combination, particularly under monomer starved conditions, as is the case in the latter stages of the polymerisations reactions undertaken here.<sup>62</sup> In order to understand the influence of block copolymer composition on order development and phase transitions in these systems, the molecular weights of the PS blocks across the three polymerisations were targeted to obtain block ratios in the final products of  $f_{\text{PMMA}} \approx f_{\text{PS}}$  (experiment 5),  $f_{\text{PMMA}} \ll f_{\text{PS}}$  (experiment 6) and  $f_{\text{PMMA}} \gg f_{\text{PS}}$  (experiment 7). A control experiment in which PMMA was chain extended with a second PMMA block of comparable  $M_n$  was also completed (experiment 8).

### Internal morphology development and evolution during the polymerisation of PMMA(31)-PS(25)

Time-resolved SAXS profiles were recorded during the chain extension of PMMA(31) to PMMA(31)-PS(25) and plotted as a 3-dimensional  $q$  ( $\text{nm}^{-1}$ ) versus intensity ( $I(q)$ ) versus time ( $t$ ) plot to illustrate the morphological transitions throughout the polymerisation (Fig. 1). A large number of SAXS profiles were removed to improve the overall visibility of the data, with the remaining profiles being separated by approximately 30 minutes intervals. A second 2-dimensional plot of the data at 10 hours intervals was also created to further highlight the changes in the scattering patterns that occurred throughout the duration of the polymerisation (ESI Fig. S8†). The small gaps in the data are due to brief pauses during the data acquisition to either adjust the pressure or due to beam loss. The SAXS profiles are initially featureless and exhibit Porod scattering with  $I(q) \propto q^{-4}$ , indicating the presence of many large structures with sharp interfaces between them that are consist-

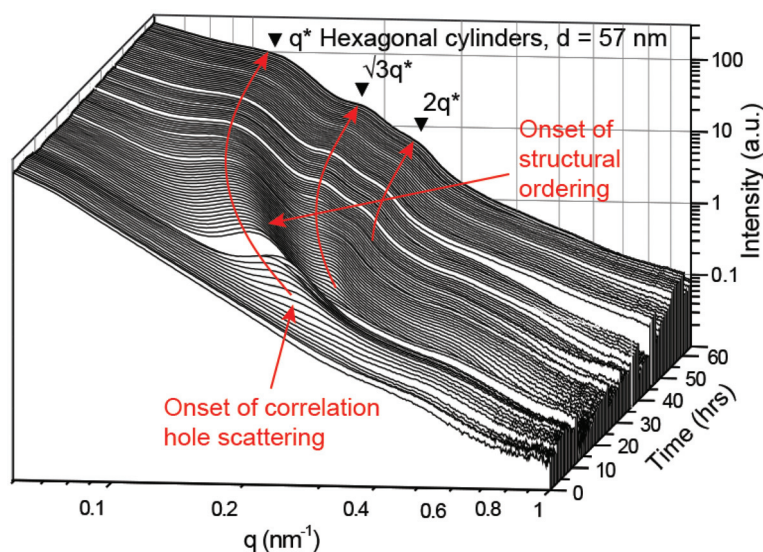


Fig. 1 Time-resolved *in situ* SAXS data collected during the chain extension of PMMA(31) to form PMMA(31)-PS(25) (experiment 5) via dispersion polymerisation in  $\text{scCO}_2$ . The time between the individual profiles included is approximately 30 minutes.

ent with the overall size of the polymer microparticles without any internal nanostructure.<sup>63</sup> This is highlighted in the ESI,<sup>†</sup> where the SAXS profile for the sample taken at  $t = 0$  is plotted alongside the  $q^{-4}$  decay data (ESI Fig. S9<sup>†</sup>). After polymerising for approximately 6 hours the first evidence of the formation of a block copolymer disordered phase is distinguishable by the formation of a very broad primary scattering ( $q^*$ ) peak centred at  $0.232 \text{ nm}^{-1}$  due to correlation hole scattering between the PMMA and PS segments enforced by their connectivity (Fig. 1,  $q^*$ ) (see ESI eqn (S1)<sup>†</sup> for the peak fitting function used to derive the peak positions).<sup>1,64</sup>

The intensity of this peak then continues to increase over the next 10 hours and it simultaneously becomes narrower, as expected for a system that is progressing towards a more ordered state (Fig. 1). After 16 hours the block copolymer undergoes a disorder-to-order transition (DOT) as evidenced by the appearance of an additional higher order scattering peak centred at  $\sqrt{3}q^*$  (Fig. 1,  $\sqrt{3}q^*$ ). A secondary peak in this position is characteristic of a hexagonally packed cylindrical morphology, an assignment that was further validated by the appearance of a third characteristic peak for this morphology centred at  $\sqrt{4} = 2q^*$  after approximately 30 hours (Fig. 1,  $2q^*$ ). The intensity of these three SAXS peaks continues to increase throughout the remainder of the polymerisation and the domain spacing of the cylindrical morphology also continues to grow at a steady rate, culminating in a  $q^*$  peak at  $0.110 \text{ nm}^{-1}$ . This corresponds with an average characteristic spacing of the cylindrical BCP morphology ( $d_{\text{CYL}}$ ) in  $\text{scCO}_2$  of 57.1 nm, as determined using Bragg's law:

$$d = 2\pi/q^* \quad (1)$$

The increase of  $d_{\text{CYL}}$  during the PS polymerization indicates that the value of  $\chi N$  for the system increased continuously

until the time when the reaction was discontinued, in agreement with our kinetic studies (ESI Fig. S6 and S7<sup>†</sup>). We also note that the SAXS maxima throughout the course of the reaction remain relatively broad. This phenomenon has been previously reported in SAXS studies on these systems and suggests that the internal morphology is composed of a distribution of domain sizes that only persist over a relatively short range order, given that the peak width is inversely proportional to the degree of ordering.<sup>36</sup>

TEM images were acquired from thin sections of the final polymer product to corroborate the hexagonally packed cylinder internal morphology of the microparticles indicated by the SAXS profiles toward the end of the reaction (Fig. 2). These images verify the occurrence of this morphology, in agreement with previous studies on this block copolymer system with comparable values of  $f_{\text{PMMA}}$ .<sup>34,36</sup> Domain size measurements taken from the TEM images returned a value of approximately 44.2 nm from 50 measurements (cylinder-to-cylinder distance of  $(2/\sqrt{3}) \times 44.2 \text{ nm} = 51.0 \text{ nm}$ ), but some variation in the domain size throughout each particle was observed, as expected from the broad nature of the reflections in the SAXS data. Nevertheless, this average value is slightly smaller than the 57.1 nm domain size calculated from the primary scattering peak in the final SAXS profile for the sample prior to depressurisation. To confirm whether the TEM measured value was representative of the sample as a whole or an artefact of the microtoming process, a post reaction SAXS profile was recorded after the final product had been collected (ESI Fig. S10<sup>†</sup>). This profile returned a value of 53.3 nm that was more comparable to that obtained prior to venting the  $\text{CO}_2$ , suggesting the discrepancy between the SAXS and TEM domain size measurements is most likely the result of sample distortion during the microtoming process, which can be difficult to avoid.<sup>34</sup>

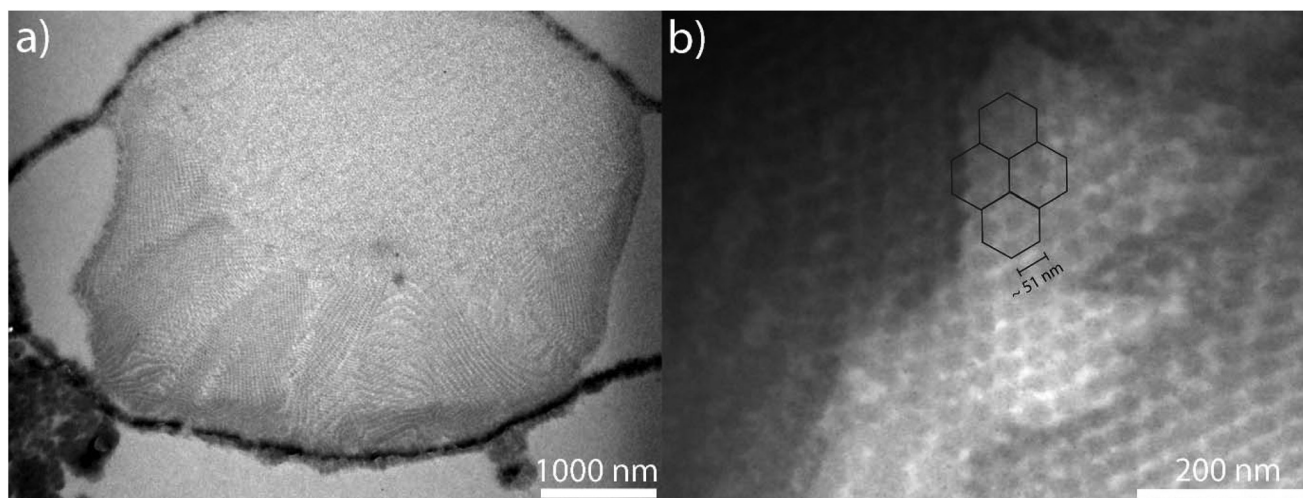


**Fig. 2** (a) TEM images of a representative cross-sectioned PMMA-*b*-PS particle obtained following the chain extension of PMMA(31) with PS(25) in the X-ray autoclave. (b) A hexagonally packed cylinder morphology can be observed throughout the sample with a cylinder-to-cylinder distance of  $\sim 51$  nm. The PS domains appear dark in both images due to staining with RuO<sub>4</sub>.

### Internal morphology development and evolution during the polymerisation of PMMA(25)-PS(50)

A three dimensional  $q$  ( $\text{nm}^{-1}$ ) versus  $I(q)$  versus  $t$  plot was generated from the SAXS data obtained during the chain extension of PMMA(25) with PS(50), with a large number of SAXS profiles again being removed to improve the overall visibility of the data (Fig. 3a). A second 2-dimensional plot of the data at 10 hours intervals was also created to further highlight the changes in the scattering patterns that occurred throughout the duration of the polymerisation (ESI Fig. S11<sup>†</sup>). As was observed for PMMA(31)-PS(25), the SAXS profiles near the beginning of the reaction exhibit the characteristic Porod scat-

tering of a microparticulate sample without internal structure. After 13.5 hours of PS polymerization, a broad and low intensity peak at around  $0.22 \text{ nm}^{-1}$  appears and continues to develop over the next 10–15 hours (Fig. 3). As in the previous case, this peak is due to correlation hole scattering between the PMMA and PS segments, not able to show ordering due to the low  $\chi N$  value at this point of the reaction. As the polymerization reaction progresses this peak gradually becomes more intense, forming a broad correlation peak that extends from  $0.140$ – $0.185 \text{ nm}^{-1}$  (Fig. 3a). This broad peak shows similarities with correlation peaks usually observed in systems comprised of interacting but poorly ordered spherical objects.<sup>50</sup> Thus, at the early stages of the reaction (before 30 hours) it appears

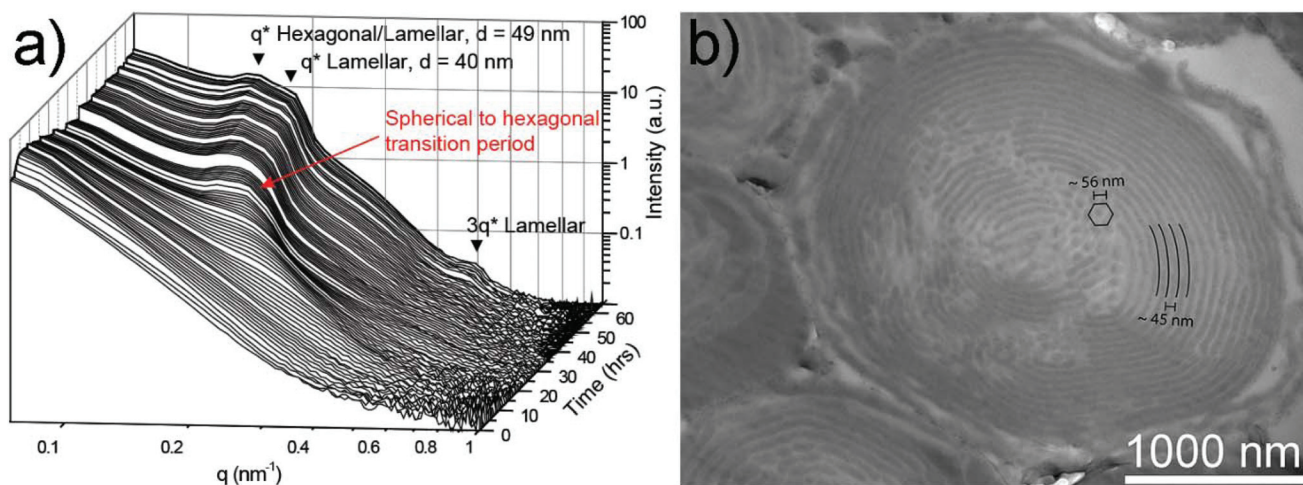


**Fig. 3** (a) Time-resolved *in situ* SAXS profiles collected throughout the dispersion polymerisation of PMMA(25)-PS(50) in  $\text{scCO}_2$ . (b) TEM images of representative cross-sectioned PMMA(25)-PS(50) microparticles synthesised in the X-ray autoclave and collected at the end of the reaction. The majority of microparticles exhibit a coexisting mix of both morphologies, with lamellar being predominant towards the particle exterior. The PS domains appear dark due to staining with RuO<sub>4</sub>. The time between the individual profiles included is approximately 30 minutes.

that spherical PS domains were beginning to form within the PMMA microparticles.

Over time this peak then continuously shifts towards lower  $q$ -values, again indicating that the molecular weight of the polystyrene block was gradually increasing. From approximately 35 hours onwards this peak then gradually begins to separate into two distinct maxima at  $0.0167\text{ nm}^{-1}$  and  $0.0194\text{ nm}^{-1}$ . This is indicative of a morphology transition within the sample, the specific nature of which cannot be assigned from this information alone. Finally, a third reflection with a much higher  $q$  value in the range of  $0.48\text{ nm}^{-1}$  also becomes apparent from approximately 50 hours onwards (Fig. 3a,  $3q^*$ ). A peak in this range is expected to be a higher order scattering reflection that suggests the sample has progressed to a more ordered state in which the domain spacing and/or morphology is more consistent throughout the microparticles. An offline SAXS profile was also recorded for the final product upon venting the autoclave, confirming almost no change in the domain size of these samples after removing the  $\text{scCO}_2$ , as for experiment 5 above (ESI Fig. S12<sup>†</sup>).

TEM images were taken from  $\sim 100\text{ nm}$  thick sections of the final product to validate the morphological transitions throughout the polymerisation (Fig. 3b). Intriguingly, the majority of the microparticles exhibit internal morphologies in which the lamellar phase is predominant, but occurs alongside a smaller population of cylindrical domains located towards the centre of many particles (Fig. 3b). In many cases the variability of the lamellar domain spacing as measured from the TEM images was small, and an average domain spacing of  $\sim 40\text{ nm}$  ( $\text{SD} = 5\text{ nm}$ ) was obtained from 50 measurements. This value corresponds with an expected primary scattering peak position at  $q = 0.156\text{ nm}^{-1}$  that closely matches the higher  $q$  portion of the broad  $q^*$  scattering reflection in the SAXS profiles recorded for this sample prior to terminating the reaction (Fig. 3a,  $d = 40\text{ nm}$  peak), suggesting that this reflection corresponds to the formation of the lamellar morphology. There are also many lamellar regions within these particles that appear to be trapped in an incomplete transition state from the hexagonal cylinder morphology, as identified by their wavy edges, irregular appearance and larger domain spacing values that we partially attribute to the broadening of the lamellar  $q^*$  peak to lower values of  $q$  (Fig. 3b,  $d = 49\text{ nm}$  peak).

By contrast, the regions of the particle interiors that possess a hexagonal cylinder morphology show a much broader range of domain sizes that are more difficult to accurately measure from the TEM images because of uneven stretching that occurs during the transition to a lamellar morphology. In spite of this, we estimate an average cylinder-to-cylinder distance of  $\sim 50\text{ nm}$  for the domains from 50 measurements, and also attribute the consistent broadening of the primary SAXS scattering peak to lower  $q$  values to their presence. Taking the midpoint of this broad peak as the primary  $q^*$  scattering reflection also enables the higher order reflection that forms towards the end of the reaction at higher  $q$  to be assigned as the expected  $3q^*$  reflection for a lamellar

morphology (Fig. 3a,  $3q^*$  peak). This is further evidence that the lamellar phase forms during the reaction and gradually becomes more prevalent. Such a transition is also anticipated based on the stability window for the lamellar phase in the classical diblock copolymer phase diagram and the  $f_{\text{PMMA}}$  value of the final product.<sup>2</sup> However, because of a lack of higher order scattering reflections in this sample during the earlier stages of the reaction, the exact sequence of transitions that eventually culminate in the formation of the lamellar morphology could not be identified from these data alone.

#### Offline evaluation of morphology evolution for PMMA(25)-PS(50)

To further elucidate the complex phase behaviour during the polymerisation and to estimate a time frame for when the spherical to lamellar phase transition (*via* hexagonal cylinders) occurs, additional TEM images and single shot SAXS data were acquired from the polymer aliquots collected during the offline kinetics evaluation of this reaction (Fig. 4). After reacting for 21 hours an internal morphology of spheres is present throughout the entirety of each particle. By 37 hours the lamellar phase becomes apparent around the edges of some particles alongside the majority spherical phase, and there are also areas within certain particles where arrays of more ordered circular domains indicative of a hexagonally packed cylinder morphology are present.

At 53 hours the prevalence of the spherical phase has declined dramatically, whereas the hexagonally packed cylinder and lamellar morphologies have become abundant to the point where both morphologies are present in roughly equal proportions within the microparticles (see ESI Fig. S13<sup>†</sup> for a higher magnification TEM image). These observations are qualitatively comparable to those for the microparticles collected at both the 60 hours kinetic time point and from the X-ray autoclave after polymerising for 64 hours during *in situ* SAXS monitoring. This further highlights the very gradual and somewhat sporadic nature of the transitions through phase space for this system and also validates the expected gradual transition of the samples away from the spherical phase and into the morphologies expected for a more symmetrical block copolymer system.<sup>2</sup> To probe the morphology transitions at even higher conversion values than possible at the synchrotron due to time limitations, the kinetics experiment was continued for a further 24 hours beyond the 60 hours time point to gain further insight of the morphological transitions at very high conversion. The final TEM images taken of the product collected after depressurising the autoclave indicated an even higher proportion of particles with a pure lamellar morphology, as expected for this reaction based on the final morphology analysis from previous reports on PMMA-*b*-PS block copolymer microparticles of similar  $f_{\text{PMMA}}$  values.<sup>34</sup>

Together these data demonstrate that the hexagonal cylinder morphology is a distinct intermediate stage formed during the transition to a lamellar morphology, but that the specific scattering reflection is obscured in the *in situ* SAXS profiles. Its

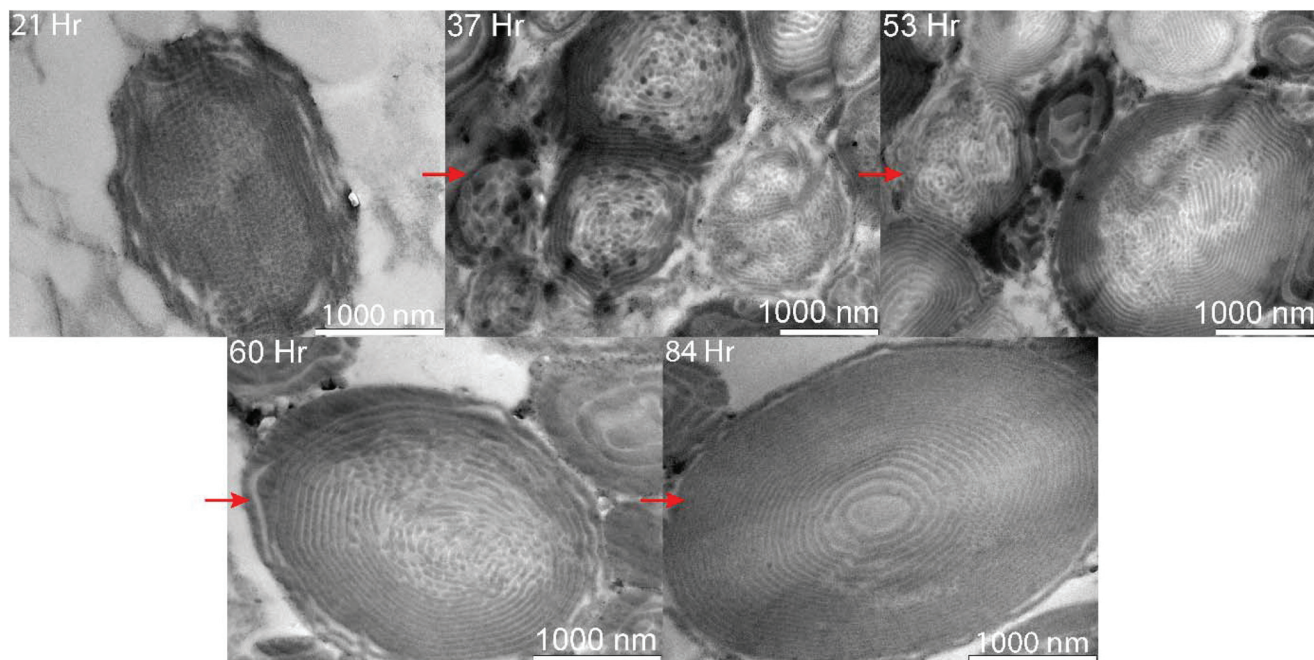


Fig. 4 TEM images of representative cross-sectioned PMMA-*b*-PS particles taken from the kinetic aliquots of the offline chain extension of PMMA(25) with PS(50) at time points of 21, 37, 53, 60 and 84 hours.

appearance within certain particles as elongated and partially fused cylinders also match those described previously by Sakurai *et al.*<sup>65</sup> when a polystyrene-*b*-polybutadiene-*b*-polystyrene (PS-*b*-PB-*b*-PS) block copolymer was thermally induced to undergo a transition from cylinders to lamellae. This occurred through a process in which neighbouring cylinders gradually approached each other before zipping into uninterrupted lamellae.<sup>65</sup> A similar mechanism has also been reported during the transition from high to low order structures in a polystyrene-*b*-polyethylene-*co*-polybutylene-*b*-polystyrene (PS-*b*-PE-*co*-PB-*b*-PS) block copolymer.<sup>66</sup> In this case the cylindrical structure breaks up and forms rippled cylinders as an intermediate prior to transforming into a spherical structure in a selective solvent, which accurately describes the reverse of the transitions observed here. It can therefore be concluded that this spherical to lamellar transition *via* the intermediate hexagonal cylinder morphology initially begins at some point during the 16 hours window between 21–37 hours, corresponding with a PS molecular weight range between ~15–27 kDa based on the kinetics monitoring data (ESI Fig. S6†). These results also suggest that the same transition is likely to have occurred during the early stages of the PMMA(31)-PS(25) polymerisation, immediately after phase separation but prior to formation of the higher order peaks characteristic of a the hexagonal cylinder morphology. For PMMA(31)-PS(25) this occurs after approximately 35 hours of polymerisation and a PS molecular weight of ~15 kDa, suggesting further agreement between the morphology transitions of the two reactions that is obscured in the SAXS data alone due to the lack of higher order scattering information owing to the domain size variation within the microparticles.

#### Control polymerisations testing the limits of block copolymer self-organisation in scCO<sub>2</sub>: synthesis of PMMA(58)-PS(12) and PMMA(54)-PMMA(44) monitored *via in situ* SAXS

As expected, the  $q$  (nm<sup>-1</sup>) *versus*  $I(q)$  *versus* time plots obtained during the synthesis of the second blocks for PMMA(58)-PS(12) and PMMA(54)-PMMA(44) are both initially featureless (Fig. 5a and ESI Fig. S14,† respectively). This remains the case for the entirety of the PMMA(54)-PMMA(44) polymerisation, indicating that no phase separation occurs during the polymerisation of the second block, and was subsequently corroborated *via* the TEM images taken of the sample post-polymerisation (ESI Fig. S14b†). On the other hand, a single broad scattering peak develops at 0.136 nm<sup>-1</sup> quite late into the polymerisation of PMMA(58)-PS(12) at approximately 65 hours (see also ESI Fig. S15† for the corresponding 2-dimensional plot of the SAXS profiles at 10 hours intervals). In conjunction with the corresponding TEM images of the final product (Fig. 5b), which lack any evidence of internal phase separated structures, this was assigned as the correlation hole scattering peak indicative of the disordered phase. We attribute the lack of order in this sample to its high degree of block asymmetry ( $f_{\text{PMMA}} = 0.81$ ), positioning it towards the edges of the phase diagram where the formation of ordered structures becomes thermodynamically unfavourable.<sup>2</sup>

#### Empirical phase diagram of PMMA-*b*-PS derived from *in situ* SAXS measurements

Block copolymer phase diagrams are powerful tools for researchers needing to target specific morphologies for a system in order to meet an application need. Although both

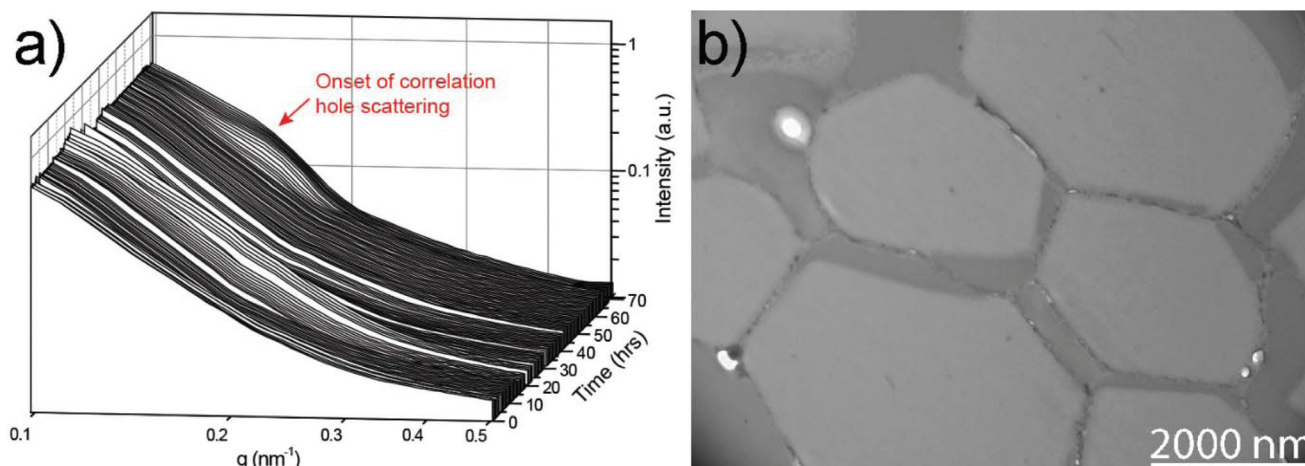


Fig. 5 (a) Time-resolved *in situ* SAXS data recorded during the chain extension of PMMA(58) to form PMMA(58)-PS(12) via dispersion polymerisation in  $\text{scCO}_2$ . The time between the individual profiles included is approximately 30 minutes. (b) TEM images taken of the final product.

theoretically and experimentally derived phase diagrams have been extensively studied and mapped out for neat diblock copolymer systems in the bulk and thin film states, their applicability to ternary systems that contain additives or dopants is often limited.<sup>2,5,12</sup> This is because the additives almost always exhibit preferential affinity for one block, leading to uneven swelling and significantly more complex system thermodynamics. As a result, phase diagrams of such systems must be plotted manually using empirical data taken from static samples, which is a time consuming and experimentally tedious task.<sup>34,58,67</sup>

Previously, Jennings *et al.* have used this approach to plot initial phase diagrams from several static samples of two block copolymer systems, PMMA-*b*-PS and PMMA-*b*-poly(benzyl methacrylate), synthesised *via* one-pot RAFT dispersion polymerisation in  $\text{scCO}_2$ .<sup>34</sup> Although comprised of only a limited number of data points, the diagrams were a more quantitative representation of previous findings that  $\text{scCO}_2$  preferentially swells methacrylate based polymers over those comprised of styrene units.<sup>36,60</sup> As a consequence, PMMA-*b*-PS block copolymers synthesised in  $\text{scCO}_2$  demonstrate markedly different morphologies when compared with those in the melt state (see Fig. 6 for the reproduced data). These morphologies are preserved upon venting the  $\text{CO}_2$  because the block copolymers rapidly revert to a glassy, immobile state at the synthesis temperature (65 °C). For example, at  $\chi N$  and  $f_{\text{PMMA}}$  values of  $\sim 30$  and  $\sim 0.5$ , respectively, a lamellar morphology is anticipated for a neat diblock copolymer,<sup>2</sup> however, a spherical morphology was observed in an equivalent PMMA-*b*-PS block copolymer synthesised in  $\text{scCO}_2$ .<sup>34</sup>

The rich morphology data that are recorded during a RAFT dispersion polymerisation monitored *in situ* using SAXS are therefore a convenient method for plotting highly accurate empirical phase diagrams from a much smaller subset of polymerisation reactions, when combined with kinetically monitored sample characteristic data. The resulting diagram was plotted using the data points taken from each of the three

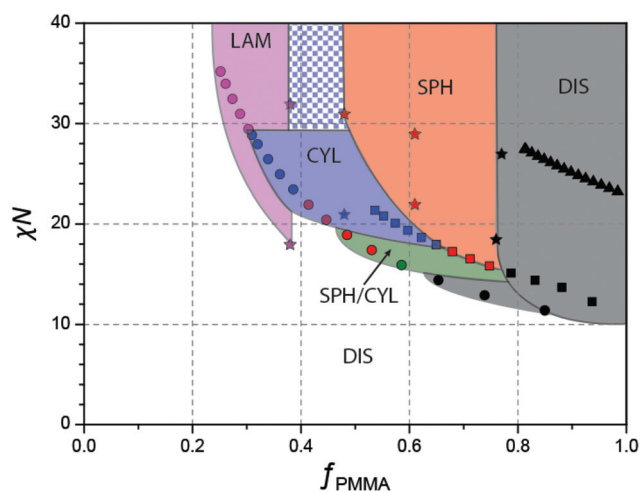


Fig. 6 Empirical phase diagram for PMMA-*b*-PS in  $\text{scCO}_2$  derived from the SAXS and kinetics data for PMMA(31)-PS(25) (squares), PMMA(25)-PS(50) (circles) and PMMA(58)-PS(12) (triangles). The data points represented by stars are taken from a previous report by Jennings *et al.* for the same system in  $\text{scCO}_2$ .<sup>34</sup> Where exact time points for morphology transitions could not be determined the phase boundaries were taken at the midpoint between the available data points. The blue checked region is an assumed stability region for the cylindrical morphology that was not observed in the data available.

block copolymer reactions undertaken here at 10 hours intervals (Fig. 6). The data previously reported by Jennings *et al.* for eight static samples of this block copolymer synthesised in  $\text{scCO}_2$  are also included for easy comparison.<sup>34</sup> In each case, the molecular weight and composition data from GPC and  $^1\text{H}$  NMR spectroscopy, respectively, were used to calculate values of  $N$  and  $f_{\text{PMMA}}$ , while the value of  $\chi$  at 65 °C was taken from the literature as 0.0395<sup>56</sup> ( $\chi = 0.0411$  for data plotted from Jennings *et al.*).<sup>34</sup> For simplicity, the molecular weight growth for the reaction of PMMA(58)-PS(12) reaction was assumed to be linear with time with a slope equal to that for PMMA(31)-PS(25).

Very good agreement between the morphology transitions for the three reactions undertaken here and the previous data was observed, thereby solidifying the validity of this approach as being on par with the more conventional approach. This is in spite of additional variables in the  $scCO_2$  system, such as temperature, and more importantly, the presence of unreacted monomer, showing that overall their contributions in these systems are low relative to the effects of the  $scCO_2$ .

## Conclusions

In conclusion, we have demonstrated that the synthesis of nanostructured block copolymer microparticles *via* RAFT dispersion polymerisation in  $scCO_2$  can be decoupled into completely independent steps. This was achieved by exploiting the living chain ends of RAFT synthesised PMMA homopolymers, even after storage for months, and their ability to be quickly redispersed in  $scCO_2$  using a small quantity of additional PDMS-MA stabiliser. Using this process a series of three PMMA-*b*-PS block copolymers with varying  $f_{PMMA}$  ratios were synthesised and the development of order and subsequent morphology evolution was monitored throughout the polymerisation *via in situ* SAXS and corroborated using post-mortem TEM imaging. For the polymerisation of PMMA(31)-PS(25) a SAXS pattern consistent with a hexagonal cylinder morphology was gradually formed following phase separation at approximately 16 hours. The characteristic spacing then gradually increased with time in response to the growing PS block until the end of the reaction and no further morphology transitions occurred. TEM imaging confirmed the presence of this morphology and additional SAXS analysis of the final product revealed that the domain size of the sample following depressurisation was almost the same value prior to venting the autoclave at the end of the reaction. This indicates that the increase in domain size of the internal morphology brought about by the swelling effects of  $scCO_2$  are mostly retained by the sample upon its removal.

By contrast, the SAXS profiles obtained during the synthesis of PMMA(25)-PS(50) were considerably more complex. Initially a single broad peak was discernible in the SAXS profiles of this sample at 13.5 hours, which from the TEM images taken at a slightly later time was revealed to be due to the initial formation of a spherical morphology. As the polymerisation progressed this SAXS peak became progressively broader and slightly bimodal in appearance as the spheres gradually transitioned into a mixed cylindrical/lamellar phase. To further elucidate the nature and time period of this transition the reaction was repeated in a sampling autoclave and aliquots were taken at various time points for TEM analysis. These images revealed that the transition from spheres begins to occur over a 16 hours window between 21–37 hours *via* a hexagonally packed cylinder morphology intermediate. This is a slow and somewhat sporadic process that remains partially incomplete until the very late stages of the polymerisation ( $t > 64$  hours). Finally, for PMMA(58)-PS(12) a disordered peak appeared late into the poly-

merisation but no self-organisation occurred due to the highly asymmetric composition of this sample, while for PMMA(54)-PMMA(44) there was no evidence of phase separation.

## Conflicts of interest

There are no conflicts to declare.

## Acknowledgements

SAXS experiments were undertaken at Beamline 26B (DUBBLE) of the European Synchrotron and Radiation Facility (ESRF) in Grenoble, France. We thank the N.W.O for providing the beam time for our experiments. We gratefully acknowledge the University of Nottingham Nanoscale and Microscale Research Centre (NMRC) for access to their instrumentation, in particular Ms Denise McClean for assistance with the FEI Tecnai TEM. MA, TMB, GH and SMH are indebted to the very high quality technical and high pressure safety support at the University of Nottingham from Peter Fields, Richard Wilson and Martin Dellar. This research was supported in part under the Leverhulme Grant Award Scheme (RPG-2014-034, for TMB, GH and SMH) as well a UNNES-IDB PhD scholarship for MA.

## References

- 1 L. Leibler, *Macromolecules*, 1980, **13**, 1602–1617.
- 2 M. W. Matsen and F. S. Bates, *Macromolecules*, 1996, **29**, 1091–1098.
- 3 M. W. Matsen and M. Schick, *Phys. Rev. Lett.*, 1994, **72**, 2660–2663.
- 4 R. A. Segalman, *Mater. Sci. Eng., R*, 2005, **48**, 191–226.
- 5 A. K. Khandpur, S. Foerster, F. S. Bates, I. W. Hamley, A. J. Ryan, W. Bras, K. Almdal and K. Mortensen, *Macromolecules*, 1995, **28**, 8796–8806.
- 6 H. Yu, X. Qiu, S. P. Nunes and K.-V. Peinemann, *Nat. Commun.*, 2014, **5**, 4110.
- 7 D. Mecerreyes, *Prog. Polym. Sci.*, 2011, **36**, 1629–1648.
- 8 V. F. Scalfani, E. F. Wiesenauer, J. R. Ekblad, J. P. Edwards, D. L. Gin and T. S. Bailey, *Macromolecules*, 2012, **45**, 4262–4276.
- 9 K.-V. Peinemann, V. Abetz and P. F. W. Simon, *Nat. Mater.*, 2007, **6**, 992–996.
- 10 Y. Fink, A. M. Urbas, M. G. Bawendi, J. D. Joannopoulos and E. L. Thomas, *J. Lightwave Technol.*, 1999, **17**, 1963–1969.
- 11 Y. Kang, J. J. Walsh, T. Gorishnyy and E. L. Thomas, *Nat. Mater.*, 2007, **6**, 957–960.
- 12 C. T. Black, R. Ruiz, G. Breyta, J. Y. Cheng, M. E. Colburn, K. W. Guarini, H. C. Kim and Y. Zhang, *IBM J. Res. Dev.*, 2007, **51**, 605–633.
- 13 J. G. Kennemur, L. Yao, F. S. Bates and M. A. Hillmyer, *Macromolecules*, 2014, **47**, 1411–1418.
- 14 T. M. Bennett, K. Pei, H.-H. Cheng, K. J. Thurecht, K. S. Jack and I. Blakey, *J. Micro/Nanolithogr., MEMS, MOEMS*, 2014, **13**, 031304.

- 15 I. Botiz and S. B. Darling, *Mater. Today*, 2010, **13**, 42–51.
- 16 H.-Y. Hsueh, H.-Y. Chen, M.-S. She, C.-K. Chen, R.-M. Ho, S. Gwo, H. Hasegawa and E. L. Thomas, *Nano Lett.*, 2010, **10**, 4994–5000.
- 17 M. G. Fischer, X. Hua, B. D. Wilts, I. Gunkel, T. M. Bennett and U. Steiner, *ACS Appl. Mater. Interfaces*, 2017, **9**, 22388–22397.
- 18 T. M. Bennett, G. He, R. R. Larder, M. G. Fischer, G. A. Rance, M. W. Fay, A. K. Pearce, C. D. J. Parmenter, U. Steiner and S. M. Howdle, *Nano Lett.*, 2018, **18**, 7560–7569.
- 19 J. Jennings, G. He, S. M. Howdle and P. B. Zetterlund, *Chem. Soc. Rev.*, 2016, **45**, 5055–5084.
- 20 B. H. Jones and T. P. Lodge, *ACS Nano*, 2011, **5**, 8914–8927.
- 21 H. Sai, K. W. Tan, K. Hur, E. Asenath-Smith, R. Hovden, Y. Jiang, M. Riccio, D. A. Muller, V. Elser, L. A. Estroff, S. M. Gruner and U. Wiesner, *Science*, 2013, **341**, 530–534.
- 22 T. Higuchi, A. Tajima, K. Motoyoshi, H. Yabu and M. Shimomura, *Angew. Chem., Int. Ed.*, 2008, **47**, 8044–8046.
- 23 T. Higuchi, A. Tajima, H. Yabu and M. Shimomura, *Soft Matter*, 2008, **4**, 1302–1305.
- 24 L. Li, K. Matsunaga, J. Zhu, T. Higuchi, H. Yabu, M. Shimomura, H. Jinnai, R. C. Hayward and T. P. Russell, *Macromolecules*, 2010, **43**, 7807–7812.
- 25 S.-J. Jeon, G.-R. Yi, C. M. Koo and S.-M. Yang, *Macromolecules*, 2007, **40**, 8430–8439.
- 26 S.-J. Jeon, G.-R. Yi and S.-M. Yang, *Adv. Mater.*, 2008, **20**, 4103–4108.
- 27 K. H. Ku, H. Yang, J. M. Shin and B. J. Kim, *J. Polym. Sci., Part A: Polym. Chem.*, 2015, **53**, 188–192.
- 28 Z. Lu, G. Liu and F. Liu, *Macromolecules*, 2001, **34**, 8814–8817.
- 29 A. Nykänen, A. Rahikkala, S.-P. Hirvonen, V. Aseyev, H. Tenhu, R. Mezzenga, J. Raula, E. Kauppinen and J. Ruokolainen, *Macromolecules*, 2012, **45**, 8401–8411.
- 30 D. J. Keddie, *Chem. Soc. Rev.*, 2014, **43**, 496–505.
- 31 B. Charleux, G. Delaittre, J. Rieger and F. D'Agosto, *Macromolecules*, 2012, **45**, 6753–6765.
- 32 N. J. Warren and S. P. Armes, *J. Am. Chem. Soc.*, 2014, **136**, 10174–10185.
- 33 M. J. Derry, L. A. Fielding and S. P. Armes, *Prog. Polym. Sci.*, 2016, **52**, 1–18.
- 34 J. Jennings, S. P. Bassett, D. Hermida-Merino, G. Portale, W. Bras, L. Knight, J. J. Titman, T. Higuchi, H. Jinnai and S. M. Howdle, *Polym. Chem.*, 2016, **7**, 905–916.
- 35 J. Jennings, M. Beija, J. T. Kennon, H. Willcock, R. K. O'Reilly, S. Rimmer and S. M. Howdle, *Macromolecules*, 2013, **46**, 6843–6851.
- 36 J. Jennings, M. Beija, A. P. Richez, S. D. Cooper, P. E. Mignot, K. J. Thurecht, K. S. Jack and S. M. Howdle, *J. Am. Chem. Soc.*, 2012, **134**, 4772–4781.
- 37 G. He, T. M. Bennett, M. Alauhdin, M. W. Fay, X. Liu, S. T. Schwab, C.-g. Sun and S. M. Howdle, *Polym. Chem.*, 2018, **9**, 3808–3819.
- 38 T. D. McAllister, L. D. Farrand and S. M. Howdle, *Macromol. Chem. Phys.*, 2016, **217**, 2294–2301.
- 39 A. I. Cooper, *J. Mater. Chem.*, 2000, **10**, 207–234.
- 40 C. Boyère, C. Jérôme and A. Debuigne, *Eur. Polym. J.*, 2014, **61**, 45–63.
- 41 S. Curia, D. S. A. De Focatiis and S. M. Howdle, *Polymer*, 2015, **69**, 17–24.
- 42 S. Curia, A. F. Barclay, S. Torron, M. Johansson and S. M. Howdle, *Philos. Trans. R. Soc., A*, 2015, 373.
- 43 I. Kikic, *J. Supercrit. Fluids*, 2009, **47**, 458–465.
- 44 E. Girard, T. Tassaing, J.-D. Marty and M. Destarac, *Chem. Rev.*, 2016, **116**, 4125–4169.
- 45 S. Hilic, S. A. E. Boyer, A. A. H. Pádua and J.-P. E. Grolier, *J. Polym. Sci., Part B: Polym. Phys.*, 2001, **39**, 2063–2070.
- 46 R. Li, Z. Zhang and T. Fang, *J. Supercrit. Fluids*, 2016, **110**, 110–116.
- 47 B. Chu and B. S. Hsiao, *Chem. Rev.*, 2001, **101**, 1727–1762.
- 48 M. J. Elwell, S. Mortimer and A. J. Ryan, *Macromolecules*, 1994, **27**, 5428–5439.
- 49 H. S. Lee, S. R. Yoo and S. W. Seo, *Fibers Polym.*, 2001, **2**, 98.
- 50 M. J. Derry, L. A. Fielding, N. J. Warren, C. J. Mable, A. J. Smith, O. O. Mykhaýlyk and S. P. Armes, *Chem. Sci.*, 2016, **7**, 5078–5090.
- 51 D. Hermida-Merino, G. Portale, P. Fields, R. Wilson, S. P. Bassett, J. Jennings, M. Dellar, C. Gommès, S. M. Howdle, B. C. M. Vrolijk and W. Bras, *Rev. Sci. Instrum.*, 2014, **85**, 093905.
- 52 J. T. Lai, D. Filla and R. Shea, *Macromolecules*, 2002, **35**, 6754–6756.
- 53 A. M. Gregory, K. J. Thurecht and S. M. Howdle, *Macromolecules*, 2008, **41**, 1215–1222.
- 54 W. Bras, I. P. Dolbnya, D. Detollenaere, R. van Tol, M. Malfois, G. N. Greaves, A. J. Ryan and E. Heeley, *J. Appl. Crystallogr.*, 2003, **36**, 791–794.
- 55 J. Brandrup, E. H. Immergut and E. A. Grulke, *Polymer Handbook*, Wiley, 4th edn, 1999.
- 56 T. P. Russell, R. P. Hjelm and P. A. Seeger, *Macromolecules*, 1990, **23**, 890–893.
- 57 H. Ahn, D. Y. Ryu, Y. Kim, K. W. Kwon, J. Lee and J. Cho, *Macromolecules*, 2009, **42**, 7897–7902.
- 58 T. M. Bennett, K. S. Jack, K. J. Thurecht and I. Blakey, *Macromolecules*, 2016, **49**, 205–214.
- 59 M. L. Hoarfrost and R. A. Segalman, *ACS Macro Lett.*, 2012, **1**, 937–943.
- 60 Y. Zhang, K. K. Gangwani and R. M. Lemert, *J. Supercrit. Fluids*, 1997, **11**, 115–134.
- 61 M. Zhong and K. Matyjaszewski, *Macromolecules*, 2011, **44**, 2668–2677.
- 62 T. Tanaka, M. Okayama, Y. Kitayama, Y. Kagawa and M. Okubo, *Langmuir*, 2010, **26**, 7843–7847.
- 63 T. Rieker, A. Hanprasopwattana, A. Datye and P. Hubbard, *Langmuir*, 1999, **15**, 638–641.
- 64 F. S. Bates, *Macromolecules*, 1985, **18**, 525–528.
- 65 S. Sakurai, T. Momii, K. Taie, M. Shibayama, S. Nomura and T. Hashimoto, *Macromolecules*, 1993, **26**, 485–491.
- 66 M. Li, Y. Liu, H. Nie, R. Bansil and M. Steinhart, *Macromolecules*, 2007, **40**, 9491–9502.
- 67 T. P. Lodge, B. Pudil and K. J. Hanley, *Macromolecules*, 2002, **35**, 4707–4717.

### 3- Co-proposer PhD Thesis project awarded; “Etude multi-échelle de l’impact de l’ajout de fluoroélastomère sur la structure du PVDF par des mesures *in situ* couplées”, Université de Lorraine.

---

I have co-applied successfully for a Ph.D. project to the Region of Lorraine together with prof. Patrice Bourson but also, we have fund-raised from an industrial partner (ARKEMA) in order to investigate by time resolved simultaneous DSC-SAXS-WAXS experiments in combination with Raman spectroscopy the effect on the nanostructure of PVDF the addition of a fluoroelastomer to enhance the mechanical properties. The total financial support was 135000 Euros. Importantly, the data simultaneously acquired by different techniques have been studied by chemometrics analysis in order to correlate subtle differences among the enormous metadata recorded. Chemometrics analysis is largely employed in the spectroscopic field but has scarcely used with X-ray data and/or in combination with spectroscopic techniques. I consider that the use of X-rays techniques with other relevant spectroscopies is crucial to correlate different length-scales. However, the enormous amount of data generated at acquisition times close to second or millisecond requires the employ of a mathematical tool that allows associating the data and its multiple interconnections. I have successfully applied for a visitor scientist grant in 2018, 2019 and 2020 at the Université de Lorraine to expand my knowledge on multivariate analysis. The grant was valued around 2500 euros in order to support my trip and stay for a month within prof. Patrice Bourson. The thesis student (Sarah Saidi) is in her last Ph.D. year and I will be the corresponding author of the 3 manuscripts under preparation. Sarah Saidi has spent most of her Ph.D in DUBBLE, supervised by me.

The student has already presented her work at ISPAC, the 32<sup>nd</sup> International Symposium on Polymer Analysis and Characterization, June 2-5, 2019 with an oral contribution entitled ‘Multi-scale study of the impact of fluoroelastomer addition on the PVDF structure by coupled *in situ* measurements’.

Poly (vinylidene fluoride) (PVDF) is an interesting material largely employed in a wide range of applications such as architectural, offshore materials, solar panels, and chemical engineering. The PVDF materials undergo extreme conditions for these applications such as high or low pressure, high and low temperature, cold or hot bending and blistering. The manufacturing of the polymeric materials must meet strict ambivalent specifications because of the variable conditions depending on the work environment. PVDF properties depend on its semi-crystalline nanostructure. Indeed, PVDF crystallizes readily and presents a polymorphism. PVDF is well known to crystallize, in a polar phase ( $\beta$ -) which exhibits interesting electrical properties, such as pyroelectricity or piezoelectricity and in a non-polar phase ( $\alpha$ -), the more mechanical resistant and stable phase. Moreover, PVDF has been blended with a fluoroelastomer (in weight fraction lower than 50wt%) in order to improve the viscoelastic behavior of the final material by changing the nanostructure of the initial neat PVDF. The understanding of PVDF

blends crystallization under conditions that mimic their life cycle is crucial to optimize and design novel PVDF derivatives to enhance the performance of the material under real conditions. With this goal, it has to be established the relation between the crystallinity, phase content and the crystallite size of a pure PVDF and a PVDF/fluoroelastomer blends. The composition of the blend influences the overall crystallinity. More precisely, different PVDF/fluoroelastomer blends have been studied to probe the influence of fluoroelastomer mixed to PVDF matrix. Raman spectroscopy imaging and time-resolved simultaneous DSC-SAXS-WAXS experiments in combination with Raman spectroscopy have been performed to identify the structure, crystallinity, shape and crystallite size. Moreover, chemometrics analysis has been performed to correlate the simultaneous data acquired.

In a first stage of the project, I have focused on the experimental optimization of the combination of scattering techniques with Raman spectroscopy.

Time-resolved small-angle X-ray scattering (SAXS) and/or wide-angle X-ray scattering (WAXS) are currently employed (Portale *et al.*, 2016a) as ordinary structural characterization techniques in the synchrotron radiation community. Moreover, SAXS lab sources have been extended throughout the solid-state physics departments as a result of the great improvement at the covered angular range, the enhancement in flux, the detectors development and the standardization of complex sample environments. However, novel technical implementations are required to design complex experimental with fine control to further study the dynamic morphological evolution upon external stimuli in a multi-technique approach. The Dutch-Belgian Beamline (DUBBLE) beamline is particularly optimized for the study of polymer science under extreme conditions, as reported by Bras *et al.* (Bras *et al.*, 2003). The versatility of DUBBLE to accommodate complex experimental setup (Portale *et al.*, 2013) with applicable advances on combined techniques has been proved to be crucial to monitor the polymer crystallization under processing-relevant conditions that mimic industrial environments. Particularly, great efforts have been focused on the crystallization understanding of the interplay of the different flow fields and thermal treatments that replicate the industrial conditions at which polymers are subjected in processing such as extrusion, injection molding, blow molding, fiber spinning, drop casting, filament deposition modeling and inkjet printing. The characterization of the crystallization mechanism of semicrystalline polymers from the melt have been largely benefited upon quiescent and non-isothermal conditions with mild cooling rates by combining DSC optical microscopy equipment (Russell & Koberstein, 1985) (Bras, Derbyshire, Devine *et al.*, 1995) with simultaneous SAXS/WAXS experiments. Moreover, the nanostructuring of semicrystalline polymers upon fast quenching cooling rates relevant to industrial environments, has been characterized upon scattering techniques subjected to ballistic cooling and recently, in combination with flash chip calorimetry (Portale *et al.*, 2016b). Likewise, the effect of shear forces on the crystallization mechanism of semicrystalline polymers has greatly probed by scattering techniques to reproduce the industrial conditions. (Ryan *et al.*, 2016) Solid-state drawability of  $\beta$  nucleated iPP films has been evaluated (Luijsterburg *et al.*, 2014) by in situ 2D WAXS measurements under uniaxial stretching at different temperatures by heated godet drawing roll units fitted with an oven that mimic industrial conditions. The mechanical and optical properties of polymeric films depend on

thermo-draw history that undergo commonly different applications such as the food and packing industry as well as cast film extrusion process. In situ WAXS and SAXS experiments using small-scale industrial equipment such as the study of 2D stretching at different temperatures and grades of low-density polyethylene (LDPE) has been conducted (Portale *et al.*, 2013; van Drongelen *et al.*, 2014; Troisi *et al.*, 2016) using a real film blowing machine connected to an extruder. The dependence of the onset of crystallinity and the crystal orientation as a function of different take-up and blow-up ratios of the polymer film has been studied. Flow-induced crystallization has been largely investigated by in situ simultaneous SAXS-WAXS experiments in combination with a slit-like rheometer (Balzano *et al.*, 2010; Ma *et al.*, 2012; Troisi *et al.*, 2015) to correlate the structure-property relationship of injection molding industrial process. The formation under high shear rates of the so-called shish-kebab structures as a function of the imposed stress in a wide range of polymers has been monitoring as well as the effect of nucleating agents upon shear (Wilsens *et al.*, 2018, 2019). Recently, the crystallization upon precise and locally controlled uniaxial extensional flow of LDPE has been investigated by dedicated rheo-SAXS experimental to decouple the effect of the extensional component from the rotational component present in shear flow and thus, attain higher extensional forces. (Pepe *et al.*, 2020) Furthermore, polymer water/CO<sub>2</sub> emulsions at extreme conditions have been monitoring (Alaimo *et al.*, 2015) by the development of a versatile high-pressure X-ray vessel (Hermida-Merino *et al.*, 2014) fitted with a large exit opening angle that permits acquired WAXS patterns. The internal structural development of block copolymer microparticles during a dispersion polymerization has been probing by in situ simultaneous SAXS-WAXS experiments (Alauhdin *et al.*, 2019) under supercritical CO<sub>2</sub> to assess the degree of CO<sub>2</sub> affinity on the different block on the final quenched structure. Moreover, Franeker *et al.* (Franeker *et al.*, 2017) reported recently the formation at different length-scales of sub-micrometer structures during the thin film formation by spin coating of polymeric blends and for block-copolymers (Fleury *et al.*, 2019), studied by ultrafast grazing incidence small angle and wide X-ray scattering (GISAXS/GIWAXS (Dong *et al.*, 2020)) coupled with laser interferometry and laser scattering.

Experimental strategies to perform simultaneous SAXS-WAXS experiments in combination with non-X-ray based techniques with different sensitivities have been extensively discussed by Bras *et al.* (Bras *et al.*, 2014) as well as the design of appropriate complex sample environments. A pioneering combination of vibrational technics with synchrotron radiation light has been reported by Bras *et al.* (Bras, Derbyshire, Bogg *et al.*, 1995) in which SAXS has been coupled to Fourier-transform infrared (FTIR) spectroscopy to study the driving force for structure development in polyurethanes. However, the technical requirements to conduct Fourier-transform infrared spectroscopy prevent to universalize the combination with other techniques and specific complex sample environments have to be integrated. In contrast, Raman spectroscopy has been widely exploited in combination with multiple techniques with the advent of the technological developments due to simple implementation, improvement of the time resolution and experimental advantages. (Gerrard & Maddam, 1986) Raman spectroscopy is a non-destructive technique that can be applied to different media (bulk, fibers, solution, gels and films), specifically aqueous solution without special experimental preparations, and requires small quantities of sample to be studied. Moreover, Raman spectroscopy is sensible

to molecular vibrations related to the bond polarization of the active moieties,(Ferraro *et al.*, 2003) which generally is attributed to apolar groups. Consequently, Raman spectroscopy conveys structural details of the chemical bonds, singularly for polymers, for both the monomer units to the macromolecular conformation and can be easily polarized to detect structural anisotropies. (2000) Furthermore, the Raman scattering response probes the covalent nature representative of polymeric backbone in particular the frequent unsaturated bonds as well as the chain stereoregularity. (Edwards *et al.*, 1993) In addition, the low frequencies spectral range is correlated to the collective motion associated with the transition time to identify and correlate the chemical conformation to the structure of nanomaterials. Quantitative analysis by Raman spectroscopy of the system composition requires the correction of the scattering bands intensity either by adding an internal standard or calibration with a different technique. (1999) The indirect relationship of Raman scattering intensity to the concentration arises from the uncertainty of the scatters volume illuminated by in the incident beam. However, the linear intensity dependence facilitates to distinguish different component concentrations. Particularly, the crystallinity content of semicrystalline polymers has been largely determined by Raman spectroscopy as well as the characterization of the related nanostructured is analyzed combined with SAXS/WAXS experiments due to the complementary sensitivities to different crystalline, interphase or amorphous phases. Moreover, the detailed description of the nanostructure composition by SAXS experiments has been greatly benefited by associated to Raman quantitative analysis to optimize the parameters of the correlation function, particularly at crystallinities around 50 % where electronic contrast hamper the phase assignment by SAXS.

Similarly to X-ray scattering techniques, polymerization under industrial has been largely employed by Raman spectroscopy to monitor both the kinetics and physical parameters of the reaction medium, especially in heterogeneous systems such as monomer droplets, polymer particles, micelles (Dropsit *et al.*, 2019). Moreover, the optimization of the polymerization conditions in solution have been studied (Chevrel *et al.*, 2012) by combined Raman spectroscopy to rheological measurements to relate the fluid mechanics with the synthetic mechanism of acrylic acid at different shear rates(Chevrel *et al.*, 2014), enabling to be scaled to industrial environments by pilot plants studies (Kohlmann *et al.*, 2016) (Chevrel *et al.*, 2016). Likewise, the gel effect during the bulk polymerization of polystyrene has been probed (Brun, Youssef *et al.*, 2013) by coupling Raman spectroscopy to rheology to correlate the viscosity development of the heterogeneous medium with the monomer conversion. Coupling Raman spectroscopy to drop tensiometry illustrated the versatility to monitor heterogenous polymerizations in a drop reaction vessel within an aqueous medium to account for the relation between monomer conversion with the interfacial tension and dilatation rheology(Dropsit *et al.*, 2018). Remarkably, the scattering nature of the Raman response has been proved to discriminate simultaneously the kinetic reaction mechanism and phase separation or phase inversion physical phenomena during the polymerization by examining the reaction media with Raman probes with different analyzed volumes. (Brun *et al.*, 2014) Moreover, the mechanism of deformation under uniaxial stretching of iPP has been monitored (Martin *et al.*, 2013) by in situ polarized Raman spectroscopy, yielding detailed nanostructure evolution of the

amorphous and the crystalline domains. Beneficially, the orientation of the polymeric amorphous domains and the stress distribution within the chemical bonds was directly probed by Raman spectroscopy, in contrast to X-ray scattering techniques, as well as the degree of crystallinity and orientation of the crystalline domains. Furthermore, ammonium nitrate phase transitions upon thermal treatment have been monitored with in situ Raman spectroscopy and DSC by relating with the group theory, the lattice vibrations to the required phase transition energy. (Harju *et al.*, 1992)

Particularly, Raman spectroscopy has been coupled to several X-ray based techniques across the synchrotron community for both scattering such as micro-XRD (Davies *et al.*, 2005), high resolution (Boccaleri *et al.*, 2007) XRD or spectroscopic techniques like UV-vis XAFS (Beale *et al.*, 2005) and sequential combinations of both as XANES-XRD. (Kongmark *et al.*, 2009) Likewise, Raman spectroscopy is beneficial to be associated with SAXS-WAXS techniques to analyze the nanostructural evolution of polymeric systems upon external stimuli whilst obtaining concurrently kinetic data as well as identifying potential X-ray beam damage. (McGeehan *et al.*, 2007) (Stanley *et al.*, 2014) Simultaneous Raman spectroscopy with high time resolution (2s) on back scattering mode using optical fiber probe with time-resolved SAXS-WAXS measurements (Bryant *et al.*, 1998) has been applied to follow in situ the phase transition of high density polyethylene upon thermal treatment in combination with a Linkam calorimeter stage. Moreover, the online combination of Raman spectroscopy with SAXS/WAXS has been proved to advance the on the understanding of complex polymer processing such as reactive solvent polymerizations where concomitant or sequential physicochemical phenomena occurs that imply kinetic and morphological variations.

Firstly, the mechanism of formation and the polymer-solvent compound as well as the phase transformation in syndiotactic polystyrene (sPS) gels was probed by harnessing the simultaneous data at different lengthscales obtained by the combined Raman spectroscopy SAXS WAXS setup (Rastogi *et al.*, 1998; Goossens *et al.*, 1999). The optical density differences detected by Raman spectroscopy to identify the developed solid liquid phase separations upon thermal treatment as well as the conformational changes during the phase transformations of sPS with different solvents, (decalin, benzyl methacrylate, and cyclohexyl methacrylate). Furthermore, the kinetics and polymerization mechanism of a reactive solvent as styrene with PE has been (Goossens *et al.*, 2001) monitored at different temperatures by the coupled Raman spectroscopy with simultaneous SAXS/WAXS to follow the temperature dependence of the sequential liquid-solid phase separation and subsequent PE crystallization that was affected by solvent removal.

The structural development of both the crystalline and amorphous region under tensile deformation of isotactic polypropylene (iPP) fiber (Ran *et al.*, 2003) have been studied by in situ simultaneous polarized Raman spectroscopy and synchrotron two-dimension (2D) WAXD measurements. Raman spectroscopy has permitted to resolve the structural evolution during the  $\alpha$  to mesophase transition upon stretching to a packing disorder instead to the backbone conformational conversion. Furthermore, Ponçot *et al.* (Ponçot *et al.*, 2015) have conducted simultaneous Raman spectroscopy and high energy wide angles X-rays scattering (HE-WAXS)

during uniaxial tensile in combination with a videotraction system of different polypropylene blends to characterize the structural polymer micromechanism under the real mechanical behavior. The multitechnique approach revealed a systematic correlation between the WAXS and Raman spectroscopy mechanism of orientation of the polymer nanostructure was found. However, WAXS orientation factors were found to be more sensible under low strain regimes whereas chain orientation ratio detected by Raman spectroscopy were more accurate at high strains values, highlighting the importance of the combined study on the same sample volume.

The coupling of SAXS with Raman spectroscopy (Haas *et al.*, 2014) has been employed to study the dispersion properties of single-wall carbon nanotubes (SWNTs) in sodium dodecyl sulfate (SDS). The multiprobe environment (UV-Raman spectroscopies) has been controlled using an interface build with Python on SPEC (Certified Scientific Software) allowing the simultaneous triggering of both X-ray scattering and Raman spectrometer. Remarkably, the fitting of the SAXS profiles has been assisted by the Raman spectra by obtaining a proportional total number density of SWNTs as a function of the SWNT concentration from both SAXS and Raman data.

Summarizing, great efforts have been devoted to the combination of scattering techniques with spectroscopic methods, in particular, vibrational techniques, to cover the structural transformations at different length scales and to establish the driven force between the morphological transitions and the chemical conversions. Consequently, large amounts of data are generated that are tedious to analyze with slight temporal shifts if different techniques are not integrated under the same control unit. Moreover, acquisition time per frames will tend to differ among techniques sensitivities with the advent of new sources at synchrotron radiation facilities, highlighting the requirement of technical control on the triggering, acquisition, and files recording to avoid time discrepancies among variables under study.

Importantly, the correlation of the variables of a complex system that define the structural transformations obtained from multiple techniques, particularly in the present study, WAXS, SAXS and Raman spectroscopy as a function of temperature, is crucial to relate ambiguous or/and unclear correlations among the crystallinity, long period, conformational changes and phase transition. Generally, data analysis is focused on an area of interest of the spectra in which evident changes are observed and compared to other techniques data, missing hidden cross-correlations to the naked eye in the complete range of the recorded data. Particularly, Raman spectra analysis typically consist in the deconvolution to a Voigt function (Sundius, 1973) (Palmö *et al.*, 1988) of the Raman band (Lorentz-Gaussian outline) pre-processed by correcting the raw data with a baseline, smoothing and normalizing the spectra to an independent band of the process under study. However, the analysis subjectivity introduced on the normalization and deconvolution inaccuracy of superimposed Raman bands entails generally tedious data treatment and previous insightful knowledge about the Raman modes. A detailed assessment of the quantification of polybutadiene content in polystyrene by Raman spectroscopy using both band fitting or chemometrics methods has shown the simplicity to obtain higher reproducible and consistency results by chemometric procedures.(Brun, Bourson *et al.*, 2013)

Multivariate analysis (MVA) is a chemometric procedure defined as a statistical method used to study complex sets of data that contain more than one variable, in particular the Principal

Component Analysis (PCA). Consequently, MVA across PCA assists to extract additional information from the data, especially in the case of very complicated phenomena and/or very weak changes. MVA have been largely employed in the spectroscopic field (Chapron *et al.*, 2019). However, it has been scarcely applied to examine different parameters obtained from scattering techniques combined other different measurement as inverse gas chromatographic (Voelkel *et al.*, 2006), SAXS/UV-vis (Haas *et al.*, 2014; Caetano *et al.*, 2017), SAXS and high performance anion exchange chromatography using pulsed amperometric detection (HPAEC-PAD) (Sanderson *et al.*, 2006). Furthermore, chemometrics models has been rarely exploited to analyze the polymer transitions upon processing conditions. The importance of the spectral data pre-treatment by the adequate algorithm to correct the experimental artefacts has been (Witschnigg *et al.*, 2010) evaluated with different material state (melt state to semi-crystalline solid state) and polymer postprocessing procedures (cooling down, heating up, ...) on the applied chemometrics model (PCA, partial least squares (PLS)). The choice of a suitable spectral range of interest to apply the chemometric model has been found to be crucial to observe negligible variations not noticeable at first sight by the naked eye. Particularly, the crystallization mechanism at quiescent conditions of molten poly(3-hydroxybutyrate) (PHB) has been analyzed in detail by MCR and both homospectral and heterospectral 2DCOS to reveal the sequential order of the multistep crystallization procedure.(Guo *et al.*, 2012) Accordingly, simultaneous time-resolved SAXS/WAXS experiments have been conducted at DUBBLE, using Linkam calorimeter stage in combination with Raman spectroscopy with fine temperature control in a reproducible, versatile and simple setup. The attribution of phase transition and the understanding of the crystallization mechanism has been achieved by a multi-technique approach to correlate the organization of the polymer chains during the crystallization from a molecular level to its nanostructure. The polymer crystallization thermodynamics is generally studied by thermal techniques, and thus, the temperature control under the influence of the combined X-ray beam and laser probe on the sample is crucial to affect the sensitivity the Linkam device thermocouple. Consequently, it has been designed a combined Raman spectroscopy with time-resolved SAXS-WAXS setup coupled to the Linkam calorimetry stage in which the scattering detectors and Linkam stage are controlled under a permanent connection in parallel of all detectors and the Linkam simultaneously to avoid time uncertainties. Moreover, rigorous calibrations of the Linkam calorimeter stage with the Raman laser and the X-ray beam has been conducted to compare reliably the results to a standard DSC. Finally, the data generated by the different techniques (WAXS, SAXS and Raman spectroscopy as a function of temperature) will be correlated by applying the MVA data analysis. The multitechnique simultaneous analysis of the mechanism crystallization upon cooling from the melt will be applied to a high molecular weight PVDF blended with a fluoroelastomer. A multiprobe and detailed post-analysis approach is required to monitor the structural similarity as well as the physical impediments due to the high molecular weight interfere with the identification of the complex nanostructure under development with narrow temporal transitions.

Time-resolved simultaneous SAXS and WAXS experiments coupled to a Linkam calorimeter stage have become a routine technique at the synchrotron light community. The Raman probe was fitted with a focal lens and located in an angle to avoid disturbing the optical path of the

scattering X-rays as well as reduced the air gap to minimize the background during the X-ray acquisition (Figure 3.1A shows a global picture of the multi-technique setup, a magnification of the sample holder is seen in Figure 3.1B). The Linkam calorimeter-stage was placed vertically to measure by simultaneous SAXS/WAXS in transmission mode whilst the Raman probe was located in the exit window side, measuring in reflection mode.

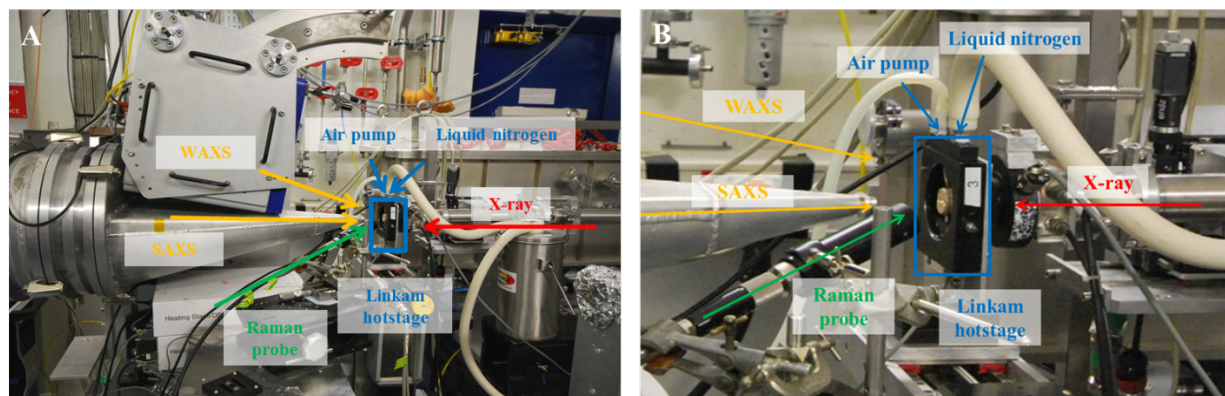
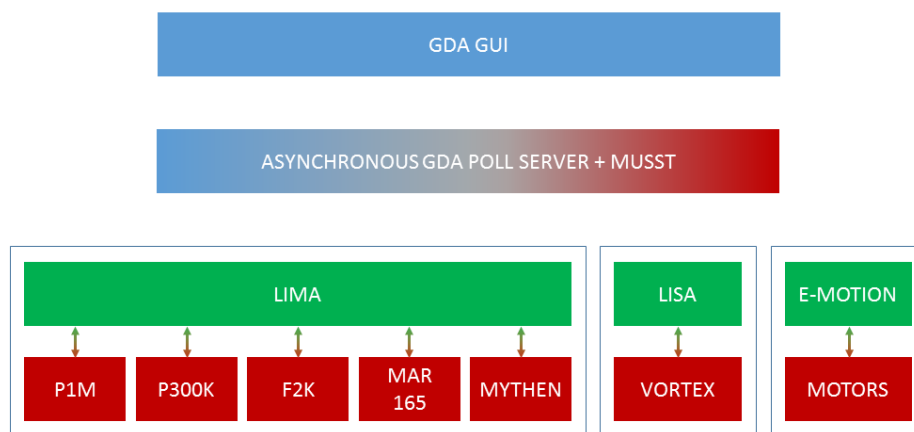


Figure 3.1. Simultaneous SAXS/WAXS combined to both Linkam DSC and Raman spectroscopy setup at DUBBLE (BM26b, ESRF) (A) and a magnification of the sample environment (B).

The experimental control of the combined DSC Linkam and X-ray scattering instrumentation has to be harmonized to assign the thermal changes to the corresponding scattering patterns due to the different technical sensibilities. A Permanent connection in parallel of all detectors simultaneously has been established by the Multipurpose Unit for Synchronization, Sequencing and Triggering (MUSST) electronic module as central unit (see Figure 3.2). The MUST unit is fitted with an internal timer that it is independent and very flexible for triggering and synchronizing different beamline components and user hardware such as the Linkam DSC. In addition, the MUST built-in data storage capability can be used as data acquisition unit in combination with other techniques with different experimental parameters. Moreover, MUST unit offers the asynchronous periodic polling up to sub-millisecond resolution over extended period. In a typical experiment, the user has to generate a configuration file with the thermal protocol and launch the experiment with the selected acquisition times for the detectors. The system will write into the header of each image the corresponding thermal data as well as a file containing the DSC data with millisecond resolution time. Furthermore, new versions of the acquisition systems will allow the motion integration and different devices (like Linkam) into a Gui (GDA) in order to program several devices in sequential experimental order.



GDA software  
Tango control system  
Hardware

Figure 3.2. Schema of the MUSST module as central unit in parallel of all detectors simultaneously link to the GDA Gui.

The versatile experimental procedure has been optimised to standardize efficiently the instrumental protocol and transfer it to DUBBLE community as well as couple it to another sample environment. The versatility to combine Raman spectroscopy with other techniques compare to FT-Infrared spectroscopy is mainly due to capacity to adapt the instrumentation to optimize the Raman spectra to the sample response. The components of the Raman spectrometer such as the laser wavelength (532 nm lasers for higher sensitivity or resonance enhancement, 633 nm lasers for cost effective solutions, 785 nm lasers for sample fluorescence suppression) and power (100-400 mW) can be tuning. Particularly, the flexibility of the probe that is fitted with a few meter fiber optics for both the incident laser beam and the back-scattering Raman radiation due to the wavelength employed falls in the visible light range. Moreover, the probe can feature focal lens that allows position distantly to the Raman spectrometer and the sample, enhancing the adaptability to combine Raman spectroscopy to a broad range of sample environments. Thanks to technological innovations of the Raman spectrometer components such as the laser, Notch and Edge filters, introduction of CCD detector, the acquisitions times are faster and compatible with synchrotron measurements, a few seconds are enough for a good quality spectrum. A probe lens with a focal length of 5 cm was arranged with angle of approximately 60 °, minimizing the sample to the flight tube distance and thus, the air scattering background (see Figure 3.1). The Raman spectra acquisition was synchronized remotely from the control cabin via the spectrometer computer. Moreover, the effect of the laser on the sample temperature and DSC profile has been assessed to avoid influencing the temperature reading, which is crucial to understand polymer crystallization and correlate it with offline measurements. Generally, spectrometers feature a shutter for the incident laser to obtain a better signal/noise ratio synchronized with the shutter aperture. An oscillating DSC signal with a superposed frequency associated to the opening shutter period was obtained (see Figure 3.3 a) when the laser shutter was on due to the intermittent laser

heat impinging on the sample whilst the deactivation of the laser shutter yields a constant DSC signal (see Figure 3.3, b).

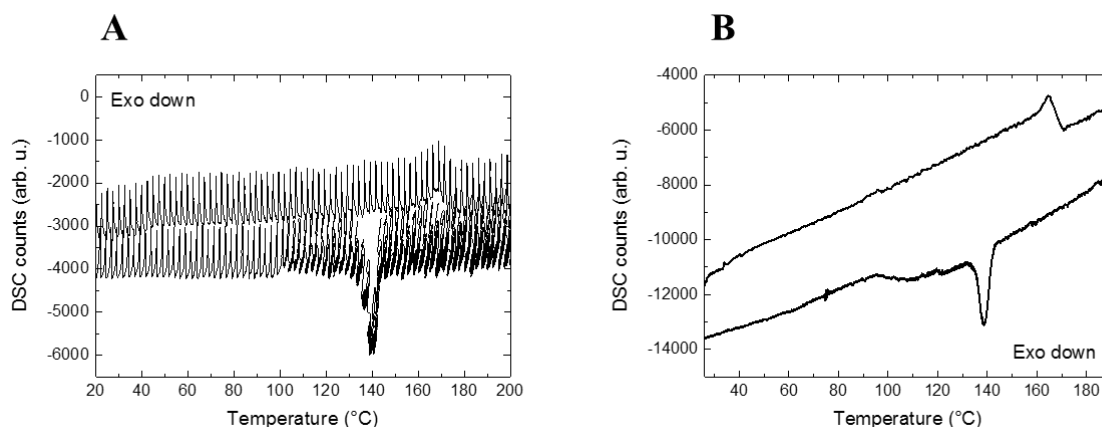


Figure 3.3. Linkam DSC profile of the cooling and second heating ramps of the PVDF sample during the simultaneous SAXS/WAXS couple to the Linkam DSC combined with the Raman spectrometer with the activated laser shutter (left) and with the deactivated laser shutter (right).

However, an output laser power of 150 mW has been selected to minimize the laser heat transfer to the sample and a calibration of the DSC temperature has to be conducted to account for both the X-rays and Raman laser on the sample temperature. The laser wavelength of the spectrometer is also a parameter that can be tailored. Commercial Raman spectrometers fitted with lasers of 532 nm and 785 nm are available and can be switched depending on the sample response. Laser wavelength of 785 nm are generally most suitable for obtaining good quality spectra to avoid the fluorescence effect (related to the aspect/color of the samples). The aspect of most of the polymers are normally white/yellowish, leading to potentially fluorescence effects on the spectra, and thus, a near infrared (IR) laser wavelength (785 nm) have been used.

Moreover, the focus of the laser beam into the sample permits to control the volume of the sample illuminated as well as the penetration by laser Gaussian-shaped beam. The beam size and penetration of the laser are parameters required to correlate the obtained data by diverse techniques with comparable sampling methodologies, consequently extinguishing the surface effects of the sample (skin effects). The waist dimension is a beam parameter that determine the amplitude of both the electric and magnetic field a long of a Gaussian beam at the focal point. The selected focal distance of 5 cm in the current experimental corresponds to a waist dimension (Long, 1977) of  $d = 20 \mu\text{m}$  and  $L = 2.1 \text{ mm}$  obtained by the following equation:

$$d = \frac{4\lambda f}{\pi\phi} \quad (1)$$

$$L = \frac{16\lambda n f^2}{\pi\phi^2} \quad (2)$$

Being  $d$ , the diameter of the convergent lens,  $\lambda$  the wavelength of the laser (785 nm),  $f$  the focal distance (5 cm),  $\phi$  the output laser beam diameter (2.6 mm, measured by the “razor blade”)(Chaudemanche, 2013; Kimura & Munakata, 1987),  $L$  the convergent lens distance and  $n$  the refractive index (1.42 for neat PVDF), the sample thickness was 0.8 mm. The selected

laser beam parameters permitted to probe throughout the sample to suppress the skin effect and surface orientation. In addition, a blank spectrum without the laser on is acquired to avoid instrumental noise and to improve the quality of the recorded spectra. However, the absorption depth and propagation of the laser beam through the material produces undesirable secondary effects related to the material response. Mainly, heat transfer to the samples occurs, the so-called photothermal effect is generated by laser beam when the energetic excitation rate of the material is slower to the thermalization time (Brown & Arnold, 2010). Typically, polymers are characterized in lower part of the thermalization times, in the order of  $10^{-6}$  seconds. Moreover, photodecomposition can be produced if the excitation energy is analog to the bond energy. Similarly, X-ray interacts with the matter (Portale *et al.*, 2016a; Bras *et al.*, 2014), producing photoelectrons that can enhance the crystallization rate of materials, the growth of nanoparticles as well as material damaged at restrained X-ray fluxes as well as increasing the temperature by  $3,4 \text{ Ks}^{-1}$  in adiabatic approximation. A compromise between the dose of both the laser and X-ray beam and the detrimental secondary effects need to be considered to design experiments with the correct time resolution of the structural and chemical process under study. Consequently, a calibration of the sample temperature in the coupled techniques experiment was conducted to correct both the X-ray and laser beam (785 nm) effects on the DSC thermocouple reading. The melting point of different well-known standards (Nylon, indium, benzoic acid, PVDF). have been used to cover the linearity response of the instrument in the temperature range under interest (see calibration curve in Figure 3.4).

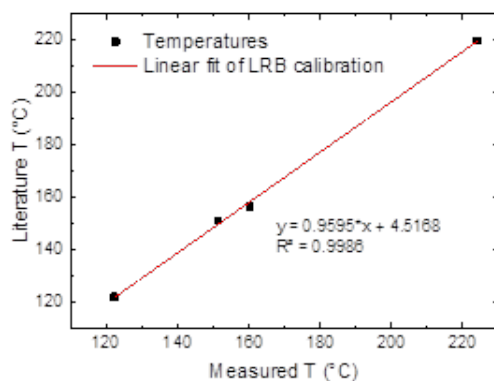


Figure 3.4. Calibration curve obtained under the simultaneous influence of both X-ray beam and Raman laser (785 nm) measured by the Linkam DSC-stage.

Likewise, the temperature recorded in the header of every single SAXS and WAXS frame as well as Raman spectra is amended accordingly to correlate the thermodynamic transformation to the precise real temperature and to compare the measurements with other offline measurements. Moreover, the effect on the thermocouple reading and the material response of the laser beam impinging the sample has been evaluated individually to assess both the temperature fluctuation as well as the impact on the Raman spectra quality that would be related to damage effects by other techniques. The quality of the in-situ Raman spectra acquired in the experimental coupled with X-ray scattering and Linkam DSC techniques has been compared with the data obtained by combining a standard DSC and the same Raman spectrometer with a laser beam wavelength of 785 nm.

### Validation of the Raman spectra quality by comparison to the DSC-Raman

A thermal protocol with identical ramp parameters has been carried out for PVDF Kynar 740 blended with a fluoroelastomer by using 3 different experimental setups to validate the temperature acquisition by either the in situ Linkam DSC combined with both Raman spectroscopy and X-ray scattering techniques or the combined DSC-Raman using a Q200 TA Instrument (Veitmann *et al.*, 2015) and a single measurement in a Q200 TA Instrument DSC as a reference. A comparison of the amended thermograms with the corresponding calibration curve has been plotted as a function of the cooling temperature. A slight deviation has been found for (see Figure 3.5) the crystallization temperature (138.7 °C, 138.1 °C and 139.5 °C) even for the corrected temperatures of the respective different experiments. The minor temperature difference between the three crystallization temperatures can be explained by the difference of experimental error sources. The temperature discrepancy highlights the advantages of combined techniques to obtain equivalent thermodynamic conditions and compare the data to other independent measurements.

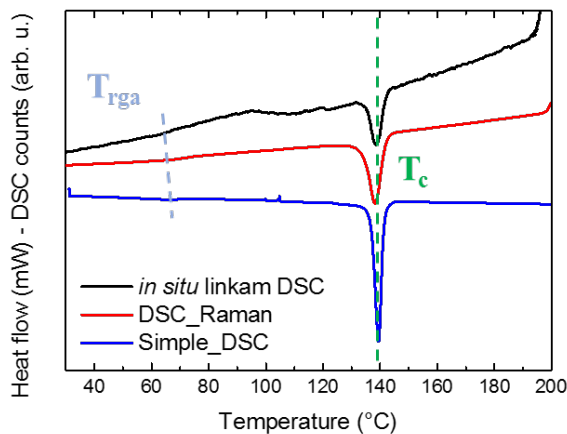


Figure 3.5. Comparison of the thermogram obtained from Linkam DSC, the Q200 TA DSC-Raman and a single Q200 TA DSC profile.

### Results

The correlation of the complementary data acquired by time resolved simultaneous SAXS-WAXS experiments coupled to the Linkam DSC stage in combination with Raman spectroscopy to study the crystallization from the melt of PVDF (Kynar 740) blended with a fluoroelastomer are briefly discussed. The nanostructure of PVDF has been largely investigated by X-ray scattering techniques as well as by Raman spectroscopy to tailor a broad range of applications in a variety of different industrial fields such as offshore pipes, construction materials, healthcare and pharmaceuticals (Ameduri, 2009). PVDF is semi-crystalline polymer that crystallize in several crystalline phases defined by different chain configurations, namely  $\alpha$  (TGTG'),  $\beta$  (TTTT), and  $\gamma$  (TTTGTTG') phases. However, PVDF crystallize from the melt mainly in the  $\alpha$  phase at moderate quenching temperatures and extremely high quenching temperatures or blending with other polymers such as PMMA, are required to obtain the desired electroactive  $\beta$  phase. PVDF has been blended with several polymers and inorganic fillers to enhance its properties. However, the effect on the crystallization of PVDF by the addition of fluoroelastomer has slightly examined yet. The multi-technique approach to

monitoring the crystallization of the PVDF/fluoroelastomer blend benefits the interpretation of complex and faint structural transformations by the complementary simultaneous information related to different chemical sensibilities and length-scales. The  $\beta$ -phase quantification for instance, is a challenging task at low contents by WAXS measurements due to the broad profile of the reflections and the superposition with the amorphous phase. Similarly, Raman spectroscopy cannot rigorously quantify the amorphous phase due to overlapping with the  $\alpha$ -phase, but is very sensitive to the  $\beta$  phase instead.

Moreover, a weak structural transition observed at 70 °C upon cooling has been controversially (Leonard *et al.*, 1984; Loufakis & Wunderlich, 1987; Nabata, 1990; Teyssedre *et al.*, 1993) assigned to the rigid amorphous phase densification. The mechanism of crystallization upon cooling from the melt (200 °C) to room temperature (25 °C) of the blend fluoroelastomer/PVDF the long period evolution and the crystallinity have been monitored simultaneously by SAXS (Figure 3.6A) and WAXS (Figure 3.6B) respectively, as a function of temperature. WAXS measurements have probed the transformation from the amorphous to the  $\alpha$ -PVDF phase represented by the characteristics main reflections at the scattering values ( $q$ ) of 12.6 nm<sup>-1</sup>, 13.1 nm<sup>-1</sup>, 14.2 nm<sup>-1</sup> and 18.8 nm<sup>-1</sup> that correspond to the (100), (020), (110) and (021) (hkl) planes of the monoclinic PVDF phase (pseudo-orthorhombic) (Loving, 1982), respectively. Note, WAXS requires a minimum of crystallinity (1% in polymer study (Wang *et al.*, 2000)) to produce at least one diffraction reflection. Moreover, the nanostructure parameters of the two phase lamellar system with diffuse boundaries has been The evolution of long period, crystallinity content, lamellar thickness and molecular conformation as a function of temperature during the crystallization from the melt of the blend PVDF/fluoroelastomer has been determined (see Figure 3.7) .

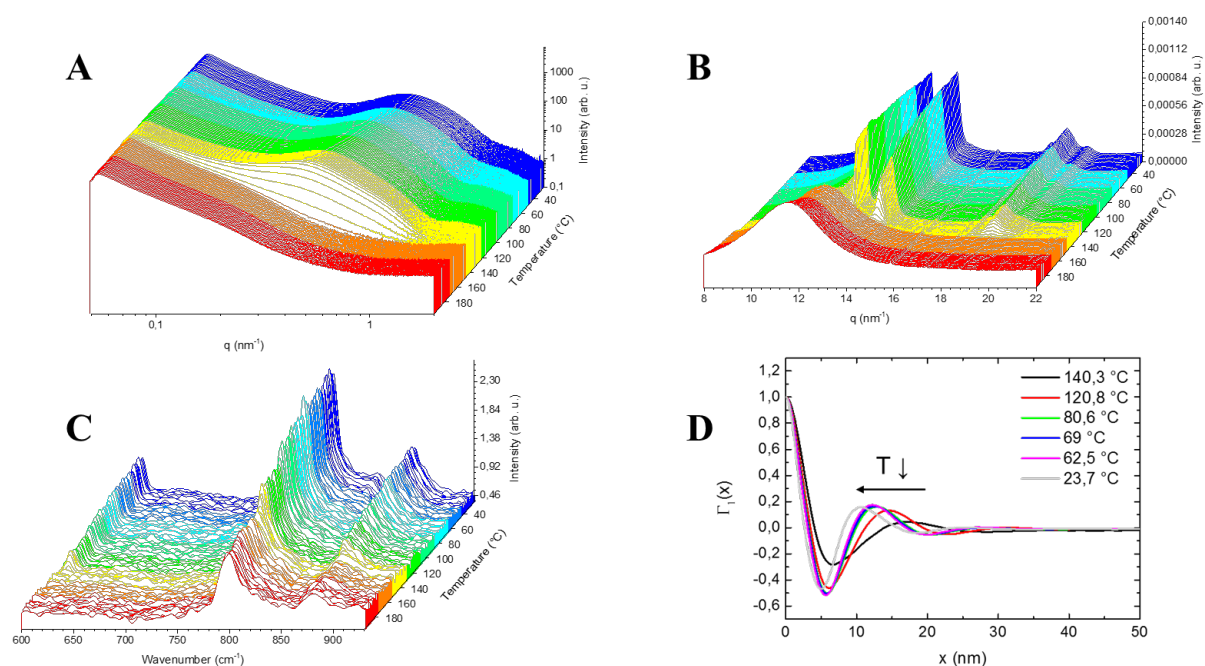


Figure 3.6. 3D plots of the time-resolved SAXS (A), WAXS (B) patterns and Raman spectra (C) obtained in the *in situ* Raman spectroscopy combined with SAXS/WAXS coupled to the Linkam DSC setup, during the cooling step from the melt to RT of the blend PVDF/fluoroelastomer

sample. Raman spectra from the Q200 TA DSC-Raman combined measurement (D) Validity of the in-situ Raman spectra quality of the blend PVDF/fluoroelastomer sample. The colour code in the 3D plot corresponds to a temperature range related to  $\Delta T = 21.6$  °C, in order to distinguish properly the evolution of the structural parameters upon temperature. The black arrows in the Raman spectra (C, D) correspond to the band position of the  $\beta$ -phase of the PVDF sample.

Raman spectroscopy is known to be sensible to phase variation in PVDF ( $\alpha/\beta$  ratio) (Veitmann et al., 2015). Indeed, the vibrational bands at  $796\text{ cm}^{-1}$  and  $840\text{ cm}^{-1}$  of the  $\alpha$ -phase (Kobayashi et al., 1975; Nallasamy & Mohan, 2005; Boerio & Koenig, 1971) corresponding to the rocking vibration mode  $r(\text{CH}_2) - \nu_s(\text{CF}_2)$  and  $r(\text{CF}_3)$  (Yang et al., 2014), respectively, are monitored as a function of temperature (see Figure 6C). Initially, at the melt ( $200$  °C) a broader band found slightly shifted to the the  $\alpha$ -phase, centered at  $799\text{ cm}^{-1}$ , correspond to the rocking vibration mode of the amorphous phase of the PVDF. Note that the identification and quantification of the PVDF amorphous phase is complicated by Raman spectroscopy as the characteristic band of amorphous phase of PVDF is convoluted with the band of the  $\alpha$ -phase at  $796\text{ cm}^{-1}$ . However, as the temperature decreases the broad band become thinner due to standstill of the vibration group  $r(\text{CH}_2) - \nu_s(\text{CF}_2)$ , the transition between amorphous to crystalline phases and the phase change will be analyzed more in detail by MVA. According to the Rama spectra, the chain conformation ( $\text{TGT}\bar{\text{G}}$ ) of crystalline phase monoclinic (pseudo-orthorhombic) form polymer blend (PVDF/fluoroelastomer) remain unchanged during the crystallization confirming the  $\beta$ -phase absence revealed by WAXS. The integrated value of the characteristic  $\alpha$ -vibration band ( $785 - 815\text{ cm}^{-1}$ ) has been plotted (see Figure 3.7), to compare all in situ data obtained (Xc, Lp, Q and  $\alpha$ -peak vs T). The slow increase of  $\alpha$ -peak before  $T_c$  compare to x-ray data (Lp, Xc and Q) suggest that the crystalline phase at a crystallinity  $\leq 1\%$  (WAXS detection limits) can be detected by Raman spectroscopy.

The crystallization temperature observed to the Raman spectroscopy is about  $139$  °C due to a shift of the broad to thinner band center at  $796\text{ cm}^{-1}$  representative of the  $\alpha$  crystalline phase, confirming the value from the Linkam DSC  $138.7$  °C (see Figure 3.5). Explication of the small difference will be explained in another part of the paper. In order to have the less possible difference between each machine a calibration curve have been elaborate according to literature melting point of standard materials.

Another point should be check, the quality of the in-situ Raman spectra. As explained previously, a combined DSC-Raman measurement has been conducted in order to verify this point. In Figure 3.6D, the 3D plot of the Raman spectra from this measurement done in the same condition than the in-situ Raman spectra is shown. The same trend and peaks are observed and present, respectively. The only difference is the smoothness of the spectra in the DSC-Raman spectra due to the background experiment. The data are comparable meaning that the in-situ Raman is of quality to follow the evolution of the characteristic peaks of the PVDF sample.

Further in detail SAXS analysis of the isotropic two-phase system (Ryan et al., 1994), as the case for the blend PVDF/elastomer (amorphous and crystalline phase) was achieved by the invariant  $Q$ , also known as Porod's invariant (Glatter & Kratky, 1982). The invariant  $Q$  is related to the

electron density fluctuation between the two phases, during phase transformation and can be express by the given equation (3):

$$Q = \int_0^\infty q^2 I(q) dq \propto 2\pi\Phi(1-\Phi)(\rho_c - \rho_a)^2 \quad (3)$$

Where  $I(q)$  is the scattering intensity, and  $q$  is the scattering vector. In the second term of the equation (3),  $\Phi$  and  $\rho_a$  are the volume fraction and the electron density of the amorphous phase, and  $(1-\Phi)$  and  $\rho_c$  are the volume fraction and electron density of the crystalline phase. The evolution of the invariant as a function of temperature (see in Figure 3.7) shows the phase transition at 140 °C (inflexion point determined by derivative, available in SI) that corresponds to the crystallization of the PVDF sample, described by an increase of the electron density of the crystalline phase. Moreover, the drop of the invariant at 69–70 °C (inflexion point determined by derivative, available in SI), suggest the compaction of the rigid amorphous part. The invariant is sensible in an evolving system to changes in the composition up to 50 vol. % ( $X_c$  PVDF sample max 51%, calculate from WAXS) when a maximum is reached, and inversion of the invariant will be observed.

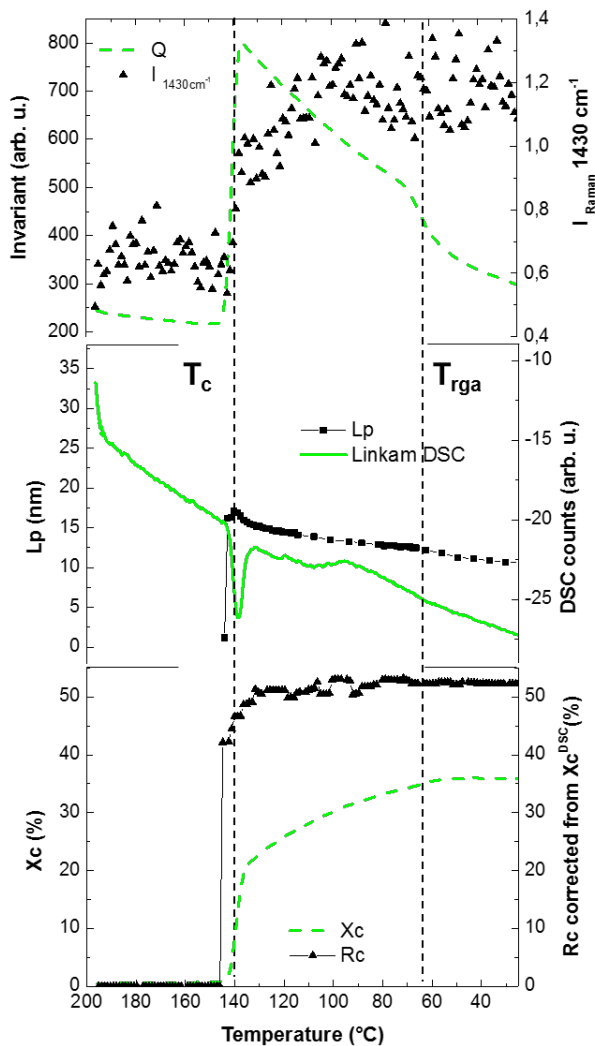


Figure 3.7. Porod's invariant, crystallinity ( $X_c$ ) and long period evolution as a function of temperature during crystallization from the melt (200 °C) of PVDF sample. The dash line ( $\approx 145$  °C) indicates the crystallization transition ( $T_c$ ) and the dash line ( $\approx 70$  °C) the transition of the rigid amorphous compaction ( $T_{rga}$ ).

### **Correlation data: chemometrics**

The PCA is a reduction method of the original data using an orthogonal transformation to convert the data into linearly uncorrelated data, the so-called principal component (PC) to represent the largest variance possible. An advantage of the use of PCA analysis on low quality data is to be able to extract the data separating it from the noise. PCA was used to transform of the different measured variables into a data matrix that represent the relationship between crystallinity, long period and vibrational mode as a function of temperature. The data matrix is reduced by PCA to scores and loadings. The scores are the weights of the spectra/scattering profiles (here) in the different dimensions (PC), and the loadings are the representation of coefficients of the linear combination of the initial variables (here, the Raman band, or the scattering vector  $q$ , that indicate also the percentage of the variance attributed to each PC. The PCA has been applied to the crystallization from the melt to the Raman spectra and from the crystallization temperature to room temperature as the crystallization event cover the entire vector variance.

## 4-Controlling of fibrillization for drug delivery.

---

During my research, I have largely worked in the supramolecular field in collaboration with several groups across Europe in order to understand the structure-activity relationship and the gelation process that drives the self-assembly of potential gelators into gels. Gelation is not fully understood and the majority of gels are found serendipitously. However, it has been established that gelation is mainly controlled by the gelator design, gelator concentration, gelation conditions and solvent effects. Attempts to understand the molecular assembly of the gelators into molecular-scale fibrils and the subsequent hierarchical organization of the fibrils into spanning network that percolates the solution by fibril-fibril interaction has also been investigated. Particularly, I have investigated the important factors that control the fibrillization mechanism that in turn, govern the gelation process from a low molecular hydrogelator that forms monodispersed fibers and has been reported in the following manuscripts.

1. Francisco Rodríguez-Llansola, Beatriu Escuder, Juan F Miravet, Daniel Hermida-Merino, Ian W Hamley, Christine J Cardin, Wayne Hayes: Selective and highly efficient dye scavenging by a pH-responsive molecular hydrogelator. *Chemical Communications* 11/2010; 46(42):7960-2., DOI:10.1039/c0cc02338h
2. Hermida-Merino, D., Trebbin, M., Foerster, S., Rodriguez-Llansola, F. and Portale, G.; *“Microfluidic Assisted Self-Assembly of pH-Sensitive Low-Molecular Weight Hydrogelators Close to the Minimum Gelation Concentration”*; *Macromol. Symp.*, (2015), 358: 59–66. doi: 10.1002/masy.

The physical characteristics of the low molecular hydrogel have triggered me to apply successfully for a visiting scientist grant in 2016 at the University of Castilla la Mancha, (1<sup>st</sup> classified) to the Pharmacy school in order to study the possibility to employ the nanofibers as nanocarriers for drug delivery applications.

Bioinspired supramolecular hydrogelators are great candidates to be employed as drug carriers as a result of their biocompatibility and capability to uptake and release specifically host molecules upon external stimuli. Drug uptake generally requires several steps and/or to covalently attach the nanocarrier resulting in inefficient industrial process to scale up. One pot passive loading of Doxorubicin by an urea-derivative hydrogelator (**HG1**) was efficiently achieved by physical interactions attaining an impressive loading rate of DOX/HG1 molecules. The viability cell study confirmed the harmless impact of **HG1** in healthy cells crucial to be applied as drug nanocarrier. Hydrogels were recently identified as ideal therapeutic local administration methodology in complex human anatomies after tumour resection due to their mechanical and adhesion properties. Particularly, glioblastoma multiforme is highly lethal tumour that is mainly treated by surgery resection and subsequently with local drug administration. However, recent studies showed limited therapeutic efficacy and local application of Doxorubicine by injection of loaded hydrogel is a great candidate to enhance

the controlled drug release in the resection cavity. Molecular release profile studies monitored the Doxorubicine regulated from the DOX discharge upon pH change from the internal fibre structure. Moreover, in vitro cells monitored the corroborated the therapeutic release efficiency whilst minimising the harmful side effects on healthy cells. Fluorescence lifetime studies on in vitro cells followed the release mechanism at the cellular scale of both DOX solution and DOX loaded in **HG1** formulations, confirming the molecular DOX release process described outside the cellular media. Fluorescence lifetime imagin probed the intracellular DOX release by both formulations (DOX solution and DOX loaded in **HG1**), highlighting the differences on the timescales and cellular pharmacological route traverse by DOX transported by **HG1**.

The design of ideal nanocarriers is a synthetic challenge that has to fulfil concomitantly ambivalent physical requirements. Bio-inspired smart materials that accomplish specific functions in complexes and dynamic environments represent a continuous synthetic challenge. The design framework required to conceive novel materials that feature targeted activities depends mainly on the structure-property relationship. Moreover, responsive smart materials to specific external stimuli involve subsequent structural developments in a dynamic media that introduce higher complexity.

Hydrogels are typically generated by the fine balance of self-assembled amphiphile monomers that can interact through covalent bonds, by noncovalent interactions or by a combination of both. The driven force that defines the internal structure of physical hydrogels together with the aqueous media equilibrium determines also the supramolecular assembled structures generated such as fibres, micelles, or ribbons. Among all, hydrogels based on small molecules or low-molecular-weight-hydrogelators (LMHG), are remarkable candidates to design responsive materials due to the dynamic nature of the non-covalent interactions that can be typically triggered by external stimuli (temperature, concentration, pH, light, salts concentration, etc).<sup>1-7</sup> Particularly, the structural complexity requisite of drug nanocarriers arise from the sequential multi functions achieved involved in different chemical media. The specifically drug upload must be efficient an, limiting the synthetic steps as well as avoiding the pharmaceutical compound damage. Moreover, the nanocarrier transport should enable the drug transference through the cellular membrane. Furthermore, the drug administration route define the initial nanocarrier mechanical properties. In addition, the therapeutic drug release must satisfy a regulated kinetic profile that minimise the pharmaceutical dosage and target the tumour cells. Importangly, pH responsive physical hydrogels combine the reversibility interaction capacity to specifically load and upload the therapuatic agents at human revelant pH and offers the mechanical characteristics to attain complex human anatomies to target explicit tumours.

Particularly, Glioblastoma multiforme (GBM) is the most common and aggressive of the primary brain tumours developed in adults. GBM appears firstly on the glial human cells and infiltrates diffusely into the unaffected surrounding parenchyma. Despite the relatively low incidence, 3.19 per 100,000 people per annum, the median survival of GBM patients is only approximately

12-18 months, and merely 10% of them currently survive for more than 5 years. The early and distant dissemination of malignant cells renders GBM a surgically incurable neoplasm.<sup>8</sup> Aggressive resection surgery increases survival time in patients, however, recurrences occur 1-1.5 years after initial therapy.<sup>9,10</sup> After resection, GBM patients generally follow the standard treatment: external beam radiation around the original tumour plus oral temozolomide (TMZ) daily.<sup>11</sup>

Among the main challenges of GBM treatment, the difficulty of drug delivery to the tumour results in an insufficient amount of the most drugs at the site of action (f). The presence of the blood brain barrier (BBB) constitutes the main obstacle for the systemic treatment of brain tumours in general and GBM in particular. An increasing demand urges to develop novel strategies able to both enhance the drug efficiency and reduce the adverse side effects without affecting normal tissue(g).

Currently, novel therapeutic agents fail to show clinical relevance in the treatment of GBM, due to their toxicity or chemoresistance and therapeutic approaches focus on local delivery of therapeutic agents after surgery resection rejection emerges as an effective alternative.<sup>12</sup> Local therapeutic agent delivery provides tumour cells targeted exposure to high drug concentrations, minimising systemic healthy tissue damage as well as preventing the growth of cancer cells unattainable by surgery resection (j). Specially, FDA has approved the application of Gliadel® wafers as post-surgery medical care, supporting the therapeutic local interstitial treatment of antitumour drug to avoid the cancer recurrence.<sup>13</sup> However, Gliadel® has shown poor and controversial results compared to the standard medical treatment from marketing approval.<sup>13,14</sup> Particularly, the drug loading and the rigidity of the wafer structure limits the therapeutic efficiency into the anatomy of the resection cavity. Hydrogels have been largely proposed as candidates for drug delivery systems and potentially substitute films due to their mechanical properties. Indeed, hydrogels can be sufficiently loaded with the appropriate drug therapeutic dose and administered locally in the <sup>16</sup>brain after a craniotomy via intracerebral implantation injection. Moreover, hydrogels have enough adherence capacity to stick to the cavity borders, covering an optimized area under treatment. Hydrogels were employed as drug delivery systems in the treatment of GBM, and in particular, a PLGA-based hydrogel, OncoGel™ was successfully tested as an adjuvant to radiation therapy.<sup>17,18</sup> Recently, photopolymerizable hydrogels enable to TMZ delivery have shown a significantly decreased in the tumor growth in mice treated compared to controls.<sup>19,20</sup> In addition, a GBM xenograft model have shown the inhibition of tumour growth by the application of Doxorubicin (DOX) loaded in Mebiol™Gel, a thermoreversible polymeric gelator which is biocompatible and non-cytotoxic.<sup>21,22</sup> Doxorubicin (DOX) is successfully employed in the treatment of several solid malignant tumours such as X.<sup>23</sup> However, high doses of DOX were required to be systemically administered to exert a therapeutic benefit.<sup>24</sup> However, the pharmacologic DOX systems currently under study feature drug carrier limitations such as low drug loading, short retention time, and thus, a rapid burst release was typically found.<sup>24,25</sup> Moreover, DOX is unable to penetrate efficiently the central nervous system (CNS) due to the blood brain barrier restraining the application for GBM treatment (i).

Previously, a non-peptidic mono urea derivative hydrogelator (**HG1**) displaying the ability to intercalate selectively planar and positively charged guests into its negative charged structure was proven to load DOX (Figure 4.1a). Moreover, **HG1** possesses a significant low minimum gelation concentration, indicating the percolation of the network formed by the self-assembled **HG1** aggregates at low monomer ratio. The triggering of the highly monodisperse **HG1** fibrillation is achieved by a fine pH change whilst maintaining constantly a low supersaturation point. The well-controlled uptake mechanism of guest molecules during fibrillation is an key **HG1** feature to both diminish the uptake process time and enhancing the uptake capability whilst preserving the mechanical properties.<sup>3</sup> In general, **HG1** combines ideal physicochemical characteristics to be a promising drug delivery system for local therapeutic agent delivery in the GBM treatment. In the present work, the therapeutic transport performance of **HG1** as nanocarrier for the local DOX delivery in the treatment of GBM is assessed. Importantly the planar molecular structure of DOX facilitates the molecular encapsulation by the intercalation with **HG1** molecules due to structural similarity and the possibility to interact through non-covalent bonds. Moreover, the passive loading of the hydrogel, the temperature dependence of the formulations as well as the interaction of DOX molecules with the hydrogel monomers within the network were evaluated. The DOX passive uptake mechanism and kinetics during the **HG1** fibrillation process is controlled by the slow acidification produced by the hydrolysis of glucono- $\delta$ -lactone (GDL). The controlled pH change by the GDL addition to the **HG1** solution generates a unperturbed homogeneous nanofibrillation that promotes the uniform drug uptake/release throughout the entire volume at the nano length scale. Moreover, the biocompatibility of unloaded **HG1** was tested in non-tumoral cells. Glioma cell lines C6 and U87 were selected as *in vitro* models for GBM and cytotoxicity of DOX-loaded **HG1** was evaluated. Remarkably, the *in vitro* responsive behaviour to pH stimuli of DOX release profiles were found to be comparable to pharmacological standards at acidic and physiological values. Finally, DOX release profile in the glioma cell line C6 as well as the DOX distribution inside cells was evaluated by confocal and fluorescence lifetime microscopy. Notably, DOX-loaded **HG1** showed a selective cytotoxic profile against glioblastoma cells without affecting the viability of non-tumoral cells.

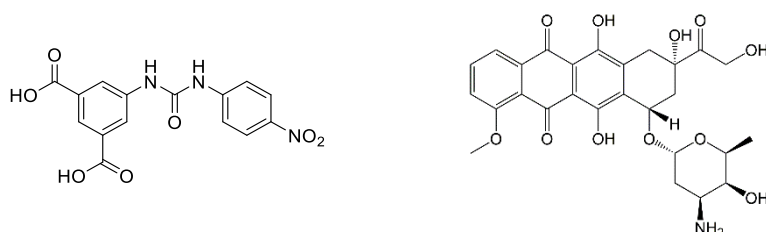


Figure 4.1. Molecular structures of a) **HG1**, b) Doxorubicin

Typically, the poor mechanical properties of physical hydrogels in the swollen state limitate the proliferation of drug release devices generated by low molecular weigh hydrogelators. The drug uncontrolled release is generally arised from the weak interactions with the matrix scaffold generated by the physical network crosslinks of the hydrogelator assemblies.

Moreover, the drug vehicule system mechanical properties and thus, the efficiency of the drug release is intimately related to the drug uptake method. In an active loading drug uptake method, the drug is discharged from the hydrogel internal structure and diffuses on the damaged supramolecular network where remains entrapped. The main advantage of the active loading is the stability of the mechanical properties, avoiding the disruption of the previously formed network. However, a low drug loading capability is typically achieved along with large uptake process times due to the infiltration difficulty of the guest drug on the formed molecular agregate. In contrast, the drug guest is entrapped during the network formation process in a passive loading, facilitating the drug uptake and increasing its loading efficiency. However, the passive loading is competitive assembly process that usually result in to detrimental poor mechanical properties of the loaded hydrogel<sup>26</sup> due to the acting as chain stoppers in physical hydrogels. The hydrogel **HG1** fibrillization mechanism was found to be controlled by the slow acidification that mantains constant a low supersaturation point. Similarly, a cooperative assembly between the drug and the hydrogelator is expected to yield also highly monodisperse nanofibers, however, affecting the kinetics of fibrillization. Importangly, the DOX addition to the **HG1** basic solution is expected to affect the GDL hydrolysis that affects the rate to attain the pKa of the monoprotonated **HG1**.

### 1. Sol-gel phase transition: fibrillation process mechanism.

The mechanism of drug uptake/release of **HG1** has been monitored at different length scales by SAXS, and FTIR to understand the key parameters that govern the passive/active loading of the DOX guest molecules by the nanofibers formed by **HG1**. The loading capacity and release/uptake profile will depend on the guest molecule incorporation method to the nanofiber carrier. The guest molecule structural features such as the molecular rigidity and planarity, as well as the interactions nature with the hydrogelator will determine the absorption method, either decorating the surface or being assimilated in the internal nanostructure. The hydrogel network formation upon pH change was monitored by SAXS from the self-assembled precursors originated from the dissolved molecules (DOX and **HG1**) at the supersaturation point to the complete percolation of the aggreagates. Previously, the gelation mechanism of **HG1** was followed by multi-length scale approach, performing several techniques such as SAXS, rheology, FTIR and NMR. The initial **HG1** aggregates were found to arise from firstly the hydrophobic pockets resulted from the monoprotonation of the carboxylic acid group with the highest pKa, 6.4. The primary **HG1** concentration determined the formed aggregates cross-section and the subsequent enlogantion through cooperative hydrogen bonds between the nitro-urea groups (see scheme 4.2). Highly monodisperse nanofibers were formed by **HG1** under 15mg/ml characterised by a core-shell hollow cylinder shape ( $r_{int}$  1.4 nm and  $r_{shell}$  ca 1.6 nm). Importantly, the supramolecular polymerization of **HG1** was controlled maintaining a low supersaturation point by the pH change through the whole volume and reaction time.

SAXS experiments were performed to probe the gelation process in the presence of the DOX guest molecules during the passive loading at two distint uptaking concentrations, specifically 3 mg/ml and 12 mg/ml of DOX (see Figure X). The DOX loading concentration assessment aimed

to identify the role of DOX on the fiber structure as well as to perturbate the initial thermodynamic conditions. In principle, the monomer availability concentration at the onset of the nucleation at the supersaturation point would be affected by the different concentration of DOX. Furthermore, the DOX occurrence disturbed the pH change by altering the hydrolysis equilibrium of GDL and thus, the growth mechanism.

Similarly to the previous nanofibrillization of **HG1**, a rod-like structure with a core-shell cylinder shape described the self-assembled aggregates morphology of DOX in **HG1** hydrogel. The rapidly length growth of the rod-like self-assembly suggests a nucleation-elongation mechanism likewise the described by **HG1** fibers. Moreover, fibers with nearly structural parameters were obtained by both DOX loading concentrations in **HG1**, increasing only the polydispersity cross-section (see Figure 4.3). A simultaneous density core thickening with a polydispersity (see Figure 4.3 and table 1) enhancement indicates that the infiltration of DOX molecules in the internal fiber structure disrupted slightly the self-assembly motif whilst retaining the main physical interactions. Moreover, the high loading capacity of DOX by the **HG1** assembly manifested the cooperative involvement of DOX in the internal fibre structure, either likely due to hydrogen bonding or  $\pi$ - $\pi$  interactions. However, the analogous cross-section for both DOX loading concentrations (3 mg/ml and 12 mg/ml)

and **HG1** nanofibers imply that the nucleation occurrence of **HG1** first determine the fibre cross-section. Subsequently, the DOX molecules compete with **HG1** in the fibre elongation process resulting in a slowdown of the self-assembly mechanism as well as the worsening of the interaction motif. However, the supramolecular interactions nature of the driven force during the elongation fibre development offered the flexibility to adapt the molecular assembly pattern. Moreover, the pH controlled change governed the monomer concentration availability in the fibre tip, avoiding the branching structure resulted from concentrations gradients.

Furthermore, the so-called Porod invariant (equation 1) ascribed to the total scattering intensity,  $Q$ , is related to volume fraction ( $\phi$ ) transformation of the electron density ( $n_e$ ) for bi-phasic systems and importantly, is independent of the scatter morphology. In the **HG1** system under supramolecular polymerization, the invariant is a powerful tool that affords to monitor the reaction kinetics and to assess the influence of DOX on the fibrillization mechanism.

$$Q = \int_0^{\infty} I(q)q^2 dq \propto \langle n_e \rangle^2 \phi_1 \phi_2 \quad \text{equation 1}$$

with  $\langle n_e \rangle^2$  being  $(\rho_{\text{gel}} - \rho_{\text{sol}})^2$  and  $\phi_i$  the volume fraction of the **HG1** solution and **HG1** gel phases with time (see Figure 4.3) affords the assessment of the morphologic transformation.

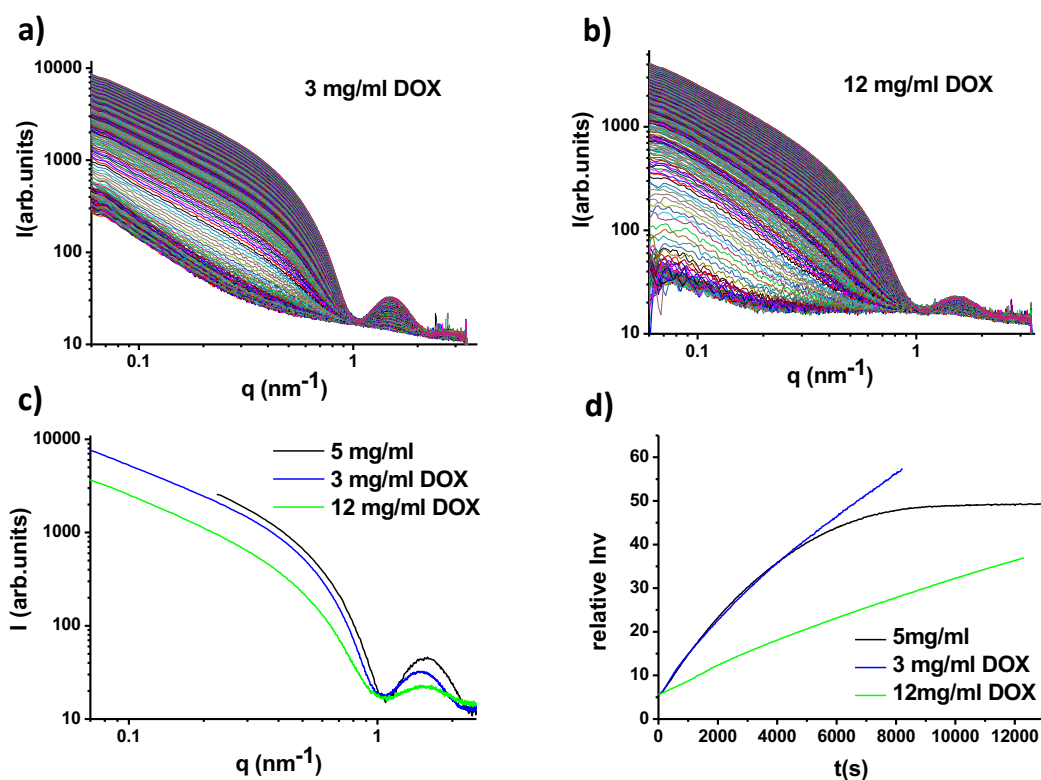


Figure 4.2. Time resolved SAXS profiles a) DOX (3 mg/ml) loaded in HG1 b) DOX (12 mg/ml) loaded in HG1. 3) Comparison of SAXS profiles at 9000 s. d) SAXS invariant of

DOX (3 mg/ml, 12 mg/ml) loaded in HG1 and HG1.

The SAXS invariant trend corresponding to either the passive loading of both DOX formulations (3 mg/ml, 12 mg/ml) in HG1 compare to HG1 gelation confirmed that DOX modified completely the kinetics of fibrillization. Recurrently, the linearization of the Avrami method to the HG1 fibrillization confirmed the formation of aggregates in 1D ( $n \sim 1$ ) in agreement with the SAXS model with different velocity constants. However, the application of the Avrami model to the passive loading of both formulations proved the polydispersity increase ( $n \sim 1,2$ , see Figure SX) in the uncomplete reaction under study. Remarkably, the mechanism of the nanofibre formation was found to depend simply on the initial HG1 concentration despite the large presence of guest molecules that strongly interact through multiple weak interactions. Particularly, the nucleation step generated the fibre cross-section precursors that subsequently were elongated with the participation of the guest molecules, retarding the kinetics of fibrillization.

The nanofibers structure of the guest molecules uptake process during the active loading.

Moreover, frequency oscillation sweep of the hydrogels generated by the corresponding DOX loading formulations (3 mg/ml and 12 mg/ml) under a non-destructive range (see Figure X) were performed to probe the fibrillar network. The characteristic independent response for the

storage and loss moduli with frequency of the gel state was described for both DOX formulations (see Figure X) in **HG1**. Moreover, the both the storage and loss components featured similar modulus for both DOX formulations and **HG1** hydrogels related to fibrillar networks with similar strength. The virtual parallel rheological properties with absence of network relaxation in the frequency range under study is associated with the lack of fibre branching and with a density of crosslinks resulted from the long **HG1** fibres, in agreement with the morphology described by SAXS. Furthermore, the  $\tan \delta$  obtained (measured at 1,3 Hz of the dynamic stress) indicated a higher strength of the DOX loaded hydrogel compared with **HG1** ( $\tan(\delta)$  **HG1** = 3.6  $\tan(\delta)$  DOX loaded in **HG1** = 8.7). However, the elastic component ( $G'$ ) was found continuously higher for **HG1** and the loss modulus component of DOX loaded in **HG1** slightly decreased, indicating larger resistance to flow.

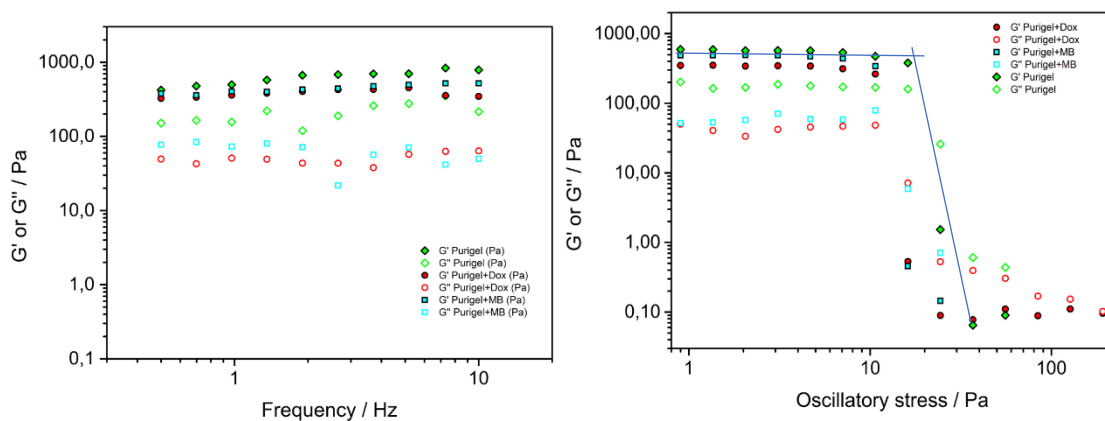


**Figure 4.3.** a) frequency sweep of hydrogels formed by the both DOX passive loading fomulations in **HG1** (3 mg/ml and 12 mg/ml) and **HG1** hydrogel passive loading DOX at pH 5 (black squares) and 7.4 (red circles).

Moreover, the yield stress of the hydrogel network DOX (12 mg/ml) loaded in **HG1** and **HG1** was evaluated by a dynamic stress sweep to determine the point of the fibrillar network disruption. The yield stress is a typical mechanical parameter defined for nanostructured liquids which is related to the processability, performance and long term storage material capability. The yield stress is largely employed in different fields such as food science, healthcare, paint applications and pharmaceutical as indicate the network stability to phase separation, sedimentation, aggregation, precipitation and resistance to vibration during transport. Particularly, the yield stress of the DOX loaded in **HG1** is a key parameter to assess the applicability of as injectable pharmacological hydrogel. The yield stress of the hydrogels under study featured a narrow transition (ca 10 Pa) with a decrease of both storage and loss modulus of 4 orders of magnitude. The yield stress was found around 22 Pa for both the DOX (12mg/ml) loaded in **HG1** and **HG1**, that confirmed the stability of the hydrogels network, similar for instance to the toothpaste (10 Pa).

## 2. Molecular Release behaviour with pH.

Monitorization of the pH-dependent DOX release from the **HG1** nanofibers after the passive loading of DOX (12 mg/mL) were conducted by fluorescence spectroscopy (see Figure 4.4 a and b). The pH functional activity of an ideal nanocarrier must target a tight pH range to deliver the drug whilst retaining the interaction with the drug at acid pH, depending on the therapeutic application methodology. The DOX release from the **HG1** at both pH 5 and pH 7.4 was selected to mimic the media conditions at appropriate physiological conditions. The pH in the body controls important functional activities and ranges from the stomach with high acid media to the intestine featuring slight basic conditions. However, human blood is characterised by a pH 7.35/7.45 gradient and cancer cells in particular, is found to be in general slightly basic. The lack of fluorescence emission by **HG1** allows to follow the release mechanism of the guest molecules only. Only a 9% of DOX was released after 120 min at pH 5 (see Figure 3) whilst a further increase in pH (pH = 7.4) produced a small further release of DOX (11%) after the releasing time (120 min). Moreover, the DOX release followed a slight different mechanism, either a biphasic or triphasic profile at pH 5 and pH 7.4, respectively. A slow diffusion from the hydrogel matrix with a linear zero-order release profile was found at pH 5 (see Figure 4.4). However, the DOX release at pH 7.4 suggested an initial rapid burst (phase I), diffusion from **HG1** matrix (phase II), and zero-order erosion stage (phase III) (see Figure 3). The release profile suggests that the DOX trapped in **HG1** matrix at pH 5 is more stable than at pH 7.4, minimizing the erosion stage and attaining easily a zero-order release. The percolated network is originated at acidic conditions due to the high hydrophobicity of the protonated **HG1** species that forms the assembly precursors at the pKa of the monoprotonated carboxylic species (pH=6.7). Moreover, the fibrillization driven force is the hydrogen bonding interactions that are maintaining acid media. The profile release suggests a dilution effect of the gel network instead of disruption of the DOX-**HG1** interactions. Moreover, the lower percentage of DOX released by **HG1** at pH 5 and 7.4 compared to methylene blue indicates that DOX participate in the inner fiber structure interacting strongly with the likely hydrogen bonds.

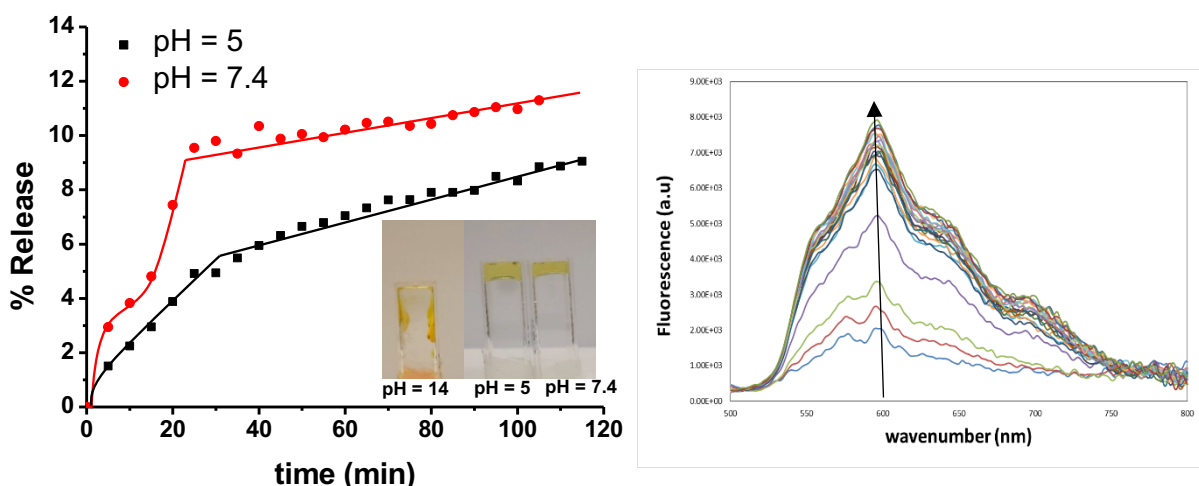


Figure 4.4. a) % Release profile of passive loading DOX in HG1 at pH 5 (black squares) and 7.4 (red circles), b) DOX fluorescence spectroscopy during the release from HG1 at pH 7.4.

Moreover, the centre of the DOX emission fluorescence band remained constant during both the uptake and release processes, (see Figure 3 b and SX in ESI), indicating the lack of  $\pi$ - $\pi$  stacking interactions between the DOX and **HG1**. The DOX fluorescence band was simply shifted by the acid-base reaction due to likely dissociation of alcohol of DOX in basic media. However, the large quenching effect on the fluorescence intensity on both media, either in the DOX loaded in **HG1** (acid media) or the DOX dissolved with **HG1** in basic media, revealed the strong interaction between the DOX and **HG1** molecules (see Figure 4.3) before and after the fibrillization process. In addition, the concurrence of the DOX fluorescence band for either the DOX in solution, or DOX dissolved together with **HG1** in basic media highlighted that DOX probed an analogous aqueous microenvironment (see Figure 4.3). Furthermore, the DOX fluorescence band monotonic increase together with the coincidence of fluorescence band position during the DOX release from the **HG1** fibrillar structure (see Figure 3b) confirmed the identical molecular DOX discharge mechanism to the upload process by **HG1**. Similarly to previous described by SAXS and rheology, the fluorescence spectra of DOX loaded in **HG1** indicated that DOX was placed inside the fibers with water molecules surrounding in an equivalent fashion than the DOX dissolved in water.

### 3. Biological studies

**Cell viability studies.** The effects of **HG1** on mitochondrial function and cell viability were investigated by determining the percentage of 3-(4,5-dimethylthiazol-2-yl)-2,5-diphenyltetrazolium bromide (MTT) transformed (% MTT transformed). MTT is metabolized at the mitochondrial level by viable and metabolically active cells to give an insoluble coloured formazan product. Insults that alter the metabolism of the cells affect the rate of MTT reduction into formazan. The reduction in the percentage of MTT has been largely employed as an index of cellular viability as the MTT transformation correlates with a reduction of the general metabolism (n).

The cell viability of the nanocarrier excipient **HG1** as a control test, has shown the innocuous effect on glioblastoma cells at the concentration range under study (% MTT transformed were  $97.2 \pm 2.7$  and  $96.3 \pm 1.9$ , in C6 and U87 cells respectively) confirming the inert nature at typical therapeutic concentrations/doses and that acts as a mere vehicle for the therapeutic agents.

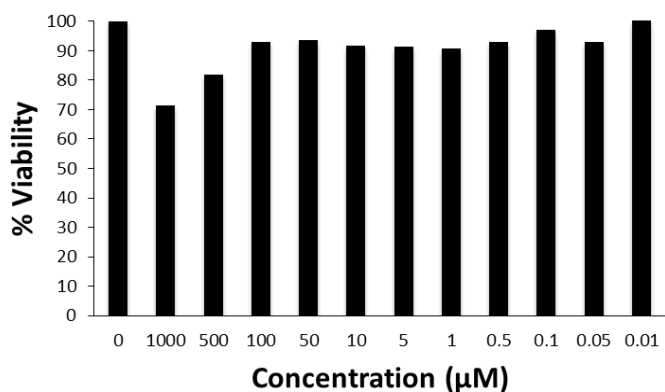
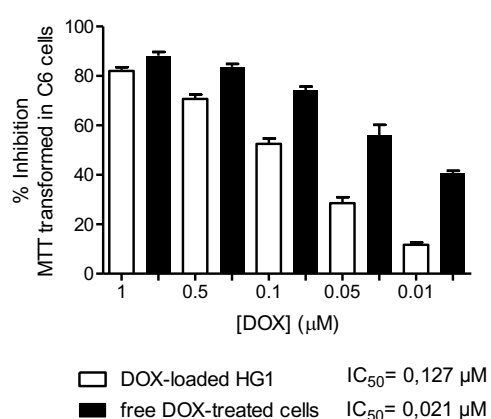


Figure 4.5. MTT assay in Mouse fibroblast C3H10T1/2 cell were treated with different concentration of HG1 hydrogel 1 (0- 1000 µM) for 72h.

Moreover, C6 and U87 cells were treated at increasing concentrations (0.01-1 µM) of free DOX and DOX-loaded **HG1** for 72 hours to determine the percentage of MTT transformed in culture media with a pH X. The treatment of C6 and U87 glioblastoma cells with free DOX or DOX-loaded in **HG1** reduced the glioblastoma viability in a concentration-dependent fashion (see Figure 4.6), producing higher potent effect in C6 cells compare to U87 at lower concentrations (see Figure 4a). Interestingly, in human glioblastoma cells, DOX-loaded in **HG1** displayed a potency very similar to free DOX, featuring nearly identical  $IC_{50}$  values (see Figure 4.56.b), whilst the inhibition % in rat glioblastoma C6 cells treated with DOX-loaded in **HG1** resulted systematically lower (see Figure 4.6a).

a)



b)

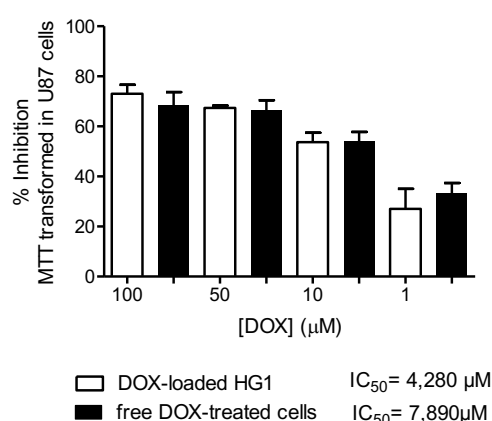


Figure 4.6. Cytotoxic effect of vehicle(HG1), DOX, and DOX-loaded in HG1 on rat glioblastoma C6 (a) and U87 human cells (b).  $IC_{50}$  values, expressed in micromolar, are included in the corresponding graph. Data are expressed as mean  $\pm$  s.e.m. from at least three independent experiments.

Moreover, the side-effect of DOX-loaded in **HG1** on non-tumoral cells have been assessed by using a primary culture of rat astrocytes as the background of C6 rat glioblastoma cells. Rat astrocytes were incubated with free-DOX or DOX-loaded in **HG1** for different times (24-72 h) to determine the inhibition percentage of MTT. Remarkably, the rat astrocytes cellular viability was unaffected by the treatment with DOX-loaded in **HG1** at the studied incubation times (see Figure 4.7), whilst free-DOX induced a drastic reduction in cellular viability, attaining a reduction in the inhibition of MTT transformed below to 50% after 72 h of incubation (see Figure 4,7).

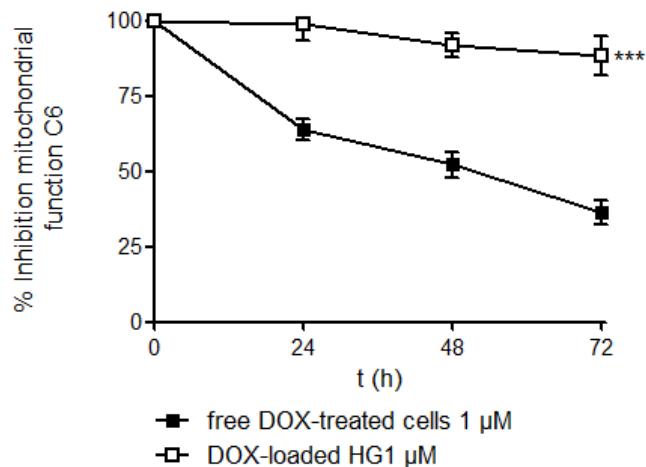


Figure 4,7. Cytotoxic effect of free DOX and DOX-loaded in **HG1** on rat astrocytes. Data are expressed as mean  $\pm$  s.e.m. from at least three independent experiments.

In summary, **HG1** combines the therapeutic properties of an ideal excipient due to its inert nature together with an efficient upload and smart controlled release. **HG1** is a great candidate to develop novel drug formulation nanocarrier systems for sustained DOX delivery in the treatment of GBM, with an adequate safety profile against non-tumoral cells.

#### In vitro release of DOX-loaded in **HG1** hydrogel in culture media.

The time-course for the DOX level remaining in the culture media of the treated C6 glioblastoma cells either with free-DOX or DOX-loaded in **HG1** has been quantified by (m). Free-DOX was rapidly incorporated by the C6 cells and diminished monotonically with the incubation time, almost disappearing from the culture media within 24h (see Figure 4.8), in agreement with previously found in cells X(m). However, the amount of free-DOX in the culture media of the C6 cells treated with DOX-loaded in **HG1** in culture media slightly increased monotonically from a negligible DOX concentration to a plateau-like range at 9h of treatment (see Figure 4.8). Importantly, the free DOX levels in the culture media of both therapeutic administration methodologies are comparable from the 9 hours onwards of the treatment. The controlled DOX release generated by the **HG1** gel avoids the initial drug burst release stage. The lack of high DOX concentrations in contact with the cells across the delivery process by **HG1** gel minimize the toxic side-effects on healthy cells, as previously observed in the treatment of healthy rat astrocytes (see Figure 4.8).

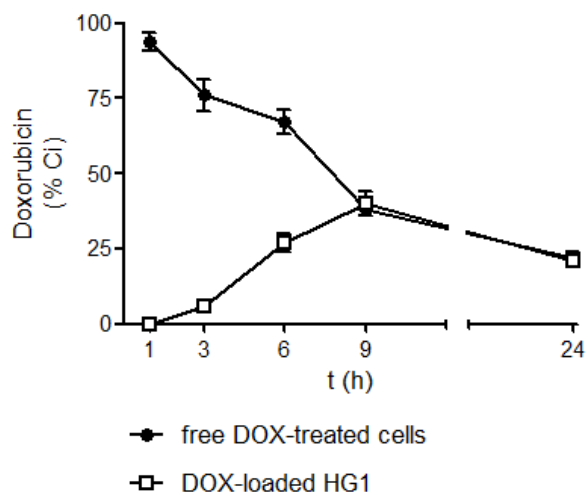


Figure 4.8. Time-course study of the percentage of DOX remaining in the culture medium of C6 cells treated with  $0.5 \mu\text{M}$  DOX or  $0.5 \mu\text{M}$  DOX-loaded in HG1. Data are expressed as mean  $\pm$  s.e.m. from at least three independent experiments.

Release Dynamic of DOX-loaded in HG1 hydrogel by a passive loading formulation in culture cells.

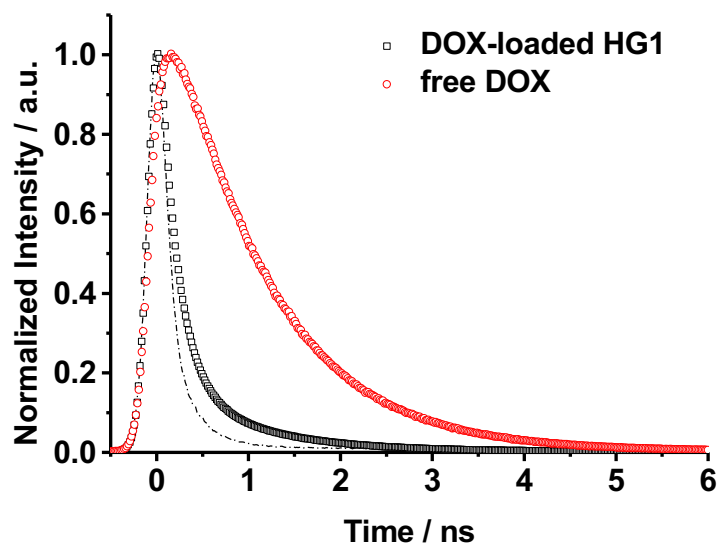


Figure 4.9. Dynamics of free DOX in buffer solution (red circles) and DOX-loaded in HG1 (black square) by a passive loading formulation.

The intracellular DOX release dynamics in culture C6 cells treated with either a PBS buffer solution of DOX and DOX-loaded in **HG1** at identical concentration ( $12 \text{ mg/mL}$ ) was monitored by following the DOX fluorescence lifetime. Remarkably, the fluorescence lifetime is a photophysical state function and thus, independent on the experimental conditions (excitation wavelength, light pulse duration, photobleaching, etc...) as well as the fluophore

concentration and fluorescence intensity. The fluorescence lifetime spectroscopy is a non-destructive technique applied to diverse media (solution, gel, films, bulk) related to nanosecond and/or picosecond structural dynamics and interactions of the fluorophore that is ideal to monitor the molecular dynamics in complex systems such as the cells. The time interval of a fluorophore in the excited state is affected by quenching the fluorescence response due to internal emission pathways such as conformation changes, side-chain rotation as well as external irradiative relaxation routes such as interactions between adjacent groups, polarity, solvent relaxation, temperature and media viscosity. Firstly, the fluorescence decay from the excited state of the exclusive fluorophore (DOX) of the delivery system in both formulations is studied by time-resolved fluorescence spectroscopy (TRF), to probe the DOX molecular environment in either solution (PBS) or within the internal fiber structure. A mono-exponential lifetime value of 1.02 ns for the DOX applied in solution was found, consistent with previously reported lifetime values (see Figure 4.9)<sup>27-30</sup> whilst DOX-loaded in **HG1** presented a biexponential decay with an average lifetime of 0.47 ns. Specifically, the biexponential decay showed a slow component of 0.93 ns (with an amplitude of 5%) related to DOX molecules at the vicinity of the fiber, and a fast component of 0.20 ns (95% of amplitude) corresponded to molecules likely trapped inside the fibres (see Figure 4.9). The molecular sensitivity of DOX to changes in the local chemical environment affects its fluorescence response, decreasing significantly the lifetime of the DOX trapped either in the neighbouring or the internal structure of **HG1** fibre. Importantly, the amplitude/ratio of the DOX fluorescence decay which is proportional to the corresponding DOX molecular state, confirmed a highly effective molecular upload by the **HG1** fibers. The fluorophore probes two different molecular environments featuring lower fluorescence lifetimes than the unassembled DOX in solution. Moreover, the shorter fluorescence lifetime at the greater viscosity of the **HG1** hydrogel, where the fluorophore is expected to possess a higher fluorescence lifetime due to a molecular rigidification. The dramatic quenching effect of the DOX fluorescence lifetime and intensity in the hydrogel is likely arising from the interaction with **HG1** or charge/proton transfer with the donor or acceptor groups such as the nitro, amino, phenyl moieties.

Moreover, fluorescence lifetime was recorded by FLIM on C6 glioblastoma cells treated with the vehicle (**HG1**, control experiment), a DOX solution (PBS), or DOX-loaded in **HG1** for different incubation times to probe the cellular DOX location. Particularly, the intracellular media at two different regions of interest, cytoplasm and nuclei, was studied by fitting the fluorescence lifetime to a biexponential decay analysis (see Figure 4.10 and Table 1). A similar decay pattern in both the cytoplasm and nuclei was found for both therapeutic formulations (DOX in solution applied to the C6 cells and DOX-loaded in **HG1**). A mono-exponential lifetime of 1.45 ns was obtained at nuclei during the incubation times under study, shifting to larger emission lifetimes than the typical DOX value in solution (c.a. 1.02 ns) due to higher molecular rigidity. Moreover, a slow component of 3 ns as well as a fast component of 0.46 ns were measured at the cytoplasm, suggesting that DOX molecules were located in areas with different local microviscosity and/or chemical environment (see Table 1). The relation between amplitudes, A(%), of both lifetimes remains constant for the incubation times under study and for both formulation methods (DOX solution applied to the C6 cells and DOX-loaded in **HG1**). The absent

of new fluorescence lifetimes, at least above the FLIM resolution time 0,2 ns, in the DOX-loaded in **HG1** compare to DOX in solution, in the intracellular release dynamics suggested that DOX cross the cell without the vehicle **HG1X**.

**Table 1.** Biexponential analysis of both formulations; DOX solution and DOX-loaded in **HG1** in the nuclei and cytoplasm of cells at different incubation times.

		time (h)	$\tau_{av}(ns)$	$\tau_1(ns)$	$A_1(\%)$	$\tau_2(ns)$	$A_2(\%)$
Nuclei	DOX	3	$1.48 \pm 0.18$	$1.48 \pm 0.18$	100	-	-
		6	$1.49 \pm 0.22$	$1.49 \pm 0.22$	100	-	-
		24	$1.44 \pm 0.20$	$1.44 \pm 0.20$	100	-	-
	DOX-Loaded	3	$1.45 \pm 0.28$	$1.45 \pm 0.28$	100	-	-
		6	$1.44 \pm 0.22$	$1.44 \pm 0.22$	100	-	-
		24	$1.51 \pm 0.22$	$1.51 \pm 0.22$	100	-	-
Cytoplasm	DOX	3	$1.95 \pm 0.24$	$3.03 \pm 0.40$	18.2	$0.49 \pm 0.22$	81.8
		6	$1.92 \pm 0.24$	$2.91 \pm 0.36$	19.1	$0.45 \pm 0.24$	80.9
		24	$1.86 \pm 0.28$	$2.97 \pm 0.44$	24.6	$0.44 \pm 0.16$	75.4
	DOX-Loaded	3	$1.60 \pm 0.16$	$2.80 \pm 0.18$	18.1	$0.43 \pm 0.24$	81.9
		6	$1.88 \pm 0.20$	$3.04 \pm 0.40$	18.6	$0.47 \pm 0.20$	81.4
		24	$2.06 \pm 0.20$	$3.36 \pm 0.36$	15.4	$0.43 \pm 0.14$	84.6

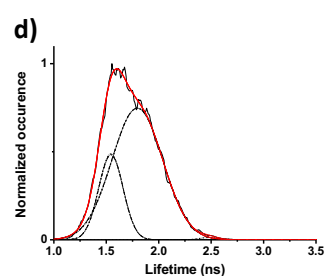
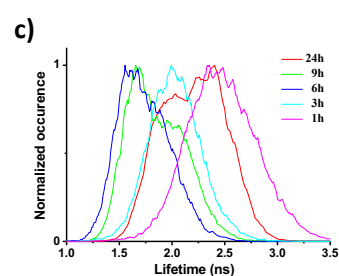
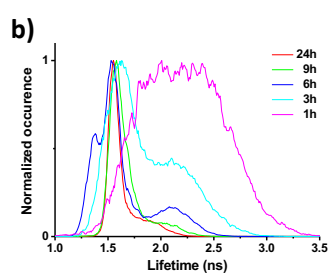
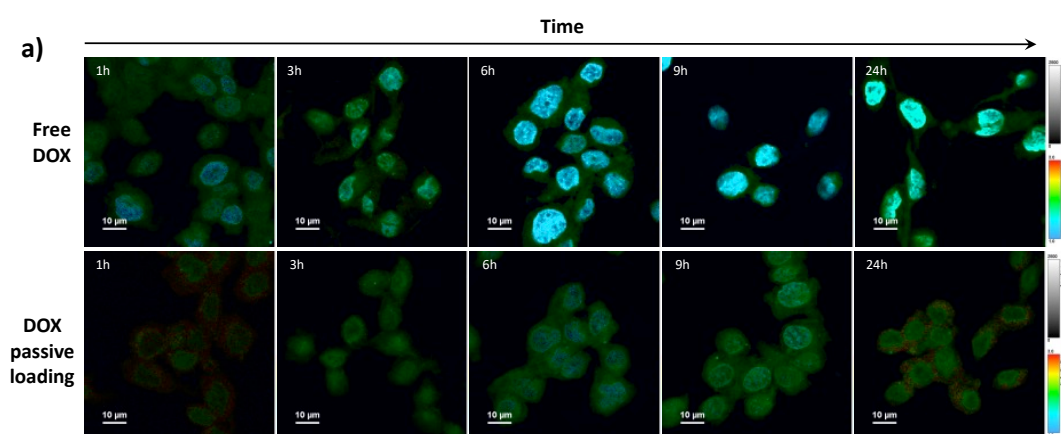
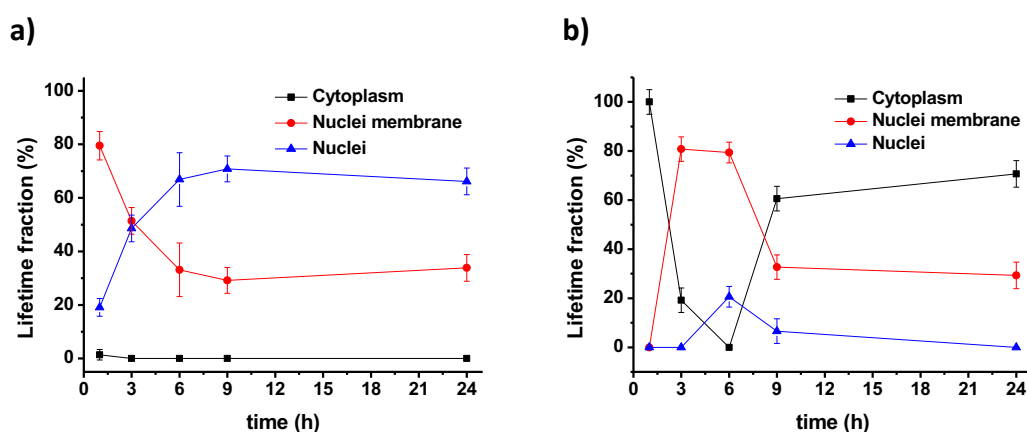


Figure 4.10. a) FLIM images of C6 cells treated with 0,5  $\mu$ M of a DOX solution and DOX-loaded in HG1(a). Lifetime histograms for DOX applied in solution (b) and DOX-loaded in HG1 (c). Deconvoluted histogram at 6h in DOX-loaded HG1 treatment.(d)

Moreover, fluorescence lifetime imaging were reconstructed from the average lifetimes on the C6 glioblastoma cells treated with both therapeutic formulations (a DOX solution(PBS), or DOX-loaded in **HG1**) for different incubation times to highlight the DOX intracellular delivery. Firstly, FLIM image of control cells showed a very slight autofluorescence with an average lifetime value of 2.4 ns (see Figure S9 in ESI). The fluorescence lifetime distribution after 1h of treatment with the DOX solution showed that the fluorescence signal is mainly located in the cytoplasm as well as the nuclei membrane with an average lifetime value of 2.2 ns. Moreover, the DOX fluorescence signal tend to be displaced towards the nuclei along with DOX solution treatment time, and within 3h, DOX was found practically only in the nuclei. Importantly, the fluorescence lifetime decreased to 1.5 ns typically attributed to DOX-DNA intercalation,<sup>27,28,30</sup> remaining at the nuclei for the incubation time under study (24 h). However, the fluorescence intensity of the C6 cells treated with DOX-loaded in **HG1** decreased due to the quenching effect of the interaction with **HG1**. As we commented above, it is only observed fluorescence lifetime of DOX when it is released. Initially, the fluorescence signal was concentrated in the cytoplasm with a lifetime of 2.5 ns at 1 h of DOX-loaded in **HG1** treatment. Similarly to the DOX solution formulation, the fluorescence signal shifted to nuclei membrane within 3h, decreasing the average lifetime decrease to 2 ns. Moreover, the DOX fluorescence signal appeared both at the nuclei membrane and nuclei at 6 h of DOX-loaded in **HG1** and, a further decreases of the lifetime fluorescence to 1.5 ns. However, the DOX fluorescence signal increase the average lifetime and shifted back to the nuclei membrane at 9 h of treatment and even to the cytoplasm after 24 h. The unusual DOX delivery behaviour is in agreement with the controlled release profile observed in “in vitro” and culture media for the DOX-loaded in **HG1** formulation (9 hours ~40% of release, see Figures 4.11b). Moreover, the lack of fluorescent activity avoided to monitor the **HG1** molecules during the DOX transport in the intracellular media. However, **HG1** deterred the initial DOX burst release stage, reducing the high concentrations of DOX in contact with the cells compared to the DOX in solution formulation.



*Figure 4.11. Lifetime fractions (%) from deconvoluted histograms extracted from FLIM images in Figure 8a, b, and c: a) buffer solution of DOX formulation, b) DOX-loaded in HG1 treatment. Errors bars represent the standard deviation as  $2\sigma$ .*

The delayed DOX cell penetration process transported by **HG1** was assessed by deconvolution of the Gaussian-like lifetime histogram, assigning the DOX average lifetimes values for cytoplasm, nuclei membrane, and nuclei to 2.5, 2.0 and 1.5 ns, respectively. The ratio of DOX molecules presents in the different areas of the cell (see Figure 4.11) was inferred from the relative areas of deconvoluted curves at each average lifetime (see Figures 4.10b, c, d). Importantly, DOX easily penetrated to the nuclei membrane and was then readily incorporated into the nuclei. However, the DOX infiltration was significantly slower for the DOX-loaded in the gel treatment and from 9 h onwards DOX mainly was found in the cytoplasm due to the critical release.

## CONCLUSION

The mono urea non-peptidic derivative hydrogelator (**HG1**) has been evaluated as a biocompatible and nontoxic carrier to local delivery of DOX in the treatment of GBM. Moreover, the remarkable controlled DOX uptake achieved by the cooperative nanofibrillization with **HG1** highlighted the key role of the specific inter-supramolecular interactions between the DOX-hydrogelator to maximize the loading rate. In addition, the maintaining of the supersaturation point low, across the nanofibrillization and DOX uptake concomitant by the regulated pH change avoided the gradient molecular concentrations and consequently, the fibre branching. The inter molecular co-assembly mechanism resulted in long fibres, circumventing the detrimental chain stopper behaviour during the fibrillization generally found for guest molecules. The monitoring of fibrillization by SAXS showed the slight increase of the fibre cross-section compared to **HG1** fibres, however, retaining the mechanism of nucleation and elongation. Moreover, the hydrogel network formed with DOX featured analogous strength and yield stress to the **HG1** gel, indicating a similar fibrillar percolation due to comparable fibre length and crosslinks. The release of DOX from **HG1** is pH dependent due to the solubility of **HG1** in basic media, yielding a controlled release over time. DOX-loaded in **HG1** reduced the glioblastoma viability in a concentration-dependent manner, resulting in slightly  $IC_{50}$  lower values than direct treatment with a DOX solution. Moreover, the application of DOX-loaded in **HG1** formulation avoided undesirable side effects over healthy cells at identical concentrations of DOX released after 24 hours of treatment with both formulations. Microscopy studies confirmed the DOX controlled release observed in the in vitro studies, with a slow DOX penetration in the DOX-loaded in **HG1** treatment. Remarkably, **HG1** hydrogel is a great candidate as local delivery super-nanocarrier. Particularly, DOX-loaded in **HG1** hydrogel is an ideal alternative to the market therapeutic treatments to be applied into the tumour resection cavity. The **HG1** hydrogel acts as DOX reservoir, releasing from the hydrogel matrix upon pH change and minimal systemic toxicity.

Moreover, I have been invited to give an oral contribution to the following conferences:

- Polymer Networks & Gels 2014 Conference, Correlating molecular structure to the mechanism of gelation of low molecular weight hydrogelators. Tokyo, Japan
- 2015 International Chemical Congress of Pacific Basin Societies Understanding the fibrillation of self-assembled low molecular weight hydrogelators. Honolulu, USA.
- XVII International Small Angle Scattering Conference - SAS2018XVII International Small Angle Scattering Conference - SAS2018, Investigation of the uptake/release during the fibrillization of self-assembled low molecular weight hydrogelators by SAXS/GISAXS. Traverse City, USA.
- 32nd Advanced Materials World Congress Conference organized by International Association of Advanced Materials entitled 'Monitoring of the drug uptake/release by a self-assembled low molecular weight hydrogelator carrier'. Sydney, Australia.

Currently, we are working on several publications that will report the promising results as drug nanocarriers as well as uptake/release mechanism.

# Selective and highly efficient dye scavenging by a pH-responsive molecular hydrogelator†

Francisco Rodríguez-Llansola,<sup>a</sup> Beatriu Escuder,<sup>\*a</sup> Juan F. Miravet,<sup>\*a</sup> Daniel Hermida-Merino,<sup>b</sup> Ian. W. Hamley,<sup>b</sup> Christine J. Cardin<sup>b</sup> and Wayne Hayes<sup>\*b</sup>

Received 2nd July 2010, Accepted 9th September 2010

DOI: 10.1039/c0cc02338h

**A structurally simple low molecular weight hydrogelator derived from isophthalic acid forms robust pH-responsive hydrogels capable of highly efficient and selective dye adsorption.**

Molecular gels represent an intriguing type of organic nanostructured soft material. Molecular gelators form elongated supramolecular aggregates that further evolve to nanofibrillar networks which entrap the solvent to yield a gel.<sup>1</sup> This type of soft matter is of interest in areas such as responsive materials, catalysis or electronic and photonic materials.<sup>2</sup> Practical applications of molecular hydrogelators are especially appealing due to the biological relevance of water as a solvent. In recent years several structurally diverse molecular hydrogelators have been described.<sup>1,fg</sup> A topical aspect within this field is the stimuli responsiveness associated with molecular gels. In addition to their characteristic temperature and concentration dependence, the formation of molecular gels can be controlled by different stimuli. In particular, the presence of pH sensitive groups in the structure of the gelator can be exploited advantageously for the controlled formation of molecular gels.<sup>1g</sup>

Herein we report a structurally very simple, pH-responsive bisaromatic hydrogelator (**1**) that is derived from isophthalic acid and contains a urea functional group. The molecule reported is a remarkable example of a molecular hydrogelator capable of selective and extremely efficient incorporation of dyes into the formed hydrogel network. In this paper we additionally report on the fascinating layered solid state structure of the gelator **1** which provides a framework to account for the dramatic dye uptake capabilities of this urea in its hydrogel form.

The interaction of molecular gel fibers with different guest species has been reported.<sup>3</sup> The incorporation of dyes in hydrogels formed by a tripeptide derivative which forms gels at basic pH values has been described revealing that molecular hydrogels can potentially be used to remove industrial dyes from waste water.<sup>4a</sup> The use of gels of ionic liquids for dye removal has also been reported recently.<sup>4b</sup>

The bisaromatic hydrogelator **1** was prepared in high yield by direct addition of 5-aminoisophthalic acid to 4-nitrophenyl isocyanate and exhaustively characterized (see SI). Hydrogels were formed above a concentration of 0.9 mM (0.3 mg mL<sup>-1</sup>)

by acidification with aqueous HCl of a solution of **1** in basic water and sonication. Alternatively, for a slow and homogeneous acidification of the system, the hydrolysis of water soluble glucono- $\delta$ -lactone can be used.<sup>5</sup> Furthermore, the gelation in neutral water was also possible in the presence of small amounts (*ca.* 10% v/v) of polar organic solvents such as methanol or DMSO when accompanied by gentle heating until complete dissolution was attained and the solution was then allowed to cool to 25 °C. The gels were found to be significantly more stable upon increasing the concentration of gelator (see SI, Fig. S1). Remarkably, the hydrogels were stable at temperatures above the boiling point of water when the gelator concentration was higher than 9 mM.

The gelation process by pH tuning provoked a colour change from red–orange to yellow associated with the protonation of the carboxylate groups (see Fig. 1). The observed yellow colour in the gel samples was attributed to intermolecular interactions. Solutions of compound **1** in MeOH are colourless but upon increasing the proportion of water in the system, aggregation takes place giving rise to the observed yellow colour which correlates with the observed absorption above 400 nm (see SI, Fig. S3 and S4).

The morphology of the gel obtained by pH-tuning was observed by Atomic Force Microscopy (AFM) to reveal the presence of a network of nanofibers that were several microns in length and less than 50 nm in width (Fig. 2).

Needle-like crystals of **1** suitable for single crystal X-ray analysis were obtained from slow evaporation of a solution of

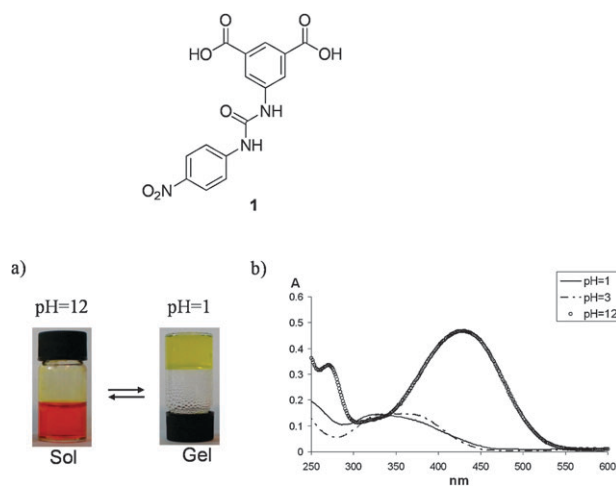


**Fig. 1** (a) Pictures of vials containing a 3 mM aqueous solution of compound **1** (left) and the hydrogel formed upon acidification (right). (b) UV-vis spectra of compound **1** (1.5 mM) at different pH values.

<sup>a</sup> Departament de Química Inorgànica i Orgànica, Universitat Jaume I, Avda. Sos Baynat s/n, 12071 Castelló, Spain. E-mail: escuder@uji.es, miravet@uji.es

<sup>b</sup> Department of Chemistry, University of Reading, Whiteknights, Reading, UK RG6 6AD. E-mail: w.c.hayes@reading.ac.uk

† Electronic supplementary information (ESI) available: Experimental details and crystal structure description. See DOI: 10.1039/c0cc02338h

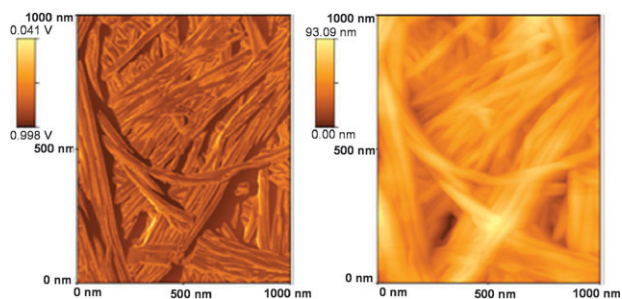


**Fig. 2** Atomic force microscopy images of xerogels obtained from the hydrogel formed by **1** (0.9 mM). Left: phase contrast, right: topography.

compound **1** in a 7 : 3 water : methanol mixture. The bisaromatic hydrogelator **1** crystallized in the monoclinic system with a dramatic layered structure. These layers are constituted by ribbons of molecules formed by intermolecular hydrogen bonding between the urea NH units and nitro moieties.<sup>6</sup> The layer is constructed by connection of the ribbons by intermolecular hydrogen bonding among the carboxylic acid functional groups at the ribbon edges (see SI, Fig. S13–S15).

The X-ray powder diffraction pattern of a xerogel from a hydrogel of **1** revealed the crystalline nature of the fibrillar network (SI, Fig. S6) and showed that the arrangement found in the fibers is a polymorph of that described in the crystal structure mentioned above, which presents different diffraction peaks.

FT-IR studies unveiled that the xerogels formed by **1** presented a 2D arrangement of intermolecular hydrogen bonds related to that found in the crystal structure. The FT-IR and ATR grazing angle spectra showed that the carbonyl stretching band intensity was reduced significantly when the sample was irradiated in grazing angle mode (see Fig. 3a). According to previous studies,<sup>7</sup> these results indicate a preferred orientation of the studied hydrogen bonding groups in a plane, suggesting that the hydrogen bonding array is oriented along the axis of a nanofiber.

Therefore, a model is proposed for **1** in which the  $\pi$ - $\pi$ -stacking and hydrogen bonding interactions are orthogonally related with weaker aromatic interactions that lie perpendicular to the fiber axis (Fig. 3b). In the model, gel fibers can be seen to result from frustrated crystallization caused by the partial ionization of carboxylic acid units that would preclude the formation of extended 2D hydrogen arrays such as those

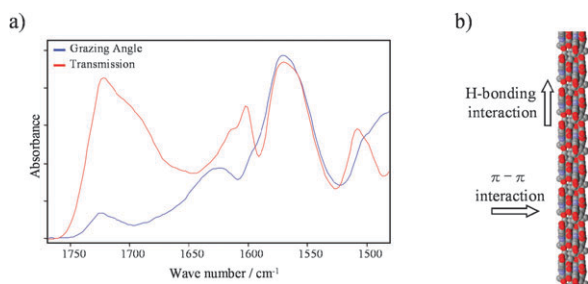


**Fig. 3** (a) Transmission vs. grazing angle ATR FT-IR spectra for xerogels of compound **1**. (b) Proposed orientation of the hydrogen bonding interactions within the fibers.

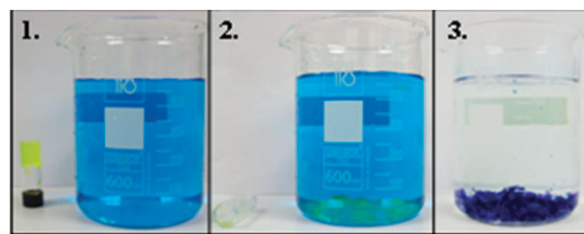


**Fig. 4** Pictures of the methylene blue removal process. (1) Solution of methylene blue in water (500 mL, 8 mg mL<sup>-1</sup>) and vial containing a hydrogel of **1** (2 mL, 20 mM). (2) Solution of methylene blue with the hydrogel fragments deposited at the bottom of the beaker. (3) Picture of the system after 72 h.

observed in the crystal structure and favour the formation of elongated assemblies.

Interestingly, the crystalline layered structures have in common an inherent ability to mimic clays by intercalation of guest molecules.<sup>8</sup> With this concept in mind, the potential for incorporation of guest molecules into the hydrogel fibers was tested. A preliminary study revealed that these hydrogels were very efficient in the adsorption of methylene blue. As shown in Fig. 4, a very small quantity of hydrogel (2 mL, 20 mM) is able to completely decolour a 500 mL solution of methylene blue with a dye concentration of 8 mg L<sup>-1</sup>. It has to be noted that the adsorption of methylene blue into molecular hydrogels is not a general property. For example, adsorption of the dye was not observed when a hydrogelator that did not feature aromatic units that was available in our laboratories was studied (see SI, Fig. S8).

In a more detailed study, the adsorption of six different compounds into the gel was studied (see Table 1) including two planar, positively charged aromatic compounds that are used commonly as dyes, methylene blue and violet blue 2B. Additionally, two cationic aromatic compounds, 1-pyrene methylammonium hydrochloride and dopamine, and an anionic dye, indigo carmine, were used as possible guests. The last substrate studied was spermine, an aliphatic tetracationic substrate that is known to interact with negatively charged DNA strands. For the adsorption studies, solutions containing the different guests were deposited over a hydrogel obtained by pH-tuning. Since spermine does not exhibit a strong UV-vis chromophore, the adsorption was monitored by <sup>1</sup>H NMR spectroscopy for all of the above dyes.

Noticeably the hydrogel formed by compound **1** was extremely selective in the adsorption of the positively charged

**Table 1** Adsorption of different species (SI, Fig. S7) on the hydrogel formed by **1**<sup>a</sup>

Adsorbate	% Adsorbed
Methylene blue	98
Methyl Violet 2B	97
1-Pyrenemethylamine	62
Spermine	< 1
Dopamine	< 1
Indigo carmine	< 1

<sup>a</sup> Determined by <sup>1</sup>H NMR. A solution in D<sub>2</sub>O of these species (7.25 mM, 1 mL) with DMSO as internal standard was deposited for 48 h on 1 mL of the hydrogel formed with D<sub>2</sub>O (14.5 mM). The structure of the adsorbates is depicted in the SI.

dyes methylene blue and methyl violet 2B. When a solution of these dyes (7.25 mM, 1 mL) was deposited on 1 mL of the hydrogel (14.5 mM), the dyes could not be detected by NMR spectroscopy in the original solution after 48 h. The fact that the aliphatic tetracation spermine was not adsorbed at all under the same conditions supports the hypothesis that intercalation constitutes the main driving force for the aggregation rather than purely electrostatic interactions. Negligible adsorption into the gel was measured for positively charged dopamine or anionic indigo carmine. In contrast, 62% of the initial concentration of 1-pyrenemethylamine was adsorbed on the hydrogel fibers. The selectivity observed in the interaction with methylene blue and methyl violet 2B in comparison to the other aromatic substrates reveals that the adsorption is also selective to the nature of the aromatic moiety.

For a solution of the dye deposited over a hydrogel formed in a vial the maximum amount of dye adsorption and the kinetics of the process are very dependent on the vial dimensions, namely, on the contact area between gel and solution (see SI, Fig. S9). These results indicate that for this experimental setup a diffusion controlled adsorption is taking place. For example, for vials with a diameter of 2.7 cm quantitative dye removal was observed in less than 6 h. Importantly, the removal of dyes from solutions was tested taking advantage of the pH-responsive nature of hydrogel formed by **1**. For example, when aqueous HCl is added to a solution of methylene blue and the gelator a gel is formed. Filtration of the system afforded a colourless solution and, according to UV-vis spectroscopy, the dye was removed very effectively (>99%) (see SI, Fig. S11). Similar results were obtained for methyl violet 2B but for indigo carmine this procedure was significantly less efficient. Noticeably, the dye removal efficiency using this procedure is unprecedented—the dye–hydrogelator ratio was almost equimolar in the formed gels (see SI, Table S1). The measured removal efficiency parameter determined by UV-vis spectroscopy for methylene blue and methyl violet 2B was *ca.* 800 mg of dye per gram of gelator, a significant enhancement when compared to the values described for related systems. For example, the tripeptide based hydrogel aforementioned exhibited values of 7.36 mg g<sup>-1</sup> for Rhodamine B and 10.56 mg g<sup>-1</sup> for the dye direct red 80.<sup>4a</sup> The dye removal efficiency is also notable when compared to the adsorption of methylene blue to a common adsorbent such as active charcoal which exhibits an efficiency of up to *ca.* 400 mg g<sup>-1</sup>.<sup>9</sup>

Regarding the interaction of the gelator and the dyes, a direct proof of the intimate interaction taking place in this system is the fact that the thermal stability of the gels was significantly affected by the presence of the dyes (see SI, Fig. S10).

Finally, gel regeneration can be achieved easily. For example, after repetitive extractions with chloroform to remove the dye, the gel can be regenerated by dissolution in basic water followed by acidification.

In summary, a new simple urea-based compound capable of forming robust, pH-responsive hydrogels with outstanding dye scavenging properties has been described. It is to be noted that the hydrogels are comprised of a self-assembled nanofibrillar network as revealed by microscopy studies. Interestingly, in this case a crystal structure of the gelator can be obtained

which serves as a reference for a possible structural arrangement in the gel nanofibers which, as shown by X-ray diffraction studies, possess a microcrystalline structure. A related hydrogen bonding array was inferred for the xerogel by grazing angle IR spectroscopy. A remarkable fact is that the nanofibers interact selectively with positively charged dyes such as methylene blue and methyl violet 2B. The nanofibrillar structure provides a stimuli responsive functional material which presents a very high aspect ratio. The pH responsiveness of the system gives an outstanding added value for potential practical applications. Dye solutions at basic pH containing the ionized, soluble, hydrogelator can be transformed easily into hydrogels upon acidification. Filtration of these systems affords colorless dye-free solution. With this procedure the hydrogels present an unprecedented capacity of dye removal with *ca.* 0.8 g of dye being captured by 1 g of the gelating component of the hydrogel. The extraordinary dye removal capabilities were found to be specific for this particular gelator and were attributed to its acidic character and its aromatic units. In addition to employment in industrial scale tasks such as waste water treatment, applications for hydrogels of this type in controlled drug release (especially gene therapy agents such as DNA intercalating drugs) are also envisaged.

Work at Reading was supported by EPSRC grant EP/G026203/1 to WCH and IWH. Work at Castelló was supported by MCI, grant CTQ2009-13961 and Universitat Jaume I, grants P1-1B2009-42 and P1-1B2007-11. F.R.-L. thanks Generalitat Valenciana for a FPI fellowship.

## Notes and references

- (a) *Molecular Gels: Materials with Self-Assembled Fibrillar Networks*, ed. R. G. Weiss and P. Terech, Springer, 2005; (b) P. Terech and R. G. Weiss, *Chem. Rev.*, 1997, **97**, 3133; (c) D. J. Abdallah and R. G. Weiss, *Adv. Mater.*, 2000, **12**, 1237; (d) J. van Esch and B. L. Feringa, *Angew. Chem., Int. Ed.*, 2000, **39**, 2263; (e) O. Gronwald and S. Shinkai, *Chem.–Eur. J.*, 2001, **7**, 4328; (f) L. A. Estroff and A. D. Hamilton, *Chem. Rev.*, 2004, **104**, 1201; (g) M. De Loos, B. L. Feringa and J. H. van Esch, *Eur. J. Org. Chem.*, 2005, 3615; (h) A. R. Hirst and D. K. Smith, *Chem.–Eur. J.*, 2005, **11**, 5496.
- (a) A. R. Hirst, B. Escuder, J. F. Miravet and D. K. Smith, *Angew. Chem., Int. Ed.*, 2008, **47**, 8002; (b) S. Banerjee, R. K. Das and U. Maitra, *J. Mater. Chem.*, 2009, **19**, 6649; (c) B. Escuder, F. Rodríguez-Llansola and J. F. Miravet, *New J. Chem.*, 2010, **34**, 1044.
- (a) M.-O. M. Piepenbrock, G. O. Lloyd, N. Clarke and J. W. Steed, *Chem. Rev.*, 2010, **110**, 1960; (b) P. Mukhopadhyay, Y. Iwashita, M. Shirakawa, S.-I. Kawano, N. Fujita and S. Shinkai, *Angew. Chem., Int. Ed.*, 2006, **45**, 1592; (c) B. Escuder, J. F. Miravet and J. A. Sáez, *Org. Biomol. Chem.*, 2008, **6**, 4378; (d) U. Maitra, S. Mukhopadhyay, A. Sarkar, P. Rao and S. S. Indi, *Angew. Chem., Int. Ed.*, 2001, **40**, 2281.
- (a) B. Adhikari, G. Palui and A. Banerjee, *Soft Matter*, 2009, **5**, 3452; (b) S. Dutta, D. Das, A. Dasgupta and P. K. Das, *Chem.–Eur. J.*, 2010, **16**, 1493.
- D. J. Adams, M. F. Butler, W. J. Frith, M. Kirkland, L. Mullen and P. Sanderson, *Soft Matter*, 2009, **5**, 1856.
- S. George, A. Nangia, C.-K. Lam, T. C. W. Mak and J.-F. Nicoud, *Chem. Commun.*, 2004, 1202.
- S. E. Paramonov, H. Jun and J. D. Hartgerink, *J. Am. Chem. Soc.*, 2006, **128**, 7291.
- M. J. Zaworotko, *Chem. Commun.*, 2001, 1.
- S. Mukherjee and S. Bhattacharya, *J. Am. Chem. Soc.*, 1949, **71**, 1725.

## 5-Caroline Grant (from Oct 1<sup>st</sup> 2017 to Nov. 30<sup>th</sup> 2020) in the project "NODENS" which is a Caroline Fellowship program co-founded by European Union Horizon 2020 Marie Skłodowska-Curie actions and Irish Research Council.

---

In order to continue the investigation on the gelation mechanism, I successfully obtained a joint application for Caroline Grant with Bing Wu, to spend 36 months (from Dec. 1<sup>st</sup> 2017 to Nov. 30<sup>th</sup> 2020) working as a guest researcher in the project "NODENS" which is a Caroline Fellowship program cofounded by European Union Horizon 2020 Marie Skłodowska-Curie actions and Irish Research Council.

The post-doctoral fellow, Bing Wu, has generated novel materials in the first part of the project that has been investigated by SAXS measurements. I have successfully applied for beamtime to both ESRF and ALBA in order to understand the structure development in situ. I have estimated the value on beamtime by the number of awarded shifts (5500€ per shift ).

- 2018093178 - Study of the nanostructure double network formation of a modified polypeptide derivativ Alba sincrotrón 2019 - 49.500,0 €
- SC-4908- In-Situ SAXS-WAXS Analyses of 'Microgel' Gel Structure in UV-cured Polyacrylate Systems, ESRF, 2019 - 49.500,0 €
- 2018022840 - Study of the structure of a microgel formation mechanism during the UV-curing of PEG-based polyacrylate. Alba sincrotrón 2018 - 49.500,0 €
- 26-02-900-Structural investigation of the double network formation of a modified polypeptide derivatives. ESRF 2018 -33.000,0 €
- 26-02-899-Investigation of the nanostructure development of a PEG-polyacrylate during UV curing, ESRF, 2018 - 49.500,0 €

We are working on the data analysis and I am focussing on the post-doctoral formation to analyze the SAXS data. I have promoted the post-doctoral fellow to apply for a world-recognized course on synchrotron techniques 'Hercules'. Bing Wu will attend it in March 2020 and we are working on 2 manuscripts on his work that are under preparation.

We have also successfully applied for beamtime for a project on (MA-4398-)In-situ SAXS-WAXS Analyses of 3D-Graphene-Nanocomposite Supercapacitor in the charging-discharging cycle at ESRF (49.500,0 €). We have recently published the obtained results:

- Cuili Xiang, Yin Liu, Ying Yin, Pengru Huang, Yongjin Zou\*, Marcus Fehse, Zhe She, Fen Xu, Dipanjan Banerjee, Daniel Hermida Merino, Alessandro Longo, Heinz-Bernhard Kraatz, Dermot F. Brougham, Bing Wu\*, Lixian Sun, ACS Appl. Energy Mater. 2019, 2, 5, 3389-3399.

## 6-Scientific granted project by Fapesp (Sao Paulo Federal Research Council) for the investigation of 'In situ studies of nanoparticles nucleation and growth assisted by simultaneous SAXS and WAXS and XAS in combination with UV-visible spectroscopy', 2017,

---

I have applied together with José Fernando Queiruga Rey from the Federal University ABC to the Fundação de Amparo à Pesquisa do Estado de São Paulo (FAPESP), for a project entitled 'Estudo de nucleação e crescimento de nanopartículas assistido simultaneamente por técnicas de Espalhamento de Raios X a baixos e médios ângulos (SAXS/ WAXS) e espectroscopia de absorção de Raios X (XAS) em combinação com Espectroscopia UV-Vis'. The project was awarded with 30.000,0 € in order to cover the subsistence as well as the traveling and accommodation of the associate Professor, José Fernando Queiruga Rey. The project has been developed at DUBBLE at ESRF from the 21/08/2017 to the 20/08/2018 under my supervision. Moreover, the project has been actively continued as a result of the promising results obtained by several accepted proposals. A Master thesis has been focused on the understanding in detail of thermal activated nucleation and growth process of CsHSO<sub>4</sub> in Nafion by in situ combined SAXS-WAXS/ EXAFS experiments. Moreover, a Master thesis has been established to study the nucleation and growth of gold nanoparticles in mild conditions to incorporate them in a future step in hydrogels for developing drug delivery systems with sensing properties.

### **SAXS-WAXS/ EXAFS in situ studies of thermal activated nucleation and growth process of CsHSO<sub>4</sub> in Nafion**

The study of metal-organic hybrid systems has been initially selected as it provides a novel approach to combine the mechanical support that offers the polymeric material with the improvement of targeted properties. Nafion has been largely employed as solid electrolytes in Polymer Electrolyte Membranes (PEM) fuel cell applications in the recent years. However, intermediates temperatures (<90 °C), relative high humidity and pure hydrogen as fuel are required to yield high conductivity performances. Hybrid materials have been suggested to be ideal candidates to improve the conductivity performance of Nafion membranes at higher temperatures and lower humidity conditions whilst maintaining the chemical stability and mechanical strength that is particularly significant to operate above 100 °C. Hybrid materials are generally generated by the incorporation of hydrophilic inorganic nanoparticles in the polymer structure. The precursor solution impregnates the Nafion membrane followed by a thermal treatment that induces the nucleation and growth of the nanoparticles inside the membrane. The nanostructure of Nafion-Cs nanoparticles (N-CSP) composites has been studied to enhance the proton conductivity at working conditions. The main advantage of hybrid membranes is the maintenance of high protonic conductivity at low humidity conditions. The objective of the synthesis of Nafion-Cs nanoparticles (N-CSP) composites is to increase protonic conductivity in relation to Nafion under anhydrous conditions. CsHSO<sub>4</sub> is an excellent protonic

conductor at high temperatures and low relative humidity when compared with pure Nafion. The addition of Cs nanoparticles to the Nafion above the percolation fraction may promote an increase in the conductivity of such composite films and allow the operation of direct ethanol fuel cells (DEFC) without gas humidification. The presence of large amounts of water in the DEFCs reduces the gases diffusion in the electrodes of the cell and limit the operating temperature of the DEFC in  $T < 100$  ° C. The nanomorphology of Nafion membranes has been studied in details in the last years, explaining the relationship between morphology and the high-water diffusion coefficient and protonic charge carriers. A detailed study of nanomorphology of the hybrid membranes can play a fundamental role in the design of novel materials.

The thermal activated nucleation and growth process of CsHSO<sub>4</sub> nanoparticles have been studied by in situ combined X-ray absorption fine structure (XAFS) with Small Angle X Ray Scattering (SAXS) measurements at Cs edge. The combined study approach permitted to determine both the chemical nature of the main species in the solution as well as to monitor their morphological evolution in situ.

A detailed study of nanomorphology of the hybrid membranes can play a fundamental role in the design of novel hybrid materials. Preliminary results (see Figure 6.1) shown an improvement in the conductivity of the hybrid membranes followed by changes at the Nafion morphology, as the ionomer peak is more resolved than the pure Nafion counterpart. Previously, it has been hypothesized the internal distribution of the Cs nanoparticles within the Nafion channels.

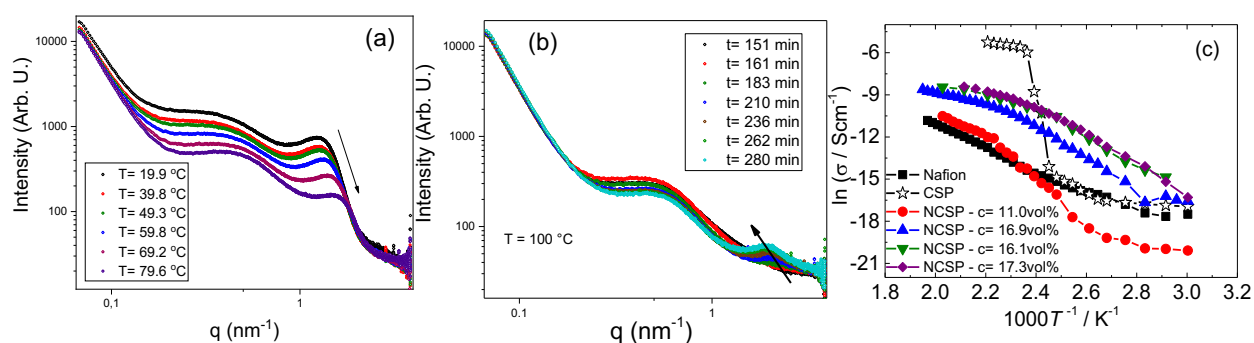


Figure 6.11. a) SAXS heating profiles of Nafion membranes impregnated with Cs precursor solution; b) SAXS isothermal profile showing the time nanoparticles grown process; c) Conductivity of Hybrid nafion nanoparticles at different temperatures.

Moreover, simultaneous XAFS/SAXS measurements performed at bm26a/DUBBLE (see Figure 6.2a) during the heating step have shown that the ionomer peak is modified during the growth of (Figure 6.2b) the Cs nanoparticles (Figure 6.2c), showing that the thermal process play an important role in the nucleation and growth of the nanoparticles.

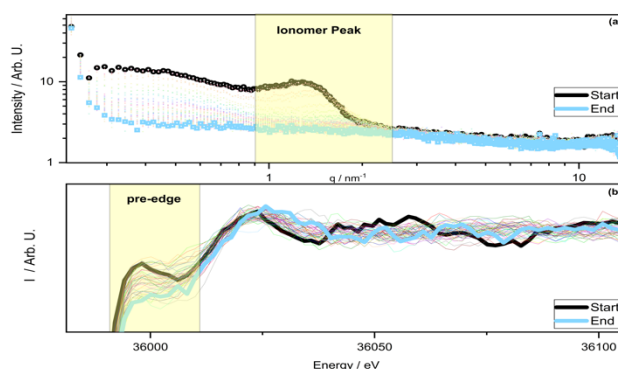


Figure 6.2. a) SAXS-XAS setup at bm26a in the ESRF; b) SAXS heating profiles of Nafion membranes impregnated with Cs precursor solution; c) EXAFS measurement of the element Cs analyzed on the K-shell

During the project, I have successfully applied for beamtime to ESRF in order to study the structure of the N-CSP composites.

- 26-01-1159-study of in situ thermal activated nucleation and growth process of CsHSO<sub>4</sub> nanoparticles by simultaneous XAFS/ SAXS measurements, 2018. ESRF, 49.500,0 €

The preliminary measurements performed have lead to the following publication:

1. Bruno R. Matos, Rodolfo Politano, José Fernando Q. Rey, Daniel Hermida-Merino, Ulrich Schade, Ljiljana Puskar, Fabio C. Fonseca: *Interplay of  $\alpha/\beta$ -Relaxation Dynamics and the Shape of Ionomer Building Blocks*. Scientific Reports 12/2018; 8(1), DOI:10.1038/s41598-018-31368-8

We are currently working on the in-depth structural characterization and more manuscripts are expected to be published in the next future as well as the Master thesis of Victor Cruz de Souza.

Furthermore, I have continued the collaboration with José Fernando Queiruga. Rey at Universidade Federal do ABC by co-directing the Master thesis of Murillo Donizeti dos Santos Rosa entitled 'Nucleação e crescimento de nanopartículas de ouro incorporado em hidrogel'.

Nanostructured materials with metallic nanoparticles, particularly gold nanoparticles, have been probed their applicability in a wide range of fields such as biomedical materials. Herein, the nucleating and grown mechanism of plasmonic nanoparticles produced by an environmental friendly chemical route have been resolved by in-situ SAXS/ UV-vis spectroscopy.

Likewise, I have firstly successfully applied to Alba sincrotrón for the investigation of gold nanoparticles in mild conditions by simultaneous SAXS/UV spectroscopy experiments.

- 2018093066 - Investigation of the nucleation and growth mechanism of gold nanoparticules by in situ UV-vis spectroscopy and SAXS. date:14/07/2019. 49.500,0 €, Alba sincrotrón

Moreover, I have developed a novel cell that allows monitoring the growth of the gold nanoparticles in flow to minimize the X-ray influence by simultaneous SAXS- UV-vis spectroscopy in order to correlate the changes on the plasmon with the morphological evolution (see Figure 6.3).

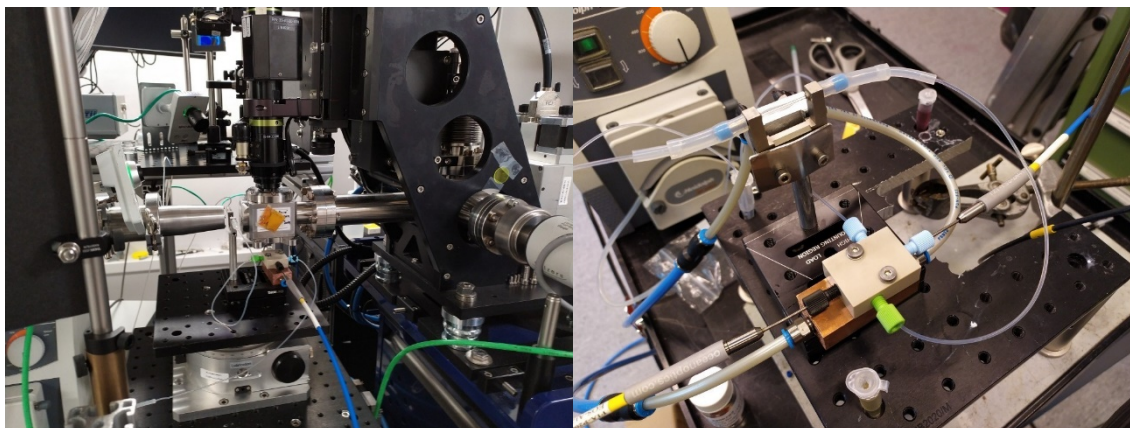


Figure 6.3. a) SAXS/UV spectroscopy setup at bm 11 in Alba. b) A magnification of the flow closed-loop system circulated with the help of a peristaltic pump.

Applications of nanostructured materials in advanced materials and biomedicine have been extremely important at the development of nanoscience and nanotechnology. Metallic nanoparticles, like gold and silver nanoparticles, are very stable and shows to be very interesting due to their electronic, magnetic and optical properties are related with the size (quantum effects). Metallic nanoparticles like gold and silver nanoparticles are interesting since they catalytic and biological properties can change the materials applications. Nowadays, synthetic routes achieve with high efficiency nanoparticles with tuning sizes and shapes at high production rates. However, the development of biocompatible chemical routes that retained the synthetic efficiency and nanoparticles stability are required to meet environmental policies. The use of biomolecules as reducing and/or stabilizing agents in a chemical or photochemical synthesis are ideal candidates to follow environmental friendly approaches. The effect of tetrachloroauric acid speciation during the nanoparticles synthesis in the replacement of Cl by H<sub>2</sub>O and D<sub>2</sub>O at the gold in aqueous medium has been studied. Thus, the process of gold speciation was subjected to the differential capacity of exchange of the deuterium dioxide associated with the gold ion by water molecules of the reaction medium. The gold speciation will be promoted by the pH variation at the gold salt precursor solution. Likewise, the gold nanoparticles could be chemically obtained by the mixture of 0.45 mM gold salt solution (AuP) at a pH 10 buffer HEPES 2.5mM /sodium phosphate (B1) or HEPES 30 mM/sodium phosphate (B2). The HEPES buffer features a piperazine molecule which act either as reductor and stabilizing agent since it can produce free radicals at the central nitrogen able to reduce the gold ion.

The in-situ measurements were carried out during the nucleation and grown of gold nanoparticles by the addition of 0.45 mM of gold salt solution (H<sub>2</sub>O or D<sub>2</sub>O) in a reductor medium (HEPES (0.25mM or 30mM) + sodium phosphate) with pH 10. According to the following scheme:  $\text{AuC}_4^- + \text{AuCl}_3(\text{OH})^- + \text{AuCl}_3(\text{H}_2\text{O})$  and  $\text{AuC}_4^- + \text{AuCl}_3(\text{OD})^- + \text{AuCl}_3(\text{D}_2\text{O})$  both

solutions with proportion 5:2:3. The precursor solution and buffer were mixed in a controlled way by the stopping flow device and injected in a capillary to follow the reaction from the beginning.

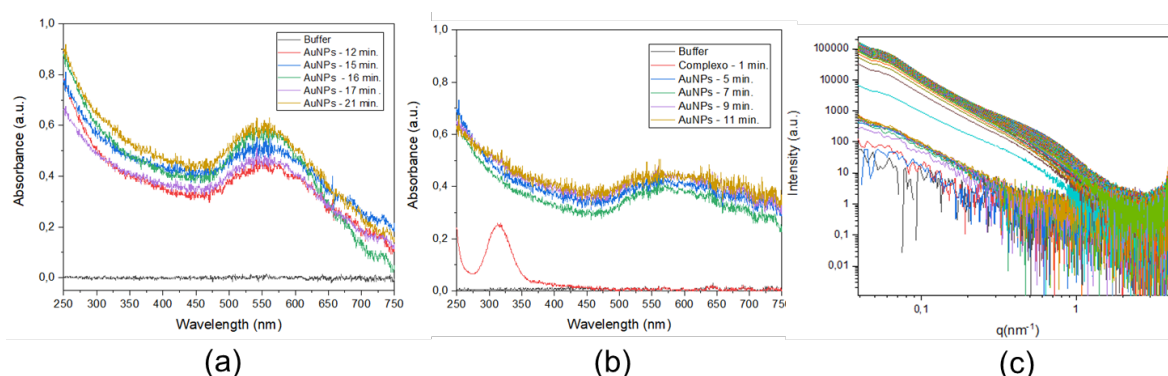


Figure 6.4 a) Uv-Vis absorption spectra of a solution mixture of HAuCl<sub>4</sub> and HEPES with different times ([AuP = 0.45 mM, H<sub>2</sub>O]/ ([B1 HEPES = 2.5 mM, D<sub>2</sub>O]). b) UV-vis absorption spectra of a solution mixture of HAuCl<sub>4</sub> and HEPES with different times ([AuP = 0.45 mM, D<sub>2</sub>O]/ (B2 [HEPES = 2.5 mM, D<sub>2</sub>O])). c) SAXS experimental data of the nucleation and growth mechanisms of a solution mixture of HAuCl<sub>4</sub> and HEPES ([AuP = 0.45 mM, D<sub>2</sub>O]/ ([B1 HEPES = 2.5 mM, H<sub>2</sub>O]))

The nanoparticle growth has been followed by SAXS measurements as well as the simultaneous monitoring of the absorption gold band at different conditions will allow us to understand the effect of the chemical environment can affect the process of nucleation and growth process to obtain a particular morphology. A detailed analysis of both the maximum absorption band of gold nanoparticles at different times of D<sub>2</sub>O/AuP suspensions in B1 Buffer (see Figure 6.4a) as well as in H<sub>2</sub>O/AuP suspensions in B2 Buffer (see Figure 6.4b) with the SAXS experiments (see Figure 6.4c) during the nucleation and grown process will permit us to correlate the plasmonic properties with the nanoparticles dimensions. Moreover, the fitting of the SAXS profiles will be used to estimate the size and size distribution of the gold nanoparticles.

## References

1. Colvin, V.L., *The potential environmental impact of engineered nanomaterials*. Nature Biotechnology, 2003. **21**(10): p. 1166-1170.
2. Daniel, M.C. and D. Astruc, *Gold nanoparticles: Assembly, supramolecular chemistry, quantum-size-related properties, and applications toward biology, catalysis, and nanotechnology*. Chemical Reviews, 2004. **104**(1): p. 293-346.
3. Sarikaya, M., et al., *Molecular biomimetics: nanotechnology through biology*. Nature Materials, 2003. **2**(9): p. 577-585.
4. Gurunathan, S., et al., *A green chemistry approach for synthesizing biocompatible gold nanoparticles*. Nanoscale Research Letters, 2014. **9**(1): p. 9-248.

# SCIENTIFIC REPORTS



OPEN

## Interplay of $\alpha/\beta$ -Relaxation Dynamics and the Shape of Ionomer Building Blocks

Bruno R. Matos<sup>1</sup>, Rodolfo Politano<sup>1</sup>, José Fernando Q. Rey<sup>3,4</sup>, Daniel Hermida-Merino<sup>4</sup>, Ulrich Schade<sup>2</sup>, Ljiljana Puskar<sup>2</sup> & Fabio C. Fonseca<sup>1</sup>

The relation between the  $\alpha/\beta$  relaxations and the shape of the building blocks of ionomer materials is a key factor for programming an important temperature-dependent property: the memory of shape. However, the morphology of ionomers is indirectly obtained via modeling of small angle X-ray scattering (SAXS) data owing to the hardly accessible image characterization of the nanometric building blocks – micelle-like cylindrical polymeric aggregates (radius ~2–6 nm and length >100 nm). Herein, broadband dielectric spectroscopy (BDS) measurements, free from electrode polarization effects, allowed identifying the time and temperature dependence of the polarization of different length scales of the ionomer matrix, and more importantly, by directly providing the aspect ratio of the radius and length of the polymeric aggregates for each desired temperature. This finding is essential for controlling the shape of ionomer based functional products under several stimuli conditions, thereby advancing remarkable applications, such as four dimensional (4D) printing.

Ionomers are considered shape memory polymers due to the ability of fixing, or programming, two or multi macroscopic shapes on different types of stimuli, such as, temperature and moisture content<sup>1</sup>. Such adaptive materials are envisioned as a revolutionary concept and a massive world trend of production of functional parts<sup>1,2</sup>. Associated with additive manufacturing, the shape memory polymers have the ability of reconfiguring the matrix structure to a temporary desired shape according to the ambient stimulus, adding a new dimension to the final product: time. The advance of shape memory ionomers is valuable for several high-performance applications such as artificial muscle design, electrocatalyst binders, polymer electrolyte fuel cells, and four dimensional (4D) printing<sup>1–5</sup>.

Perfluorinated ionomers (PIs) are a specific family of ionomeric materials that displays outstanding physical properties, such as, thin-film nanoconfinement, exceedingly high ion transport, elevated mechanical resistance, and memory of shape<sup>3,6,7</sup>. All of these properties are known to be linked to the PIs morphology. The PIs morphology has been extensively modeled by SAXS in which the building blocks of their microstructure are assigned to long cylinder like polymeric aggregates ( $r \sim 2.5$  nm and  $L > 100$  nm), adjacently packed together mainly by temporary ionic crosslinks and a low degree of crystallinity<sup>5,6</sup>. Many efforts have been made to characterize the shape of such polymeric aggregates by image characterization techniques<sup>8,9</sup>. The most promising results have been obtained by transmission electron microscopy (TEM) and atomic force microscopy (AFM)<sup>8,9</sup>. However, due to instability of the sample during TEM measurements and the interaction of the sample with the tip in AFM, most of the available data display artifacts and are not representative of the PI morphology<sup>8,9</sup>. Moreover, by means of such techniques, the *in situ* temperature characterization of the polymeric aggregates is very problematic. This issue is aggravated if the morphology information as a function of relative humidity is required. Such drawbacks have been overcome with the use of small angle X-ray scattering (SAXS) in which the ionomer morphology at different sets of temperature and relative humidity can be indirectly obtained via modeling<sup>9,10</sup>. In addition, usually at the  $\alpha$ -transition, the peak associated with the radial correlation of the polymeric aggregates (ionomer peak) disappears, and as such, the mechanism for this thermal-triggered disordering, or loss of correlation of the polymeric aggregates, has not been fully understood or modeled<sup>9,11</sup>. The absence of a solid empirical finding relating

<sup>1</sup>Instituto de Pesquisas Energéticas e Nucleares, IPEN-CNEN/SP, São Paulo, 05508000, Brazil. <sup>2</sup>Methoden der Materialentwicklung, Helmholtz-Zentrum für Materialien und Energie GmbH, Berlin, 12489, Germany. <sup>3</sup>Universidade Federal do ABC, UFABC, Santo André, 09219170, Brazil. <sup>4</sup>Netherlands Organisation for Scientific Research (NWO), DUBBLE@ESRF, Grenoble, 38000, France. Correspondence and requests for materials should be addressed to B.R.M. (email: [brmatos@usp.br](mailto:brmatos@usp.br))

the temperature and shape of the polymeric aggregates makes the SAXS modeling arbitrary and speculative. Therefore, this issue requires a modeling-independent characterization of the shape and size of the polymeric aggregates as a function of  $T$  for understanding the shape memory property and advancing 4D printing, for example.

Broadband dielectric spectroscopy (BDS) is a powerful tool to study the dynamics of the polarization due to ion-hopping within ionomeric matrices in a wide range of length scales<sup>6,12</sup>. However, the dielectric spectrum usually displays electrode polarization contributions that mask the characteristic relaxation frequencies within the ionomer matrix<sup>13</sup>. Specifically, this feature has been a main issue for the characterization of PIs, due to the high ion conductivity, and for more than 40 years the assignment of the dielectric spectrum of PIs is an open problem<sup>6,14,15</sup>. Even more recently, from 2014 up to the present day, the old interpretations of PI dielectric spectra have not thrived over the years<sup>6,15</sup>. From 2014 onwards, more recent findings showed a careful characterization of the dielectric spectrum of solutions and hydrated solid films of a one of the mostly studied PI, Nafion®<sup>16</sup>. Dilute Nafion solutions represented a simple system for the characterization of the mechanisms of ion-hopping polarization within the polymeric aggregates<sup>16</sup>. The striking result was that PIs exhibit polyelectrolyte-like polarizations instead of the conventional segmental motion relaxations observed in hydrocarbon ionomers, for example. The  $\alpha$  and  $\beta$  relaxations observed in the dielectric spectrum were assigned to the ion-hopping polarization along the longitudinal and radial directions of the polymeric aggregates, respectively<sup>16,17</sup>. By adding salt to Nafion solution a rod-to-coil transition occurred and the size and shape of the polymeric aggregates were estimated considering the position of  $\alpha$  and  $\beta$  relaxations<sup>16</sup>. An excellent match was obtained for the dimensions of the polymeric aggregates as estimated by SAXS and BDS<sup>16,17</sup>. This finding opens the investigation of the shape/relaxation relation for solid PI films.

Here, the aspect ratio of the polymeric aggregates was directly obtained at a broad range of temperature for Nafion by BDS. The electrode polarizations at very low frequencies ( $f < 10^{-2}$  Hz) were eliminated in this work by the use of a 4-probe setup or a two-probe having high specific surface area electrodes. Initially we performed variable temperature SAXS, infrared spectroscopy (FTIR), and dynamic mechanical analysis (DMA) on Nafion in order to determine the morphology of the ionic domains, state of the electrostatic interactions among ionic groups, and the thermal transition within the ionic phase, respectively, at rigorously the same experimental conditions. Posteriorly, the SAXS, FTIR and DMA data are confronted to BDS measurements of Nafion.

Mid and far infrared (MIR and FIR) spectroscopy and SAXS measurements were performed on Nafion during increasing temperature in the 30–200 °C  $T$ -range ( $RH \sim 0\%$ ) under  $N_2$ . Figure 1a and b shows the MIR data in the functional groups region (4000–1250  $cm^{-1}$ ) collected during the first and second heating, respectively. Figure 1c shows the 2D plot of FIR (400–20  $cm^{-1}$ ) data for Nafion measured in the first heating. Figure 1d shows the SAXS patterns for Nafion during the first heating, and the inset shows  $I^{-1/2}$  vs  $q^2$  plot in the low  $q$ -range.

Relevant features in the Nafion MIR spectra are observed on the first and second heating: (i) at 200 °C, the OH stretching at 2980  $cm^{-1}$  displays a blueshift ( $\sim 220$   $cm^{-1}$ ); followed by the development of a high frequency (3500  $cm^{-1}$ ) band assigned to dangling OH groups in  $SO_3H$ ; (ii) the water bands at 1660, 1710 and 2200  $cm^{-1}$  disappeared revealing the underlying  $CF_2$  overtone at 2370  $cm^{-1}$ ; and (iii) the bands associated with  $RSO_3^-$  (1060  $cm^{-1}$ , not shown<sup>18</sup>) gradually disappeared leading to the gradual appearance of  $SO_2$  vibration in  $RSO_3H$  (1410  $cm^{-1}$ )<sup>18,19</sup>. Notably, the initial coordination water of Nafion samples results is monohydrated sulfonic groups ( $RSO_3H \cdot H_2O$ )<sup>20</sup>. Previous thermogravimetric analysis on vacuum dried Nafion samples evidenced that heating from 30–200 °C removed the residual water molecules in the samples<sup>20</sup>. The water removal is in agreement with absence of MIR water bands and the association of the protonic charges with the sulfonic groups at  $T > 100$  °C (hereafter mentioned as “dry samples”) indicating that the proton diffusion takes place mostly via ion-hopping. Further minimization of the water content is attained in the second heating (Fig. 1b) in which protons are associated with the sulfonic groups from 40 to 200 °C, due to the presence of the 1410  $cm^{-1}$  band in the entire  $T$ -range; whilst the broad OH stretching MIR band (3000  $cm^{-1}$ ) is mostly due to clustering  $RSO_3H$  in the sample<sup>19</sup>. Importantly, the ionic crosslinks persisted in the entire temperature range investigated. The blueshift of the OH stretching in  $RSO_3H$  (2980  $cm^{-1}$ ) takes place in the  $\alpha$ -transition  $T$ -range ( $T_\alpha \sim 120$  °C), having the onset and endset at 100 and 140 °C, respectively. A blueshift of the OH stretching frequency is reported for solid-liquid-vapor transition of  $H_2O$  and corresponds to the weakening of the hydrogen bonding<sup>21</sup>. The weakening of the OH bonding in Nafion with increasing  $T$  can be understood considering the counterelastic forces imposed by the main and side chains against the ionic aggregation as the temperature increases. This feature suggests that the enough  $KT$  energy is being provided allowing segments of the polymer chains to escape from the temporary ionic crosslinks.

Cation exchange experiments in the FIR region reported the cation motion frequency of the  $H^+ \cdot SO_3^-$  form in Nafion appearing as broad band centered at 240  $cm^{-1}$ , which can also be seen in Fig. 1c<sup>19,22</sup>. The most prominent features reported in the spectral region of 50–400  $cm^{-1}$  are the  $CF_2$  rocking band at 204  $cm^{-1}$ , and three bands present in the proton form of Nafion  $\sim 240$ , 335, and 375  $cm^{-1}$ , which are assigned to H-bond stretching involving the hydronium ion<sup>19,22</sup>. It was previously observed that decrease of hydration promoted a decrease of the intensity of 335 and 375  $cm^{-1}$  bands<sup>19</sup>, following the behavior of the water bands in the MIR range (Fig. 1a and b). However, these bands persisted for  $T > 120$  °C, suggesting that these bands are also probably related to OH stretching in  $RSO_3H$ .

It is difficult to infer feature changes of the cation motion band (240  $cm^{-1}$ ) upon heating due to the partial overlapping with 335  $cm^{-1}$  band (Fig. 1c). Nonetheless, it is possible to notice a broadening and intensity reduction for  $T > 140$  °C of the cation motion band. At high  $T$  ( $> 180$  °C), the absorbances of both 240 and 335  $cm^{-1}$  bands are diminished and only a broad coalesced absorbance is observed. These findings reveal important aspects of the cation-motion band of perfluorinated ionomers. As the cation motion band of ionomers is related to the proton transport across the length scales of the ionic heterogeneities of the sample, the broadening of such band for  $T > 140$  °C suggests that the ion-hopping occurs over more disordered ionic aggregates.

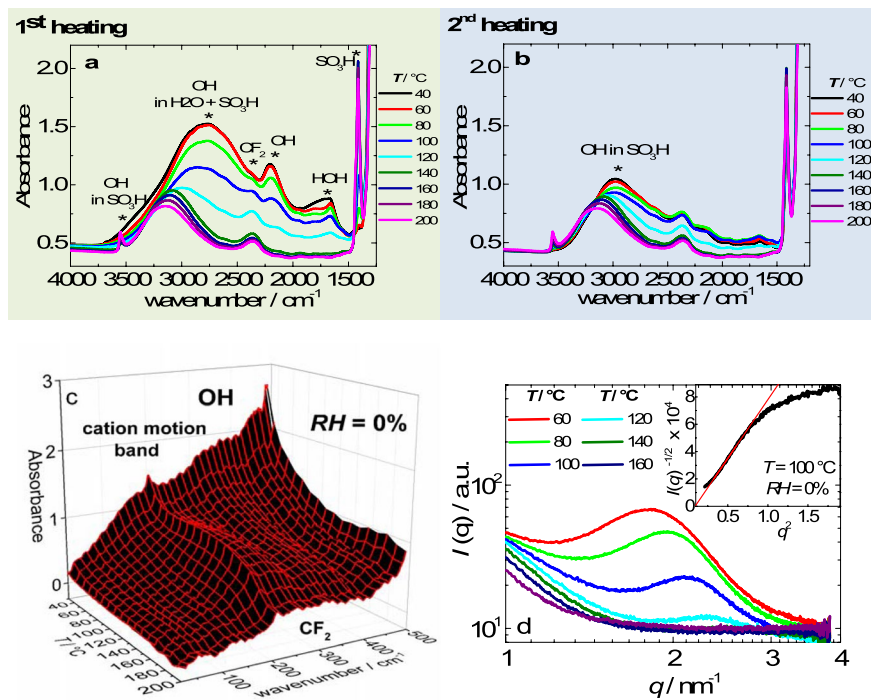


**Figure 1.** *In situ* MIR temperature measurements of Nafion during the first and second heating in the transmission mode in the functional groups region, 4000–1250  $\text{cm}^{-1}$  (a and b). *In situ* FIR temperature measurements of Nafion during the first heating in the transmission mode using the synchrotron source from the IRIS beamline (c). *In situ* SAXS temperature measurements of Nafion during the first heating using the synchrotron source from the ESRF beamline (d). The inset shows  $I^{-1/2}$  vs  $q^2$  plot in the low  $q$ -range.

Usually, SAXS patterns of Nafion membranes at low RH ( $RH \sim 10\%$ ) display a scattering maxima centered at  $q \sim 1.9 \text{ nm}^{-1}$  due to the ionomer peak<sup>23</sup>, which can be clearly observed in Fig. 1d for low temperatures. Previously, ultra small angle X-ray scattering (USAXS) measurements of Nafion in the hydrated form displayed low- $q$  scattering upturn ( $q < 0.03 \text{ nm}^{-1}$ ), being attributed to large-scale density fluctuations associated with the length of the polymeric aggregates ( $l \approx 350 \text{ nm}$ )<sup>23,24</sup>. Similarly, the Zimm approximation ( $I^{-1/2} \text{ vs } q^2$ ) is shown in the inset of Fig. 1d to estimate the length of the polymeric aggregates of Nafion in the dry form<sup>23,24</sup>. In the first and second heatings, the length exhibits a weak dependence on temperature. For the first heating, the length decreases from 182 to 174 nm in the 20–200 °C  $T$ -range, whereas in the second heating the length decreases from 154 to 150 nm at the same  $T$ -interval. The reduction of the size of the polymeric aggregates, in the sequence 350 nm (hydrated Nafion)<sup>23</sup> > 182 nm (1<sup>st</sup> heating) > 150 nm (2<sup>nd</sup> heating), is possibly due to the less expanded polymeric aggregates due to the water elimination and coordination of protons with the sulfonic acid groups, minimizing the electrostatic repulsions among bare sulfonic acid groups in the sample containing water molecules.

The ionomer peak corresponds to the radial correlation of the cylindrical polymeric aggregates, and at 120 °C the radius is 2.74 nm (Fig. 1d). The SAXS patterns of Nafion measured in the first and second heatings are similar in the 30–200 °C  $T$ -range. With increasing  $T$ , in the 30–140 °C range, the ionomer peak decreases in intensity, broadens, and displaces to higher  $q$ -values (from 1.72 to 2.48  $\text{nm}^{-1}$ ). In the second heating, the reduction in SAXS peak intensity in the 30–140 °C range is minimized. Such a less temperature-dependent peak intensity is supported by FTIR (Fig. 1b) and can be related to the loss of residual water molecules and irreversible modification of the ionic network arrangement during the first heating. Most pronounced changes in the SAXS patterns are observed at  $T \sim 140$  °C, for which the ionomer peak is totally suppressed. The reduction of the ionomer peak intensity could be linked to the water evaporation. However, MIR results evidenced that the effect of the removal of coordinated water from sulfonic acid groups for  $T > 100$  °C are minimal. Therefore, the changes of the ionomer peak features for  $T > 140$  °C can be attributed to a loss of ordering of the polymeric aggregates. Such finding is in good agreement with the FIR data, confirming that a structuring of the ionic phase takes place due to the weakening of the electrostatic interactions at the  $\alpha$ -transition. Previously, the disappearance of the ionomer peak has been observed for drawn Nafion films in the direction perpendicular to the stretching axis, which was attributed to a misalignment of the polymeric aggregates<sup>24</sup>. In this scenario, a tentative explanation for the suppression of the ionomer peak at the  $\alpha$ -transition would be the misalignment of the polymeric aggregates, possibly due to the minimization of the electrostatic repulsion among sulfonic acid groups due to water removal and the weakening of the electrostatic interactions among  $\text{SO}_3\text{H}$  dipoles, which are the “pillars” for the cylindrical shape of the polymeric aggregates. However, the water removal effect and the weakening of the electrostatic interactions do not explain the reason why the suppression of the ionomer peak takes place at 140 °C. It is also worth noting that the only information that can be extracted from both FIR and SAXS measurements is a disordering of the ionic phase

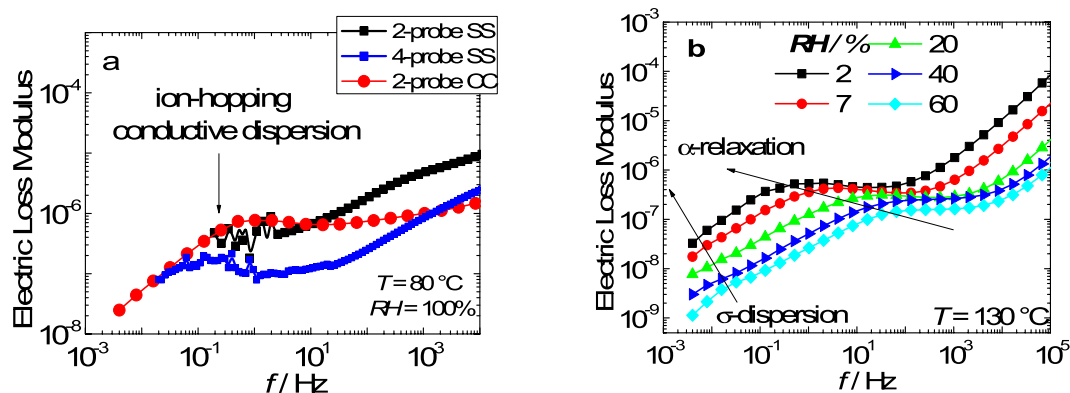


**Figure 2.** Electric loss modulus of Nafion using three different electrodes setup: 2-probe SS; 4-probe SS; and 2-probe CC (a). Electric loss modulus of Nafion with decreasing relative humidity using 2-probe CC (b).

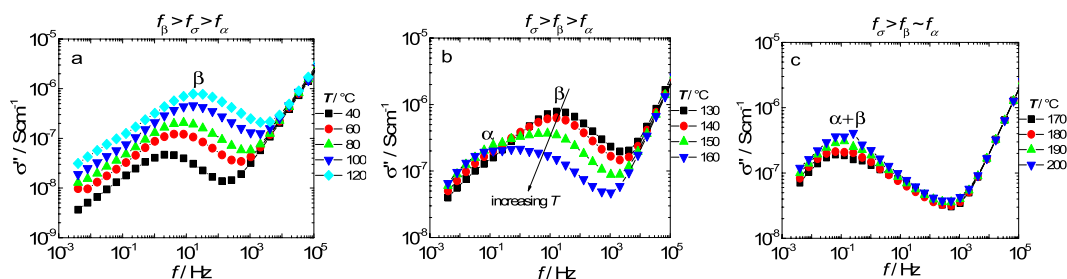


**Figure 3.** Imaginary component of the proton conductivity as a function of frequency in three temperature ranges: (a) from 40 to 120 °C; (b) from 130 to 160 °C; and (c) from 170 to 200 °C.

with increasing  $T$ . Both techniques remain silent with respect to the mechanism of this disordering transition, mechanism of which can be assessed by BDS<sup>25</sup>.

In BDS, the characteristic frequencies of both ion-hopping and  $\alpha$ -relaxation are commonly overlapped with electrode polarization at low frequency (typically in the  $10^{-2}$ – $10^2$  Hz range), hindering the investigation of the dynamics of the dielectric dispersions<sup>17,25</sup>. BDS measurements of Nafion using 4-probe and 2-probe (using high surface specific area electrodes) in the through-plane setup are free from electrode contributions. Such measurements allowed identifying the ion-hopping (proton hopping) as well as the  $\alpha$  and  $\beta$  relaxations.

Figure 2 shows the dielectric spectroscopy measurements (in the electric modulus formalism/ $M^* = M' + iM''$ ) of Nafion performed with decreasing relative humidity from 100% to 2%. Such measurement allows determining the position of the relaxations at high RH in which the ion-hopping dispersion (Fig. 2a) and  $\alpha$ -relaxation (Fig. 2b) are more easily identified<sup>17</sup>, and monitor its displacement as the sample dries, thereby determining the position of the relaxations in the dry film. The identification of ion-hopping dispersion ( $\sigma$ -dispersion) of Nafion, as showed in Fig. 2a, was performed using three different setups: (i) 2-probe using flat stainless steel (SS) electrodes; (ii) 4-probe SS electrodes; and (iii) 2-probe carbon cloth (CC) electrodes. Both the  $M''(f)$  representation and the 4-probe setup eliminates electrode polarization effects revealing the  $\sigma$ -dispersion at  $f \sim 10^{-1}$  Hz for Nafion at  $RH = 100\%$ <sup>13</sup>. Such a feature cannot be detected using the 2-probe SS setup. However, highly reproducible DS measurements with a well-defined  $\sigma$ -dispersion are obtained using high specific surface area 2-probe CC electrodes in a broad range of frequency and temperature. The elimination of the electrode polarization in such frequency range allows determining the position of the  $\sigma$ -dispersion and  $\alpha$ -relaxation as the relative humidity decreases, as shown in Fig. 2b.

At 130 °C ( $RH = 60\%$ ) the relaxations are displaced to a higher frequency range in which the  $\sigma$ -dispersion and the  $\alpha$ -relaxation are identified at  $f_\sigma \sim 10^{-1}$  and  $f_\alpha \sim 10^2$  Hz, respectively (Fig. 2b). As the RH decreases from 60 to 2%, the  $\alpha$ -relaxation decreases in frequency from  $10^2$  to  $10^{-1}$  Hz, superposing with  $\sigma$ -dispersion ( $\sim 10^{-2}$  Hz), indicating a lower RH-dependence of  $f_\sigma$  compared to  $f_\alpha$ . The  $\sigma$ -dispersion frequency of Nafion at dry conditions is in good agreement with previous investigations of *ac* conductive dispersion ( $f \sim 10^{-2}$ – $10^{-3}$  Hz)<sup>17</sup>. Therefore, the results of Fig. 2b indicate that at dry conditions ( $T = 30$  °C and  $RH \sim 0\%$ ) initial position of the  $\alpha$  and  $\beta$  relaxations with respect to the  $\sigma$ -dispersion are:  $f_\sigma \sim f_\alpha$  and  $f_\sigma < f_\beta$ . Such relations are helpful to understand the dynamics role of the ion-hopping on the  $T$ -dependence of the relaxation dynamics of the ionomer, as shown in Fig. 3.

Figure 3 shows the imaginary conductivity spectra ( $\sigma^* = \sigma' + i\sigma''$ ) of Nafion at three  $T$ -ranges at  $RH \sim 0\%$  during the second heating. In Fig. 3a, only the  $\beta$ -relaxation can be observed in the 40–120 °C  $T$ -range, indicating that at  $RH \sim 0\%$ , the alpha-relaxation is displaced even further to lower frequencies.

The ion-hopping characteristic frequency,  $f_\sigma$ , refers to the dynamics of the temporary crosslinks<sup>25</sup>, while  $\alpha$ - and  $\beta$ -relaxations represent the ion-hopping polarization due to the higher activation energy across the length scales

of the polymeric aggregates<sup>13</sup>. The protonic charges diffuse via ion-hopping in the polymeric matrix and polarize at the polymeric aggregates. In this context, two limiting cases are relevant for understanding of Nafion spectra: (i) for  $f_\beta > f_\sigma > f_\alpha$ , the proton diffusion is not limited by the longitudinal polarization of the polymeric aggregates; and (ii) for  $f_\beta > f_\alpha > f_\sigma$ , the proton diffusion is reduced by the polarization of the protonic charges across the radius and length of the polymeric aggregates. The change from behavior (i) to (ii) takes place at 120 °C, as shown in Fig. 3c and d, indicating that the  $\alpha$ -transition of Nafion is associated with the presence of an additional polarization of charges existing at  $T > 120$  °C.

Figure 3b shows that as the temperature increases from 40 to 120 °C, the  $\beta$ -relaxation displaces to higher  $f$  and a shoulder is seen at 120 °C due to  $\alpha$ -relaxation high- $f$  displacement. In the 140–170 °C  $T$ -interval (Fig. 3c), the  $\beta$ -relaxation displaces to low  $f$  until it superposed with the  $\alpha$ -relaxation at  $f = 10^{-1}$  Hz. Both the high- $f$  and low- $f$  displacements of  $\alpha$  and  $\beta$ -relaxations, respectively, represent a change of conformation of the polymeric aggregates. Therefore, the blueshift of  $\alpha$ -relaxation indicates a reduction of the length of the polymeric aggregates, whereas the redshift of  $\beta$ -relaxation indicates a thickening of the polymeric aggregates. The coincidence of both relaxations for  $T > 170$  °C suggests a reduction of the aspect ratio of the polymeric aggregates to a nearly spherical shape.

The length and radius of the polymeric aggregates ( $L$ ) are associated with the radial ( $f_\beta$ ) and longitudinal ( $f_\alpha$ ) polarization frequencies by the following equation<sup>12,25</sup>:

$$f_{\alpha,\beta}^{-1} \approx \frac{L^2}{D}, \quad (1)$$

where  $D$  is the diffusion coefficient of protons counterions obtained by Nernst-Einstein relation:  $D = \sigma k_b T / ne^2$ ; where  $k_b$  is the Boltzmann constant,  $T$  is the absolute temperature,  $e$  is the elementary charge, and  $n$  is the charge concentration. In the  $f_\beta > f_\sigma > f_\alpha$  regime, at 120 °C, the radius of the polymeric aggregates is ~6.47 nm. Due to the difficulty in assessing the  $\alpha$ -relaxation from 30 to 120 °C it is not possible to precisely obtain the length of the polymeric aggregates. However, the high- $f$  shift of the  $\alpha$ -relaxation in Fig. 2b ( $f \sim 10^{-2}$  to  $10^{-1}$  Hz) suggests a reduction of the length from 287 to 90 nm, in which the latter is the lowest length achieved by the aggregates at  $T = 160$  °C (the endset of  $\alpha$ -transition). In the 170–200 °C range, the  $\alpha$ -relaxation frequency is nearly constant resulting in an increase of the length of the polymeric aggregates ranges from ~141 to 210 nm, which can be an outcome of the thermal expansion of the aggregates. It is worth emphasizing that the radius and length obtained by BDS have similar magnitude as the ones obtained by SAXS. The FIR, SAXS and BDS are in very good agreement indicating that the properties of Nafion membranes are profoundly modified above the  $\alpha$ -transition due to the crossover from the two regimes and the suppression of the radial correlation of the polymeric aggregates.

Figure 4a shows the radial correlation of the polymeric aggregates ( $r$ ) estimated by SAXS and DS. Figure 4b combines FIR, SAXS and BDS data evidencing the suppression of the radial correlation length at the  $\alpha$ -transition, as determined by dynamic mechanical analysis (DMA). Figure 4c shows a schematic representation of the proposed conformation transition of Nafion due to the crossover from regime *i* to *ii*.

In Fig. 4a, as the temperature increases from 30 to 120 °C, the radius obtained by SAXS and BDS of the polymeric aggregates decreases, following a similar power law with increasing  $T$ ,  $-0.02$  and  $-0.05$ , respectively.

The  $\alpha$ -transition as determined by DMA, the elastic modulus drops to values close to zero confirming that the long-range motion of the main chains is no longer restricted by the ionic crosslinks. Since the ion-hopping is correlated with the motion of the main and side chains, the  $\alpha$ - and  $\beta$ -relaxations are associated with the long and short range motions of the polymer backbone, respectively. Similarly, considering the segmental motion of the main chains, the two limiting cases can be devised as: (i) For  $f_\beta > f_\sigma > f_\alpha$ , the long range motion of the main chains is restricted by the ionic crosslinks; and (ii) for  $f_\beta > f_\alpha > f_\sigma$ , only the short range motions are restricted by the ionic clustering. This conformation transition is only possible due to the  $f_\beta > f_\alpha > f_\sigma$  relation at  $T > 120$  °C, which allowed the long range motion to escape from the restrictions imposed by the ionic crosslinks.

The combined techniques showed that the length scales of the polarizations probed by BDS are compatible with the ones observed by SAXS. Such findings allow correlating conformation changes of the polymeric aggregates with the ion-hopping. Therefore, the understanding of the evolution of the size and ordering of the polymeric aggregates and the ion-hopping with increasing  $T$  would help establish the relationship between the ionic network and microstructure of PIs, which is crucial for tailoring new high-performance ionomers<sup>26</sup>. The reversibility of the shape of the polymeric aggregates due to annealing and water swelling of Nafion is the next step of this investigation.

## Conclusions

Broadband dielectric spectroscopy (BDS) with free electrode polarization effects is shown to be a unique tool capable of revealing the origin of the atypical dynamics of  $\alpha$ -transition in perfluorinated ionomers. The combination of variable temperature IR, SAXS, and DS allowed for monitoring of the electrostatic interactions and morphology from different length scales in Nafion membranes. These characterizations provide further insights into the origin of  $\alpha$ -transition. Namely, the  $\alpha$ -transition is a critical temperature ( $T = 120$  °C) separating two regimes. Below  $\alpha$ -transition ( $T < 120$  °C) the shape of the polymeric aggregates are locked into nanocylinders due to the fast ion-hopping, which restricts the translational motion of the main and side chains. Above  $\alpha$ -transition ( $T > 120$  °C), the relaxation frequency of  $\alpha$  surpasses the ion-hopping permitting the long-range motion of the main chains, which relaxes in a more spherical conformation. Such finding allows mastering the temperature-shape relationship in ion-containing polymers as well as tuning the desired shape of the building blocks of the ionomer morphology.

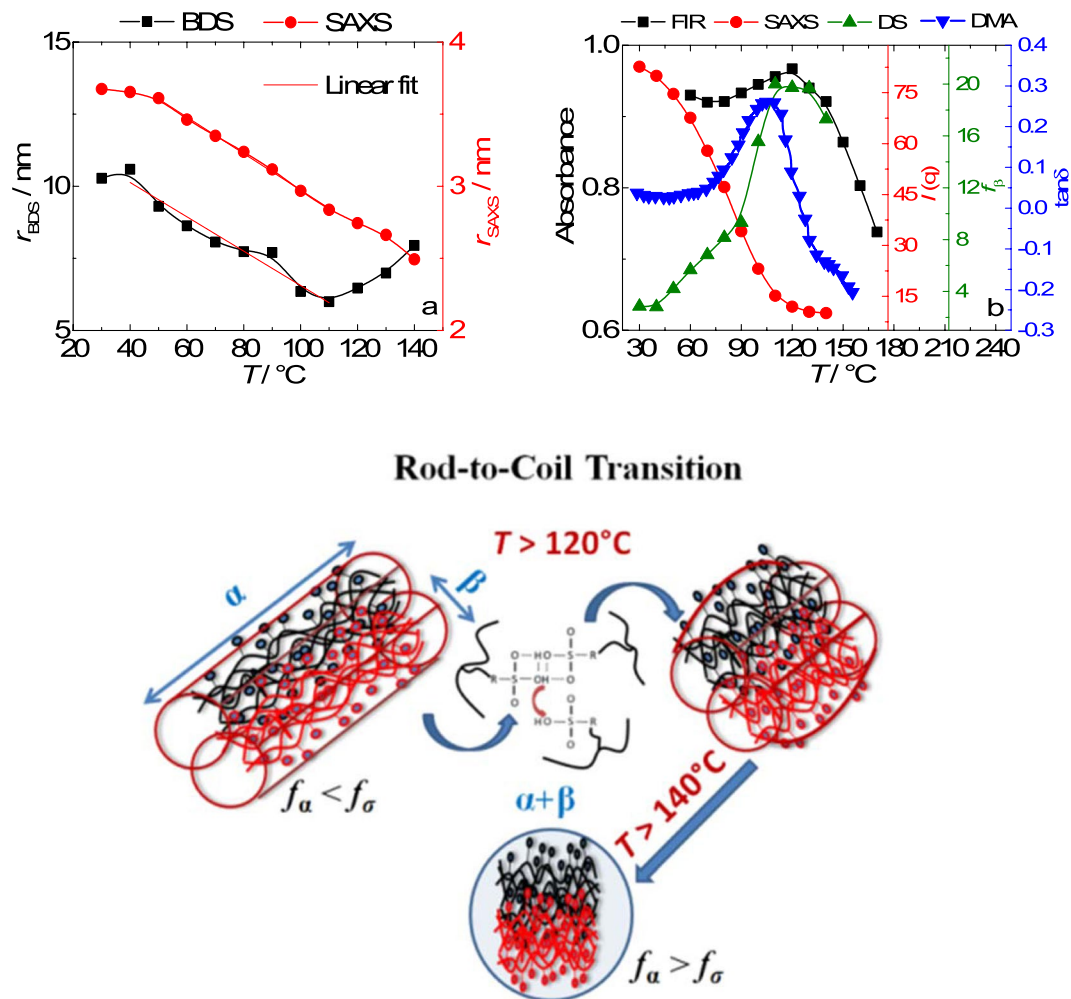


**Figure 4.** The  $\alpha$ -transition as measured by DMA and the disordering of ionic domains of the polymeric aggregates as determined by different techniques, FIR (band position), SAXS (ionomer peak position) and BDS ( $\beta$ -relaxation position) (a); the radius of the polymeric aggregates as estimated by SAXS and BDS (b); and schematic representation of the proposed conformation transition of Nafion due to the crossover from regime *i* to *ii* (c).

## Methods

Commercial Nafion membranes ( $EW = 1,100 \text{ g eq}^{-1}$ ) were obtained from DuPont with different thicknesses (N211, N115). The membranes were pre-treated by standard cleaning and activation protocols<sup>17</sup>. The obtained film was then post-treated in 3% (w/w)  $\text{H}_2\text{O}_2$  and 0.5 M  $\text{H}_2\text{SO}_4$ , with intermediate steps in  $\text{H}_2\text{O}$  to remove excess chemicals. Nafion membranes in the non-ionic form ( $\text{RSO}_2\text{F}$ ) were used to help identifying the IR bands. In all measurements, the water content in commercial Nafion samples ( $EW = 1100 \text{ meqg}^{-1}$ ) was minimized by keeping them in  $\text{N}_2$  for 24 h, which also allowed us to better estimate the initial hydration condition of the membrane<sup>20</sup>.

Variable temperature mid infrared (MIR FT) and far infrared (FIR FT) spectra were measured at the IRIS beamline at the electron storage ring BESSY II of Helmholtz Zentrum Berlin. MIR FT was measured in transmission mode in the Bruker Vertex 70/v using a KBr beamsplitter, a DLaTGS detector fitted with an internal global source. For these measurements a modified Harrick demountable FT IR transmission cell was employed which allowed in-vacuum heating. The cell was equipped with ZnSe windows of 2 mm thickness and a 630  $\mu\text{m}$  PTFE spacer. The spectra were acquired with  $4 \text{ cm}^{-1}$  resolution and 32 scans were averaged. The references were recorded through the empty channel inside the spectrometer sample compartment under vacuum. FIR FT measurements in spectral region between 600 and  $30 \text{ cm}^{-1}$  were performed using the Harrick cell equipped with 2 mm thick Ge windows, with  $2 \text{ cm}^{-1}$  resolution using infrared synchrotron radiation as a source together with a liquid helium cooled silicon bolometer and a silicon beamsplitter. The reference was obtained by measuring the empty Harrick cell with identical conditions in the entire range of temperature investigated. Previous to the measurements, the membranes were preconditioned in the Harrick cell by purging  $\text{N}_2$  ( $RH \sim 0.1\%$ ) for 24 h at room  $T$ . The relative humidity was recorded using a humidity sensor (Sensirion EK-H4) at the outlet of the cell. The data collection was performed on N211 and N115 samples in the 30–200  $^\circ\text{C}$   $T$ -range with a step of 10 degrees in two successive heatings. The FTIR bands in the 1100–1200  $\text{cm}^{-1}$  range are saturating (not shown). Measurements

were performed after ~10 min at each temperature for system stabilization, when no noticeable spectral changes were observed.

The samples were examined by SAXS at the beam line BM26-B<sup>27,28</sup> at the European Synchrotron Radiation Facility (ESRF) in Grenoble, France. The energy of X-ray source was 12 keV ( $\lambda$  eV0.1033 nm), and sample to detector distance was 3005 mm. Data was recorded using the Pilatus 1 M detector, with  $172 \times 172 \mu\text{m}$  pixel size. The samples were heated at  $2^\circ\text{C}/\text{min}$  from  $20^\circ\text{C}$  to  $250^\circ\text{C}$ , cooled at  $40^\circ\text{C}/\text{min}$  to  $20^\circ\text{C}$ , heated again at  $2^\circ\text{C}/\text{min}$  to  $300^\circ\text{C}$  and finally cooled at  $10^\circ\text{C}/\text{min}$  to  $20^\circ\text{C}$ , in a Linkam DSC600 hot stage for the simultaneous SAXS temperature-dependent study. The SAXS patterns were reduced by BUBBLE and by the homemade XRTools software. The scattering Intensity ( $I$ ) vs scattering vector,  $q$   $\text{sc}4\pi \sin \theta/\lambda^{-1}$ , where  $\lambda$  is the X-ray wavelength and  $2\theta$  is the scattering angle. The scattering vector was calibrated using silver behenate. The scattering patterns were also corrected for transmission, normalized upon primary beam fluctuations and background scattering before data integration.

Dynamic mechanical analysis (DMA) was carried out under nitrogen flow in a Netzsch DMA 242 E in tensile mode. Rectangular Nafion samples ( $15 \times 6 \text{ mm}^2$ ) were cut and tested, respecting the machine direction. The measurements were performed from  $30$ – $200^\circ\text{C}$  with  $10^\circ\text{C}$  steps under  $\text{N}_2$  flow and amplitude of  $4 \mu\text{m}$  and oscillation frequency of  $1 \text{ Hz}$ .

Broadband dielectric spectroscopy (BDS) data were collected in a specially designed air-tight sample holder able to measure the proton conductivity in the range  $T = 30$ – $200^\circ\text{C}$  with  $RH = 0\%$  (dry  $\text{N}_2$  purge)<sup>17</sup>. Temperature controllers connected to band heaters placed externally around the cylindrical chambers are monitored by thermocouples (type K) inserted inside the metallic walls. The sample holder is capable of controlling both the temperature (from room temperature up to  $\sim 200^\circ\text{C}$ ) and the relative humidity ( $RH$ , from  $\sim 3$  to  $100\%$ ). Nafion samples were sandwiched between stainless steel spring-load contact terminals (electrically insulated from the chamber walls) with carbon cloth to facilitate water equilibration. In this experimental apparatus, the  $RH$  of the sample chamber can be calculated by,  $RH = \rho(T_r)/P(T_r) \times 100$ , where  $\rho$  is the vapor partial pressure,  $P$  is the saturated vapor partial pressure, and  $T_r$  and  $T_s$  are, respectively, the water reservoir and sample chamber temperatures. A Solartron 1260 frequency response analyzer was used in the frequency ( $f$ ) range of  $4 \text{ mHz}$  to  $3 \text{ MHz}$  applying an  $ac$  amplitude of  $100 \text{ mV}$ . The complex conductivity ( $\sigma^* = 2\pi f \epsilon_0 \epsilon''^*$ ) and electric modulus ( $M^* = M' + iM'' = 1/\epsilon^*$ ) representations were used throughout this study, in which the dielectric loss ( $\epsilon''(f)$ ) was obtained from:

$$\epsilon''(f) = -\frac{dcos(\theta(f))}{2\pi f \epsilon_0 S |Z(f)|}, \quad (2)$$

where  $\epsilon'$  and  $\epsilon''$  are the real and imaginary parts of the dielectric permittivity;  $\epsilon_0$  is the vacuum permittivity ( $\sim 8.854 \times 10^{-14} \text{ Fcm}^{-1}$ );  $S$  is the electrode active area,  $d$  is the thickness of the membrane;  $|Z|$  and  $\theta$  are the modulus and phase angle of impedance. The frequency dependent conductivity was obtained using the relation:  $\sigma' = 2\pi f \epsilon_0 \epsilon''^{13}$ .

## References

- Tibbits, S. 4D Printing: Multi-Material Shape Change. *Architec. Design*. **84**, 116–121 (2014).
- Ge, Q., Qi, H. J. & Dunn, M. L. Active materials by four-dimension printing. *Appl. Phys. Lett.* **103**, 131901 (2013).
- Xie, T. Tunable polymer multi-shape memory effect. *Nature* **464**, 267–270 (2010).
- Zhao, Z. *et al.* Three-Dimensional Printed Shape Memory Objects Based on an Olefin Ionomer of Zinc-Neutralized Poly(ethylene-co-methacrylic acid). *ACS Appl. Mater. Interfaces* **9**, 27239–27249 (2017).
- Page, K. A., Park, J. K., Moore, R. B. & Sakai, V. G. Direct Analysis of the Ion-Hopping Process Associated with the  $\alpha$ -Relaxation in Perfluorosulfonate Ionomers Using Quasielastic Neutron Scattering. *Macromolecules* **42**, 2729–2736 (2009).
- Osborn, S. J. *et al.* Glass Transition Temperature of Perfluorosulfonic Acid Ionomers. *Macromolecules* **40**, 3886–3890 (2007).
- Matos, B. R., Goulart, G. A., Santiago, E. I., Muccillo, R. & Fonseca, F. C. Proton conductivity of perfluorosulfonate ionomers at high temperature and high relative humidity. *Appl. Phys. Lett.* **104**, 091904 (2014).
- Lopez-Haro, M. *et al.* Three-dimensional analysis of Nafion layers in fuel cell electrodes. *Nature Comm.* **5**, 5229 (2014).
- Kusoglu, A. & Weber, A. Z. New Insights into Perfluorinated Sulfonic-Acid Ionomers. *Chem. Rev.* **117**, 987–1104 (2017).
- Schmidt-Rohr, K. & Chen, Q. Parallel cylindrical water nanochannels in Nafion fuel-cell membranes. *Nature Mater.* **7**, 75–83 (2008).
- Jackson, D. A., Koberstein, J. T. & Weiss, R. A. Small-Angle X-Ray Scattering Studies of Zinc Stearate-Filled Sulfonated Poly(ethylene-co-propylene-co-ethylidene-propylene-co-ethylidene norbornene) Ionomers. *J. Polym. Sci.: Part B: Polym. Phys.* **37**, 3141–3150 (1999).
- Colby, R. H. *et al.* Dynamics of Lightly Sulfonated Polystyrene Ionomers. *Phys. Rev. Lett.* **81**, 3976 (1998).
- Schonhals, A. & Kremer, F., In *Broadband Dielectric Spectroscopy*, Schonhals, A. & Kremer, F., Editors, p. 59 (Springer Verlag, Berlin, 2003).
- Yeo, S. C. & Eisenberg, A. Physical properties and supermolecular structure of perfluorinated ion-containing (nafion) polymers. *J. Appl. Polym. Sci.* **21**, 875 (1977).
- Di Noto, V., Negro, E., Sanchez, J.-Y. & Iojoiu, C. Structure-relaxation interplay of a new nanostructured membrane based on tetraethylammonium trifluoromethanesulfonate ionic liquid and neutralized nafion 117 for high-temperature fuel cells. *J. Am. Chem. Soc.* **132**, 2183 (2010).
- Matos, B. R., Santiago, E. I., Rey, J. F. Q. & Fonseca, F. C. Origin of  $\alpha$  and  $\beta$  relaxations of Nafion. *Phys. Rev. E* **89**, 052601 (2014).
- Matos, B. R. *et al.*  $dc$  Proton conductivity at low-frequency in Nafion conductivity spectrum probed by time-resolved SAXS measurements and impedance spectroscopy. *J. Polym. Sci. Part B: Polym. Phys.* **53**, 822 (2015).
- Puskar, L. *et al.* Infrared dynamics study of thermally treated perfluoroimide acid proton exchange membranes. *Phys. Chem. Chem. Phys.* **19**, 626–635 (2017).
- Bernardina, S. D. *et al.* Mechanism of Ionization, Hydration, and Intermolecular H-Bonding in Proton Conducting Nanostructured Ionomers. *J. Phys. Chem. C* **118**, 25468–25479 (2014).
- Matos, B. R. *et al.* Proton and cesium conductivity in perfluorosulfonate ionomers at low and high relative humidity. *Solid State Ionics* **301**, 86–94 (2017).
- Eisenberg, D. & Kauzmann, W. *The Structure and Properties of Water*. (Oxford University Press, New York, 1969; pp. 300).
- Bawagana, A. D. O. *et al.* Far-infrared studies on Nafion and perfluoroimide acid (PFIA) and their alkali salts. *Vibr. Spectr.* **75**, 213–217 (2014).

23. Gebel, G. & Lambard, J. Small-Angle Scattering Study of Water-Swollen Perfluorinated Ionomer Membranes. *Macromolecules* **30**, 7914–7920 (1997).
24. van der Heijden, P. C., Rubatat, L. & Diat, O. Orientation of Drawn Nafion at Molecular and Mesoscopic Scales. *Macromolecules* **37**, 5327–5336 (2004).
25. Tierney, N. K. & Register, R. A. Ion Hopping in Ethylene-Methacrylic Acid Ionomer Melts As Probed by Rheometry and Cation Diffusion Measurements. *Macromolecules* **35**, 2358–2364 (2002).
26. Matos, B. R. In Situ Fabrication of Nafion–Titanate Hybrid Electrolytes for High-Temperature Direct Ethanol Fuel Cell, <https://doi.org/10.1021/jp405754v>.
27. Bras, W. *et al.* Recent experiments on a combined small-angle/wide-angle X-ray scattering beam line at the ESRF. *J. Appl. Cryst.* **36**, 791–794 (2013).
28. Portale, G., Cavallo, D., Alfonso, G. C., Hermida-Merino, D. & Van Drongelen, M. Polymer crystallization studies under processing-relevant conditions at the SAXS/WAXS DUBBLE beamline at the ESRF. *J. Appl. Cryst.* **46**, 1681–1689 (2013).

## Acknowledgements

We thank the Brazilian funding agencies CAPES, CNPq, and FAPESP (grant number 2013/50151-5, 2014/09087-4, 2014/50279-4 and 2016/14785-8). Thanks are also due to LNLS (18801 and 20160239) and CNEN. FCF is a CNPq fellow. We thank the ESRF and the HZB for the allocation of synchrotron radiation beamtime.

## Author Contributions

R.P. and B.R.M. performed the DMA experiments and analyzed the data. B.R.M., L.P. and U.S. performed the FTIR experiments and discussed the data. J.F.Q.R. and D.H.M. performed the SAXS experiments and analyzed the data. B.R.M. and F.C.F. performed the BDS experiments and discussed the data. B.R.M. wrote the manuscript. All the authors revised the manuscript.

## Additional Information

**Competing Interests:** The authors declare no competing interests.

**Publisher's note:** Springer Nature remains neutral with regard to jurisdictional claims in published maps and institutional affiliations.



**Open Access** This article is licensed under a Creative Commons Attribution 4.0 International License, which permits use, sharing, adaptation, distribution and reproduction in any medium or format, as long as you give appropriate credit to the original author(s) and the source, provide a link to the Creative Commons license, and indicate if changes were made. The images or other third party material in this article are included in the article's Creative Commons license, unless indicated otherwise in a credit line to the material. If material is not included in the article's Creative Commons license and your intended use is not permitted by statutory regulation or exceeds the permitted use, you will need to obtain permission directly from the copyright holder. To view a copy of this license, visit <http://creativecommons.org/licenses/by/4.0/>.

© The Author(s) 2018

## 7- Co-proposer PhD Thesis project awarded ; ‘Nouvelle génération de biopolymères nanostructurés pour la fabrication additive et l’électrofilage, Université de Lorraine.

I have been awarded with 92.500,0 € as co-applicant with prof. Patrice Bourson by the Region of Grand Est to finance the development of a thesis to investigate novel nanostructured biopolymers to generate fibers by electrospinning. The thesis has recently started, 01/10/2019 and the funds will cover the project until the 30/09/2022. The project involves several scientific partners to integrate different expertise to cover from the tailored synthesis of novel biodegradable polyesters to the characterization of the structure-properties relationship and their applications in the biomedical field (see Figure 7.1). I have led the organization of the scientific cooperation using my previous connections across Europe to identify the task required as well as the timelines to achieve the project. Firstly, I have conceived the polymer derivatives to proceed with the nanostructural investigation to initiate the formulation of drug delivery systems. We have implemented an Erasmus project between the Université de Lorraine and Universidad de Castilla la Mancha at a first stage to synthesise the aimed polymer derivatives and the nanostructure characterization will be continued in DUBBLE under my supervision.

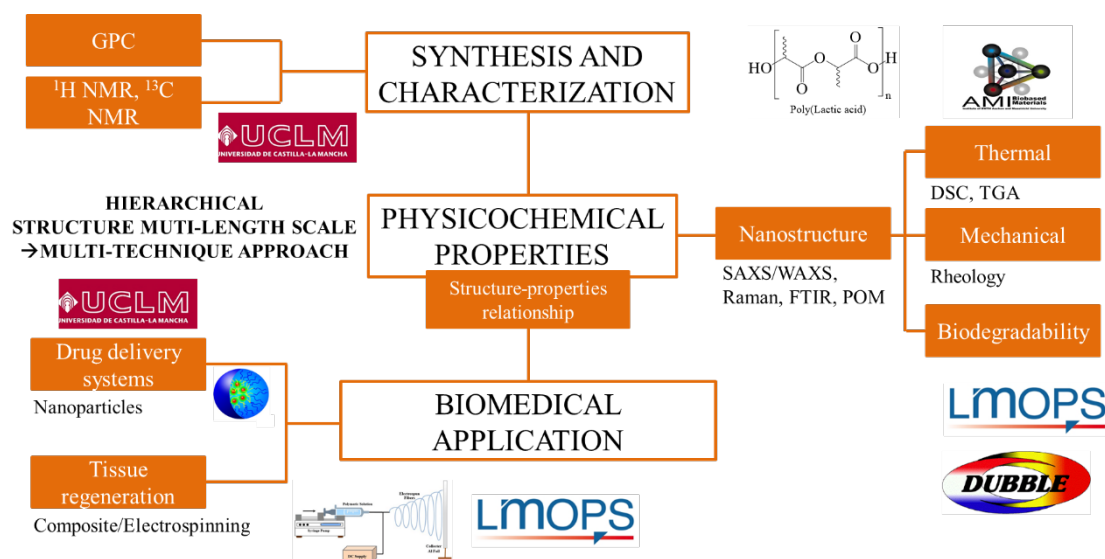


Figure 7.1. Planning of the objectives for the generation of novel stereo-PLA-block-copolymers from the synthesis to the applications.

Plastics revolution started in 1869 when John Wesley Hyatt found that a practical plastic material could be made by mixing nitrocellulose, camphor and alcohol: celluloid(1). Since then, plastics have replaced a large number of materials on the market due to the synthesis of a wide variety of new polymers with a great variability of applications and properties (i.e., polyvinyl chloride, polystyrene). In 2018, the production of plastics worldwide was 359 million metric tons (2) and it is expected to double within the next 20 years. According to the United Nations, five billion plastic bags are used each year and one million plastic bottles are bought every

minute. Plastic production projections based on current trends estimate that will be nearly 12 billion tons of plastic waste in landfills and oceans and consequences could be devastating by 2050 (3,4). Plastic debris in oceans was first observed in 1960s and since then, plastics reputation has worsened due to the lack of biodegradability as well as the potential threat to the human health. Over time, plastics in the sea break down into smaller fragments called micro-plastics that when consumed by marine animals could enter the human food chain.

Among the actions that could reduce the magnitude of the problem (public education, regulatory and economic policy instruments), the substitution of polyolefin for bio-based and biodegradable plastics is one of the most important. However, the reduction of plastic production is limited due to the lack of substitute materials that can satisfy the perceived advantages of plastic and consumer practices. Bio-based plastics such as starch blends, bio-PET and bio-PE are already been employed in several industrial applications and its production is expected to increase to 6.1 million tons by 2021.

During my second granted scientific visit to the Universidad de Castilla la Mancha, at the Pharmacy School, I have established a collaboration to synthesize novel block copolymers stereocomplexes of PLLA-PLDA at high  $M_w$  in order to generate bio-based plastics with properties similar to polyolefins. The grant as a senior scientific visitor has been awarded 2500 € to cover my subsistence, traveling and accommodation for a month.

PLA is a well-studied bio-based polymer that is usually synthesized by ROP generating two enantiomers, poly (L-lactic acid) (PLLA) and poly (D-lactic acid) (PDLA) due to the presence of a carbon chiral centre in its backbone. PLA is the bio-based polymer most widely employed in diverse fields such as food handling, fibre manufacturing, textile industry or biomedical. Particularly, biomedical field applications include tissue engineering (tissue regeneration, internal fixation, wound treatment, suture thread), stents, drug delivery systems.

Poly(lactic acid) (PLA) possesses particular interest to manufacturers due to its biocompatibility, processability (easy to be handled in fused deposition modeling machines -3D printing-) and its eco-friendliness (derived from sugar resources by well-known chemical processes, biodegradable, recyclable and compostable).

One of the main advantages of PLA is to be bioassimilable, i.e. it is completely metabolized to water and carbon dioxide in the human body and as such totally eliminated (Food and drugs administration (FDA) approved). Moreover, toxicity studies have shown the inert effect as a solid form in humans. The degradation kinetics depend on several physicochemical parameters such as pH, molecular weight or thickness of the sample, and thus, can be modulated by playing with the PLA chirality to continue or reduce the degradation rate, respectively. In addition, the degradation of a highly crystalline form to lactic acid will last for months whilst an amorphous derivative will degrade in weeks.

However, the PLA applicability is slightly inferior to conventional petroleum-based polymers in terms of thermal resistance, mechanical properties and crystallinity.

Isotactic PLA, composed of identical repeat units of either L-LA or D-LA, is a semicrystalline polymer that generates either PLLA or PDLA respectively, that crystallize in two enantiomeric

homochiral strands. Moreover, PLA can cocrystallize if both enantiomers are present as a stereocomplex (SC) phase, featuring properties superior to the homochiral (HC) crystal phase.

Different strategies have been evaluated to improve the physicochemical properties such as the use of plasticizers or nucleating agents. Moreover, the equimolar blend of PLLA and PDLA enantiomers is a strategy largely used to generate SC crystallites, which present a melting point 50°C higher than its homocrystals (HC) counterparts due to the strong interactions between L- and D-lactyl unit sequences (Tsuji, 2016). However, the SC crystallization of the blended enantiomers (PLLA and PDLA) diminishes for high molecular weight ( $HM_w$ ) PLA and enantiomeric HC are obtained instead (Competitive Stereocomplexation 2015). Block copolymers formed by enantiomeric PLA strands are required to retain the SC crystallization in  $HM_w$  polymers.

Previous synthetic strategies for obtaining stereo-block-PLA have been focused on the lengthening of building blocks from pre-polymers by a stepwise fashion or the attachment of pre-synthesized PDLA and PLLA strands by reactive end-group linkers. However, limitations on the preciseness and complexity of the desired polymer architecture are the main drawbacks of the prepolymer extension synthetic approaches. A straightforward strategy to achieve stereo-regularity in the polymeric backbone is the one-pot sequential monomer addition to a truly living polymerization catalyst, requiring catalysts that are extremely rare. Recently, highly active Zn (II) and chloro-magnesium complexes in the ROP catalysis of homo-chiral lactides have been introduced to synthesize  $HM_w$  stereo-n-block co-polymers. Stereo-di-block copolymers characterized with a high  $T_m$  and  $\Delta H_m$  have been successfully synthesized, suggesting the formation of SC crystals (Rosen, Goldberg, Venditto, & Kol, 2016). Nevertheless, an exhaustive characterization of the stereo di-block-copolymers is needed to understand the mechanism of crystallization of the SC phase as well as to correlate the crystalline structure to its physicochemical properties. The crystallization mechanism of enantiomeric PLA (PLLA and PDLA) has been largely investigated as well as the equimolar PLLA/PDLA physical blend. The latter, showed the exclusive formation of SC crystals only at low  $M_w$  samples, and a progressive transformation of the HC/SC ratio as  $M_w$  increased. Importantly, the crystallization mechanism of stereo di-block co-polymers PLA has never been investigated.

Chiral N,N,O-scorpionate zinc alkyls previously synthesized by the group at Universidad de Castilla la Mancha (Otero 2012) showed to be effective and stereoselective initiators for ROP of lactides, acting as single-site initiators at mild conditions and without the need for a cocatalyst or activator. Herein, a series of PLA stereo-diblock-copolymers attaining different  $M_w$  were synthesized, through a scorpionate zinc alkyl catalyst, as a proof of concept, to achieve highly stereo-regular derivatives.

Summarising, the aim of thesis during the first year was the optimization of the synthetic route and its characterization (see Table 1). Polymerizations of homochiral L- and D-LA, and stereo di-block co-polymers were conducted in toluene at 90°C.

Entry	Di-block copolymer (theoretical block length)	Temperature (°C)	Time (min)	% conversion	$M_w$ (theor.) (Da)	$M_w$ (exper.) (Da)	$M_w/M_n$	Di-block copolymer ( block length)
1	PLLA-b-PLLA (50L-b-50D)	90	50	95	14400	32823	1.93	PLLA-b-PLLA (115L-b-115D)
2	PLLA-b-PLLA (100D-b-100L)	90	60	94	28800	79107	2.38	PLLA-b-PLLA (275D-b-275L)
3	PLLA-b-PLLA (100L-b-100D)	90	60	95	28800	79320	2.25	PLLA-b-PLLA (275L-b-275D)
4	PLLA-b-PLLA (200L-b-200D)	75	120	81	57600	72508	2.20	PLLA-b-PLLA (250L-b-250D)
5	PLLA-b-PLLA (200L-b-200D)	90	90	90	57600	63313	2.20	PLLA-b-PLLA (220L-b-220D)
6	PLLA-b-PLLA (300L-b-300D)	90	100	97	86400	107912	1.69	PLLA-b-PLLA (375L-b-375D)
7	PLLA-b-PLLA (500L-b-500D)	90	120	84	144000	94181	2.11	PLLA-b-PLLA (330L-b-330D)
8	PLLA-b-PLLA (500L-b-500D)	90	7h	85	144000	150094	2.31	PLLA-b-PLLA (520L-b-520D)

Table 1. Summary of the PLLA polymers synthesis optimization.

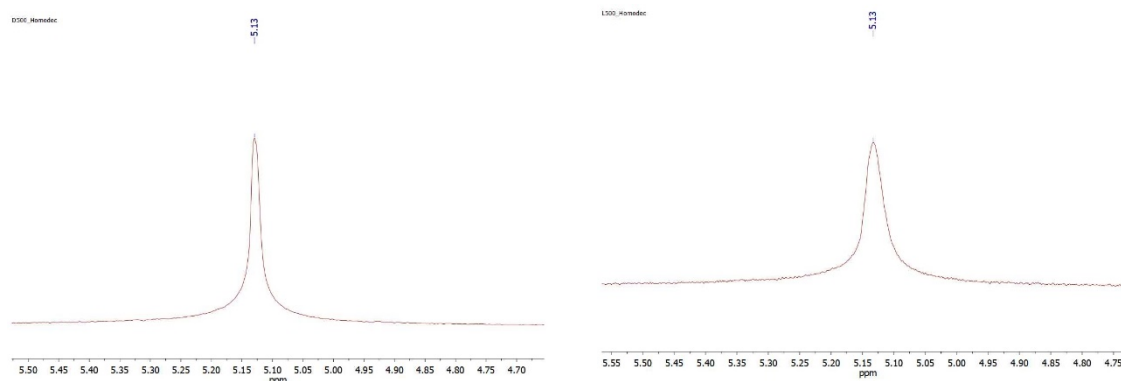


Figure 7.2.  $^1\text{H}$  NMR.

Different  $M_w$  were obtained by varying the ratio  $[\text{LA}]/[\text{catalyst}]$  and  $M_w$  distributions obtained were fairly narrow ( $\sim 2$ ). The polymerizations kinetics shown, including high molecular weight polymerizations, high conversion rates, above 80%. Polymerization of L-lactide and D-Lactide yielded stereochemically pure PLA ( $^1\text{H}$  NMR and homonuclear decoupling  $^1\text{H}$  NMR, see Figure 7.2), indicating that epimerization of the monomer and polymer was absent under the polymerization conditions. Stereo di-block co-polymers were readily prepared by the one-pot sequential addition method.

tetrad	Probability of ESC (non-Bernoullian)	Probability of CEC (Bernoullian)
<i>mmm</i>	$[P_m^2 + (1 - P_m)^2 + P_m^3 + (1 - P_m)^3]/2$	$P_m^2 + 0.5 P_m P_r$
<i>mnr</i>	$[P_m^2(1 - P_m) + P_m(1 - P_m)^2]/2$	$0.5 P_m P_r$
<i>rmr</i>	$[P_m^2(1 - P_m) + P_m(1 - P_m)^2]/2$	$0.5 P_m P_r$
<i>rrr</i>	$[P_m^2(1 - P_m) + P_m(1 - P_m)^2]/2$	$0.5 P_r^2$
<i>mrm</i>	$[P_m(1 - P_m)]$	$0.5 (P_m^2 + P_m P_r)$

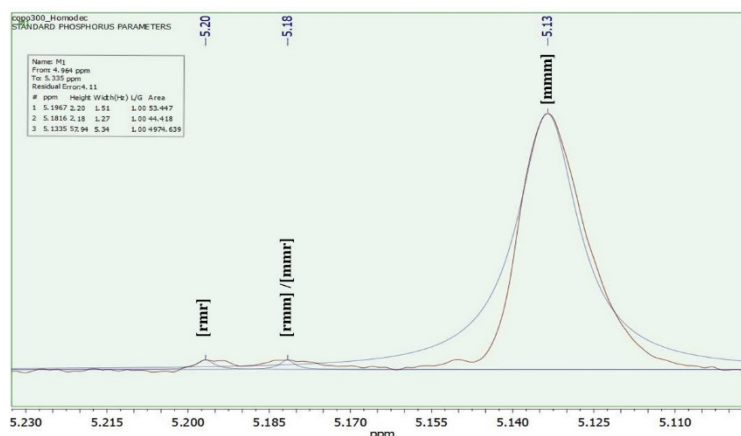


Figure 7.3. Homonuclear decoupling  $^1\text{H}$  NMR

Monomer consumption was found higher than 85% for both block sequences followed by  $^1\text{H}$  NMR. Moreover, stereo di-block co-polymers tacticity was calculated from deconvoluted

homonuclear decoupling  $^1\text{H}$  NMR spectra by using both Bernoullian and non-Bernoullian statistics (see Figure 7.3). The stereocontrol achieved by a particular initiator is expressed in terms of probability to generate certain stereosequences.  $P_m$ : probability of isotactic enchainment and  $P_r$ : probability of syndio/heterotactic enchainment (platel2008). Besides,  $P_m + P_r = 1$  and while  $P_m=0.5$  indicates a random insertion,  $P_m=1.0$  indicates isotactic PLA (orhan2018). The deconvoluted methine region of the homonuclear decoupled  $^1\text{H}$  NMR spectrum of 300L-*b*-300D stereo di-block co-polymer is shown in Figure 3, as an example. The peaks were assigned to the appropriate tetrads in accordance with literature (Ovitt2002).

Stereocontrolled polymerization can be mediated by two distinct mechanisms, namely, chain end control (CEC) or enantiomorphic site control (ESC). In the former case, control of the chirality is associated with the propagating chain end that in the transition state of the next monomer insertion defines the chirality of the next monomer unit to be inserted. In contrast, in polymerizations mediated through an ESC mechanism, the chirality of the catalyst determines the chirality of the next monomer unit.

	$P_m$ (ESC)	$P_m$ (CEC)
PLLA- <i>b</i> -PLLA (50L- <i>b</i> -50D)	0.96	0.88
PLLA- <i>b</i> -PLLA (100D- <i>b</i> -100L)	0.93	0.83
PLLA- <i>b</i> -PLLA (100L- <i>b</i> -100D)	0.90	0.96
PLLA- <i>b</i> -PLLA (200L- <i>b</i> -200D)		
PLLA- <i>b</i> -PLLA (200L- <i>b</i> -200D)		
PLLA- <i>b</i> -PLLA (300L- <i>b</i> -300D)	0.99	0.96
PLLA- <i>b</i> -PLLA (500L- <i>b</i> -500D)_20	0.82	0.69
PLLA- <i>b</i> -PLLA (500L- <i>b</i> -500D)_19	0.98	0.92

Table 2. Summary of the tacticity of PLA derivatives for both methodologies.

The isomer monomer insertion creates a stereoerror from which « standard » growth would form a new stereoblock of opposite configuration to the previous formed (-LLLLLDDDDDLLLLL-). Assuming isotactic-PLA would be formed by a CEC mechanism exclusively when polymerization is run from rac-LA, the following relative tetrad intensities would be expected:  $[\text{mrm}] = [\text{rmm}] \neq [\text{rmr}]$ . Conversely, the ESC mechanism should generate single insertion stereoerrors of the type -LLLLLLDLLLLL-. In ESC mechanism, the tetrad ratio should then follow the sequent probabilities;  $[\text{rmr}] = [\text{mmr}] = [\text{rmm}] = 2/[\text{mrm}]$  (Orhan2018\_homodecoupling). Generally, stereocontrol in the ROP of PLA is more commonly achieved by CEC, even if the catalyst contains a chiral component. However, any conclusion related to the mechanism followed by our catalyst can not be drawn from the tetrad probabilities, due to the assumptions of the models applied do not correspond to those of our synthesis, i.e., the model is usually applied for polymerizations run from rac-or meso-LA, while our synthesis is based on the one-pot sequential addition of enantiopure LA monomers. However, the polymerization mechanism followed by our catalyst can be elucidated from a racemic PLA polymerization and thus, the appropriate  $P_m$  values (those obtained from ESC or CEC mechanism) will be considered.

Moreover, it has been investigated the polymer crystallization mechanism of those derivatives in collaboration with the group of prof. Sanjay Rastogi at Maastricht University.

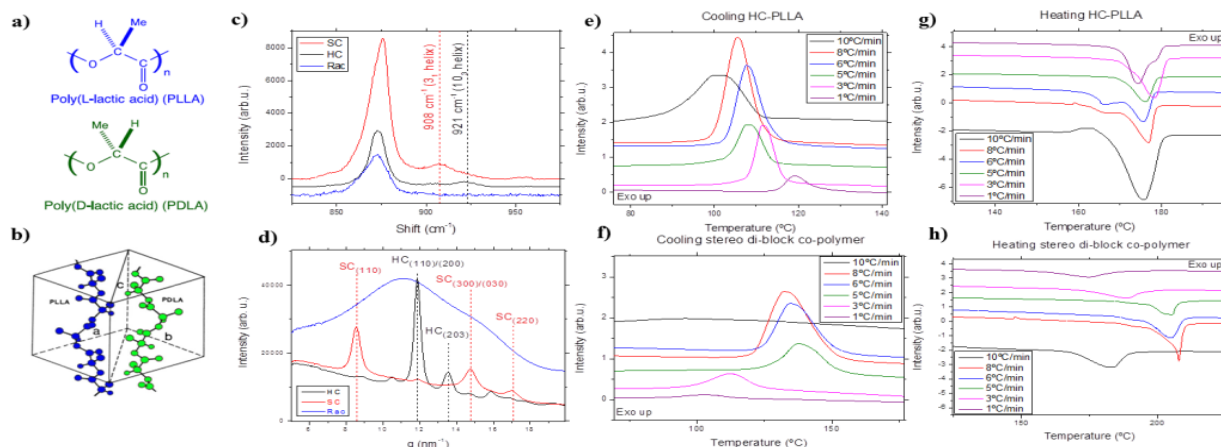


Figure 4. a) PLLA and PDLA structure; b) SC crystalline lattice; c) Raman studies; d) WAXS studies; e) HC- cooling curve ; f) SC- cooling curve ; g) HC- heating curve ; h) SC- heating curve .

Cooling rate	HC-PLLA			SC-PLLA		
	$T_c$ (°C)	$T_m$ (°C)	$\Delta H_m$ (J.g <sup>-1</sup> )	$T_c$ (°C)	$T_m$ (°C)	$\Delta H_m$ (J.g <sup>-1</sup> )
10°C/min	100.48	175.50	57.04	108.70*	183.55	30.82
8°C/min	105.51	176.90	55.03	132.40	207.93	47.91
6°C/min	107.73	175.70	55.48	134.69	205.32	49.34
5°C/min	107.81	176.12	55.67	137.94	205.41	54.03
3°C/min	111.48	178.28	55.34	112.35	188.82	30.06
1°C/min	119.25	174.29	59.14	103.13	174.10	26.88

\*: cold crystallization

**Table 3.** DSC results of HC-PLLA and SC-PLLA upon non-isothermal melt crystallization and subsequent melting.

The crystallization mechanism of enantiomeric PLA (PLLA and PDLA) has been largely investigated as well as the equimolar PLLA/PDLA physical blend. The latter, showed the exclusive formation of SC crystals only at low  $M_w$  samples, and a progressive transformation of the HC/SC ratio as  $M_w$  increased. Importantly, the crystallization mechanism of stereo di-block co-polymers PLA has never been investigated as previously mentioned. Preliminary independent Raman and SAXS/WAXS measurements at room temperature confirmed that stereo-diblock-copolymers crystallize exclusively as SC (see Figure 7.4 c and d), compared to physically blended equimolar enantiomers, in which a competition between stereocomplexation and homoenantiomeric crystallization occurs. Moreover, crystallization studies on PLA stereo-diblock-copolymers by DSC (Image 4e-h) showed dramatic differences on the crystalline populations depending on cooling rate (see  $\Delta H_m$  and  $T_m$  in table 3). Importantly, PLA stereo-diblock-copolymer crystalline populations could be associated to either SC (8, 6 and 5°C/min) or HC (1°C/min) despite been covalently linked. Moreover, a non-reported crystalline phase is obtained when cooling at 10 and 3°C/min that could be related to the number of monomeric units participating in the SC. A fully characterization of the crystallization mechanism from the melt will be performed by simultaneous SAXS-WAXS in combination with Raman spectroscopy in the next future and compare them to the corresponding enantiomeric and physically blended counterparts. Raman spectroscopy will be used to correlate the chain conformation evolution of either the SC phase ( $3_1$  helix 908  $\text{cm}^{-1}$ ) or the  $\alpha$  phase ( $10_3$  helix 921  $\text{cm}^{-1}$ ) to the crystallinity triggering resolved by WAXS as well as possible phase transformations, as suggested by DSC depending on the thermal history. The long period will be monitored by SAXS and detailed multivariate 2D analysis will be carried out to correlate Raman spectra to scattering profiles to understand complex multistep crystallization mechanism. Moreover, crystallization studies

have been conducted by polarized optical microscopy (POM) of both PLLA and PDLA homopolymers as well as  $HM_w$  stereo di-block co-polymer at different isothermal crystallization temperatures ( $T_{ic}$ ) after 5 and 15 min, respectively, from the start of the isothermal step. It has been found that the higher the selected  $T_{ic}$  the lower the density of spherulites for all PLA derivatives. Moreover, higher density of spherulites in PLLA samples were observed compared to that of PDLA, indicating that crystallization in PLLA is faster than in PDLA. Photomicrographs of  $HM_w$  co-polymer were acquired after 15 minutes from the start of the isothermal step, rather than 5, because the latency period until spherulites start to grow up is higher for the co-polymer than for homopolymers (see Figure 7.5).

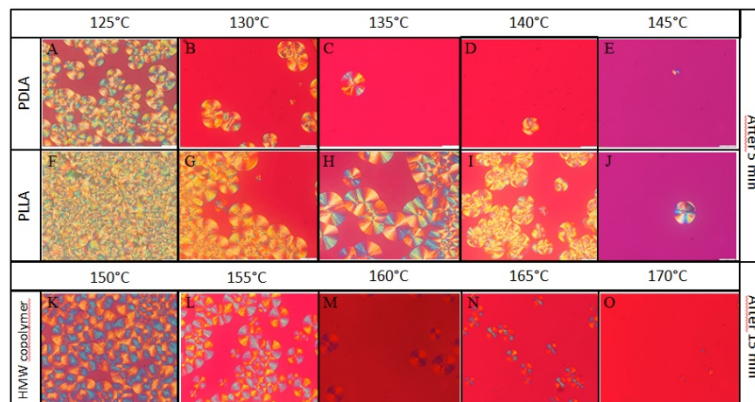


Figure 5. Polarization photomicrographs of PLLA (A-E) and PDLA (F-J) homopolymers and (K-O)  $HM_w$  stereo di-block co-polymer at different isothermal crystallization temperatures ( $T_{ic}$ ) after 5 and 15 min, respectively, from the start of the isothermal step.

Moreover, the thesis student has initiated to investigate the possibility to use the novel generated derivatives as drug carriers at Universidad de Castilla la Mancha following our recent work distributed as research highlight by Alba to the National press:

:Enrique Niza, Cristina Nieto-Jiménez, María del Mar Noblejas-López, Iván Bravo, José Antonio Castro-Osma, Felipe de la Cruz-Martínez, Marc Martínez de Sarasa Buchaca, Daniel Hermida-Merino, Eduardo Solano, Alberto Ocaña, Carlos Alonso-Moreno. Poly(Cyclohexene Phthalate) Nanoparticles for Controlled Dasatinib Delivery in Breast Cancer Therapy. *Nanomaterials* 2019, 9, 1208. DOI: 10.3390/nano9091208 en la prensa por ser elegido por su importancia en la investigación fundamental y en la aplicación de los rayos X por el sincrotrón ALBA. <https://www.sincrotronalba.es/es/actualidad/noticias/nuevas-nanoparticulas-biocompatibles-contra-el-cancer-de-mama>

Novel drug delivery systems (DDS) are a crucial strategy to target specifically a smart therapeutic dose and local administration at a suitable rate, for an established period and at a set concentration. Generally, the drug can diffuse through paths or pores in polymer matrices or alternatively, the drug is physisorbed on the nanocarrier surface and undergoes a very rapid release ("burst release").

As previously described, PLA is a great candidate for the design of drug delivery systems due to its degradable nature in humid environments and the nontoxic resorbed products or excreted by the human body. Drug release rates from PLA depend on a range of variables such as the physicochemical properties of the polymer, the type of formulation and the percentage

of drug loading. DDS generated from PLA block co-polymers feature progressive drug release profiles for long term treatments, due to the strong interactions with the therapeutic drug. A series of PLA derivatives were synthesized by ROP to formulate nanoparticles drug delivery systems of Doxorubicin (DOX) and Dasatinib (DAS) to elucidate the relationship between the crystalline phase of the internal nanoparticles structure and the drug release. DOX has demonstrated very limited efficacy in the treatment of gliomas due to the short half-life of DOX in biological experiments. DAS is an FDA-approved multi-target compound for the treatment of chronic myeloid leukemia. However, the extremely low solubility of DAS diminishes its efficacy. The development of efficient delivery systems of DOX and DAS could potentially improve the therapeutic efficacy. Three different formulations (racemic-PLA, homopolymer-PLA and diblock-copolymer-PLA) for both drugs were recently synthesized by double emulsion and solvent evaporation method with a final hydrodynamic radius smaller than 200 nm, and loading efficacy (LE) results show important differences among them presenting higher loading efficacy for DOX than for DAS (see Table 4).

Formulation	Drug load (mg)	DASATINIB		DOXORUBICIN	
		Average size (nm)	LE (%)	Average size (nm)	LE (%)
SC-PLA	0,5	147,4	0,01	130,9	0,11
RAC-PLA	0,5	143,1	0,03	140,4	0,10
HC-PLA	0,5	143,9	0,09	171,2	0,18
SC-PLA	1	133,0	0,13	144,1	0,25
RAC-PLA	1	191,4	0,13	125,1	0,10
HC-PLA	1	129,7	0,11	119,3	0,22
SC-PLA	1,5	133,2	0,03	133,4	0,16
RAC-PLA	1,5	127,3	0,01	160,7	0,16
HC-PLA	1,5	161,6	0,03	106,7	0,04

Table 4. Hydrodynamic radius (nm) and loading efficacy (LE) of three different formulations. SC: copolymer; RAC: racemic; HC: homopolymer.

Different release profiles among formulations are expected from the kinetically trapped structure generated during the nanoparticles formation from the double emulsion system. Different crystalline domains were observed by thermal analysis during the 1st heating cycle of the formed nanoparticles after precipitation compared to the raw material. SAXS/WAXS previewed measurements will elucidate the effect of the nanostructure on the interaction between the DOX and DAS and the PLA derivatives and particularly, the effect of the drugs on the crystallinity of the PLA derivative that will determine the drugs release profile.

Finally, I am currently working in the first manuscript about the synthesis of the stereo-block PLA copolymers of the project together with the student Carmen Moya.

## 8- Study of the nanostructure of the fish gelatin hydrogels for drug delivery applications

---

Biomaterials are ideal candidates to supply sustainably functionalised nanomaterials that in turn, could potentially substitute synthetic materials in daily use applications. However, the structure-properties relationship of biomaterials have been scarcely investigated. Particularly, marine bioresources are uncommonly employed for designing novel soft matter systems with relevant industrial applications. Likewise, I have been stimulated to contact the Institute of marine research of the CSIC organization (Spanish council research) to obtain fish gelatin to characterise the physicochemical properties and its structural correlation in collaboration with the University of Vigo. Gelatin is a biopolymer, widely used in the food, pharmaceutical, and and photographic industries, due to its excellent biocompatibility, biodegradability properties. Gel colloids offer functionality and versatility in a wide variety of applications such as hygienic products, agriculture, drug delivery systems, food additives, pharmaceuticals, biomedical. Recently, gelatin was proved to promote joint and skin health. The skin and bones of cattle and pigshave often been used commercially for the production of gelatin. However, in recent years, fish gelatin has become increasingly important as a natural alternative source due to the livestock crisis and the increased demand for non-bovine and non-swine gelatin for religious and social reasons. In addition, fish skin is an important by-product of the fish processing industry considered for a long-time waste and pollutant. The valorization of value-added products derived from fisheries waste sources is a key step towards the improvement of fishing industry environmental sustainability and as a contribution to the circular economy.

In particular, shark and tuna have been identified as source species to obtain gelatin due to the abundance as a by-product of the fisheries industries, and their properties have been subject to study.

However, Shark/Tuna fish gelatin possess structural inherent limitations to replace mammalian sources despite a similar composition. The main limitations of Shark and Tuna fish gelatin are the low melting point and the gel strength whilst possessing a higher viscosity than mammalian gelatin, although the relatively lower gel strength and melting temperature than mammalian gelatin, may provide a better alternative in the food industry. Food systems require low melting points and moderate storage modulus to simplify the flavor release and thus, provide better sensory characteristics.

Particularly, the shark fish gel formed is often unstable and has poor rheological properties, limiting its field of application. However, the physical properties of tuna skin gelatin are comparable to mammalian gels. Thermal analysis of Shark/Tuna fish gels has determined various phases according to water content and the temperature of formation. Importantly, glass transition temperature has been determined to correlate the structural to the physical properties such as crystallization temperature, adhesion, collapse, and molecular mobility of biological materials.

Moreover, gelatine-based fish and Bovine gels have been extensively studied in the field of drug delivery systems as a versatile biomaterial and have numerous advantageous capabilities such as biocompatibility, biodegradability, low antigenicity, and multifunctionality.

The general objective of this study is to characterize the nanostructure of Tuna/Shark gelatin based hydrogels to exploit them as drug nanocarrier vehicles.

Hydrogels are polymer networks extensively expanded by the incorporation of water. Hydrogels that are usually referred to as hydrophilic gels are covalent or physical networks of polymeric chains eventually found as colloidal gels[1], in which water is the dispersion medium.

The ability of hydrogels to absorb water arises from hydrophilic functional groups attached either to the main chain or as pendant groups to the polymeric backbone, while their resistance to dissolution arises from cross-links between network chains.

Natural polymers are popular for current biomedical applications as are typically derived from living organisms. Moreover, natural polymers are generally non-toxic, biocompatible, and produce negligible inflammatory response in the host organism due to their biological origin[2],[3].

The desired mechanical property of the hydrogel can be achieved, by changing the degree of crosslinking, Hence, there is an optimum degree of crosslinking to achieve a relatively strong and yet elastic hydrogel.

Current physicochemical studies extensively focus on the understanding of the structure-properties of natural polymers to design bioinspired functional nanomaterials. In particular, gelatin has been an attractive candidate for preparing hydrogels with long-term biomedical applications due to the large number of functional groups in the backbone and the facility to be crosslinked to enhance their mechanical properties[2].

As previously mentioned, the vast majority of commercial gelatin is obtained from mammalian species in particular from pig, cattle and bovine gelatins [4]. However, the increased demand for an alternative to gelatin sources is increasingly required due to socio-cultural and religious reasons related to mammalian species. By-products from the fish processing industry represent a potential and promising source for gelatin production [5], [6].

Moreover, novel environmental and economic policy guidelines promote the rational use of marine resources, and in particular, the revaluation of fishing industry waste. Fish is an excellent nutritional source due to the high content of proteins in the muscles as well as high levels of essential amino acids. Collagen is the main structural protein in the animal kingdom that is estimated to represent the 75% of the total weight in fish processing industry residue [7], and thus further processing to yield gelatin can help to offset harmful environmental effects.

Moreover, a large part of the by-products generated during the fish filleting consists of skin and bones with large amounts of collagen that possess a wide range of applications[8].

Furthermore, obtaining valuable by-products from fisheries and reducing industrial waste is an attractive research topic due to sustainability issues. The effective use of fishery resources turns increasingly important and thus the demand for more efficient use of fish waste will only increase. Moreover, fish gelatin materials comply with the recommendations of the European Union to develop the Circular Economy [9], specifically, in the field of fishing, aquaculture, and exploitation of marine resources.

Sustainable development is an overarching objective that requires an interdisciplinary strategy to address the societal challenge concerning climate action, environment, resource efficiency, and raw materials. In a green environmental society valorization of abundant and available biowastes with high potential to manufacture value-added products is the first step to close the loop between waste and consumption in line with the main goal of the circular economy.

Collagen is mainly composed by glycine, proline, and hydroxyproline, which denature in the presence of dilute acid standards (% H<sub>2</sub>SO<sub>4</sub>, citric acid), turning in a soluble protein such as

gelatin in dissolved solutions [10]. Several methods are used by the industry to manufacture gelatin from collagen. In general, gelatin is obtained using a sequence of three types of processing steps: pretreatments to remove noncollagen impurities and prepare the collagen for extraction, one or more water extraction steps to convert collagen into gelatin, and finally, a series of refinement and recovery processes to get a highly purified dried gelatin. The main step of the gelatin production process is firstly to remove undesirable side-products that will interfere with the gelatin extraction. Subsequently, the water insoluble collagen thus obtained, is converted into the water soluble gelatin while maintaining maximum yield and functional properties [11].

For gelatin production the raw material may be any collagen-containing tissue. Hides, skins and bones from mammalian sources such as porcine and bovine are preferred, but gelatins are also produced from the skins of cold and warm water fish species as well as minor quantities from avian sources.

Different mammalian and fish gelatin sources. Mammalian gelatins have significantly superior physical properties such as higher viscosity, melting and setting temperature, and faster setting time compared to fish gelatin counterparts. Porcine skin-derived gelatin is the most popular source (46%), followed by bovine skin (29.4%), bovine bone (23.1%) and other sources (1.5%) [12].

The lower content of amino acids in fish gelatin is the main structural difference with the mammalian counterparts. The higher amino acid sequence enhances the ordered interchain interactions that stabilises the network formed in a hydrogel. Fish gelatin gel contains fewer physical cross-links as a result, between clusters compared to mammalian gelatin, or alternatively exhibits weaker interaction between clusters [13].

The mechanical properties of most commercial gelatins, derived from mammalian sources, has been conducted. However very little work has been performed on gelatins from fish origin.

Importantly, the unhydrolyzed collagen coil–helix or renaturation temperature that will define the mechanical properties, depends upon the proportion of the iminoacid in both proline and hydroxyproline.

The iminoacid proportion is generally, 24% for mammals and 16%–18% for most fish species. The collagen from cold-water fish, has a very low hydroxyproline content. Consequently, the gelatin extracted from cold water fish collagen has a very low gelling and melting temperature [14]. Mammalian gelatin possesses a gelation temperatures values of 25°C, in contrast at warm-water fish gelatin that features a gelation temperature of 29°C and cold-water fish gelatin that gellates at 10°C.

Mammalian gelatin is characterised by the highest concentration of proline and hydroxy proline that help to stabilize the triple helical structures. The triple helical structures act as junctions in a network that eventually forms the gel[15].

The applicability, functionality, and commercial value of fish gelatins depend essentially on physicochemical properties such as viscosity, strength and gel rigidity, intumescent capacity, thermal stability, as well as pH. The physicochemical properties are influenced in particular by amino acids composition, molecular weight, and proportion of  $\alpha$ -chains.

The melting and gelling temperatures (the temperature at which a gelatin solution changes from solid to liquid and vice versa) of fish gelatin hydrogel are relatively low compared to cattle and pig gelatins due to their smaller amounts of proline and hydroxyproline [16]. Gelatin fish is

characterized by similar thermal stability to mammalian gelatins that depends on raw materials source and processing conditions. The extraction temperature is a key factor in gelatin processing, as the increase in temperature from 60 to 75°C leads to a reduction in rheological properties.

Moreover, gelatin interacts strongly with molecules that are highly soluble in aqueous media and in particular, with ionic counterparts. A strategy to enhance the fish gelatin hydrogels mechanical properties is the formation of double-network gels with co-hydrogelators by the establishment of either physical or chemical crosslinks. In this study the shark/tuna gelatin has been used as a drug nanocarrier with a series of pharma derivatives, Doxorubicin and Crocine.

One strategy to improve their mechanical properties is the formation of double network gels using a cohydrogelator. In this sense, ionic liquids (ILs) are considered green solvents due to their biodegradability and low toxicity. ILs are potentially ideal candidates as solvents or cosolvents for gelatin, together with water, due to their ionic nature, generating the so-called Ion-Gelatin. Strong interactions between these species are expected due to the ionic character of both gelatin and ILs. Thus, gelatin polypeptide strands will tend to reorganized into the most thermodynamically favorable structure during the protein re-naturalization. Xray diffraction experiments evidence important differences between water-based gelatin and Ion-based gelatin, indicating a pronounced modification in the conformation of the gelatin lefthand helix. Recently, a perfluorinated IL, [C<sub>2</sub>C1py] [C<sub>4</sub>F<sub>9</sub>SO<sub>3</sub>], has been studied, featuring a thermophysical profile promising to be a co-hydrogelator for fish gelatin due to the lack of cytotoxicity and polar nanosegregated structure. Therefore, the overall aim of this part of the project is to characterize the nanostructure formation of Ionic hydrogels obtained from the gelation process upon cooling (around 273 K) of an aqueous Shark/Tuna gelatin solution with perfluorinated IL by using X-ray techniques to understand the structure-property relationship in comparison with previously characterized fish gelatin hydrogels.

Moreover, the ionic hydrogels were successfully passive loaded with two drugs: Doxorubicin, a potential chemotherapeutic agents widely used in several cancers treatments; and Crocin, a carotenoid antioxidant used as neural protective agent and with antiproliferative action against cancer cells. The structure-property relationship between drugs and internal ion hydrogel matrix of the nanocarriers will be evaluated to understand the structural parameters to design specific drug delivery systems for targeted and local administration.

Fourier transform infrared (FTIR) and thermal analysis (DSC) of the Ion Gelatin have been performed to assess the supramolecular interactions between the perfluorinated IL and the gelatin.

A characteristic band of the collagen triple helix structure appears in the FTIR bands. The amide bands I, II, III, are related to the secondary structure of proteins ( $\beta$ -sheet and  $\alpha$ -helix). A slight systemic red shift was found when fluorinated IL was introduced, suggesting an interaction between FIL and fish gelatin. The absorption band of amide I and II of the hydrogels formed by the mixture of shark gelatin and fluorinated IL has a lower intensity associated with the dilution effect. However, the absence of gelatin displacement and the constant rate between amide I and II suggest that the collagen helix structure is retained in the mixed gelatin-ion hydrogel. In addition, recent preliminary SAXS have shown swelling of the fibrillar nanostructure of the gelatin hydrogel after the addition of the FILs. Ion-Gelatin hydrogels have been characterized also by thermal analysis, (see Figure 8.1), observing that with the addition of IL to the solution, the T<sub>g</sub> of the hydrogel disappeared, indicating that the addition of IL is more likely to hinder protein-protein interactions, thus increasing the mobility of the gelatin chains. Moreover, the

FIL within the gelating hydrogel has modified the crystallization mechanism as well as enhancing the strength of the final network (see Figure 1), confirming the interaction with the gelatin fibers.

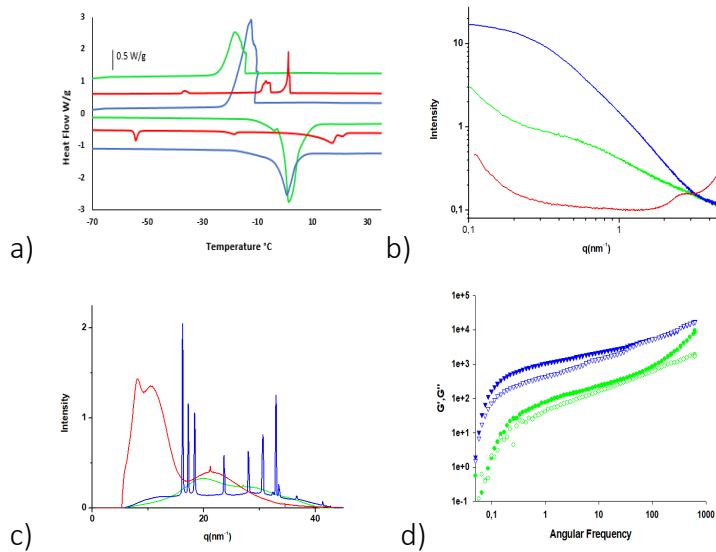


Figure 8.1. a) DSC thermograms of shark gelatin/Ionic Liquid hydrogel at  $5^{\circ}\text{C}\cdot\text{min}^{-1}$ , b) SAXS and c) WAXS of shark gelatin/Ionic Liquid hydrogel at  $5^{\circ}\text{C}\cdot\text{min}^{-1}$  at  $25^{\circ}\text{C}$ ; d) Frequency Sweep (—) 25% Shark gelatin, (—) (25:25)% Shark Gelatin/IL, (—) Ionic Liquid

Furthermore, the structure-loading properties of fish hydrogels have been investigated as nanocarrier devices for pharmaceutical applications by the uptake and release of Doxorubicin, and Crocin. Release profiles showed a typical triphasic aspect whose extension clearly depends on the internal interaction between gelatin fibres and drug species (see Figure 8.2).

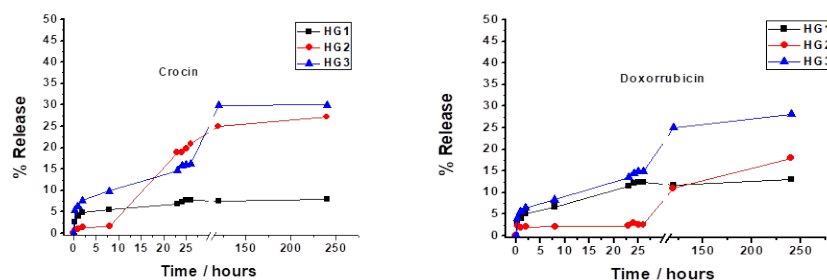


Figure 8.2. HG1 = Tuna Gelatin, HG2 = Blue Shark Head Chondroitin Sulfate, HG3 = Blue Shark Gelatin.

Currently, we are working on a manuscript that reports the formation of fish gelatin hydrogels and the influence on the ionic liquids in its nanostructure. Simultaneous SAXS/WAXS have allowed to elucidate the nanostructure of a series of Ionic-gelatin hydrogels, as well as the effect of the gelatin on the ionic phase transitions upon temperature. A detailed SAXS analysis will characterize the size of the nanosegregated ionic domains within hydrogels network. The addition of the fluorinated IL as cohydrogelator modifies the complex structure of the tuna/shark corresponding hydrogel that determine the tunability of the thermophysical and carrier properties profile related to the different domains molecular structure, in order to meet the optimal conditions required to load specifically drugs with different complementary therapeutic targets.

Moreover, a detailed assessment of the fish gelatin hydrogels as drug delivery systems will be described. Moreover, fish gelatin from other fish species have been identified to continue with the research study.

## 9- Main applicant as well as co-applicant of a series of synchrotron proposals as well as other polymer research projects.

---

I am the main applicant of around 70 synchrotron proposals around Europe with an average of 9 shifts per proposal. Each shift is evaluated as 5500 €.

Moreover, I am also a co-applicant of the successful project “Procesos catalíticos para la conversión de CO<sub>2</sub> en productos de interés industrial” of the science ministry of Spain. I am in the project as ‘colaborador de equipo’. In this project, the researchers from Universidad de Castilla la Mancha synthesize novel polymeric derivatives that I am responsible for the characterization within my scientific network.

I have participated in order to advance the polymer science research at the beamline particularly at relevant industrial conditions as a co-proposer of the successful DPI project “Online Polyolefin structuring during Cast Film Extrusion” granted on June the 1<sup>st</sup> of 2018 by Dr. Portale. I also supervised the thesis student, Federico Di Sacco during his synchrotron experiments and I assist him in the development of novel SAXS-WAXS experiments combined with other relevant techniques.

## 10- Part of the scientific panel of bl11 NCD in Alba sincrotrón.

---

I have been invited to be a member of the scientific panel of the proposals for the beamline bl 11 NCD at ALBA sincrotrón.

I have been participating for 5 panels so far:

- ALBA Review Panel for Evaluation of Scientific Proposals for the 2021-I Call, 20/10/2020.
- ALBA Review Panel for Evaluation of Scientific Proposals for the 2020-II Call, 20/04/2020.
- ALBA Review Panel for Evaluation of Scientific Proposals for the 2020-I Call, 11/10/2019
- ALBA Review Panel for Evaluation of Scientific Proposals for the 2019-II Call, 11/04/2019.
- ALBA Review Panel for Evaluation of Scientific Proposals for the 2019-I Call, 11/10/2018.

## 11-Beamline scientist responsible of bm26/ DUBBLE at ESRF from July 2015.

---

I am responsible for managing general operations in the beamline as well as the chemical laboratory. As senior beamline scientist in a world-renowned scientific facility in soft condensed matter research, I have been able to expand my extensive organizational skills and develop an in-depth understanding on how to effectively perform a range of responsibilities including project management, scheduling and the preparation of scientific reports while providing scientific and technical support to visiting scientists in a competitive environment. During this period, bm26b has been ranking as the SAXS beamline at ESRF with the highest scientific cut-off to obtain beamtime. In addition, I have acquired an outstanding knowledge at the forefront of X-ray instrumentation. I have benefited from close interaction with the most prominent research groups in materials science, and specifically soft condensed matter, in the Netherlands and Europe. This has encouraged me to develop novel sample environments and performed cutting edge X-ray experiments in combination with other techniques.

Currently, I am responsible for the design of the new beamline during the ESRF upgrade. I have worked in collaboration with other ESRF scientists to formulate the Ray tracing of the new source and the selection and the optical components for the beamline.

My candidature to obtain the HDR has been prompted as an opportunity to work with excellent French and international research groups with whom I would like to continue and expand my collaborations as well as the excellent scientific environment for performing X-ray experiments that offers both Soleil synchrotron within the French research community. I could provide long experience on the management of a highly productive beamline on continue development in order to satisfy and attract new users with new challenging research activities. Moreover, I have worked with unique X-ray facilities from both technical and work environments that it would be of great benefit to further advance in my scientific career.

The main focus of my research has been the study of the structure-property relationships in the soft matter area in different medium such as bulk, solution as well as thin films. Particularly, I have devoted my scientific in-house research activity to perform scattering experiments both in transmission and grazing angle mode, in combination with several spectroscopies and mechanical techniques in the polymeric field such as polymer crystallization, self-assembled supramolecular polymers, advanced functional polymeric systems and metal-organic hybrid systems.

As beamline scientist of bm26-b, I have benefited from the long standing and extensive investigation of polymer crystallization studies in quiescent and industrial processing conditions conducted at the beamline. A wide range of polyofines, polyamides, etc ... have been investigated at extreme conditions in order to understand the mechanism of crystallization and the kinetics of expected mesophases and oriented structures formations.

I have also extensively worked in the implementation of grazing angle scattering techniques at DUBBLE. In particular, the combination GiXS techniques with other millisecond relevant techniques in order to investigate the main parameters that defined the polymeric film formation by performing in-situ GISAXS/GIWAXS experiments that allows to describe the crystallinity and microphase separation of block copolymers as well as polymer blends. The assessment of the role of as several phenomena such as macrophase separation, nanostructure

development and film percolation, occur concomitantly is crucial to control the film formation. We have recently published some of our work on the field and we have several manuscripts submitted.

1. Jacobus J. van Franeker, Daniel Hermida-Merino, Cedric Gommès, Kirill Arapov, Jasper J. Michels, René A. J. Janssen, Giuseppe Portale (2017) *Sub-Micrometer Structure Formation during Spin Coating Revealed by Time-Resolved In Situ Laser and X-Ray Scattering*. *Adv. Funct. Mater.* 2017, 1702516.
2. Guillaume Fleury, Daniel Hermida-Merino, Dong Jingjin, Karim Aissou, Aleksei Bytchkov, Giuseppe Portale: *Micellar-Mediated Block Copolymer Ordering Dynamics Revealed by In Situ Grazing Incidence Small-Angle X-Ray Scattering during Spin Coating*. *Advanced Functional Materials* 01/2019; DOI:10.1002/adfm.201806741.
3. Jingjin Dong; Shuyan Shao; Simon Kahmann; Alexander J Rommens; Daniel Hermida-Merino; Gert H ten Brink; Maria A Loi; Giuseppe Portale. *Mechanism of Crystal Formation in Ruddlesden--Popper Sn-Based Perovskites*. *Advanced Functional Materials*. pp. 2001294 - 2001294. 2020.

As with conventional, covalently bonded polymers, the macroscopic properties of supramolecular polymers (such as viscosity and tensile strength) are intimately related to its nanostructure. The versatility of the supramolecular architectures offers the possibility of constructing chemical architectures displaying notable structural complexity, from linear H polymeric chains to networks and hyperbranched systems. These supramolecular entities can, in turn, enable the production of new thermoplastic elastomers, superglues, hot adhesives, and tuneable polymer materials. A systematic study of the effect of the end group and linkers on the nanostructure of self-assembled polymers has been the aim of the research on the supramolecular field.

1. Kelly Melia, Barnaby W. Greenland, Daniel Hermida-Merino, Lewis R. Hart, Ian W. Hamley, Howard M. Colquhoun, Andrew T. Slark, Wayne Hayes (2018) *Self-assembling unsymmetrical bis-ureas*. *Reactive and Functional Polymers* 124 (2018) 156–161.
2. Daniel Hermida-Merino, Ben O’Driscoll, Lewis R. Hart, Peter J. Harris, Howard M. Colquhoun, Andrew T. Slark, Cristina Prisacariu, Ian W. Hamley and Wayne Hayes (2018) *Enhancement of microphase ordering and mechanical properties of supramolecular hydrogen-bonded polyurethane networks*. *Polym. Chem.*, DOI: 10.1039/c8py00604k .
3. Daniel Hermida Merino, Antonio Feula, Kelly Melia, Andrew T. Slark, Ioannis Giannakopoulos, Clive R. Siviour, C. Paul Buckley, Barnaby W. Greenland, Dan Liu, Yu Gan, Peter J. Harris, Ann M. Chippindale, Ian W. Hamley, Wayne Hayes; “A systematic study of the effect of the hard end-group composition on the microphase separation, thermal and mechanical properties of supramolecular polyurethanes”; *Polymer*, 107 (2016), 368-378. <http://dx.doi.org/10.1016/j.polymer.2016.07.029>
4. Hermida-Merino, D., Trebbin, M., Foerster, S., Rodriguez-Llansola, F. and Portale, G.; “Microfluidic Assisted Self-Assembly of pH-Sensitive Low-Molecular Weight

*Hydrogelators Close to the Minimum Gelation Concentration*"; Macromol. Symp., (2015), 358: 59–66. doi: 10.1002/masy.

5. Daniel Hermida Merino, Gemma E Newby, Ian W Hamley, Wayne Hayes, Andrew Slark; *"Microphase separation induced in the melt of Pluronic copolymers by blending with a hydrogen bonding urea–urethane end-capped supramolecular polymer"*; Soft Matter, (2015) **11**, 5799-5803; DOI: 10.1039/C5SM01461A
6. D Hermida-Merino, M Belal, B.W. Greenland, P Woodward, A.T. Slark, F.J. Davis, G.R. Mitchell, I.W. Hamley, W Hayes: *Electrospun supramolecular polymer fibres*. European Polymer Journal 04/2012; 48(7):1249-1255., DOI:10.1016/j.eurpolymj.2012.04.015.
7. Daniel Hermida Merino, Andrew T. Slark, Howard M. Colquhoun, Wayne Hayes, Ian W. Hamley: *Thermo-responsive microphase separated supramolecular polyurethanes*. 09/2010; 1(8):1263-1271., DOI:10.1039/C0PY00122H.



Cite this: *Polym. Chem.*, 2018, **9**, 3406

## Enhancement of microphase ordering and mechanical properties of supramolecular hydrogen-bonded polyurethane networks†

Daniel Hermida-Merino,<sup>‡a</sup> Ben O'Driscoll,<sup>a</sup> Lewis R. Hart,<sup>a</sup> Peter J. Harris,<sup>b</sup> Howard M. Colquhoun,<sup>a</sup> Andrew T. Stark,<sup>c</sup> Cristina Prisacariu,<sup>§d</sup> Ian W. Hamley <sup>a</sup> and Wayne Hayes <sup>\*a</sup>

The improvement of the mechanical properties of supramolecular polymer networks is currently receiving significant interest both within academic and industrial circles in order to enable the application of these desirable stimuli-responsive materials in real world situations. In this study, structural units within phase separated supramolecular polyurethane (SPU) networks have been changed to assess the role of the hard segment composition on the mechanical characteristics of the resultant materials. Notably, increasing the degrees of conformational freedom within the hard segment component of a SPU was found to improve the phase separation and as a consequence also increase the storage modulus of the polymer network. Specifically, replacing 4,4'-methylene diphenyl diisocyanate with 4,4'-dibenzyl diisocyanate within a SPU improved the packing efficiency of the isocyanate derived hard segments and improved the physical properties of the supramolecular polymer network. This study utilised a combination of SAXS, WAXS and AFM analysis to assess the degree of crystallinity within the hard segment component of the polymer network whilst rheological analysis was used to establish the mechanical characteristics of the polymers.

Received 19th April 2018,  
Accepted 1st June 2018

DOI: 10.1039/c8py00604k

rsc.li/polymers

## Introduction

First disclosed over 80 years ago,<sup>1</sup> polyurethanes (PUs) are now a widely utilised class of materials which have traditionally been accessed *via* reaction of polyols with polyisocyanates<sup>2–5</sup> to yield a versatile and diverse range of materials. As a result of their facile synthesis and attractive physical properties, PUs have found use as thermoplastic, thermosetting and elastomeric materials<sup>6</sup> in applications including adhesives, protective coatings, foams, fibers, elastomers and medicine.<sup>7–10</sup> Numerous polyols have been harnessed as building blocks,

however, from the range of commercially available isocyanates, methylene diphenyl diisocyanate (MDI) has found the most extensive use on account of its attractive chemistries and relatively low toxicity.<sup>11,12</sup>

A recent development in PU chemistries has been the investigation of supramolecular polyurethane (SPU) networks<sup>13–18</sup> which are able to self-assemble through weak non-covalent interactions.<sup>19–27</sup> These materials are attractive on account of their thermo-reversible characteristics.<sup>28–32</sup> Gooch and co-workers have reported<sup>33</sup> SPU-based elastomers which assemble through triple hydrogen bonding interactions and provide access to different degrees of crystallinity. By altering the feed ratio of the hetero-complementary polymers the mechanical properties were also enhanced. Gao *et al.* have described<sup>34</sup> the synthesis and properties of PU 'cationomers' with an imidazolium-diol based chain extender which demonstrated a modulus of approximately 180 MPa as a result of enhanced immiscibility between the hard and soft segments. Burattini and co-workers have studied<sup>35</sup> the intramolecular interactions between chain-folding polyimide and telechelic polyurethane featuring electronically complementary pyrenyl end groups. The supramolecular blend formed by a combination of hydrogen bonding and  $\pi$ - $\pi$  stacking interactions produced a healable material with a tensile modulus of 0.3 MPa and a modulus of toughness of 510 MPa. More recently, Feula *et al.*<sup>36</sup>

<sup>a</sup>Department of Chemistry, University of Reading, Whiteknights, Reading, RG6 6AD, UK. E-mail: w.c.hayes@reading.ac.uk

<sup>b</sup>Electron Microscopy Laboratory, University of Reading, Whiteknights, Reading, RG6 6AD, UK

<sup>c</sup>Henkel Adhesive Technologies, Wood Lane End, Hemel Hempstead, HP2 4RQ, UK

<sup>d</sup>Petru Poni Institute of Macromolecular Chemistry of the Romanian Academy, Aleea Grigore Chica Voda, Nr. 41 A, Iasi 700487, Romania

†Electronic supplementary information (ESI) available. See DOI: 10.1039/c8py00604k

‡Present address: DUBBLE CRG, BM26, ESRF-The European Synchrotron, Netherlands Organization for Scientific Research, 6 rue Jules Horowitz, 38043, Grenoble, France.

§This paper is dedicated to our dear friend and colleague, Dr Cristina Prisacariu, who sadly passed away during preparation of this manuscript.

have developed a well-defined hydrogen bonded SPU with a low dissociation temperature which permits healing at physiological temperatures. The biocompatible synthetic skin was able to fully recover its mechanical performance after healing for 1 hour at 37 °C.

It has been reported<sup>15</sup> that the mechanical properties of chain extended PUs are influenced by the chemistries of the polymer which control the phase separation between rigid *hard* and flexible *soft* segments of the polymer architecture. Furthermore, the improvement in mechanical properties<sup>37</sup> and resulting surface hydrophobicity<sup>38</sup> have been attributed to phase separation in the polymer matrix. For example, Yilgör and co-workers have investigated the local packing of the urea moieties in segmented PUs in order to obtain high degrees of microphase separation.<sup>13,14,39–41</sup> Furthermore, phase separation can be promoted by using an apolar soft segment with low surface energies such as polydimethylsiloxane (PDMS).<sup>42–44</sup> Incorporation of a range of hard segments as chain extenders has also led to the generation of tuneable thermo-reversible materials.<sup>28,29,45</sup> Prisacariu and co-workers have reported<sup>46</sup> recently the use of 4,4'-dibenzyl diisocyanate (DBDI) in PU synthesis as alternative to MDI. DBDI features an ethylene linkage between the aromatic isocyanate moieties which permits free rotation about the linker, resulting in optimal alignment of the urethane or urea containing motifs between polymer chains. In principle this more flexible linkage enhances the ordering of the hard segments in linear PUs.<sup>47</sup> Indeed, the use of the more flexible diisocyanate (DBDI) in covalent and chain-extended PUs ( $M_n = 60\,000$ – $120\,000$  g mol<sup>-1</sup>) has enhanced the ordering of the hard segments with appreciable improvement in the mechanical properties relative to MDI-derived analogues.<sup>46,48–55</sup>

Herein we report the synthesis and properties of a novel series of self-assembled low molecular weight (>12 000 g mol<sup>-1</sup>) and phase separated supramolecular polyurethanes which feature DBDI derived hard segments with a view to improving both the thermal and mechanical characteristics of supramolecular polymers. The effect of incorporating a flexible ethylene linkage into the urethane/urea component of these self-assembling materials is reported and evaluated.

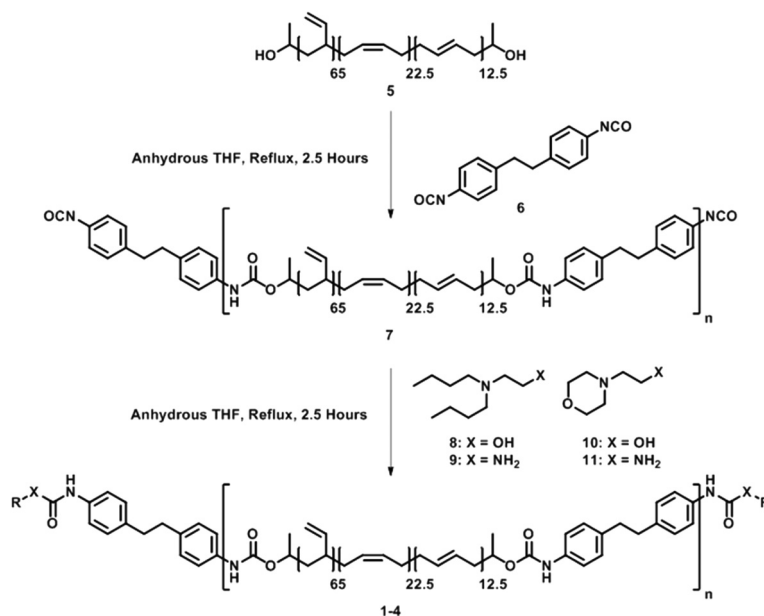
## Results and discussion

In order to understand the role of the diisocyanate-derived hard segment within the self-assembled polymer network, SPUs 1–4 (Scheme 1 and Table 1) with 4,4'-DBDI residues were synthesised by first end-capping the apolar polybutadiene 5 (Krasol LBH 2000,  $M_w = 2020$  g mol<sup>-1</sup>) mid-block, with DBDI 6 to afford the pre-polymer 7.<sup>29,56</sup>

To allow sole focus on the physical properties arising as a consequence of the hard segment, end-groups were selected with predictable contributions to the self-assembly process,

**Table 1** End group and yields from the synthesis of SPUs 1–4

Compound	R	Yield (%)
1		80
2		89
3		87
4		80



**Scheme 1** Synthesis of polyurethanes 1–4 with DBDI 6 derived hard segments.

thus allowing comparison to analogues derived from MDI.<sup>26,29,46,57–60</sup> Termination of the pre-polymer 7 was successfully achieved by addition of either derivatives containing morpholine or dibutylamine motifs (8–11) with amino or hydroxyl functionalities, respectively (Table 1). The chosen end-groups have previously been reported in structurally similar SPUs containing 4,4'-MDI derived hard segments. The SPUs reported by Woodward *et al.*<sup>29</sup> were shown to be weakly hydrogen bond, or indeed not at all in the case of the dibutylamine motif. Details of the materials and methods, as well as full spectroscopic characterisation for the SPUs 1–4 can be found in the ESI.†

To investigate the packing of hard segments between SPU chains containing both DBDI and MDI derived hard segments and the efficiency of intermolecular hydrogen bonding, energy minimised molecular models (Fig. 1) were generated. A single repeat unit of the polyol soft segment capped by two DBDI or MDI moieties with terminal methyl units (hard segments) was modelled using Cerius<sup>2</sup> software and the Dreiding II<sup>61</sup> force field. Examination of the models reveals the packing within DBDI derived hard segments is more efficient (Fig. 1a and b). Close contacts forming linear hydrogen bonds of lengths 2.3–2.6 Å between the hydrogen bond donors (NH of urethane/urea) and the hydrogen bond acceptors (carbonyl oxygen) were observed. These distances are in good agreement with hydrogen bond lengths measured in crystals.<sup>62,63</sup> The polymers are also observed to be well-ordered in the DBDI derived SPU array as demonstrated by examination of the polymer chains, end on. Visually, the phenyl rings of the DBDI motifs were rotated into the same plane as a result of the increased flexibility of the ethylene linkage. When the MDI derived SPU model was subjected to the same constraints, less efficient packing was observed in both the hard and soft segments as well as increased hydrogen bonding (NH...O) distances (2.3–2.8 Å) between the polymer chains (Fig. 1c and d). It was also noted

that the polymer chains are contracted in length in the model of the MDI derived polymers when compared to the DBDI derived analogue, possibly related to the packing efficiency of the isocyanate moiety.

Variable temperature FT-IR spectroscopic analysis was conducted on the SPUs 1–4 (Fig. 2) and revealed a thermo-responsive behaviour similar to structurally related MDI analogues.<sup>26,29</sup> A strong absorbance for both the free (1730 cm<sup>-1</sup>) and hydrogen-bonded (1710 cm<sup>-1</sup>) urethane groups<sup>64</sup> was observed in all SPUs at room temperature, arising from the urethane bonds in the pre-polymer in addition to the end-groups in polymers 1 and 2. The ordered hydrogen bonded urea band at *ca.* 1640 cm<sup>-1</sup> was observed to be the predominant absorbance within the urea vibration modes for polymers 3 and 4 in addition to the hydrogen bonded urethane absorbance. The intensity of both the urethane and urea absorbance bands were seen to diminish with increased temperature for all SPUs 1–4, as a result of dissociation of the hydrogen bonded network. However, after heating to 120 °C, hydrogen bonding was still present above 50% in all cases. This effect may be attributed to the more efficient packing in the hard segments, resulting in increased hydrogen bond strength and crystallinity. After approximately 30 minutes at room temperature, full recovery of the relative percentage of hydrogen bonding was observed within the SPUs 1–4 as determined spectroscopically. The recovery of the relative percentage of hydrogen bonding over time demonstrates the thermoreversible nature of the SPUs and is in good agreement with our previous studies for analogues SPUs previously reported by Woodward *et al.*<sup>29</sup> Therefore, it is proposed that the presence of a DBDI derived moiety in the SPUs (1–4) improves the efficiency of packing within the polymer network, whilst retaining the hydrogen bonding characteristics of the urethane/urea functional groups.

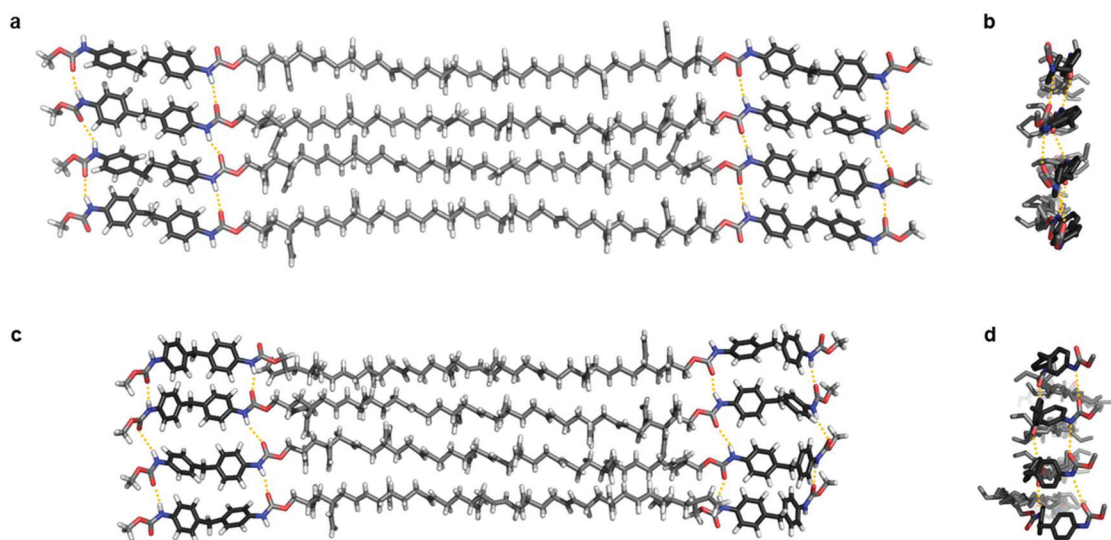


Fig. 1 To scale, energy minimised molecular models of (a) DBDI derived oligomer and (b) chain-end on view of the same molecular assembly showing more efficient stacking when compared to analogous MDI derivatives (c & d).

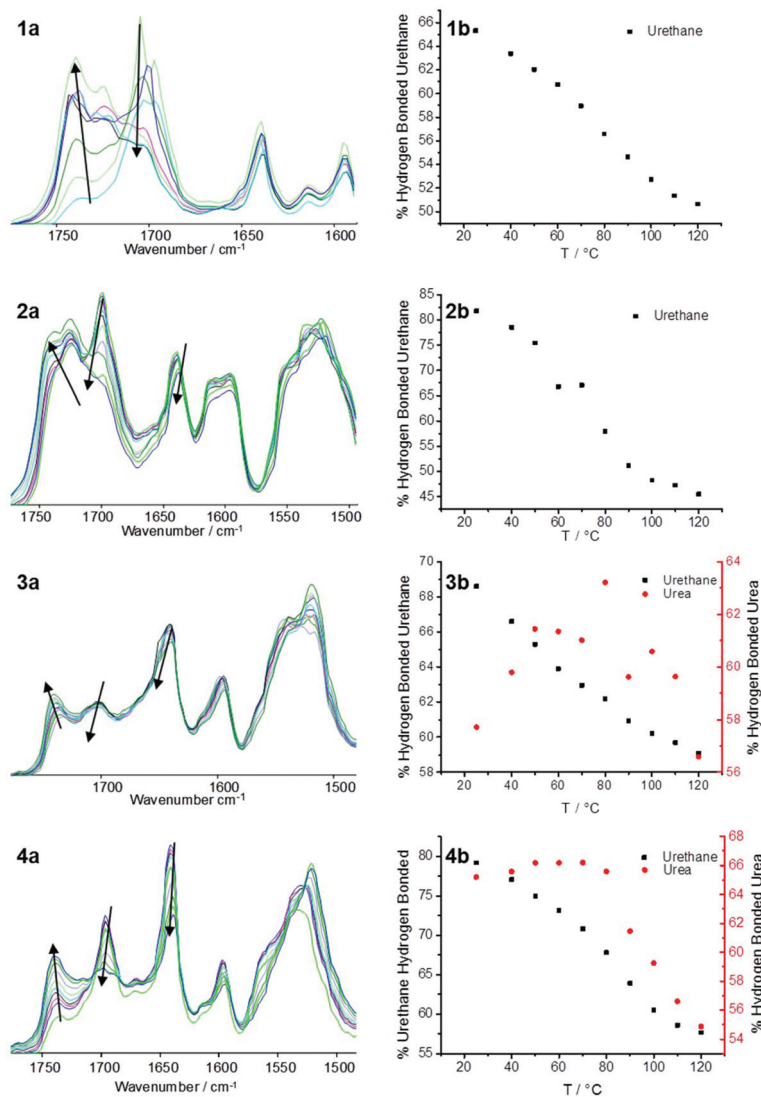


Fig. 2 (a) VT-FTIR spectra (25–120 °C) of DBDI-derived SPUs 1–4 and (b) hydrogen bonded urethane and urea content for the DBDI SPUs (1–4).

### Morphological analysis

To assess the crystallinity within the hard segments of the polymers obtained with DBDI (18.0 wt% of structural components in the polymer which includes the DBDI unit) and compare their morphology to that of MDI analogues<sup>26,29</sup> (17.4–18.3 wt% hard segment), the SPUs 1–4 were probed *via* SAXS, WAXS and AFM analyses.

Temperature dependant SAXS experiments (Fig. 3) revealed that the DBDI derived linker indeed promotes organisation of the hard segments as a result of the ethylene bridging residue's increased rotational freedom. Microphase separation is observed for all SPUs 1–4 as indicated by the reflection at  $0.047 \text{ \AA}^{-1}$  for the morpholine derivatives (2 & 4) and  $0.067 \text{ \AA}^{-1}$  for the corresponding dibutylamine analogues (1 & 3). The domain spacing within the DBDI derivatives was thus determined to be *ca.* 13.2 nm for morpholine derivatives (urethane 2 and urea 4 analogues) and *ca.* 9.0 nm for both dibutylamine

derivatives (urethane 1 and urea 3 analogues). These domain spacings are approximately twice those observed for the MDI derived analogues (MDI-dibutylamine = 4.31 nm and 5.12 nm and MDI-morpholine = 5.20 nm and 5.70 nm),<sup>26,28,29</sup> suggesting that the SPU chains are able to adopt a more extended configuration permitted by enhanced stacking of the DBDI units. Interestingly, the SAXS profile of SPU 3 possesses two reflections centred at  $0.067 \text{ \AA}^{-1}$  (9 nm) and  $0.11 \text{ \AA}^{-1}$  (5.7 nm) which is a novel pattern for supramolecular polyurethane-urea systems of this type.<sup>26,28,29</sup> The second order SAXS peak ( $q\sqrt{3}$ ) corresponds to hexagonal packing of cylinders within the micro-domains as a result of association of the urethane-urea motifs which are allowed to form without disruption from the dibutylamine end-groups. These results suggest a higher degree of microphase separation compared to analogues materials with MDI hard segments. The thermo-responsive behaviour of the SPUs 1–4 were investigated by heat/cool cycle between  $-60 \text{ }^\circ\text{C}$  and  $70 \text{ }^\circ\text{C}$  conducted at

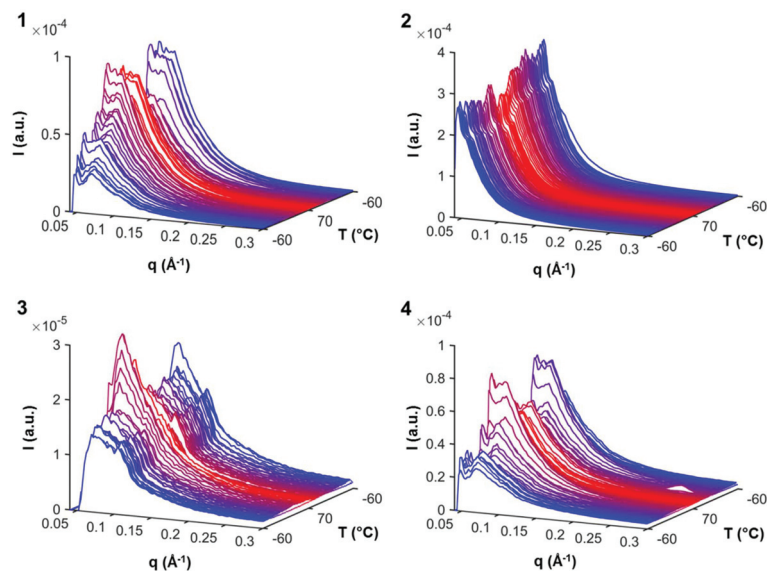


Fig. 3 Variable temperature SAXS analysis of 1–4. The samples were heated at  $5\text{ °C min}^{-1}$  between  $-60\text{ °C}$  (nearest) and  $70\text{ °C}$  before cooling to  $-60\text{ °C}$  (furthest).

$5\text{ °C min}^{-1}$ . The temperature response of the microphase separation exhibited an analogous trend to systems reported previously.<sup>26,29</sup> Upon heating from  $-60\text{ °C}$ , the thermal history of the material was initially removed and an equilibrium reached as demonstrated by an increase in the intensity of the SAXS peak at  $0.067\text{ Å}^{-1}$ . The intensity of the SAXS peak then decreases at *ca.*  $70\text{ °C}$ , indicating the phase mixing of the hard and soft segments *via* disruption of the hydrogen bonding interactions. Upon cooling, the intensity of the SAXS peak at  $0.067\text{ Å}^{-1}$  increases once again as a result of the hydrogen bonding network being restored. This trend further supports the thermo-responsive properties of the SPUs 1–4 reported by IR spectroscopy.

WAXS studies were performed to investigate the nanostructure of DBDI segments in the SPUs. In principle, the conformation adopted by the DBDI linker should enable ‘crystalline’ like micro-domains to form in the bulk as a result of the ordered hydrogen bonding and aromatic  $\pi$ – $\pi$  stacking interactions as indicated in the SAXS profiles of the SPUs (Fig. 3). Notably, the WAXS profiles (Fig. 4) of the DBDI derivative SPUs 1–4 feature several reflections on the broad amorphous scattering signal, especially in the case of SPU 2. Notably, the crystalline pattern corresponds to a urethane derivative which confirms the ordering potential of the DBDI linker. The reflections observed in the WAXS profiles correspond to association of the urethane/urea chain ends ( $4.5$ – $4.7\text{ Å}$ ) in the polymer matrix, in excellent agreement with structurally related SPUs ( $4.6$ – $4.7\text{ Å}$ ).<sup>29,65</sup> Furthermore, the WAXS profiles of SPUs 1–4 all exhibit a broad shoulder at *ca.*  $2\theta = 20^\circ$  within the crystalline region. These signals correspond to domain spacings of  $3.5\text{ Å}$ , which strongly suggests  $\pi$ – $\pi$  stacking interactions between the aromatic motifs within the hydrogen bonding hard segments.<sup>26</sup> This result along with the absence of these features

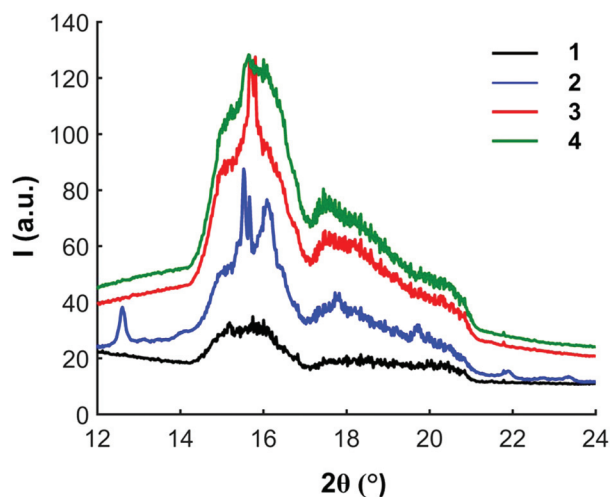


Fig. 4 Comparison of WAXS profiles for DBDI-based SPUs (1–4).

in structurally related materials<sup>29</sup> incorporating MDI further supports the hypothesis that the ethylene bridge provides greater rotational freedom allowing more efficient packing of the hard segments.

The thermo-responsive dynamics of the ‘crystalline’ micro-domains was probed by VT-WAXS analysis to understand the thermally induced disruption of the hydrogen bonding interactions (Fig. 5) within the hard segments. In agreement with the VT-SAXS experiments, the VT-WAXS profiles follow a similar temperature trend and demonstrate the thermoreversibility of the ordering within these materials.

To further analyse the self-assembly of the SPUs 1–4, AFM studies (Fig. 6 and Fig. S9†) were carried out to visualize the

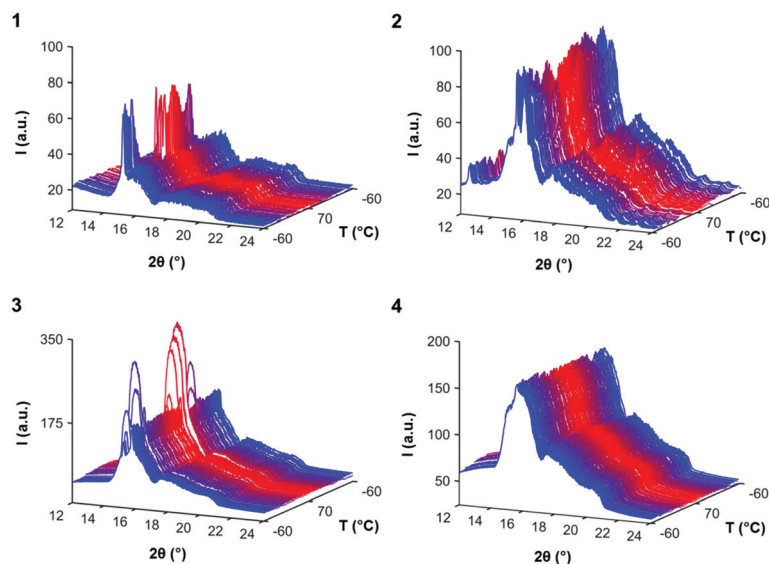


Fig. 5 Variable temperature WAXS analysis of SPUs 1–4. The samples were heated at  $5\text{ °C min}^{-1}$  between  $-60\text{ °C}$  and  $70\text{ °C}$  over three cycles.

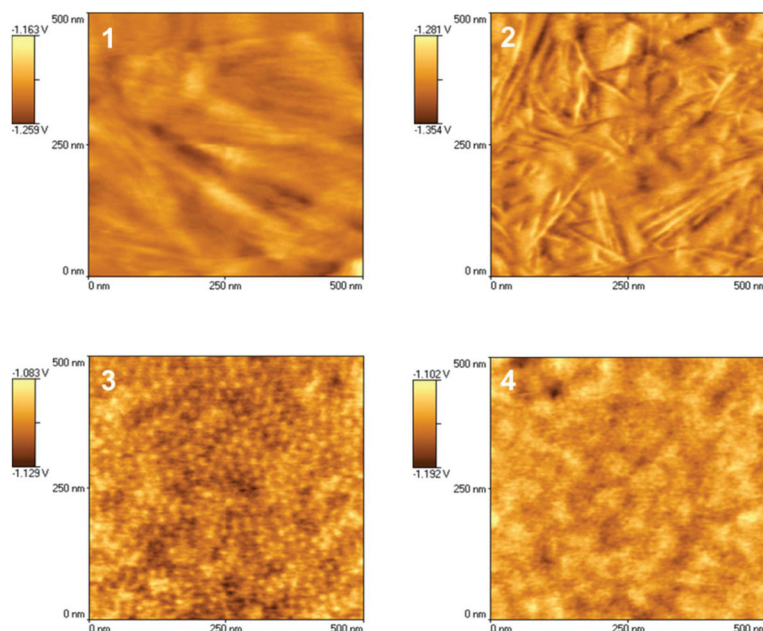


Fig. 6 AFM phase micrographs of DBDI based SPUs 1–4.

changes in the morphology attained by the DBDI derived SPUs when compared to the MDI-based analogues.<sup>26,29</sup> The ordered stacking of the DBDI linkers has been observed<sup>46</sup> to promote the packing of both urethane and urea moieties. As a result, the microphase separation of the DBDI supramolecular derivatives should favour alignment of the urea/urethane moieties within fibrillar aggregates. Remarkably, the all-urethane SPUs 1 and 2 are present as fibres with high aspect ratios (*i.e. ca.* 100 nm in length and *ca.* 10 nm in width). Increased phase mixing is observed in SPU 1 as a result of the relatively weak hydrogen bonds between urethane motifs (5.1 wt% end groups

in 1, comprising terminal DBDI unit and the covalently bound end-group). In contrast, SPU 2 forms more defined fibre like structures on account of association of the morpholine end-group (3.4 wt% end group content) with the urethanes of the PU residues. Interestingly, spheres or cylinder like morphologies are observed in SPUs 3 and 4. SPU 3 gives rise to defined structures as a result of the relatively strong bifurcated hydrogen bonding interactions between urea moieties within the hard segments which are not disrupted by the dibutyl terminal-groups (4.2 wt% end group content). In comparison, disruption to the hard segment assembly is observed in the

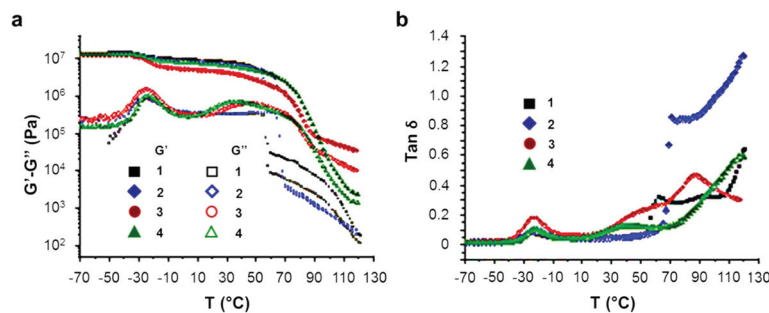


Fig. 7 (a) Thermal dependence of dynamic shear moduli for DBDI derived polymers 1–4. (b) Plot of  $\tan \delta$  versus temperature for DBDI based SPUs 1–4.

morphology of SPU 4 as a consequence of the morpholine terminal group (3.8 wt% end group content) hydrogen bonding to the urethane/urea groups. The resulting disruption in the hydrogen bonding network and decreased crystallinity results, however, in the formation of 3D structures as the morpholine residues allow interactions between self-assembled arrays. These observations from AFM imaging are in good agreement with the SAXS profiles obtained for the SPUs 1–4, where features *ca.* 9–13 nm were observed. Perhaps this is most clearly demonstrated in the case of SPU 3 which revealed a reflection at 9 nm which corresponds to the diameter of spheres or cylinders (Fig. 6 [3]).

### Rheological analysis

To probe the effect of hard segment composition (18.0 wt%) on the mechanical properties of the SPUs, rheological analysis was undertaken. The storage modulus ( $G'$ ) for all DBDI derived materials was observed at *ca.*  $10^7$  Pa which is approximately an order of magnitude greater than those observed for structurally related polymers containing MDI moieties<sup>26,29</sup> with comparable molecular weights and polymeric composition. This observation provides strong evidence that the efficiency of packing within the hard segment is closely related to the mechanical properties of the SPUs. Interestingly, the storage moduli of SPUs 1–4 were approximately an order of magnitude greater when compared to supramolecular polymers which self-assemble through recognition motifs<sup>66,67</sup> which possess association constants which are  $10^4$   $M^{-1}$  larger than those reported herein. In addition, the storage moduli of SPUs 1–4 are also comparable to DBDI derived linear, high molecular weight PUs previously reported by Priscariu *et al.*<sup>50,52,53,55</sup> This result can be attributed to the decrease of phase mixing of the hard and soft segments within the polymer architecture which is known<sup>68</sup> to improve the mechanical properties of the polymer. The plateau of the viscoelastic region is recorded at a higher modulus when compared to analogous SPUs.<sup>29</sup> Furthermore, the sharper transition of both the storage and loss moduli at high temperature confirms the ‘crystalline’ nature of the micro-domains afforded. This melting transition also occurs over a narrow temperature range (*ca.* 15 °C) for the urethane derivatives 1 & 2 and *ca.* 35 °C for the urea derivatives

3 & 4. Both temperature windows are significantly more defined than those observed for structurally related MDI analogues (*ca.* 75 °C).<sup>26,29</sup> For all SPUs 1–4, the melting transition onset is also observed at a higher temperature (70 °C) when compared to MDI analogues (20 °C),<sup>26,29</sup> demonstrating a stiffer material at elevated temperatures as a result of enhanced packing between the polymer chains. These thermal characteristics could be considered an attractive feature for industrial applications with respect to materials processing and properties. The temperature difference at which the viscoelastic transition occurs as well as the magnitude of the plateau of the storage modulus, are consistent with the differences in ordering of the nano-domains produced by the DBDI derived linkers and the potential for the enhancement of the mechanical properties. The profile of  $\tan \delta$  (Fig. 7b) also corroborates the presence of a glass transition at higher temperatures (in excess of 80 °C) which can be assigned to the hard segment phase within the polymer matrix.

### Conclusion

The investigation of the use of diisocyanate DBDI within supramolecular polyurethanes 1–4 has revealed that packing of the hard segments leads to the improvement of the mechanical properties and thermal processing window of these supramolecular polymers when compared to analogues with less ordered MDI segments. Moreover, these materials offer comparable stiffness to chain-extended and high molecular weight PUs containing DBDI and other supramolecular polymers that are assembled through recognition motifs with higher association constants. Notably, the ordering effect of the DBDI derivatives led to well-defined structures such as fibres, spheres or cylinders, observed by AFM. Interestingly, the SAXS profile of 3 revealed two reflections is a novel SAXS pattern for a urethane-based supramolecular polymer which is consistent with the presence of well-defined microphase separated domains in the AMF images. The domain spacing of the DBDI derivatives (9–13 nm) revealed by SAXS, indicates that the DBDI derivatives possess an extended configuration. Remarkably, the WAXS profiles showed a ‘crystalline’ like morphology that confirms the close packing of the hard segments.

Variable temperature SAXS and WAXS analysis also demonstrated the thermo-reversibility of the ordering within the SPUs. The attractive rheological and thermal properties of the DBDI derived SPUs also provide scope for their use in industrial applications as a result of transitions observed in the narrow temperature range and higher temperatures. These results, when compared with the MDI derivatives,<sup>26,28,29</sup> show the potential of the employment of DBDI for generating materials with improved mechanical properties.

## Conflicts of interest

There are no conflicts to declare.

## Acknowledgements

The authors would like to thank Henkel Adhesive Technologies (post-graduate studentship for DHM), EPSRC (EP/N024818/1, post-doctoral research fellowship in support of LRH) and the University of Reading for financial support of this research. The authors would also like to acknowledge the University of Reading for access to analytical instrumentation within the Chemical Analysis Facility. Mr Oliver Balmford is also thanked for his insight in reproducing scattering data.

## References

- O. Bayer, W. Siefken, H. Rinke, L. Orthner and H. Schild, *Ger. Pat. DRP*, DE728981, 1937, 728981.
- W. Yu, M. Du, D. Zhang, Y. Lin and Q. Zheng, *Macromolecules*, 2013, **46**, 7341–7351.
- I. Lee and F. S. Bates, *Macromolecules*, 2013, **46**, 4529–4539.
- T. Saito, J. H. Perkins, D. C. Jackson, N. E. Trammel, M. A. Hunt and A. K. Naskar, *RSC Adv.*, 2013, **3**, 21832–21840.
- P. Król, *Prog. Mater. Sci.*, 2007, **52**, 915–1015.
- H.-W. Engels, H.-G. Pirkel, R. Albers, R. W. Albach, J. Krause, A. Hoffmann, H. Casselmann and J. Dormish, *Angew. Chem., Int. Ed.*, 2013, **52**, 9422–9441.
- I. Yilgor and E. Yilgor, *Polym. Rev.*, 2007, **47**, 487–510.
- D. K. Chattopadhyay and K. V. S. N. Raju, *Prog. Polym. Sci.*, 2007, **32**, 352–418.
- J. Courtois, I. Baroudi, N. Nouvel, E. Degrandi, S. Pensec, G. Ducouret, C. Chanéac, L. Bouteiller and C. Creton, *Adv. Funct. Mater.*, 2010, **20**, 1803–1811.
- Z. Pan, L. Yu, N. Song, L. Zhou, J. Li, M. Ding, H. Tan and Q. Fu, *Polym. Chem.*, 2014, **5**, 2901–2910.
- The Polyurethanes Book*, ed. D. Randall and S. Lee, Wiley-Blackwell UK, 1st edn, 2003.
- Z. S. Petrovic and J. Ferguson, *Prog. Polym. Sci.*, 1991, **16**, 695–836.
- T. F. A. De Greef, M. M. J. Smulders, M. Wolffs, A. P. H. J. Schenning, R. P. Sijbesma and E. W. Meijer, *Chem. Rev.*, 2009, **109**, 5687–5754.
- M. C. Stuparu, A. Khan and C. J. Hawker, *Polym. Chem.*, 2012, **3**, 3033–3044.
- K. A. Houton and A. J. Wilson, *Polym. Int.*, 2015, **64**, 165–173.
- B. Isare, S. Pensec, M. Raynal and L. Bouteiller, *C. R. Chim.*, 2016, **19**, 148–156.
- K. A. Houton, G. M. Burslem and A. J. Wilson, *Chem. Sci.*, 2015, **6**, 2382–2388.
- A. Gooch, N. S. Murphy, N. H. Thomson and A. J. Wilson, *Macromolecules*, 2013, **46**, 9634–9641.
- X. Callies, C. Fonteneau, C. Véchambre, S. Pensec, J. M. Chenal, L. Chazeau, L. Bouteiller, G. Ducouret and C. Creton, *Polymer*, 2015, **69**, 233–240.
- K. Melia, B. W. Greenland, D. Hermida-Merino, L. R. Hart, I. W. Hamley, H. M. Colquhoun, A. T. Slark and W. Hayes, *React. Funct. Polym.*, 2018, **124**, 156–161.
- A. Feula, A. Pethybridge, C. R. Siviour, C. P. Buckley, I. W. Hamley and W. Hayes, *Macromolecules*, 2015, **48**, 6132–6141.
- L. R. Hart, S. Li, C. Sturgess, R. Wildman, J. R. Jones and W. Hayes, *ACS Appl. Mater. Interfaces*, 2016, **8**, 3115–3122.
- A. Feula, X. Tang, I. Giannakopoulos, A. M. Chippindale, I. Hamley, F. Greco, C. P. Buckley, C. R. Siviour and W. Hayes, *Chem. Sci.*, 2016, **7**, 4291–4300.
- D. M. Wood, B. W. Greenland, A. L. Acton, F. Rodriguez-Llansola, C. A. Murray, C. J. Cardin, J. F. Miravet, B. Escuder, I. W. Hamley and W. Hayes, *Chem. – Eur. J.*, 2012, **18**, 2692–2699.
- B. C. Baker, C. L. Higgins, D. Ravishankar, H. M. Colquhoun, G. C. Stevens, F. Greco, B. W. Greenland and W. Hayes, *ChemistrySelect*, 2016, **1**, 1641–1649.
- D. Hermida-Merino, A. Feula, K. Melia, A. T. Slark, I. Giannakopoulos, C. R. Siviour, C. P. Buckley, B. W. Greenland, D. Liu, Y. Gan, P. J. Harris, A. M. Chippindale, I. W. Hamley and W. Hayes, *Polymer*, 2016, **107**, 368–378.
- D. Hermida-Merino, M. Belal, B. W. Greenland, P. Woodward, A. T. Slark, F. J. Davis, G. R. Mitchell, I. W. Hamley and W. Hayes, *Eur. Polym. J.*, 2012, **48**, 1249–1255.
- D. Hermida-Merino, A. T. Slark, H. M. Colquhoun, W. Hayes and I. W. Hamley, *Polym. Chem.*, 2010, **1**, 1263–1271.
- P. Woodward, D. Hermida-Merino, B. W. Greenland, I. W. Hamley, Z. Light, A. T. Slark and W. Hayes, *Macromolecules*, 2010, **43**, 2512–2517.
- C. B. St Pourcain and A. C. Griffin, *Macromolecules*, 1995, **28**, 4116–4121.
- M. C. Kuo, R. J. Jeng, W. C. Su and S. A. Dai, *Macromolecules*, 2008, **41**, 682–690.
- J.-M. Lehn, *Chem. Soc. Rev.*, 2007, **36**, 151–160.
- A. Gooch, C. Nedolisa, K. A. Houton, C. I. Lindsay, A. Saiani and A. J. Wilson, *Macromolecules*, 2012, **45**, 4723–4729.

- 34 R. Gao, M. Zhang, S. W. Wang, R. B. Moore, R. H. Colby and T. E. Long, *Macromol. Chem. Phys.*, 2013, **214**, 1027–1036.
- 35 S. Burattini, D. Hermida-Merino, W. Weng, J. Seppala, H. M. Colquhoun, W. Hayes, M. E. Mackay, I. W. Hamley and S. J. Rowan, *J. Am. Chem. Soc.*, 2010, **132**, 12051–12058.
- 36 A. Feula, X. Tang, I. Giannakopoulos, A. M. Chippindale, I. W. Hamley, F. Greco, C. P. Buckley, C. R. Siviour and W. Hayes, *Chem. Sci.*, 2016, **7**, 4291–4300.
- 37 A. Mishra, B. P. Das Purkayastha, J. K. Roy, V. K. Aswal and P. Maiti, *J. Phys. Chem. C*, 2012, **116**, 2260–2270.
- 38 K. Wei, L. Wang and S. Zheng, *Polym. Chem.*, 2013, **4**, 1491–1501.
- 39 S. Das, D. F. Cox, G. L. Wilkes, D. B. Klinedinst, I. Yilgör, E. Yilgor and F. L. Beyer, *J. Macromol. Sci., Part B: Phys.*, 2007, **46**, 853–875.
- 40 P. R. Laity, J. E. Taylor, S. S. Wong, P. Khunkamchoo, K. Norris, M. Cable, G. T. Andrews, A. F. Johnson and R. E. Cameron, *Polymer*, 2004, **45**, 5215–5232.
- 41 J. P. Sheth, D. B. Klinedinst, G. L. Wilkes, I. Yilgör and E. Yilgor, *Polymer*, 2005, **46**, 7317–7322.
- 42 E. Yilgor, I. Yilgor and E. Yurtsever, *Polymer*, 2002, **43**, 6551–6559.
- 43 D. J. Buckwalter, D. L. Inglefield, J. S. Enokida, A. G. Hudson, R. B. Moore and T. E. Long, *Macromol. Chem. Phys.*, 2013, **214**, 2073–2082.
- 44 L. M. Pitet, A. H. M. Van Loon, E. J. Kramer, C. J. Hawker and E. W. Meijer, *ACS Macro Lett.*, 2013, **2**, 1006–1010.
- 45 Y. Ni, F. Becquart, J. Chen and M. Taha, *Macromolecules*, 2013, **46**, 1066–1074.
- 46 C. Prisacariu, R. H. Olley, A. A. Caraculacu, D. C. Bassett and C. Martin, *Polymer*, 2003, **44**, 5407–5421.
- 47 A. A. Caraculacu, I. Agherghinei, C. Prisacariu and V. Cozan, *J. Macromol. Sci., Part A: Chem.*, 1990, **27**, 1547–1570.
- 48 C. Prisacariu, E. Scortanu and C. P. Buckley, *Int. J. Polym. Anal. Charact.*, 2009, **14**, 527–539.
- 49 C. Prisacariu, E. Scortanu and P. C. Buckley, in *Proceedings of the World Congress on Engineering*, 2008, vol. II, pp. 1468–1471.
- 50 C. Prisacariu, E. Scortanu, B. Agapie, V. A. Prisacariu and S. Coseri, *Polym. Int.*, 2013, **62**, 1600–1607.
- 51 C. Prisacariu, E. Scortanu, S. Coseri and B. Agapie, *Int. J. Polym. Anal. Charact.*, 2013, **18**, 154–161.
- 52 C. Prisacariu, E. Scortanu, I. Stoica, B. Agapie and V. Barboiu, *Polym. J.*, 2011, **43**, 613–620.
- 53 C. Prisacariu, E. Scortanu, A. Airinei, B. Agapie, M. Iurzhenko and Y. P. Mamunya, *Procedia Eng.*, 2011, **10**, 446–454.
- 54 C. Guo, L. Zhou and J. Lv, *J. Appl. Polym. Sci.*, 2011, **122**, 3544–3550.
- 55 C. Prisacariu, E. Scortanu and B. Agapie, *Procedia Eng.*, 2011, **10**, 984–989.
- 56 P. Woodward, A. Clarke, B. W. Greenland, D. Hermida-Merino, L. Yates, A. T. Slark, J. F. Miravet and W. Hayes, *Soft Matter*, 2009, **5**, 2000–2010.
- 57 C. Prisacariu and E. Scortanu, *High Perform. Polym.*, 2008, **20**, 117–125.
- 58 C. Prisacariu, C. P. Buckley and A. A. Caraculacu, *Polymer*, 2005, **46**, 3884–3894.
- 59 C. Prisacariu, E. Scortanu, G. E. Hitruc and A. A. Caraculacu, *Rev. Roum. Chim.*, 2007, **52**, 415–422.
- 60 D. Hermida-Merino, M. Belal, B. W. Greenland, P. Woodward, A. T. Slark, F. J. Davis, G. R. Mitchell, I. W. Hamley and W. Hayes, *Eur. Polym. J.*, 2012, **48**, 1249–1255.
- 61 S. L. Mayo, B. D. Olafson and W. A. Goddard, *J. Phys. Chem.*, 1990, **94**, 8897–8909.
- 62 W. Fuller, *J. Phys. Chem.*, 1959, **63**, 1705–1717.
- 63 S. Subramanian and M. J. Zaworotko, *Coord. Chem. Rev.*, 1994, **137**, 357–401.
- 64 L. Ning, W. De-Ning and Y. Sheng-Kang, *Polymer*, 1996, **37**, 3045–3047.
- 65 F. Lortie, S. Boileau, L. Bouteiller, C. Chassenieux, B. Demé, G. Ducouret, M. Jalabert, F. Lauprêtre and P. Terech, *Langmuir*, 2002, **18**, 7218–7222.
- 66 J. H. K. Ky Hirschberg, F. H. Beijer, H. A. van Aert, P. C. M. M. Magusin, R. P. Sijbesma and E. W. Meijer, *Macromolecules*, 1999, **32**, 2696–2705.
- 67 B. Folmer, R. P. Sijbesma, R. M. Versteegen, J. A. J. van der Rijt and E. W. Meijer, *Adv. Mater.*, 2000, **12**, 874–878.
- 68 J. Zheng, R. Ozişik and R. W. Siegel, *Polymer*, 2006, **47**, 7786–7794.

# Conclusions

During my scientific career, I have the opportunity to conduct cutting-edge research with some of the most prominent scientific groups across Europe and I have been stimulated to advance in the understanding of soft matter nanostructure in different media by scattering techniques using synchrotron light sources. Especially, I have probed the nanostructure formation upon extreme conditions that occur in industrial environments.

I have engaged my own research in the structure-property relationship area of polymers through a multi-technique approach to correlate several lengthscales by coupling complex techniques in situ to simultaneous SAXS-WAXS experiments. Accordingly, I have actively applied to different fellowships as well as public and public founding agencies worldwide to finance my research activities in collaboration with other scientific groups. Particularly, I have recently optimised the coupling of Raman spectroscopy to simultaneous time-resolved SAXS/WAXS experiments in combination with a Linkam DSC to investigate the crystallization from the melt of PVDF. Moreover, multivariate analysis has been conducted in simultaneously acquired data from in situ experiments to correlate among them at different lengthscales and simplify the data analysis.

Currently, I have focused my research on the design of different areas of bio-nanomaterials. Particularly, novel bio-sourced polymers have been generated by tailoring the chain architecture for tailored applications on the biomedical field.

Moreover, I have largely investigated the role of low molecular hydrogelators as bioinspired nanomaterials for the development of responsive drug nanocarriers with remarkable passive upload rates and controlled release profiles.

In addition, the valorization of biowaste such as fish gelatins obtained as by-products of the fisheries was aimed for the design of novel drug delivery systems by the design of hydrogels in combination with other co-hydrogelators as ionic liquids.

In the next future, I will continue to study in greater depth the structure-properties relationship of biomaterials by simultaneous SAXS/WAXS experiments in combination with other spectroscopies techniques. Moreover, the development of hybrid biomaterials with metallic-nanoparticles will expand the application in the nanomedicine field coupling the sensing and therapeutic applications as well as harnessing from the mechanical features that permit the local drug administration in corporal areas with impeded accessibility.

# PROJETS ET PRODUCTIONS SCIENTIFIQUES

## Cours et séminaires de formation pédagogique universitaire

---

1. Type d'événement: Séminaire  
Dénomination de l'événement: X-ray Metrology Workshop  
Ville: Utrecht, Pays-Bas  
Établissement organisateur: University of Utrecht/Netherlands center for multiscale catalytic energy conversion  
Objectifs du cours: Explicar la reducción de datos SAXS/WAXS al igual que dar nociones de SAXS a estudiantes de postgrado  
5 heures en Anglais  
Date: 22/05/2018
2. Type d'événement: Séminaire  
Dénomination de l'événement: Overview of SAXS/WAXS data reduction and analysis using WiSAXS  
Ville: Grenoble, Rhône-Alpes, France  
European Synchrotron  
Objectifs du cours: Expliquer aux utilisateurs de l'ESRF les méthodes avancées de réduction des données de SAXS/WAXS  
2 h en Anglais le 06/02/2017

## Expérience scientifique et technologique

---

### Activité scientifique ou technologique

#### *Participation à des projets de R&D&I financés à travers des procédures concurrentielles d'organismes publics ou privés*

1. Intitulé du projet: Nouvelle génération de biopolymères nanostructurés pour la fabrication additive et l'électrofilage  
Modalité du projet: De recherche fondamentale (y compris fouilles archéologiques, etc.)      Secteur du projet: Régionale compris  
Établissement où l'expérience a été réalisée: Université de Lorraine /DUBBLE  
Ville: Metz, Lorraine, France  
Chercheur/s responsable/s: Patrice Bourson; David Chapron; Daniel Hermida Merino  
Nombre de chercheurs participants: 3  
Début-Fin: 01/10/2019 - 30/09/2022      Durée du projet: 3 ans Montant total: 92.500 €
2. Intitulé du projet : Online Polyolefin structuring during Cast Film Extrusion  
Modalité du projet: De recherche et de développement y compris translationnel  
Établissement où l'expérience a été réalisée: University of Groningen  
Ville: Groningen, Groningen, Pays-Bas  
Chercheur/s responsable/s: Giuseppe Portale; Daniel Hermida Merino  
Type de participation: Equipo de colaboración

Nom du programme: Financiacion del Dutch Polymer Institute  
Début-Fin: 01/10/2018 - 30/09/2021  
Montant total: 242.000 €

3. Intitulé du projet: CTQ2017-84131-R/Procesos cataliticos para la conversion de CO2 en productos de interest industrial  
Modalité du projet: De recherche fondamentale (y            Secteur du projet: Nationale compris fouilles archéologiques, etc.)  
Type de participation: colaborador del equipo  
Établissement où l'expérience a été réalisée: Universidad de Castilla-La Mancha  
Ville: Ciudad Real, Castille-La Manche, Espagne  
Chercheur/s responsable/s: Agustín Lara Sanchez; Antonio Leandro Otero Montero; Juan Fernandez, Baeza Fernandez Baeza; Juan Tejeda Soto; Santiago García Yuste; Luis Fernando Sanchez-Barba Merlo; Carlos Alonso Moreno; José Antonio Castro Osma; Andres Garcés Osado; Ana María Rodríguez Fernandez-Pacheco; Iván Bravo Pérez Nombre de chercheurs participants: 12 Organisme/s de financement: Ministerio de Economía, Industria y Competitividad  
Type d'organisme: Agence d'État  
Ville: Madrid, Communauté de Madrid, Espagne  
Type de participation: Miembro de equipo  
Début-Fin: 01/01/2018 - 31/12/2020    Durée du projet: 2 ans  
Montant total: 138.000 €
4. Intitulé du projet: Novel pOlymeric materials DEsigNed for drug delivery System (NODENS)/CAROLINE – “Collaborative Research Fellowships for a Responsive and Innovative Europe’ provides experienced researchers”  
Établissement où l'expérience a été réalisée: Martin Luther University Halle-Wittenberg, DUBBLE Ville: Halle/Grenoble, France  
Chercheur/s responsable/s: Andreas Heise; Bing Wu; Daniel Hermida Merino; Kay Saalwaechter  
Nombre de chercheurs participants: 4 Organisme/s de financement: European Commission (Horizon 2020)/Marie Skłodowska-Curie actions Irish Research Council    Type d'organisme: Agence d'État  
Ville: Dublin, Irlande  
Début-Fin: 01/10/2017 - 30/09/2020  
Montant total: 23.391 €
5. Intitulé du projet: 2019093904 - SAXS/WAXS analyses of the dynamic heterogeneity of PVDF/PMMA and PVDF-HFP/PC blends  
Modalité du projet: De recherche fondamentale  
Type de participation: Coordinateur scientifique  
Établissement où l'expérience a été réalisée: Alba Type d'établissement: Organisme public de synchrotron  
Ville: Cerdanyola del Valles, Catalogne, Espagne  
Chercheur/s responsable/s: Bing Wu; Daniel Hermida Merino  
Nombre de chercheurs participants: 2  
Type de participation: Miembro de equipo  
Nom du programme: Propuesta sincrotrón  
Début-Fin: 12/06/2020 - 13/06/2020  
Montant total: 16.500 €

6. Intitulé du projet: 2019093942 - X-ray probing of bent-core nematic films: effects of lateral groups and alkyl tail length  
 Modalité du projet: De recherche fondamentale  
 Type de participation: Coordinateur scientifique  
 Établissement où l'expérience a été réalisée: Alba Type d'établissement: Organisme public de synchrotron  
 Ville: Cerdanyola del Valles, Catalogne, Espagne  
 Chercheur/s responsable/s: Adamo Fabrizio Corrado; Daniel Hermida Merino; Oriano Francescangeli; Michela Pisani; Francesco Vita  
 Nombre de chercheurs participants: 5  
 Type de participation: Miembro de equipo  
 Nom du programme: Propuesta sincrotrón  
 Début-Fin: 12/05/2020 - 13/05/2020  
 Montant total: 33.000 €
  
7. Intitulé du projet: 2019093948 - Structural investigation by in situ simultaneous SAXS/WAXS of the strain and melt crystallization of novel renewable itaconic acid polymer derivatives  
 Modalité du projet: De recherche fondamentale  
 Établissement où l'expérience a été réalisée: Alba Type d'établissement: Organisme public de synchrotron  
 Ville: Cerdanyola del Valles, Catalogne, Espagne  
 Chercheur/s responsable/s: Daniel Hermida Merino; Carolus Wilsens  
 Nombre de chercheurs participants: 2  
 Type de participation: Investigador principal  
 Nom du programme: Propuesta sincrotrón  
 Début-Fin: 03/03/2020 - 04/03/2020  
 Montant total: 33.000 €
  
8. Intitulé du projet: 2019023566 - Optimization of nanofluids derived from Graphene and Fluorinated Ionic Liquids for applications of capture of fluorinated gases  
 Modalité du projet: De recherche fondamentale  
 Type de participation: Coordinateur scientifique  
 Établissement où l'expérience a été réalisée: Alba Type d'établissement: Organisme public de synchrotron  
 Ville: Cerdanyola del Valles, Catalogne, Espagne  
 Chercheur/s responsable/s: Carolina Natalia Hermida Merino; Daniel Hermida Merino  
 Nombre de chercheurs participants: 2  
 Type de participation: Miembro de equipo  
 Nom du programme: Propuesta sincrotrón  
 Début-Fin: 28/11/2019 - 29/11/2019  
 Montant total: 33.000 €
  
9. Intitulé du projet: 2019023571 - in situ Structural investigation of the uptake and release of guest molecules during the fibrillization of a low molecular weight hydrogelator  
 Modalité du projet: De recherche fondamentale  
 Établissement où l'expérience a été réalisée: Alba Type d'établissement: Organisme public de synchrotron  
 Ville: Cerdanyola del Valles, Catalogne, Espagne  
 Chercheur/s responsable/s: Daniel Hermida Merino; Iván Bravo Pérez  
 Nombre de chercheurs participants: 2

Type de participation: Investigador principal  
Nom du programme: Propuesta sincrotrón  
Début-Fin: 20/11/2019 - 21/11/2019  
Montant total: 33.000 €

10. Intitulé du projet: Etude multi-échelles de polymères fonctionnels par mesures couplées in situ Modalité du projet:

Secteur du projet: Union européenne développement y compris translationnel  
Type de participation: Coordinateur scientifique  
Établissement où l'expérience a été réalisée: Université de Lorraine/DUBBLE  
Ville: Grenoble/Metz, France  
Chercheur/s responsable/s: Patrice Bourson; David Chapron; Daniel Hermida Merino  
Nombre de chercheurs participants: 3  
Nom du programme: Thèses  
Début-Fin: 01/11/2016 - 01/11/2019 Durée du projet: 3 ans  
Montant total: 135.000 € Montant du sous-projet: 45.000 €  
Pourcentage de subvention: 33%  
Engagement: Temps complet

11. Intitulé du projet: I-20190643 EC-In-situ time-resolved characterization of extensional flow induced crystallization

Modalité du projet: De recherche fondamentale  
Type de participation: Coordinateur scientifique  
Établissement où l'expérience a été réalisée Organisme public de PETRA III synchrotron  
Ville: Hamburg, Hamburg, Allemagne  
Chercheur/s responsable/s: Gerrit Peters; Jessica Pepe; Ruth Cardinaels; Daniel Hermida Merino  
Nombre de chercheurs participants: 4  
Début-Fin: 30/09/2019 - 04/10/2019  
Montant total: 49.500 €

12. Intitulé du projet: 2019023408 - In-situ time-resolved characterization of extensional flow induced crystallization

Modalité du projet: De recherche fondamentale  
Type de participation: Coordinateur scientifique  
Établissement où l'expérience a été réalisée: Alba Type d'établissement: Organisme public de synchrotron  
Ville: Cerdanyola del Valles, Catalogne, Espagne  
Chercheur/s responsable/s: Gerrit Peters; Daniel Hermida Merino; Ruth Cardinaels; Jessica Pepe Nombre de chercheurs participants: 4  
Type de participation: Miembro de equipo  
Nom du programme: Propuesta sincrotrón  
Début-Fin: 19/07/2019 - 21/07/2019  
Montant total: 49.500 €

13. Intitulé du projet: 2018093066 - Investigation of the nucleation and growth mechanism of gold nanoparticles by in situ UV-vis spectroscopy and SAXS

Modalité du projet: De recherche fondamentale  
Établissement où l'expérience a été réalisée: Alba Type d'établissement: Organisme public de synchrotron  
Ville: Cerdanyola del Valles, Catalogne, Espagne

Chercheur/s responsable/s: Daniel Hermida Merino; José Fernando Queiruga Rey  
Nombre de chercheurs participants: 2  
Type de participation: Investigador principal  
Nom du programme: Propuesta sincrotrón  
Début-Fin: 14/07/2019 - 16/07/2019  
Montant total: 49.500 €

14. Intitulé du projet: 2018093178 - Study of the nanostructure double network formation of a modified polypeptide derivatives  
Modalité du projet: De recherche fondamentale  
Établissement où l'expérience a été réalisée: Alba Type d'établissement: Organisme public de synchrotron  
Ville: Cerdanyola del Valles, Catalogne, Espagne  
Chercheur/s responsable/s: Daniel Hermida Merino  
Nombre de chercheurs participants: 1  
Type de participation: Investigador principal  
Nom du programme: Propuesta sincrotrón  
Début-Fin: 29/03/2019 - 31/03/2019  
Montant total: 49.500 €
15. Intitulé du projet: 26-02-873-The morphology of expandable thermoplastic polyurethane during high temperature treatments under supercritical CO<sub>2</sub>  
Modalité du projet: De recherche fondamentale  
Type de participation: Coordinateur scientifique  
Établissement où l'expérience a été réalisée: Type d'établissement: Organisme public de European Synchrotron Radiation Facility (ESRF)  
Ville: Grenoble, Rhône-Alpes, France  
Chercheur/s responsable/s: Steven Howdle; Kristien Van der flaas; Bart Goderis; Daniel Hermida Merino  
Nombre de chercheurs participants: 4  
Type de participation: Miembro de equipo  
Nom du programme: Propuesta sincrotrón  
Début-Fin: 26/11/2018 - 30/11/2018  
Montant total: 49.500 €
16. Intitulé du projet: SC-4908- In-Situ SAXS-WAXS Analyses of 'Microgel' Gel Structure in UV-cured Polyacrylate Systems  
Modalité du projet: De recherche fondamentale  
Type de participation: Coordinateur scientifique  
Établissement où l'expérience a été réalisée: European Synchrotron Radiation Facility (ESRF)  
Ville: Grenoble, Rhône-Alpes, France  
Chercheur/s responsable/s: Kay Saalwächter; Daniel Hermida Merino; Bing Wu  
Nombre de chercheurs participants: 3  
Type de participation: Miembro de equipo  
Nom du programme: Propuesta sincrotrón  
Début-Fin: 12/11/2018 - 16/11/2018  
Montant total: 49.500 €
17. Intitulé du projet: 2018022840 - Study of the structure of a microgel formation mechanism during the UV-curing of PEG-based polyacrylate  
Modalité du projet: De recherche fondamentale

Établissement où l'expérience a été réalisée: Alba Type d'établissement: Organisme public de synchrotron

Ville: Cerdanyola del Valles, Catalogne, Espagne

Chercheur/s responsable/s: Daniel Hermida Merino

Nombre de chercheurs participants: 1

Type de participation: Investigador principal

Nom du programme: Propuesta sincrotrón

Début-Fin: 11/10/2018 - 13/10/2018

Montant total: 49.500 €

18. Intitulé du projet: 26-02-900-Structural investigation of the double network formation of a modified polypeptide derivatives

Modalité du projet: De recherche fondamentale

Type de participation: Coordinateur scientifique

Établissement où l'expérience a été réalisée: European Synchrotron Radiation Facility (ESRF)

Ville: Grenoble, Rhône-Alpes, France

Chercheur/s responsable/s: Daniel Hermida Merino; Bing Wu

Nombre de chercheurs participants: 2

Type de participation: Investigador principal

Nom du programme: Propuesta sincrotrón

Début-Fin: 01/10/2018 - 02/10/2018

Montant total: 33.000 €

19. Intitulé du projet: 26-02-890-Shear enhanced relaxation in thermotropic polyesters:

Identifying the role of pressure, stress and shear rates on molecular orientation and relaxation

Modalité du projet: De recherche fondamentale

Type de participation: Coordinateur scientifique

Établissement où l'expérience a été réalisée: European Synchrotron Radiation Facility (ESRF)

Ville: Grenoble, Rhône-Alpes, France

Chercheur/s responsable/s: Carolus Wilsens; Daniel Hermida Merino; Sanjay Rastogi; Gerrit Peters

Nombre de chercheurs participants: 4

Type de participation: Miembro de equipo

Nom du programme: Propuesta sincrotrón

Début-Fin: 26/09/2018 - 01/10/2018

Montant total: 66.000 €

20. Intitulé du projet: MA-4398-In-situ SAXS-WAXS Analyses of 3D-Graphene-Nanocomposite

Supercapacitor in the charging-discharging cycle

Modalité du projet: De recherche fondamentale

Type de participation: Coordinateur scientifique

Établissement où l'expérience a été réalisée: European Synchrotron Radiation Facility (ESRF)

Ville: Grenoble, Rhône-Alpes, France

Chercheur/s responsable/s: Daniel Hermida Merino; Bing Wu

Nombre de chercheurs participants: 2

Type de participation: Investigador principal

Nom du programme: Propuesta sincrotrón

Début-Fin: 10/09/2018 - 14/09/2018

Montant total: 49.500 €

21. Intitulé du projet: 26-02-899-Investigation of the nanostructure development of a PEG-polyacrylate during UV curing  
 Modalité du projet: De recherche fondamentale  
 Type de participation: Coordinateur scientifique  
 Établissement où l'expérience a été réalisée: European Synchrotron Radiation Facility (ESRF)  
 Ville: Grenoble, Rhône-Alpes, France  
 Chercheur/s responsable/s: Daniel Hermida Merino; Bing Wu  
 Nombre de chercheurs participants: 2  
 Type de participation: Investigador principal  
 Nom du programme: Propuesta sincrotrón  
 Début-Fin: 03/09/2018 - 06/09/2018  
 Montant total: 49.500 €
22. Intitulé du projet: 26-01-1170-Investigation of the effect of gallium ion on the overall medical glass structures  
 Modalité du projet: De recherche fondamentale  
 Type de participation: Coordinateur scientifique  
 Établissement où l'expérience a été réalisée: European Synchrotron Radiation Facility (ESRF)  
 Ville: Grenoble, Rhône-Alpes, France  
 Chercheur/s responsable/s: Daniel Hermida Merino; Bing Wu  
 Nombre de chercheurs participants: 2  
 Type de participation: Investigador principal  
 Nom du programme: Propuesta sincrotrón  
 Début-Fin: 27/08/2018 - 31/08/2018  
 Montant total: 49.500 €
23. Intitulé du projet: LS-2882-X-ray fiber diffraction of microtubules: Analysis of the secondary structure dynamics of tubulin molecules within native microtubules  
 Modalité du projet: De recherche fondamentale  
 Type de participation: Coordinateur scientifique  
 Établissement où l'expérience a été réalisée: European Synchrotron Radiation Facility (ESRF)  
 Ville: Grenoble, Rhône-Alpes, France  
 Chercheur/s responsable/s: Juan Estevez Gallego; José Fernando Diaz Pereira; Daniel Hermida Merino; Shinji Kamimura  
 Nombre de chercheurs participants: 4  
 Type de participation: Miembro de equipo  
 Nom du programme: Propuesta sincrotrón  
 Début-Fin: 21/08/2018 - 23/08/2018  
 Montant total: 33.000 €
24. Intitulé du projet: Étude de la nucléation et de la croissance des nanoparticules assistée simultanément par des techniques de diffusion des rayons X à angle faible et moyen (SAXS/WAXS) et la spectroscopie d'absorption des rayons X (XAS) en combinaison avec la spectroscopie UV-Vis  
 Établissement où l'expérience a été réalisée: DUBBLE @ ESRF  
 Ville: Grenoble, France  
 Chercheur/s responsable/s: Jose Fernando Queiruga Rey; Daniel Hermida Merino  
 Nombre de chercheurs participants: 2  
 Organisme/s de financement: Fundação de Amparo à Pesquisa do Estado de São Paulo  
 Type d'organisme: Organisme public de recherche Paulo (FAPESP)

Ville: Sao Paulo, Brésil  
Début-Fin: 21/08/2017 - 20/08/2018  
Montant total: 30.000 €

25. Intitulé du projet: 26-02-874-Oxalamide based organic compounds in polymer melts: How are self-assembly, shear enhanced crystallization and viscosity suppression related?

Modalité du projet: De recherche fondamentale  
Type de participation: Coordinateur scientifique  
Établissement où l'expérience a été réalisée: European Synchrotron Radiation Facility (ESRF)  
Ville: Grenoble, Rhône-Alpes, France  
Chercheur/s responsable/s: Carolus Wilsens; Daniel Hermida Merino; Gerrit Peters; Sanjay Rastogi  
Nombre de chercheurs participants: 4  
Type de participation: Miembro de equipo  
Nom du programme: Propuesta sincrotrón  
Début-Fin: 18/07/2018 - 24/07/2018  
Montant total: 82.500 €

26. Intitulé du projet: 2017092500 - Crystallization investigation of PVDF/fluoroelastomer blends

Modalité du projet: De recherche fondamentale  
Établissement où l'expérience a été réalisée: Alba  
Type d'établissement: Organisme public de synchrotron  
Ville: Cerdanyola del Valles, Catalogne, Espagne  
Chercheur/s responsable/s: Daniel Hermida Merino  
Nombre de chercheurs participants: 1  
Type de participation: Investigador principal  
Nom du programme: Propuesta sincrotrón  
Début-Fin: 22/05/2018 - 24/05/2018  
Montant total: 49.500 €

27. Intitulé du projet: SC-4791- Structural development during hot stretching of disentangled UHMWPE as determined by simultaneous SAXS/WAXS: Origin of thermal conductivity

Modalité du projet: De recherche fondamentale  
Type de participation: Coordinateur scientifique  
Établissement où l'expérience a été réalisée:  
Type d'établissement: Organisme public de European Synchrotron Radiation Facility (ESRF)  
Ville: Grenoble, Rhône-Alpes, France  
Chercheur/s responsable/s: Daniel Hermida Merino; Sara Ronca; Stavros Drakopoulos; Ignacio Martin Fabiani  
Nombre de chercheurs participants: 4  
Type de participation: Miembro de equipo  
Nom du programme: Propuesta sincrotrón  
Début-Fin: 05/03/2018 - 09/03/2018  
Montant total: 49.500 €

28. Intitulé du projet: 26-01-1159-study of in situ thermal activated nucleation and growth process of CsHSO<sub>4</sub> nanoparticles by simultaneous XAFS/ SAXS measurements

Modalité du projet: De recherche fondamentale  
Type de participation: Coordinateur scientifique  
Établissement où l'expérience a été réalisée: European Synchrotron Radiation Facility (ESRF)  
Ville: Grenoble, Rhône-Alpes, France

Chercheur/s responsable/s: Daniel Hermida Merino; José Fernando Queiruga Rey  
Nombre de chercheurs participants: 2  
Type de participation: Investigador principal  
Nom du programme: Propuesta sincrotrón  
Début-Fin: 02/03/2018 - 05/03/2018  
Montant total: 49.500 €

29. Intitulé du projet: 26-02-843-Morphological aspects of making the world's strongest fiber  
Modalité du projet: De recherche fondamentale  
Type de participation: Coordinateur scientifique  
Établissement où l'expérience a été réalisée: European Synchrotron Radiation Facility (ESRF)  
Ville: Grenoble, Rhône-Alpes, France  
Chercheur/s responsable/s: Dario Cavallo; Luigi Balzano; Daniel Hermida Merino  
Nombre de chercheurs participants: 3  
Type de participation: Coordinateur  
Nom du programme: Propuesta sincrotrón  
Début-Fin: 02/03/2018 - 05/03/2018  
Montant total: 49.500 €
30. Intitulé du projet: 26-02-856-Renwable thermotropic polyesters: optimizing molecular orientation for enhanced nucleating efficiency and reinforcement in polyester blends  
Modalité du projet: De recherche fondamentale  
Type de participation: Coordinateur scientifique  
Établissement où l'expérience a été réalisée: European Synchrotron Radiation Facility (ESRF)  
Ville: Grenoble, Rhône-Alpes, France  
Chercheur/s responsable/s: Enrico Troisi; Carolus Wilsens; Sanjay Rastogi; Daniel Hermida Merino; Gerrit Peters  
Nombre de chercheurs participants: 5  
Type de participation: Miembro de equipo  
Nom du programme: Propuesta sincrotrón  
Début-Fin: 03/02/2018 - 06/02/2018  
Montant total: 49.500 €
31. Intitulé du projet: LS-2732-X-ray fiber diffraction of microtubule: Structural dynamics of native microtubules with anti-cancer tubulin-binding compounds  
Modalité du projet: De recherche fondamentale  
Type de participation: Coordinateur scientifique  
Établissement où l'expérience a été réalisée: European Synchrotron Radiation Facility (ESRF)  
Ville: Grenoble, Rhône-Alpes, France  
Chercheur/s responsable/s: Shinji Kamimura; José Fernando Diaz Pereira; Daniel Hermida Merino  
Nombre de chercheurs participants: 3  
Type de participation: Miembro de equipo  
Nom du programme: Propuesta sincrotrón  
Début-Fin: 06/10/2017 - 10/10/2017  
Montant total: 66.000 €
32. Intitulé du projet: 26-02-853-Crystallization investigation of PVDF/fluoroelastomer blends  
Modalité du projet: De recherche fondamentale  
Type de participation: Coordinateur scientifique  
Établissement où l'expérience a été réalisée: European Synchrotron Radiation Facility (ESRF)

Ville: Grenoble, Rhône-Alpes, France  
Chercheur/s responsable/s: Daniel Hermida Merino; Sarah Saidi  
Nombre de chercheurs participants: 2  
Type de participation: Investigador principal  
Nom du programme: Propuesta sincrotrón  
Début-Fin: 25/09/2017 - 29/09/2017  
Montant total: 49.500 €

33. Intitulé du projet: 26-02-855-Structure development during blending of polyamides and cellulose nano fibers in the superheated water  
Modalité du projet: De recherche fondamentale  
Type de participation: Coordinateur scientifique  
Établissement où l'expérience a été réalisée: European Synchrotron Radiation Facility (ESRF)  
Ville: Grenoble, Rhône-Alpes, France  
Chercheur/s responsable/s: Daniel Hermida Merino; Carolus Wilsens; Ele De boer; Jules Harings; Sanjay Rastogi  
Nombre de chercheurs participants: 5  
Type de participation: Miembro de equipo  
Nom du programme: Propuesta sincrotrón  
Début-Fin: 22/09/2017 - 25/09/2017 Montant total: 49.500 €
34. Intitulé du projet: 26-02-842-Evolution of water density as function pore size in hydrophobic confinement: reverse phase silica materials  
Modalité du projet: De recherche fondamentale  
Type de participation: Coordinateur scientifique  
Établissement où l'expérience a été réalisée: European Synchrotron Radiation Facility (ESRF)  
Ville: Grenoble, Rhône-Alpes, France  
Chercheur/s responsable/s: Eric Breynaert; Johan Martens; Maarten Houllberghs; Daniel Hermida Merino  
Nombre de chercheurs participants: 4  
Type de participation: Coordinateur  
Nom du programme: Propuesta sincrotrón  
Début-Fin: 18/09/2017 - 22/09/2017  
Montant total: 49.500 €
35. Intitulé du projet: 26-02-841-Structure and Kinetics of nanocrystal-based Supercrystals  
Modalité du projet: De recherche fondamentale  
Type de participation: Coordinateur scientifique  
Établissement où l'expérience a été réalisée: European Synchrotron Radiation Facility (ESRF)  
Ville: Grenoble, Rhône-Alpes, France  
Chercheur/s responsable/s: Emanuele Marino; Daniel Hermida Merino; Gerard Wegdam; Thomas Kodger; Peter Schall  
Nombre de chercheurs participants: 5  
Type de participation: Miembro de equipo  
Nom du programme: Propuesta sincrotrón  
Début-Fin: 15/09/2017 - 18/09/2017  
Montant total: 49.500 €
36. Intitulé du projet: 26-02-825-Nucleation and Growth Phenomena of Oriented HKUST-1 Thin Films  
Modalité du projet: De recherche fondamentale  
Type de participation: Coordinateur scientifique

Établissement où l'expérience a été réalisée: European Synchrotron Radiation Facility (ESRF)  
Ville: Grenoble, Rhône-Alpes, France  
Chercheur/s responsable/s: Mrinal Bera; Daniel Hermida Merino; Matthias Filez; Bert Weckhuysen; Florian Meirer  
Nombre de chercheurs participants: 5  
Type de participation: Miembro de equipo  
Nom du programme: Propuesta sincrotrón  
Début-Fin: 17/07/2017 - 25/07/2017  
Montant total: 82.500 €

37. Intitulé du projet: SC-4521-Fine crystalline structure of fullerene nanowires prepared by Laser Induced Periodic Surface Structures (LIPSS) as revealed by GIWAXS  
Modalité du projet: De recherche fondamentale  
Type de participation: Coordinateur scientifique  
Établissement où l'expérience a été réalisée: European Synchrotron Radiation Facility (ESRF) Type d'établissement: Organisme public de  
Ville: Grenoble, Rhône-Alpes, France  
Chercheur/s responsable/s: Edgar Gutierrez Fernandez; Daniel Hermida Merino; Alvaro Rodriguez; Tiberio Ezquerro; Aurora Nogales; Mari Cruz Garcia Gutierrez; Esther Rebollar  
Nombre de chercheurs participants: 7  
Type de participation: Coordinateur  
Nom du programme: Propuesta sincrotrón  
Début-Fin: 03/07/2017 - 07/07/2017  
Montant total: 49.500 €
38. Intitulé du projet: 2017032183 - Crystallization behaviour of novel PLA derivatives for drug release applications  
Modalité du projet: De recherche fondamentale  
Établissement où l'expérience a été réalisée: Alba Type d'établissement: Organisme public de synchrotron  
Ville: Cerdanyola del Valles, Catalogne, Espagne  
Chercheur/s responsable/s: Daniel Hermida Merino; Iván Bravo Pérez; Carlos Alonso Moreno  
Nombre de chercheurs participants: 3  
Type de participation: Investigador principal  
Nom du programme: Propuesta sincrotrón  
Début-Fin: 04/07/2017 - 06/07/2017  
Montant total: 49.500 €
39. Intitulé du projet: SC-4515-In-situ nanostructuring of P(VDF-TrFE) during melt crystallization  
Modalité du projet: De recherche fondamentale  
Type de participation: Coordinateur scientifique  
Établissement où l'expérience a été réalisée: European Synchrotron Radiation Facility (ESRF)  
Ville: Grenoble, Rhône-Alpes, France  
Chercheur/s responsable/s: Patrice Bourson; Marie Veitmann; Daniel Hermida Merino  
Nombre de chercheurs participants: 3  
Type de participation: Miembro de equipo  
Nom du programme: Propuesta sincrotrón  
Début-Fin: 09/05/2017 - 12/05/2017  
Montant total: 49.500 €

40. Intitulé du projet: 2016091938 - Investigation by SAXS of the uptake of drug/dye by a self-assembled low molecular weight Hydrogelator by pH change  
 Modalité du projet: De recherche fondamentale  
 Établissement où l'expérience a été réalisée: Alba  
 Type d'établissement: Organisme public de synchrotron  
 Ville: Cerdanyola del Valles, Catalogne, Espagne  
 Nombre de chercheurs participants: 1  
 Type de participation: Investigador principal  
 Nom du programme: Propuesta sincrotrón  
 Début-Fin: 23/03/2017 - 25/03/2017  
 Montant total: 49.500 €
41. Intitulé du projet: SC-4419-SAXS/WAXS study of the pH-dependent mechanism of formation of twisted ribbons using bioderived sophorolipid bolaform glycolipids agents  
 Modalité du projet: De recherche fondamentale  
 Type de participation: Coordinateur scientifique  
 Établissement où l'expérience a été réalisée: European Synchrotron Radiation Facility (ESRF)  
 Ville: Grenoble, Rhône-Alpes, France  
 Chercheur/s responsable/s: Niki Baccile; Daniel Hermida Merino  
 Nombre de chercheurs participants: 2  
 Type de participation: Miembro de equipo  
 Nom du programme: Propuesta sincrotrón  
 Début-Fin: 30/01/2017 - 03/02/2017  
 Montant total: 49.500 €
42. Intitulé du projet: 26-02-814-In situ investigation by microbeam SAXS-WAXS of self-assembled low molecular weight micro-organogelators by pH turning in a microfluidic device  
 Modalité du projet: De recherche fondamentale  
 Type de participation: Coordinateur scientifique  
 Établissement où l'expérience a été réalisée:  
 Type d'établissement: Organisme public de European Synchrotron Radiation Facility (ESRF)  
 Ville: Grenoble, Rhône-Alpes, France  
 Chercheur/s responsable/s: Daniel Hermida Merino; Giuseppe Portale  
 Nombre de chercheurs participants: 2  
 Type de participation: Investigador principal  
 Nom du programme: Propuesta sincrotrón  
 Début-Fin: 23/01/2017 - 27/01/2017  
 Montant total: 49.500 €
43. Intitulé du projet: 26-01-1097-In situ investigation of structure development by simultaneous of novel nanostructured silver-block copolymer composites by combined SAXS-XAS  
 Modalité du projet: De recherche fondamentale  
 Type de participation: Coordinateur scientifique  
 Établissement où l'expérience a été réalisée:  
 Type d'établissement: Organisme public de European Synchrotron Radiation Facility (ESRF)  
 Ville: Grenoble, Rhône-Alpes, France  
 Chercheur/s responsable/s: Daniel Hermida Merino; Wim Bras; Mohammad Alauhdin; Steve Howdle  
 Nombre de chercheurs participants: 4  
 Type de participation: Investigador principal

Nom du programme: Propuesta sincrotrón  
Début-Fin: 23/11/2016 - 27/11/2016  
Montant total: 66.000 €

44. Intitulé du projet: 26-02-800-Enhancing the nucleation efficiency of biopolymers with oxalamide-based nucleating agents  
Modalité du projet: De recherche fondamentale  
Type de participation: Coordinateur scientifique  
Établissement où l'expérience a été réalisée: European Synchrotron Radiation Facility (ESRF)  
Ville: Grenoble, Rhône-Alpes, France  
Chercheur/s responsable/s: Daniel Hermida Merino; Carolus Wilsens; Jules Harings; Dietmar Auhl  
Nombre de chercheurs participants: 4  
Type de participation: Miembro de equipo  
Nom du programme: Propuesta sincrotrón  
Début-Fin: 17/11/2016 - 21/11/2016  
Montant total: 66.000 €
45. Intitulé du projet: 26-01-1079-The role of silver during the synthesis of gold nanorods studied by simultaneous SAXS-EXAF agents  
Modalité du projet: De recherche fondamentale  
Type de participation: Coordinateur scientifique  
Établissement où l'expérience a été réalisée: European Synchrotron Radiation Facility (ESRF)  
Ville: Grenoble, Rhône-Alpes, France  
Chercheur/s responsable/s: Marek Grzelczak; Alessandro Longo; Luis Liz Marzan; Daniel Hermida Merino  
Nombre de chercheurs participants: 4  
Type de participation: Coordinateur  
Nom du programme: Propuesta sincrotrón  
Début-Fin: 08/07/2016 - 11/07/2016  
Montant total: 49.500 €
46. Intitulé du projet: 26-02-781-SAXS analysis of polymerization-induced self-assembly in supercritical-CO<sub>2</sub>  
Modalité du projet: De recherche fondamentale  
Type de participation: Coordinateur scientifique  
Établissement où l'expérience a été réalisée:  
Type d'établissement: Organisme public de European Synchrotron Radiation Facility (ESRF)  
Ville: Grenoble, Rhône-Alpes, France  
Chercheur/s responsable/s: Daniel Hermida Merino; Antoine Debuigne  
Nombre de chercheurs participants: 4  
Type de participation: Investigador principal  
Nom du programme: Propuesta sincrotrón  
Début-Fin: 12/04/2016 - 15/04/2016  
Montant total: 49.500 €
47. Intitulé du projet: 26-02-793-In-situ SAXS-WAXS investigation of the internal structure development of block copolymers in sc-CO<sub>2</sub>  
Modalité du projet: De recherche fondamentale  
Type de participation: Coordinateur scientifique  
Établissement où l'expérience a été réalisée:  
Type d'établissement: Organisme public de European Synchrotron Radiation Facility (ESRF)  
Ville: Grenoble, Rhône-Alpes, France  
Chercheur/s responsable/s: Daniel Hermida Merino; Giuseppe Portale; Mohammad Alauhdin;

Steve Howdle  
Nombre de chercheurs participants: 4  
Type de participation: Investigador principal  
Nom du programme: Propuesta sincrotrón  
Début-Fin: 08/04/2016 - 12/04/2016  
Montant total: 49.500 €

48. Intitulé du projet: 26-02-736-Microwave annealing of block copolymer samples in grazing incidence geometry

Modalité du projet: De recherche fondamentale  
Type de participation: Coordinateur scientifique  
Établissement où l'expérience a été réalisée:  
Type d'établissement: Organisme public de European Synchrotron Radiation Facility (ESRF)  
Ville: Grenoble, Rhône-Alpes, France  
Chercheur/s responsable/s: Giuseppe Portale; Paul Topham; Wim Bras; Derek Irvine; Daniel Hermida Merino  
Nombre de chercheurs participants: 5  
Type de participation: Miembro de equipo  
Nom du programme: Propuesta sincrotrón  
Début-Fin: 26/02/2016 - 29/02/2016  
Montant total: 49.500 €

49. Intitulé du projet: SC-4212-Micellization and Phase Change Dynamics of a Model Block Copolymer using Time Resolved X-ray Scattering

Modalité du projet: De recherche fondamentale  
Type de participation: Coordinateur scientifique  
Établissement où l'expérience a été réalisée:  
Type d'établissement: Organisme public de European Synchrotron Radiation Facility (ESRF)  
Ville: Grenoble, Rhône-Alpes, France  
Chercheur/s responsable/s: Gemma Newby; Daniel Hermida Merino  
Nombre de chercheurs participants: 2  
Type de participation: Miembro de equipo  
Nom du programme: Propuesta sincrotrón  
Début-Fin: 11/02/2016 - 16/02/2016  
Montant total: 82.500 €

50. Intitulé du projet: MA-2600-The influence of graphene oxide in blending of low and ultra-high molar mass polymers and its implications on orientation and crystallization during flow

Modalité du projet: De recherche fondamentale  
Type de participation: Coordinateur scientifique  
Établissement où l'expérience a été réalisée:  
Type d'établissement: Organisme public de European Synchrotron Radiation Facility (ESRF)  
Ville: Grenoble, Rhône-Alpes, France  
Chercheur/s responsable/s: Enrico Troisi; Gerrit Peters; Sanjay Rastogi; Ele de Boer; Daniel Hermida Merino; Efren Andablo Reyes  
Nombre de chercheurs participants: 6  
Type de participation: Miembro de equipo  
Nom du programme: Propuesta sincrotrón  
Début-Fin: 22/07/2015 - 27/07/2015  
Montant total: 77.000 €

51. Intitulé du projet: SC-3978-In-situ investigation of structure development by simultaneous SAXS-WAXS of novel nanostructured silver-block copolymer composites  
 Modalité du projet: De recherche fondamentale  
 Type de participation: Coordinateur scientifique  
 Établissement où l'expérience a été réalisée: European Synchrotron Radiation Facility (ESRF)  
 Ville: Grenoble, Rhône-Alpes, France  
 Chercheur/s responsable/s: Steven Howdle; Daniel Hermida Merino  
 Nombre de chercheurs participants: 2  
 Type de participation: Miembro de equipo  
 Nom du programme: Propuesta sincrotrón  
 Début-Fin: 10/07/2015 - 13/07/2015  
 Montant total: 49.500 €
52. Intitulé du projet: 26-02-769-Effect of hydration properties of platinum complex anions on cluster growth dynamics and their distribution for the control of electrodeposition within nanoporous electrodes  
 Modalité du projet: De recherche fondamentale  
 Type de participation: Coordinateur scientifique  
 Établissement où l'expérience a été réalisée:  
 Type d'établissement: Organisme public de European Synchrotron Radiation Facility (ESRF)  
 Ville: Grenoble, Rhône-Alpes, France  
 Chercheur/s responsable/s: Alessandro Longo; Daniel Hermida Merino  
 Nombre de chercheurs participants: 2  
 Type de participation: Investigador principal  
 Nom du programme: Propuesta sincrotrón  
 Début-Fin: 27/10/2015 - 30/05/2015  
 Montant total: 49.500 €
53. Intitulé du projet: 26-02-722-In situ study of a gelation mechanism by simultaneous Rheo-SAXS of a low molecular weight hydrogelator  
 Modalité du projet: De recherche fondamentale  
 Type de participation: Coordinateur scientifique  
 Établissement où l'expérience a été réalisée: European Synchrotron Radiation Facility (ESRF)  
 Ville: Grenoble, Rhône-Alpes, France  
 Chercheur/s responsable/s: Giuseppe Portale; Daniel Hermida Merino  
 Nombre de chercheurs participants: 2  
 Type de participation: Investigador principal  
 Nom du programme: Propuesta sincrotrón  
 Début-Fin: 30/01/2015 - 02/02/2015  
 Montant total: 49.500 €
54. Intitulé du projet: SC-3751-Structure Development during Polymerization in Bio-based Liquid Crystalline Polymers; SAXS study continuation (part 2)  
 Modalité du projet: De recherche fondamentale  
 Type de participation: Coordinateur scientifique  
 Établissement où l'expérience a été réalisée:  
 Type d'établissement: Organisme public de European Synchrotron Radiation Facility (ESRF)  
 Ville: Grenoble, Rhône-Alpes, France  
 Chercheur/s responsable/s: Sanjay Rastogi; Carolus Wilsens; Bart Noordover; Daniel Hermida Merino  
 Nombre de chercheurs participants: 4

Type de participation: Miembro de equipo  
Nom du programme: Propuesta sincrotrón  
Début-Fin: 02/09/2013 - 06/09/2013  
Montant total: 49.500 €

55. Intitulé du projet: 26-02-650-Gelation investigation of a supramolecular hydrogel by in situ rheo SAXS-WAXS studies  
Modalité du projet: De recherche fondamentale  
Type de participation: Coordinateur scientifique  
Établissement où l'expérience a été réalisée:  
Type d'établissement: Organisme public de European Synchrotron Radiation Facility (ESRF)  
Ville: Grenoble, Rhône-Alpes, France  
Chercheur/s responsable/s: Francisco Rodriguez Llansola; Giuseppe Portale; Daniel Hermida Merino  
Nombre de chercheurs participants: 3  
Type de participation: Investigador principal  
Nom du programme: Propuesta sincrotrón  
Début-Fin: 15/07/2013 - 19/07/2013  
Montant total: 49.500 €
56. Intitulé du projet: 26-02-648-Controlling the lamellar orientation in confined semi-crystalline polymers  
Modalité du projet: De recherche fondamentale  
Type de participation: Coordinateur scientifique  
Établissement où l'expérience a été réalisée:  
Type d'établissement: Organisme public de European Synchrotron Radiation Facility (ESRF)  
Ville: Grenoble, Rhône-Alpes, France  
Chercheur/s responsable/s: Altug Altay; Giuseppe Portale; Johannes Goossens; Daniel Hermida Merino  
Nombre de chercheurs participants: 4  
Type de participation: Miembro de equipo  
Nom du programme: Propuesta sincrotrón  
Début-Fin: 13/05/2013 - 17/05/2013  
Montant total: 49.500 €
57. Intitulé du projet: 26-02-623-Temperature- vs. strain-induced crystallization in poly(lactic acid) (PLA)  
Modalité du projet: De recherche fondamentale  
Type de participation: Coordinateur scientifique  
Établissement où l'expérience a été réalisée:  
Type d'établissement: Organisme public de European Synchrotron Radiation Facility (ESRF)  
Ville: Grenoble, Rhône-Alpes, France  
Chercheur/s responsable/s: Johannes Goossens; Denka Hristova-bogaerds; Daniel Hermida Merino  
Nombre de chercheurs participants: 3  
Type de participation: Miembro de equipo  
Nom du programme: Propuesta sincrotrón  
Début-Fin: 25/02/2013 - 01/03/2013  
Montant total: 49.500 €
58. Intitulé du projet: 26-02-625-The influence of nanofillers on the maximum drawability of isotactic poly(propylene)  
Modalité du projet: De recherche fondamentale

Type de participation: Coordinateur scientifique  
Établissement où l'expérience a été réalisée:  
Type d'établissement: Organisme public de European Synchrotron Radiation Facility (ESRF)  
Ville: Grenoble, Rhône-Alpes, France

59. Chercheur/s responsable/s: Ton Peijs; Johannes Goossens; Daniel Hermida Merino; Benny Lijsterburg  
Nombre de chercheurs participants: 4  
Type de participation: Miembro de equipo  
Nom du programme: Propuesta sincrotrón  
Début-Fin: 22/02/2013 - 25/02/2013  
Montant total: 49.500 €
60. Intitulé du projet: 26-02-631-Photo-switchable dynamic surface topologies in chiral nematic media  
Modalité du projet: De recherche fondamentale  
Type de participation: Coordinateur scientifique  
Établissement où l'expérience a été réalisée:  
Type d'établissement: Organisme public de European Synchrotron Radiation Facility (ESRF)  
Ville: Grenoble, Rhône-Alpes, France  
Chercheur/s responsable/s: Giuseppe Portale; Dirk Broer; Daniel Hermida Merino  
Nombre de chercheurs participants: 3  
Type de participation: Miembro de equipo  
Nom du programme: Propuesta sincrotrón  
Début-Fin: 18/02/2013 - 22/02/2013  
Montant total: 49.500 €
61. Intitulé du projet: 26-02-632-CaCO<sub>3</sub> Precipitation in Bicontinuous Polymer Capsules: An Organic-Inorganic Hybrid System  
Modalité du projet: De recherche fondamentale  
Type de participation: Coordinateur scientifique  
Établissement où l'expérience a été réalisée:  
Type d'établissement: Organisme public de European Synchrotron Radiation Facility (ESRF)  
Ville: Grenoble, Rhône-Alpes, France  
Chercheur/s responsable/s: Beulah Mckenzie; Nico Sommerdijk; Fiona Meldrum Llansola; Daniel Hermida Merino  
Nombre de chercheurs participants: 4  
Type de participation: Miembro de equipo  
Nom du programme: Propuesta sincrotrón  
Début-Fin: 03/12/2012 - 07/12/2012  
Montant total: 49.500 €
62. Intitulé du projet: 26-02-629-Study of the dynamic morphology of an in-situ RAFT polymerization in supercritical CO<sub>2</sub> of novel block copolymers  
Modalité du projet: De recherche fondamentale  
Type de participation: Coordinateur scientifique  
Établissement où l'expérience a été réalisée: European Synchrotron Radiation Facility (ESRF)  
Ville: Grenoble, Rhône-Alpes, France  
Chercheur/s responsable/s: Steven Howdle; James Jennings; Wim Bras; Daniel Hermida Merino  
Nombre de chercheurs participants: 4  
Type de participation: Investigador principal

Nom du programme: Propuesta sincrotrón  
Début-Fin: 12/11/2012 - 16/11/2012  
Montant total: 49.500 €

63. Intitulé du projet: 26-02-630-Investigations of the mechanism of self-assembly of a pH-sensitive low molecular weight hydrogelator  
Modalité du projet: De recherche fondamentale  
Type de participation: Coordinateur scientifique  
Type d'établissement: Organisme public de European Synchrotron Radiation Facility (ESRF)  
Ville: Grenoble, Rhône-Alpes, France  
Chercheur/s responsable/s: Francisco Rodriguez Llansola; Giuseppe Portale; Daniel Hermida Merino  
Nombre de chercheurs participants: 3  
Type de participation: Investigador principal  
Nom du programme: Propuesta sincrotrón  
Début-Fin: 09/10/2012 - 12/10/2012  
Montant total: 49.500 €
64. Intitulé du projet: 26-02-619-Structure Development during Polymerization in Bio-based Liquid Crystalline Polymers  
Modalité du projet: De recherche fondamentale  
Type de participation: Coordinateur scientifique  
Établissement où l'expérience a été réalisée:  
Type d'établissement: Organisme public de European Synchrotron Radiation Facility (ESRF)  
Ville: Grenoble, Rhône-Alpes, France  
Chercheur/s responsable/s: Sanjay Rastogi; Carolus Wilsens; Bart Noordover; Daniel Hermida Merino  
Nombre de chercheurs participants: 4  
Type de participation: Miembro de equipo  
Nom du programme: Propuesta sincrotrón  
Début-Fin: 28/09/2012 - 30/09/2012  
Montant total: 33.000 €
65. Intitulé du projet: 26-02-616-Solid-state modification as a tool to control the chemical microstructure and the morphology of novel bio-based copolyesters  
Modalité du projet: De recherche fondamentale  
Type de participation: Coordinateur scientifique  
Type d'établissement: Organisme public de European Synchrotron Radiation Facility (ESRF)  
Ville: Grenoble, Rhône-Alpes, France  
Chercheur/s responsable/s: Johannes Goossens; Bart Noordover; Daniel Hermida Merino  
Nombre de chercheurs participants: 3  
Type de participation: Miembro de equipo  
Nom du programme: Propuesta sincrotrón  
Début-Fin: 10/09/2012 - 14/09/2012  
Montant total: 49.500 €
66. Intitulé du projet: 26-02-596-A Time-Resolved SAXS/WAXS Study on Self-Healing Polymers: Correlation Between Structure and Mechanical Properties  
Modalité du projet: De recherche fondamentale  
Type de participation: Coordinateur scientifique  
Type d'établissement: Organisme public de European Synchrotron Radiation Facility (ESRF)

Ville: Grenoble, Rhône-Alpes, France  
Chercheur/s responsable/s: Giuseppe Portale; Wayne Hayes; Ian Hamley; Daniel Hermida Merino  
Nombre de chercheurs participants: 4  
Type de participation: Investigador principal  
Nom du programme: Propuesta sincrotrón  
Début-Fin: 15/06/2012 - 18/06/2012  
Montant total: 49.500 €

67. Intitulé du projet: 26-02-586-Calcium Carbonate Precipitation in a Collagen Framework  
Modalité du projet: De recherche fondamentale  
Type de participation: Coordinateur scientifique  
Type d'établissement: Organisme public de European Synchrotron Radiation Facility (ESRF)  
Ville: Grenoble, Rhône-Alpes, France  
Chercheur/s responsable/s: Nico Sommerdijk; Fiona Meldrum Llansola; Daniel Hermida Merino  
Nombre de chercheurs participants: 3  
Type de participation: Miembro de equipo  
Nom du programme: Propuesta sincrotrón  
Début-Fin: 21/11/2011 - 25/11/2011  
Montant total: 49.500 €
68. Intitulé du projet: 26-02-568-Drawing behaviour of polyamide(4,10) films  
Modalité du projet: De recherche fondamentale  
Type de participation: Coordinateur scientifique  
Type d'établissement: Organisme public de European Synchrotron Radiation Facility (ESRF)  
Ville: Grenoble, Rhône-Alpes, France  
Chercheur/s responsable/s: Daniel Hermida Merino; Giuseppe Portale; Johannes Goossens; Sainath Vaidya  
Nombre de chercheurs participants: 4  
Type de participation: Miembro de equipo  
Nom du programme: Propuesta sincrotrón  
Début-Fin: 01/07/2011 - 04/07/2011  
Montant total: 49.500 €
69. Intitulé du projet: 26-02-571-Study of the effect of diisocyanate structure, linker and end-group on the morphology of the hard segments  
Modalité du projet: De recherche fondamentale  
Type de participation: Coordinateur scientifique  
Type d'établissement: Organisme public de European Synchrotron Radiation Facility (ESRF)  
Ville: Grenoble, Rhône-Alpes, France  
Chercheur/s responsable/s: Wim Bras; Daniel Hermida Merino  
Nombre de chercheurs participants: 2  
Type de participation: Investigador principal  
Nom du programme: Propuesta sincrotrón  
Début-Fin: 28/04/2011 - 01/05/2011  
Montant total: 49.500 €
70. Intitulé du projet: SC-2736-A SAXS/WAXS/DSC Study of Novel Hydrogen-Bonded Supramolecular Polymer Structures  
Modalité du projet: De recherche fondamentale

Type de participation: Chercheur  
Type d'établissement: Organisme public de European Synchrotron Radiation Facility (ESRF)  
Ville: Grenoble, Rhône-Alpes, France  
Chercheur/s responsable/s: Iam Hamley; Wayne Hayes; Daniel Hermida Merino  
Nombre de chercheurs participants: 3  
Type de participation: Miembro de equipo  
Nom du programme: Propuesta sincrotrón  
Début-Fin: 24/04/2009 - 27/04/2009  
Montant total: 49.500 €

71. Intitulé du projet: LS-2805-X-ray fibre diffraction of microtubule: Analysis of structural dynamics of native microtubules on a second time scale  
Modalité du projet: De recherche fondamentale  
Type de participation: Coordinateur scientifique  
Établissement où l'expérience a été réalisée: European Synchrotron Radiation Facility (ESRF)  
Ville: Grenoble, Rhône-Alpes, France  
Chercheur/s responsable/s: Shinji Kamimura; José Fernando Diaz Pereira; Daniel Hermida Merino  
Nombre de chercheurs participants: 3  
Type de participation: Miembro de equipo  
Nom du programme: Propuesta sincrotrón  
Date de début: 27/03/2018  
Montant total: 66.000 €

72. Intitulé du projet: 26-02-852-Structural dynamics of tubulin dimers based on wide-angle X-ray fiber diffraction analysis of aligned native microtubules  
Modalité du projet: De recherche fondamentale  
Type de participation: Coordinateur scientifique  
Établissement où l'expérience a été réalisée: European Synchrotron Radiation Facility (ESRF)  
Ville: Grenoble, Rhône-Alpes, France  
Chercheur/s responsable/s: Daniel Hermida Merino; Shinji Kamimura  
Nombre de chercheurs participants: 2  
Type de participation: Investigador principal  
Nom du programme: Propuesta sincrotrón  
Montant total: 49.500 €

### **Participation à des contrats, conventions ou projets de R&D&I ne résultant pas de procédures concurrentielles, avec des entreprises (ou dans le cadre d'entreprises) et/ou des administrations**

Intitulé du projet: Formulator/R&D Chemist-Scientist Henkel UK. Slough. Berkshire, UK  
Type de participation: Chercheur  
Nombre de chercheurs: 2  
Date de début: 01/09/2009  
Durée du projet: 6 mois  
Montant total: 6.000 €

## Publications, documents scientifiques et techniques ou technologiques ou autre publication

- 1 Ghazi Ben Messaoud; Patrick Le Griel; Daniel Hermida-Merino; Niki Baccile. Effects of pH, temperature and shear on the structure--property relationship of lamellar hydrogels from microbial glucolipids probed by in situ rheo-SAXS. *Soft Matter*. 16 - 10, pp. 2540 - 2551. Royal Society of Chemistry, 2020.  
Type de production: Article Scientifique Type de support: Revue
- 2 Marie Gestranius; Issei Otsuka; Sami Halila; Daniel Hermida-Merino; Eduardo Solano; Redouane Borsali; Tekla Tammelin. High-Resolution Patterned Biobased Thin Films via Self-Assembled Carbohydrate Block Copolymers and Nanocellulose. *Advanced Materials Interfaces*. 7 - 7, pp. 1901737 - 1901737. 2020.  
Type de production: Article Scientifique Type de support: Revue
- 3 Eduardo Solano; Jolien Dendooven; Ji-Yu Feng; Philipp Bruner; Matthias M Minjauw; Ranjith K Ramachandran; Michiel Van Daele; Kevin Van de Kerckhove; Thomas Dobbelaere; Alessandro Coati; others. In situ study of the thermal stability of supported Pt nanoparticles and their stabilization via atomic layer deposition overcoating. *Nanoscale*. 12 - 21, pp. 11684 - 11693. Royal Society of Chemistry, 2020.  
Type de production: Article Scientifique Type de support: Revue
- 4 Jingjin Dong; Shuyan Shao; Simon Kahmann; Alexander J Rommens; Daniel Hermida-Merino; Gert H ten Brink; Maria A Loi; Giuseppe Portale. Mechanism of Crystal Formation in Ruddlesden--Popper Sn-Based Perovskites. *Advanced Functional Materials*. pp. 2001294 - 2001294. 2020.  
Type de production: Article Scientifique Type de support: Revue
- 5 Karin A Jansen; Artem Zhmurov; Bart E Vos; Giuseppe Portale; D Hermida Merino; Rustem I Litvinov; Valerie Tutwiler; Nicholas A Kurniawan; Wim Bras; John W Weisel; others. Molecular packing structure of fibrin fibers resolved by X-ray scattering and molecular modeling. *bioRxiv*. Cold Spring Harbor Laboratory, 2020.  
Type de production: Article Scientifique Type de support: Revue
- 6 Ghazi Ben Messaoud; Patrick Le Griel; Sylvain Prevost; Daniel Hermida-Merino; Wim Soetaert; Sophie LKW Roelants; Christian V Stevens; Niki Baccile. Single-molecule lamellar hydrogels from bolaform microbial glucolipids. *Soft Matter*. 16 - 10, pp. 2528 - 2539. Royal Society of Chemistry, 2020.  
Type de production: Article Scientifique Type de support: Revue
- 7 Pedro J Pacheco-Liñán; Cristina Martín; Carlos Alonso-Moreno; Alberto Juan; Daniel Hermida-Merino; Andrés Garzón-Ruiz; José Albaladejo; Mark Van der Auweraer; Boiko Cohen; Iván Bravo. The role of water and influence of hydrogen bonding on the self-assembly aggregation induced emission of an anthracene-guanidine-derivative. *Chemical Communications*. 56 - 29, pp. 4102 - 4105. Royal Society of Chemistry, 2020.  
Type de production: Article Scientifique Type de support: Revue
- 8 Cuili Xiang; Yin Liu; Ying Yin; Pengru Huang; Yongjin Zou; Marcus Fehse; Zhe She; Fen Xu; Dipanjan Banerjee; Daniel Hermida-Merino; others. A Facile Green Route to Ni/Co Oxide Nanoparticle Embedded 3D Graphitic Carbon Nanosheets for High Performance Hybrid Supercapacitor Device. *ACS Applied Energy Materials*. American Chemical Society, 2019.  
Type de production: Article Scientifique Type de support: Revue
- 9 Kousik Gayen; Kingshuk Basu; Nibedita Nandi; Krishna Sundar Das; Daniel Hermida-Merino; Ian W Hamley; Arindam Banerjee. A self-assembled peptide-appended naphthalene diimide: a fluorescent switch for sensing acid and base vapors. *ChemPlusChem*. 84 - 11, pp. 1673 - 1680. 2019.  
Type de production: Article Scientifique Type de support: Revue

- 10 Yasmine Sakhawoth; Laurent Michot; Pierre Levitz; Anne-Laure Rollet; Juliette Sirieix-Plenet; Daniel Hermida Merino; Natalie Malikova. Aggregation of Plate-like Colloids Induced by Charged Polymer Chains: Organization at the Nanometer Scale Tuned by Polymer Charge Density. *Langmuir*. 35 - 33, pp. 10937 - 10946. American Chemical Society, 2019.  
Type de production: Article Scientifique Type de support: Revue
- 11 Robin Harkins; Tatum Tauscher; Jason Nguyen; Sunny Lewis; Fabrizio C Adamo; Michela Pisani; Daniel Hermida-Merino; Edward T Samulski; Francesco Vita; Oriano Francescangeli; others. Biaxial ordering in the supercooled nematic phase of bent-core mesogens: effects of molecular symmetry and outer wing lateral groups. *Liquid Crystals*. pp. 1 - 13. Taylor & Francis, 2019.  
Type de production: Article Scientifique Type de support: Revue
- 12 Andrea Lassenberger; Andrea Scheberl; Krishna Chaithanya Batchu; Viviana Cristiglio; Isabelle Grillo; Daniel Hermida-Merino; Erik Reimhult; Niki Baccile. Biocompatible Glyconanoparticles by Grafting of Sophorolipid Monolayers on Monodisperse Iron Oxide Nanoparticles. *ACS Applied Bio Materials*. American Chemical Society, 2019.  
Type de production: Article Scientifique Type de support: Revue
- 13 Carolus HRM Wilsens; Laurence GD Hawke; Gijs W de Kort; Sarah Saidi; Manta Roy; Nils Leoné; Daniel Hermida-Merino; Gerrit WM Peters; Sanjay Rastogi. Effect of Thermal History and Shear on the Viscoelastic Response of i PP Containing an Oxalamide-Based Organic Compound. *Macromolecules*. 52 - 7, pp. 2789 - 2802. American Chemical Society, 2019.  
Type de production: Article Scientifique Type de support: Revue
- 14 Brian R Pauw; Andrew J Smith; Tim Snow; Olga Shebanova; John P Sutter; Jan Ilavsky; Daniel Hermida-Merino; Glen J Smales; Nicholas J Terrill; Andreas F Th<sup>u</sup>mann; others. Extending SAXS instrument ranges through addition of a portable, inexpensive USAXS module. arXiv preprint arXiv:1904.00080. 2019.  
Type de production: Article Scientifique Type de support: Revue
- 15 Nils Leoné; Manta Roy; Sarah Saidi; Gijs de Kort; Daniel Hermida-Merino; Carolus HRM Wilsens. Improving Processing, Crystallization, and Performance of Poly-l-lactide with an Amide-Based Organic Compound as Both Plasticizer and Nucleating Agent. *ACS Omega*. 4 - 6, pp. 10376 - 10387. American Chemical Society, 2019. Type de production: Article Scientifique Type de support: Revue
- 16 Apostolos Vagias; Qi Chen; Gert H ten Brink; Daniel Hermida-Merino; Jurgen Scheerder; Giuseppe Portale. Investigation of the Nanoscale Morphology in Industrially Relevant Clearcoats of Waterborne Polymer Colloids by Means of Variable-Angle Grazing Incidence Small-Angle X-ray Scattering. *ACS Applied Polymer Materials*. 1 - 9, pp. 2482 - 2494. American Chemical Society, 2019.  
Type de production: Article Scientifique Type de support: Revue
- 17 Guillaume Fleury; Daniel Hermida-Merino; Dong Jingjin; Karim Aissou; Aleksei Bytchkov; Giuseppe Portale. Micellar-Mediated Block Copolymer Ordering Dynamics Revealed by In Situ Grazing Incidence Small-Angle X-Ray Scattering during Spin Coating. *Advanced Functional Materials*. 29 - 10, pp. 1806741 - 1806741. 2019.  
Type de production: Article Scientifique Type de support: Revue
- 18 Mohammad Alauhdin; Thomas M Bennett; Guping He; Simon P Bassett; Giuseppe Portale; Wim Bras; Daniel Hermida-Merino; Steven M Howdle. Monitoring morphology evolution within block copolymer microparticles during dispersion polymerisation in supercritical carbon dioxide: a high pressure SAXS study. *Polymer Chemistry*. 10 - 7, pp. 860 - 871. Royal Society of Chemistry, 2019.  
Type de production: Article Scientifique Type de support: Revue
- 19 Enrique Niza; Cristina Nieto-Jiménez; María del Mar Noblejas-López; Iván Bravo; José Antonio Castro-Osma; Felipe de la Cruz-Martínez; Marc Martínez de Sarasa Buchaca; Inmaculada Posadas; Jesús Canales-Vázquez; Agustín Lara-Sánchez; others. Poly (Cyclohexene Phthalate) Nanoparticles for Controlled Dasatinib Delivery in Breast Cancer

- Therapy. *Nanomaterials*. 9 - 9, pp. 1208 - 1208. Multidisciplinary Digital Publishing Institute, 2019.
- Type de production: Article Scientifique Type de support: Revue
- 20 S Salimi; LR Hart; A Feula; D Hermida-Merino; ABR Tour{\e}; EA Kabova; L Ruiz-Cantu; DJ Irvine; R Wildman; K Shankland; others. Property enhancement of healable supramolecular polyurethanes. *European Polymer Journal*. 118, pp. 88 - 96. Pergamon, 2019.
- Type de production: Article Scientifique Type de support: Revue
- 21 Dipayan Bairagi; Parijat Biswas; Kingshuk Basu; Soumyajit Hazra; Daniel Hermida-Merino; Deepak Kumar Sinha; Ian W Hamley; Arindam Banerjee. Self-Assembling Peptide-Based Hydrogel: Regulation of Mechanical Stiffness and Thermal Stability and 3D Cell Culture of Fibroblasts. *ACS Applied Bio Materials*. American Chemical Society, 2019.
- Type de production: Article Scientifique Type de support: Revue
- 22 Charlotte JC Edwards-Gayle; Valeria Castelletto; Ian W Hamley; Glyn Barrett; Francesca Greco; Daniel Hermida-Merino; Robert P Rambo; Jani Seitsonen; Janne Ruokolainen. Self-Assembly, Antimicrobial Activity, and Membrane Interactions of Arginine-Capped Peptide Bola-Amphiphiles. *ACS applied bio materials*. American Chemical Society, 2019.
- Type de production: Article Scientifique Type de support: Revue
- 23 Ghazi Ben Messaoud; Patrick Le Griel; Sylvain Prevost; Daniel Hermida-Merino; Wim Soetaert; Sophie LKW Roelants; Christian V Stevens; Niki Baccile. Single-Lipid Lamellar Hydrogels: from Gel Engineering to Soft Materials Design. arXiv preprint arXiv:1907.02223. 2019.
- Type de production: Article Scientifique Type de support: Revue
- 24 Ghazi Messaoud; Patrick Le Griel; Sylvain Prevost; Daniel Hermida-Merino; Wim Soetaert; Sophie Roelants; Christian Stevens; Niki Baccile. Single-Molecule Lamellar Hydrogels from Bolaform Microbial Glucolipids. *Soft Matter*. 2019.
- Type de production: Article Scientifique Type de support: Revue
- 25 Alberto Alvarez-Fernandez; Fernando Valdes-Vango; Jos{\e} Ignacio Mart{\i}n; Mar{\i}a V{\e}lez; Carlos Quir{\o}s; Daniel Hermida-Merino; Giuseppe Portale; Jos{\e} Mar{\i}a Alameda; Francisco Javier Garc{\i}a Alonso. Tailoring block copolymer nanoporous thin films with acetic acid as a small guest molecule. *Polymer International*. John Wiley & Sons, Ltd, 2019.
- Type de production: Article Scientifique Type de support: Revue
- 26 Ghazi Ben Messaoud; Patrick Le Griel; Daniel Hermida-Merino; Sophie LKW Roelants; Wim Soetaert; Christian Victor Stevens; Niki Baccile. pH-Controlled Self-Assembled Fibrillar Network Hydrogels: Evidence of Kinetic Control of the Mechanical Properties. *Chemistry of Materials*. American Chemical Society, 2019.
- Type de production: Article Scientifique Type de support: Revue
- 27 Chen Sun; Marta Magdalena Mr{\o}z; Jos{\e} Ra{\u}l Castro Smirnov; Larry L{\u}er; Daniel Hermida-Merino; Chunhui Zhao; Masayuki Takeuchi; Kazunori Sugiyasu; Juan Cabanillas-Gonz{\a}lez. Amplified spontaneous emission in insulated polythiophenes. *Journal of Materials Chemistry C*. 6 - 24, pp. 6591 - 6596. Royal Society of Chemistry, 2018.
- Type de production: Article Scientifique Type de support: Revue
- 28 Carolus HRM Wilsens; Laurence GD Hawke; Enrico M Troisi; Daniel Hermida-Merino; Gijs De Kort; Nils Leoné; Keti Saralidze; Gerrit WM Peters; Sanjay Rastogi. Effect of self-assembly of oxalamide based organic compounds on melt behavior, nucleation, and crystallization of isotactic polypropylene. *Macromolecules*. 51 - 13, pp. 4882 4895. American Chemical Society, 2018.
- Type de production: Article Scientifique Type de support: Revue
- 29 Daniel Hermida-Merino; Ben O'Driscoll; Lewis R Hart; Peter J Harris; Howard M Colquhoun; Andrew T Slark; Cristina Prisacariu; Ian W Hamley; Wayne Hayes. Enhancement of microphase ordering and mechanical properties of supramolecular hydrogen-bonded polyurethane networks. *Polymer Chemistry*. 9 - 24, pp. 3406 3414. Royal Society of Chemistry, 2018.
- Type de production: Article Scientifique Type de support: Revue
- 30 Niels L Meereboer; Ivan Terzić; Sarah Saidi; Daniel Hermida Merino; Katja Loos. Nanoconfinement-induced  $\beta$ -phase formation Inside poly (vinylidene fluoride)-based block copolymers. *ACS macro letters*. 7 - 7, pp. 863 - 867. American Chemical Society, 2018.

- Type de production: Article Scientifique Type de support: Revue  
 31 T Nikolaeva; R Den Adel; E Velichko; WG Bouwman; D Hermida-Merino; H Van As; A Voda; J Van Duynhoven. Networks of micronized fat crystals grown under static conditions. *Food & function*. 9 - 4, pp. 2102 - 2111. Royal Society of Chemistry, 2018.
- Type de production: Article Scientifique Type de support: Revue  
 32 Kelly Melia; Barnaby W Greenland; Daniel Hermida-Merino; Lewis R Hart; Ian W Hamley; Howard M Colquhoun; Andrew T Slark; Wayne Hayes. Self-assembling unsymmetrical bis-ureas. *Reactive and functional polymers*. 124, pp. 156 - 161. Elsevier, 2018.
- Type de production: Article Scientifique Type de support: Revue  
 33 Xuegang Tang; Antonio Feula; Benjamin C Baker; Kelly Melia; Daniel Hermida Merino; Ian W Hamley; C Paul Buckley; Wayne Hayes; Clive R Siviour. A dynamic supramolecular polyurethane network whose mechanical properties are kinetically controlled. *Polymer*. 133, pp. 143 - 150. Elsevier, 2017.
- Type de production: Article Scientifique Type de support: Revue  
 34 O Korculanin; D Hermida-Merino; Helmut Hirsemann; B Struth; SA Rogers; MP Lettinga. Anomalous structural response of nematic colloidal platelets subjected to large amplitude stress oscillations. *Physics of Fluids*. 29 - 2, pp. 023102 - 023102. AIP Publishing, 2017.
- Type de production: Article Scientifique Type de support: Revue  
 35 Eduardo Solano; Jolien Dendooven; Matthias M Minjauw; Ranjith K Ramachandran; Kevin Van de Kerckhove; Thomas Dobbelaere; Daniel Hermida-Merino; Christophe Detavernier. Correction: Key role of surface oxidation and reduction processes in the coarsening of Pt nanoparticles. *Nanoscale*. 9 - 45, pp. 18109 - 18109. Royal Society of Chemistry, 2017.
- Type de production: Article Scientifique Type de support: Revue  
 36 Andres Garzon; Maria Fernandez-Liencres; Mónica Moral; Tomas Peña-Ruiz; Amparo Navarro; Juan Tolosa; Jesus Canales-Vázquez; Daniel Hermida-Merino; Ivan Bravo; Jose Albaladejo; others. Effect of the Aggregation on the Photophysical Properties of a Blue-Emitting Star-Shaped. *The Journal of Physical Chemistry C*. 121 - 8, pp. 4720 - 4720. 2017.
- Type de production: Article Scientifique Type de support: Revue  
 37 Ilya V Roslyakov; Dmitry S Koshkodaev; Andrei A Eliseev; Daniel Hermida-Merino; Vladimir K Ivanov; Andrei V Petukhov; Kirill S Napolskii. Growth of porous anodic alumina on low-index surfaces of Al single crystals. *The Journal of Physical Chemistry C*. 121 - 49, pp. 27511 - 27520. American Chemical Society, 2017.
- Type de production: Article Scientifique Type de support: Revue  
 38 Valeria Castelletto; Amanpreet Kaur; IW Hamley; RH Barnes; K-A Karatzas; D Hermida-Merino; S Swioklo; CJ Connon; Joanna Stasiak; M Reza; others. Hybrid membrane biomaterials from self-assembly in polysaccharide and peptide amphiphile mixtures: controllable structural and mechanical properties and antimicrobial activity. *Rsc Advances*. 7 - 14, pp. 8366 - 8375. Royal Society of Chemistry, 2017.
- Type de production: Article Scientifique Type de support: Revue  
 39 Eduardo Solano; Jolien Dendooven; Ranjith K Ramachandran; Kevin Van de Kerckhove; Thomas Dobbelaere; Daniel Hermida-Merino; Christophe Detavernier. Key role of surface oxidation and reduction processes in the coarsening of Pt nanoparticles. *Nanoscale*. 9 - 35, pp. 13159 - 13170. The Royal Society of Chemistry, 2017.
- Type de production: Article Scientifique Type de support: Revue  
 40 Alessandro Longo; Dirk-Jan Mulder; Huub PC van Kuringen; Daniel Hermida-Merino; Dipanjan Banerjee; Debarshi Dasgupta; Irina K Shishmanova; Anne B Spoelstra; Dirk J Broer; Albert PHJ Schenning; others. On the Dimensional Control of 2 D Hybrid Nanomaterials. *Chemistry--A European Journal*. 23 - 51, pp. 12534 - 12541. 2017.
- Type de production: Article Scientifique Type de support: Revue  
 41 Daniel TW Toolan; Kevin Adlington; Anna Isakova; Alexis Kalamiotis; Parvaneh Mokarian-Tabari; Georgios Dimitrakis; Christopher Dodds; Thomas Arnold; Nick J Terrill; Wim Bras; others. Selective molecular annealing: in situ small angle X-ray scattering study of microwave-assisted

- annealing of block copolymers. *Physical Chemistry Chemical Physics*. 19 - 31, pp. 20412 - 20419. Royal Society of Chemistry, 2017.  
 Type de production: Article Scientifique Type de support: Revue
- 42 Valeria Castelletto; Pavel Ryumin; Rainer Cramer; IW Hamley; M Taylor; David Allsop; M Reza; J Ruokolainen; T Arnold; D Hermida-Merino; others. Self-assembly and anti-amyloid cytotoxicity activity of amyloid beta peptide derivatives. *Scientific reports*. 7, pp. 43637 - 43637. Nature Publishing Group, 2017.  
 Type de production: Article Scientifique Type de support: Revue
- 43 Jacobus J van Franeker; Daniel Hermida-Merino; Cedric Gommès; Kirill Arapov; Jasper J Michels; Ren{\'e} AJ Janssen; Giuseppe Portale. Sub-Micrometer Structure Formation during Spin Coating Revealed by Time-Resolved In Situ Laser and X-Ray Scattering. *Advanced Functional Materials*. 27 - 46, pp. 1702516 - 1702516. 2017.  
 Type de production: Article Scientifique Type de support: Revue
- 44 Elif Arslan; Meryem Hatip Koc; Ozge Uysal; Begum Dikecoglu; Ahmet E Topal; Ruslan Garifullin; Alper D Ozkan; Aykutlu Dana; Daniel Hermida-Merino; Valeria Castelletto; others. Supramolecular peptide nanofiber morphology affects mechanotransduction of stem cells. *Biomacromolecules*. 18 - 10, pp. 3114 - 3130. American Chemical Society, 2017.  
 Type de production: Article Scientifique Type de support: Revue
- 45 Luis M De Leon-Rodriguez; Meder Kamalov; Yacine Hemar; Alok K Mitra; Valeria Castelletto; Daniel Hermida-Merino; Ian W Hamley; Margaret A Brimble. A peptide hydrogel derived from a fragment of human cardiac troponin C. *Chemical Communications*. 52 - 21, pp. 4056 - 4059. Royal Society of Chemistry, 2016.  
 Type de production: Article Scientifique Type de support: Revue
- 46 Abhishek Baral; Subhasish Roy; Srabanti Ghosh; Daniel Hermida-Merino; Ian W Hamley; Arindam Banerjee. A peptide-based mechano-sensitive, proteolytically stable hydrogel with remarkable antibacterial properties. *Langmuir*. 32 - 7, pp. 1836 - 1845. American Chemical Society, 2016.  
 Type de production: Article Scientifique Type de support: Revue
- 47 Daniel Hermida Merino; Antonio Feula; Kelly Melia; Andrew T Slark; Ioannis Giannakopoulos; Clive R Siviour; C Paul Buckley; Barnaby W Greenland; Dan Liu; Yu Gan; others. A systematic study of the effect of the hard end-group composition on the microphase separation, thermal and mechanical properties of supramolecular polyurethanes. *Polymer*. 107, pp. 368 - 378. Elsevier, 2016.  
 Type de production: Article Scientifique Type de support: Revue
- 48 {\A}lvaro Mu{\~n}oz-Noval; Kazuhiro Fukami; Akira Koyama; Dario Gallach; Daniel Hermida-Merino; Giuseppe Portale; Atsushi Kitada; Kuniaki Murase; Takeshi Abe; Shinjiro Hayakawa; others. Accelerated growth from amorphous clusters to metallic nanoparticles observed in electrochemical deposition of platinum within nanopores of porous silicon. *Electrochemistry Communications*. 71, pp. 9 - 12. Elsevier, 2016.  
 Type de production: Article Scientifique Type de support: Revue
- 49 Ranjith K Ramachandran; Jolien Dendooven; Matthias Filez; Vladimir V Galvita; Hilde Poelman; Eduardo Solano; Matthias M Minjauw; Kilian Devloo-Casier; Emiliano Fonda; Daniel Hermida-Merino; others. Atomic layer deposition route to tailor nanoalloys of noble and non-noble metals. *ACS nano*. 10 - 9, pp. 8770 - 8777. American Chemical Society, 2016.  
 Type de production: Article Scientifique Type de support: Revue
- 50 Ilya V Roslyakov; Dmitry S Koshkodaev; Andrei A Eliseev; Daniel Hermida-Merino; Andrei V Petukhov; Kirill S Napolskii. Crystallography-induced correlations in pore ordering of anodic alumina films. *The Journal of Physical Chemistry C*. 120 - 35, pp. 19698 - 19704. American Chemical Society, 2016.  
 Type de production: Article Scientifique Type de support: Revue
- 51 J Jennings; SP Bassett; D Hermida-Merino; G Portale; W Bras; L Knight; Jeremy J Titman; T Higuchi; H Jinnai; SM Howdle. How does dense phase CO<sub>2</sub> influence the phase behaviour of block copolymers synthesised by dispersion polymerisation?. *Polymer Chemistry*. 7 - 4, pp. 905 - 916. Royal Society of Chemistry, 2016.

- Type de production: Article Scientifique Type de support: Revue
- 52 Kangsheng Liu; Efren Andablo-Reyes; Nilesh Patil; Daniel Hermida Merino; Sara Ronca; Sanjay Rastogi. Influence of reduced graphene oxide on the rheological response and chain orientation on shear deformation of high density polyethylene. *Polymer*. 87, pp. 8 - 16. Elsevier, 2016.
- Type de production: Article Scientifique Type de support: Revue
- 53 Erik Meers; Stefanie Scheidl; Franz Kirchmeyer; Susanna Pfluger; Jan Stambasky. Mechanisms of the contribution of anaerobic digestion (AD) to GHG-emission abatement: more than only the substitution of fossil energy. *EUROPEAN ENERGY INNOVATION*. Autumn 2016, pp. 28 - 29. The Magazine Printing Company, 2016.
- Type de production: Article Scientifique Type de support: Revue
- 54 IV Roslyakov; NS Kuratova; DS Koshkodaev; D Hermida Merino; AV Lukashin; KS Napolskii. Morphology of anodic alumina films obtained by hard anodization: Influence of the rate of anodization voltage increase. *Journal of Surface Investigation. X-ray, Synchrotron and Neutron Techniques*. 10 - 1, pp. 191 - 197. Pleiades Publishing, 2016.
- Type de production: Article Scientifique Type de support: Revue
- 55 SD Tillmann; D Hermida-Merino; M Winter; I Cekic-Laskovic; K Loos. Nanoporous polymer foams derived from high molecular PS-b-P4VP (PDP) x for template-directed synthesis approaches. *RSC Advances*. 6 - 58, pp. 52998 - 53003. Royal Society of Chemistry, 2016.
- Type de production: Article Scientifique Type de support: Revue
- 56 Giuseppe Portale; Daniel Hermida-Merino; Wim Bras. Polymer research and synchrotron radiation perspectives. *European Polymer Journal*. 81, pp. 415 - 432. Pergamon, 2016.
- Type de production: Article Scientifique Type de support: Revue
- 57 Steven Kirkham; Valeria Castelletto; Ian William Hamley; Mehedi Reza; Janne Ruokolainen; Daniel Hermida-Merino; Panayiotis Bilalis; Hermis Iatrou. Self-Assembly of Telechelic Tyrosine End-Capped PEO and Poly (alanine) Polymers in Aqueous Solution. *Biomacromolecules*. 17 - 3, pp. 1186 - 1197. American Chemical Society, 2016.
- Type de production: Article Scientifique Type de support: Revue
- 58 Ian W Hamley; Samuel Burholt; Jessica Hutchinson; Valeria Castelletto; Emerson Rodrigo Da Silva; Wendel Alves; Philipp Gutfreund; Lionel Porcar; Rajeev Dattani; Daniel Hermida-Merino; others. Shear alignment of bola-amphiphilic arginine-coated peptide nanotubes. *Biomacromolecules*. 18 - 1, pp. 141 - 149. American Chemical Society, 2016.
- Type de production: Article Scientifique Type de support: Revue
- 59 Anthony J Ryan; Wim Bras; Daniel Hermida-Merino; Dario Cavallo. The interaction between fundamental and industrial research and experimental developments in the field of polymer crystallization. *Journal of Non-Crystalline Solids*. 451, pp. 168 - 178. North-Holland, 2016.
- Type de production: Article Scientifique Type de support: Revue
- 60 Claudio De Rosa; Finizia Auriemma; Anna Malafronte; Rocco Di Girolamo; Massimo Lazzari; Marina Nieto-Suárez; Daniel Hermida-Merino; Ian William Hamley; Giuseppe Portale. Tuning Ordered Pattern of Pd Species through Controlled Block Copolymer Self-Assembly. *The Journal of Physical Chemistry B*. 120 - 27, pp. 6829 - 6841. American Chemical Society, 2016.
- Type de production: Article Scientifique Type de support: Revue
- 61 Lian R Hutchings; Serena Agostini; Ian W Hamley; Daniel Hermida-Merino. Chain architecture as an orthogonal parameter to influence block copolymer morphology. Synthesis and characterization of hyperbranched block copolymers: HyperBlocks. *Macromolecules*. 48 - 24, pp. 8806 - 8822. American Chemical Society, 2015. Type de production: Article Scientifique
- Type de support: Revue
- 62 Gemma E Newby; Erik B Watkins; Daniel Hermida Merino; Paul A Staniec; Oier Bikondoa. In situ Rheo-GISANS of triblock copolymers: gelation and shear effects on quasi-crystalline structures at interfaces. *RSC Advances*. 5 126, pp. 104164 - 104171. Royal Society of Chemistry, 2015.
- Type de production: Article Scientifique Type de support: Revue
- 63 Alessandro Longo; Dipanjan Banerjee; Daniel Hermida-Merino; Giuseppe Portale; Pietro Calandra; Vincenzo Turco Liveri. Induced Chirality in Confined Space on Halogen Gold

- Complexes. *The Journal of Physical Chemistry C*. 119 - 32, pp. 18798 - 18807. American Chemical Society, 2015.  
 Type de production: Article Scientifique Type de support: Revue
- 64 Daniel Hermida-Merino; Gemma E Newby; Ian W Hamley; Wayne Hayes; Andrew Slark. Microphase separation induced in the melt of Pluronic copolymers by blending with a hydrogen bonding urea--urethane end-capped supramolecular polymer. *Soft matter*. 11 - 29, pp. 5799 - 5803. Royal Society of Chemistry, 2015.  
 Type de production: Article Scientifique Type de support: Revue
- 65 Peter C Roozmond; Martin van Drongelen; Zhe Ma; Anne B Spoelstra; Daniel Hermida-Merino; Gerrit WM Peters. Self-Regulation in Flow-Induced Structure Formation of Polypropylene. *Macromolecular rapid communications*. 36 - 4, pp. 385 - 390. 2015.  
 Type de production: Article Scientifique Type de support: Revue
- 66 David Alaimo; Daniel Hermida Merino; Bruno Grignard; Wim Bras; Christine Jérôme; Antoine Debuigne; Cedric J Gommès. Small-angle X-ray scattering insights into the architecture-dependent emulsifying properties of amphiphilic copolymers in supercritical carbon dioxide. *The Journal of Physical Chemistry B*. 119 - 4, pp. 1706 1716. American Chemical Society, 2015.  
 Type de production: Article Scientifique Type de support: Revue
- 67 JP MacDonald; MP Parker; BW Greenland; D Hermida-Merino; IW Hamley; MP Shaver. Tuning thermal properties and microphase separation in aliphatic polyester ABA copolymers. *Polymer Chemistry*. 6 - 9, pp. 1445 - 1453. Royal Society of Chemistry, 2015.  
 Type de production: Article Scientifique Type de support: Revue
- 68 EM Troisi; G Portale; Z Ma; Martin van Drongelen; D Hermida-Merino; GWM Peters. Unusual melting behavior in flow induced crystallization of LLDPE: effect of pressure. *Macromolecules*. 48 - 8, pp. 2551 - 2560. American Chemical Society, 2015.  
 Type de production: Article Scientifique Type de support: Revue
- 69 Daniel Hermida-Merino; Giuseppe Portale; Peter Fields; Richard Wilson; Simon P Bassett; James Jennings; Martin Dellar; Cedric Gommès; Steven M Howdle; Benno CM Vrolijk; others. A high pressure cell for supercritical CO<sub>2</sub> on-line chemical reactions studied with x-ray techniques. *Review of Scientific Instruments*. 85 - 9, pp. 093905 093905. AIP, 2014.  
 Type de production: Article Scientifique Type de support: Revue
- 70 Inbal Davidi; Daniel Hermida-Merino; Keren Keinan-Adamsky; Giuseppe Portale; Gil Goobes; Roy Shenhar. Dynamic Behavior of Supramolecular Comb Polymers Consisting of Poly (2-Vinyl Pyridine) and Palladium-Pincer Surfactants in the Solid State. *Chemistry--A European Journal*. 20 - 23, pp. 6951 - 6959. WILEY-VCH Verlag Weinheim, 2014.  
 Type de production: Article Scientifique Type de support: Revue
- 71 Inbal Davidi; Debabrata Patra; Daniel Hermida-Merino; Giuseppe Portale; Vincent M Rotello; Uri Raviv; Roy Shenhar. Hierarchical Structures of Polystyrene-block-poly (2-vinylpyridine)/Palladium--Pincer Surfactants: Effect of Weak Surfactant--Polymer Interactions on the Morphological Behavior. *Macromolecules*. 47 - 16, pp. 5774 5783. American Chemical Society, 2014.  
 Type de production: Article Scientifique Type de support: Revue
- 72 Yi-An Lin; Andrew G Cheetham; Pengcheng Zhang; Yu-Chuan Ou; Yuguo Li; Guanshu Liu; Daniel Hermida-Merino; Ian W Hamley; Honggang Cui. Multiwalled nanotubes formed by cationic mixtures of drug amphiphiles. *ACS nano*. 8 - 12, pp. 12690 - 12700. American Chemical Society, 2014. Type de production: Article Scientifique Type de support: Revue
- 73 Erik Gubbels; Lidia Jasinska-Walc; Daniel Hermida-Merino; Michael Ryan Hansen; Bart Noordover; Anne Spoelstra; Han Goossens; Cor Koning. Phase separation in poly (butylene terephthalate)-based materials prepared by solid-state modification. *Polymer*. 55 - 16, pp. 3801 - 3810. Elsevier, 2014.  
 Type de production: Article Scientifique Type de support: Revue
- 74 Benny Luijsterburg; Peter Jobse; Daniel Hermida Merino; Ton Peijs; Han Goossens. Solid-state drawing of  $\beta$ -nucleated polypropylene: Effect of additives on drawability and mechanical properties. *Journal of Polymer Science Part B: Polymer Physics*. 52 - 16, pp. 1071 - 1082. 2014.

- Type de production: Article Scientifique Type de support: Revue
- 75 Halina B Stanley; Dipanjan Banerjee; Lambert Van Breemen; Jim Ciston; Christian H Liebscher; Vladimir Martis; Daniel Hermida Merino; Alessandro Longo; Philip Pattison; Gerrit WM Peters; others. X-ray irradiation induced reduction and nanoclustering of lead in borosilicate glass. *CrystEngComm*. 16 - 39, pp. 9331 - 9339. Royal Society of Chemistry, 2014.
- Type de production: Article Scientifique Type de support: Revue
- 76 Vincent SD Voet; Daniel Hermida-Merino; Gerrit ten Brinke; Katja Loos. Block copolymer route towards poly (vinylidene fluoride)/poly (methacrylic acid)/nickel nanocomposites. *Rsc Advances*. 3 - 21, pp. 7938 - 7946. Royal Society of Chemistry, 2013.
- Type de production: Article Scientifique Type de support: Revue
- 77 Giuseppe Portale; Dario Cavallo; Giovanni Carlo Alfonso; Daniel Hermida-Merino; M van Drongelen; Luigi Balzano; GWM Peters; JGP Goossens; Wim Bras. Polymer crystallization studies under processing-relevant conditions at the SAXS/WAXS DUBBLE beamline at the ESRF. *Journal of applied crystallography*. 46 - 6, pp. 1681 - 1689. International Union of Crystallography, 2013.
- Type de production: Article Scientifique Type de support: Revue
- 78 Ivana Vukovic; Heiner Friedrich; Daniel Hermida Merino; Giuseppe Portale; Gerrit ten Brinke; Katja Loos. Shear-Induced Orientation of Gyroid PS-b-P4VP (PDP) Supramolecules. *Macromolecular rapid communications*. 34 - 15, pp. 1208 - 1212. Wiley Online Library, 2013.
- Type de production: Article Scientifique Type de support: Revue
- 79 Erik Gubbels; Lidia Jasinska-Walc; Daniel Hermida Merino; Han Goossens; Cor Koning. Solid-state modification of poly (butylene terephthalate) with a bio-based fatty acid dimer diol furnishing copolyesters with unique morphologies. *Macromolecules*. 46 - 10, pp. 3975 - 3984. ACS Publications, 2013.
- Type de production: Article Scientifique Type de support: Revue
- 80 Ivana Vukovic; Thomas P Voortman; Daniel Hermida Merino; Giuseppe Portale; Panu Hiekkataipale; Janne Ruokolainen; Gerrit ten Brinke; Katja Loos. Double gyroid network morphology in supramolecular diblock copolymer complexes. *Macromolecules*. 45 - 8, pp. 3503 - 3512. ACS Publications, 2012. Type de production: Article Scientifique Type de support: Revue
- 81 N{\a}gila MPS Ricardo; Nadja MPS Ricardo; Fl{\a}via de MLL Costa; Francisco WA Bezerra; Chiraphon Chaibundit; Daniel Hermida-Merino; Barnaby W Greenland; Stefano Burattini; Ian W Hamley; S Keith Nixon; others. Effect of water-soluble polymers, polyethylene glycol and poly (vinylpyrrolidone), on the gelation of aqueous micellar solutions of Pluronic copolymer F127. *Journal of colloid and interface science*. 368 - 1, pp. 336 - 341. Academic Press, 2012.
- Type de production: Article Scientifique Type de support: Revue
- 82 D Hermida-Merino; Mohammad Belal; Barnaby W Greenland; P Woodward; AT Slark; Fred J Davis; Geoffrey R Mitchell; IW Hamley; Wayne Hayes. Electrospun supramolecular polymer fibres. *European Polymer Journal*. 48 7, pp. 1249 - 1255. Pergamon, 2012.
- Type de production: Article Scientifique Type de support: Revue
- 83 Francisco Rodr{\i}guez-Llansola; Daniel Hermida-Merino; Bel{\e}n Nieto-Ortega; Francisco J Ram{\i}rez; Juan T L{\o}pez Navarrete; Juan Casado; Ian W Hamley; Beatriu Escuder; Wayne Hayes; Juan F Miravet. Self-assembly studies of a chiral bisurea-based superhydrogelator. *Chemistry--A European Journal*. 18 - 46, pp. 14725 - 14731. WILEY-VCH Verlag Weinheim, 2012.
- Type de production: Article Scientifique Type de support: Revue
- 84 Rose Mary Michell; Alejandro J M{\u}ller; Mariya Spasova; Philippe Dubois; Stefano Burattini; Barnaby W Greenland; Ian W Hamley; Daniel Hermida-Merino; Nicolas Cheval; Amir Fahmi. Crystallization and stereocomplexation behavior of poly (D-and L-lactide)-b-poly (N, N-dimethylamino-2-ethyl methacrylate) block copolymers. *Journal of Polymer Science Part B: Polymer Physics*. 49 - 19, pp. 1397 - 1409. Wiley Online Library, 2011.
- Type de production: Article Scientifique Type de support: Revue
- 85 N{\a}gila MPS Ricardo; Nadja MPS Ricardo; Fl{\a}via de MLL Costa; Chiraphon Chaibundit; Giuseppe Portale; Daniel Hermida-Merino; Stefano Burattini; Ian W Hamley; Christopher A Muryn; S Keith Nixon; others. The effect of n-, s-and t-butanol on the micellization and gelation

- of Pluronic P123 in aqueous solution. *Journal of colloid and interface science*. 353 - 2, pp. 482 - 489. Academic Press, 2011.  
Type de production: Article Scientifique Type de support: Revue
- 86 Stefano Burattini; Barnaby W Greenland; Daniel Hermida Merino; Wengui Weng; Jonathan Seppala; Howard M Colquhoun; Wayne Hayes; Michael E Mackay; Ian W Hamley; Stuart J Rowan. A healable supramolecular polymer blend based on aromatic pi- pi stacking and hydrogen-bonding interactions. *Journal of the American Chemical Society*. 132 - 34, pp. 12051 - 12058. American Chemical Society, 2010.  
Type de production: Article Scientifique Type de support: Revue
- 87 Philip J Woodward; Daniel Hermida Merino; Barnaby W Greenland; Ian W Hamley; Zoe Light; Andrew T Slark; Wayne Hayes. Hydrogen bonded supramolecular elastomers: correlating hydrogen bonding strength with morphology and rheology. *Macromolecules*. 43 - 5, pp. 2512 - 2517. American Chemical Society, 2010. Type de production: Article Scientifique Type de support: Revue
- 88 Francisco Rodr\iguez-Llansola; Beatriu Escuder; Juan F Miravet; Daniel Hermida-Merino; Ian W Hamley; Christine J Cardin; Wayne Hayes. Selective and highly efficient dye scavenging by a pH-responsive molecular hydrogelator. *Chemical communications*. 46 - 42, pp. 7960 - 7962. Royal Society of Chemistry, 2010.  
Type de production: Article Scientifique Type de support: Revue
- 89 V Castelletto; GE Newby; D Hermida Merino; IW Hamley; D Liu; L Noirez. Self-assembly of an amyloid peptide fragment--PEG conjugate: lyotropic phase formation and influence of PEG crystallization. *Polymer Chemistry*. 1 4, pp. 453 - 459. Royal Society of Chemistry, 2010.  
Type de production: Article Scientifique Type de support: Revue
- 90 Daniel Hermida Merino; Andrew T Slark; Howard M Colquhoun; Wayne Hayes; Ian W Hamley. Thermo-responsive microphase separated supramolecular polyurethanes. *Polymer Chemistry*. 1 - 8, pp. 1263 - 1271. Royal Society of Chemistry, 2010.  
Type de production: Article Scientifique Type de support: Revue
- 91 Philip Woodward; Alex Clarke; Barnaby W Greenland; Daniel Hermida Merino; Laura Yates; Andrew T Slark; Juan F Miravet; Wayne Hayes. Facile bisurethane supramolecular polymers containing flexible alicyclic receptor units. *Soft Matter*. 5 - 10, pp. 2000 - 2010. Royal Society of Chemistry, 2009.  
Type de production: Article Scientifique Type de support: Revue
- 92 Philip Woodward; Daniel Hermida Merino; Ian W Hamley; Andrew T Slark; Wayne Hayes. Thermally responsive elastomeric supramolecular polymers featuring flexible aliphatic hydrogen-bonding end-groups. *Australian journal of chemistry*. 62 - 8, pp. 790 - 793. CSIRO, 2009.  
Type de production: Article Scientifique Type de support: Revue
- 93 Chiraphon Chaibundit; N\gila MPS Ricardo; N\aja MPS Ricardo; Flávia de MLL Costa; Marcus GP Wong; Daniel Hermida-Merino; Jose Rodriguez-Perez; Ian W Hamley; Stephen G Yeates; Colin Booth. Effect of Ethanol on the Micellization and Gelation of Pluronic P123. *Langmuir*. 24 - 21, pp. 12260 - 12266. American Chemical Society, 2008.  
Type de production: Article Scientifique Type de support: Revue
- 94 Phil Woodward; Alex Clarke; Daniel Hermida Merino; Andrew T Slark. SELF-ASSEMBLED URETHANE AND UREA'PSEUDO'-POLYMERS. *Polymer Preprints*. 48 - 2, 2007.  
Type de production: Article Scientifique Type de support: Revue
- 95 KA Jansen; A Zhmurov; G Portale; DH Merino; RI Litvinov; BE Vos; V Tutwiler; IK Piechocka; NA Kurniawan; W Bras; others. 4. Fibrinogen Unfolding During Fibrin Gel Stretching.  
Type de production: Article Scientifique Type de support: Revue
- 96 Arindam Banerjee; Kousik Gayen; Kingshuk Basu; Nibedita Nandi; Krishna Sundar Das; Daniel Hermida-Merino; Ian W Hamley. A Self-Assembled Peptide-Appended Naphthalene Diimide: A Fluorescent Switch for Sensing Volatile Acid and Basic Vapors. *ChemPlusChem*. John Wiley & Sons, Ltd,  
Type de production: Article Scientifique Type de support: Revue

## Travaux présentés lors de congrès nationaux ou internationaux

1. Titre: Monitoring of the drug uptake/release by a self-assembled low molecular weight hydrogelator carrier  
Nom du congrès: Advanced Materials World Congress  
Autor de correspondencia: Oui  
Ville d'une réalisation: Sydney, Australie  
Date de tenue de l'événement: 02/02/2020  
Date de fin: 05/02/2020  
Établissement organisateur: International      Type d'établissement: Associations et groupements Association of Advanced Materials  
Ville: Ulrika, Suède  
Daniel Hermida Merino; Ivan Bravo Perez; Inmaculada Posadas Mayo; Giuseppe Portale.
2. Titre: INVESTIGATION OF THE UPTAKE/RELEASE PROCESS DURING THE FIBRILLIZATION OF SELF-ASSEMBLED LOW MOLECULAR WEIGHT HYDROGELATORS BY SAXS/GISAXS  
nom du congrès: XVII International Small Angle Scattering Conference - SAS2018XVII  
International Small Angle Scattering Conference - SAS2018  
Autor de correspondencia: Oui  
Ville d'une réalisation: Traverse city (Michigan), États-Unis  
Date de tenue de l'événement: 12/10/2018  
Date de fin: 12/10/2018  
Établissement organisateur: Advanced Photon Source  
Ville: Lemont (Illinois), États-Unis  
Daniel Hermida Merino; Ivan Bravo Perez; Gisepepe Portale.
3. Titre: Understanding the fibrillation of self-assembled low molecular weight hydrogelators  
Nom du congrès: 2015 International Chemical Congress of Pacific Basin Societies  
Autor de correspondencia: Oui  
Ville d'une réalisation: HONOLULU, HAWAII, États-Unis  
Date de tenue de l'événement: 15/12/2015  
Date de fin: 20/12/2015  
Établissement organisateur: American chemistry Society, Chemical Society of Japan, Canadian Society for Chemistry, New Zealand Institute of Chemistry, Royal Australian Institute of Chemistry, Korean Chemical and Chinese Chemical  
Ville: Washington, États-Unis  
Daniel Hermida Merino; Giuseppe Portale.
4. Titre: The influence of graphene oxide in blending of low and ultra-high molar mas polymers and its implications on orientation and crystallization during flow  
Nom du congrès: Fourth International Conference Frontiers in Polymer Science  
Autor de correspondencia: Oui  
Ville d'une réalisation: Riva del Garda, Italie  
Date de tenue de l'événement: 20/05/2015  
Date de fin: 22/05/2015  
Établissement organisateur: Elsevier      Type d'établissement: Editorial  
Ville: Amsterdam, Pays-Bas  
Daniel Hermida Merino; Giuseppe Portale; Wim Bras; Enrico Troisi; Gerrit Peters; Efen Andablo Reyes; Ele de Boer; Sanjay Rastogi.
5. Titre: Correlating molecular structure to mechanism of gelation of low molecular weight hydrogelators

Nom du congrès: Polymer Networks & Gels 2014 Conference

Autor de correspondencia: Oui

Ville d'une réalisation: Tokyo, Japon

Date de tenue de l'événement: 10/11/2014

Date de fin: 14/11/2014

Établissement organisateur: University of Tokyo Type d'établissement: Université

Ville: Tokyo, Japon

Daniel Hermida Merino; Francisco Rodriguez Llansola; Alessandro Longo; Giuseppe Portale.  
"Microfluidic Assisted Self-Assembly of pH-Sensitive Low-Molecular Weight Hydrogelators  
Close to the Minimum Gelation Concentration".

6. Titre: Study of the dynamic morphology of an in-situ RAFT polymerization in supercritical CO<sub>2</sub> of novel block copolymers

Nom du congrès: Third International Conference Frontiers in Polymer Science

Autor de correspondencia: Oui

Ville d'une réalisation: Sitges, Espagne

Date de tenue de l'événement: 21/05/2013

Date de fin: 23/05/2013

Établissement organisateur: Elsevier Type d'établissement: Editorial

Ville: Amsterdam, Pays-Bas

Daniel Hermida Merino; Giuseppe Portale; Wim Bras; James Jennings; Simon Bassett; Steven Howdle.

7. Titre: Drawing behaviour of polyamide(4,10) films

Nom du congrès: Second International Conference Frontiers in Polymer Science

Autor de correspondencia: Oui

Ville d'une réalisation: Lyon, France

Date de tenue de l'événement: 29/05/2011

Date de fin: 31/05/2011

Établissement organisateur: Elsevier Type d'établissement: Editorial

Ville: Amsterdam, Pays-Bas

Daniel Hermida Merino; Han Goossens; S Vaidya.

## Comités consultatifs scientifiques, sociétés scientifiques

1. Intitulé du comité: ALBA Review Panel for Evaluation of Scientific Proposals for the 2020-I Call  
Organisme responsable: Alba Type d'organisme: Organisme public de recherche  
Ville: Cerdanyola del Vallès, Catalogne, Espagne  
Début-Fin: 20/10/2020 - 20/10/2020
2. Intitulé du comité: ALBA Review Panel for Evaluation of Scientific Proposals for the 2020-I Call  
Organisme responsable: Alba Type d'organisme: Organisme public de recherche  
Ville: Cerdanyola del Vallès, Catalogne, Espagne  
Début-Fin: 20/04/2020 - 20/04/2020
3. Intitulé du comité: ALBA Review Panel for Evaluation of Scientific Proposals for the 2020-I Call  
Organisme responsable: Alba Type d'organisme: Organisme public de recherche  
Ville: Cerdanyola del Vallès, Catalogne, Espagne  
Début-Fin: 11/10/2019 - 11/10/2019

4. Intitulé du comité: ALBA Review Panel for Evaluation of Scientific Proposals for the 2019-II Call  
Organisme responsable: Alba Type d'organisme: Organisme public de recherche  
Ville: Cerdanyola del Vallès, Catalogne, Espagne  
Début-Fin: 11/04/2019 - 11/04/2019
  
5. Intitulé du comité: ALBA Review Panel for Evaluation of Scientific Proposals for the 2019-I Call  
Organisme responsable: Alba Type d'organisme: Organisme public de recherche  
Ville: Cerdanyola del Vallès, Catalogne, Espagne  
Début-Fin: 11/10/2018 - 11/10/2018

## Expérience de gestion de R&D&I

### **Intitulé/dénomination de l'activité : Responsable de Ligne de synchrotron bm26 @ ESRF**

Type de gestion : Gestion d'organisme

Responsabilité exercée : Caractéristiques générales: Les lignes lumineuses de Dubble ont une présence de haut niveau internationalement reconnue dans la recherche en temps réel concernant la matière condensée molle et toutes les corrélations croisées concernant la biologie et la physique. Le travail du scientifique supérieur et chef de la ligne lumière et de son laboratoire de chimie est réalisé dans un environnement de recherche international dans un environnement très interdisciplinaire. Tâche principale: Exploitation et développement de lignes lumineuses synchrotron et assistance aux utilisateurs en participant à des expériences, en éduquant les utilisateurs externes, en conseillant les utilisateurs sur leur plan de travail scientifique et leurs stratégies d'analyse de données, et en menant leurs propres recherches. Principales composantes du poste: - Traduire les questions scientifiques en un programme expérimental efficace et créer l'environnement physique dans lequel ces expériences peuvent être menées; - est bien mis à jour avec la littérature existante, capable de comprendre les corrélations croisées pratiques et scientifiques requises dans ce domaine interdisciplinaire, mène ses propres expériences, analyse et interprète les données et rend compte au chef de projet. Prend en charge les expériences des utilisateurs externes, prend en charge l'analyse des données et participe à l'interprétation des données et est co-auteur de vos manuscrits; - Contacter et conseiller les utilisateurs de la ligne lumineuse avant les sessions expérimentales dans des environnements échantillons, des protocoles expérimentaux et concevoir les stratégies optimales pour obtenir les résultats que les utilisateurs attendent d'obtenir; - Présente des propositions de recherche pour ses propres recherches; - Supervise les doctorants et apprentis; - Supervise le personnel technique concernant l'exploitation et la maintenance de la ligne électrique SAXS et, en l'absence de chefs de projet, assure cette supervision pour l'ensemble du projet DUBBLE; - Il est responsable du programme scientifique de la ligne lumineuse SAXS. Cela implique de créer un planning utilisateur efficace, d'adapter le statut technique aux demandes des utilisateurs, d'agir préventivement par rapport aux demandes des utilisateurs en fonction de leurs connaissances scientifiques et de lancer de nouveaux développements. Pour cela, l'organisation du personnel technique et des spécialistes externes doit être coordonnée; - Dans le cadre d'exigences scientifiques interdisciplinaires et transdisciplinaires, développer davantage les capacités techniques de la ligne de lumière, notamment en ce qui concerne les environnements d'échantillonnage, l'acquisition de données, l'analyse de données; - Coordonner les exigences de la ligne lumineuse SAXS dans le contexte plus large du projet DUBBLE. Ceci en programmant des ressources expérimentales en coordination avec le chef de projet et d'autres scientifiques chevronnés et en définissant clairement la main-d'œuvre et les demandes financières pour le programme existant et les

nouveaux développements; Assure le bon fonctionnement de la ligne lumineuse SAXS, encourage les utilisateurs à terminer leur travail à temps, tant en analyse expérimentale qu'en analyse de données et en rédaction de publications; - Publier les résultats de ses propres résultats dans des revues scientifiques à comité de lecture de renommée internationale. Co-auteurs avec des messages d'utilisateurs. Il présente les travaux lors de réunions internationales et scientifiques et organise également de telles réunions; - Conseille au sens le plus large dans le domaine sur les futures possibilités de recherche. Ceci à la plus grande communauté d'utilisateurs également à la demande d'organisations externes; - Attirer de nouveaux groupes d'utilisateurs au sein de la communauté d'utilisateurs néerlandais-flamands et créer / conserver avec ces groupes d'utilisateurs une communauté d'utilisateurs de haut niveau in...

Établissement où la formation a été réalisée : Type d'établissement: Organisme public de DUBBLE @ ESRFrecherche

Date de début: 01/07/2015

Durée: 4 ans - 6 mois

## Séjour dans des centres de R&D&I ou bien des entreprises nationales ou internationales

1. Établissement où la formation a été réalisée: Type d'établissement: Organisme public de European Synchrotron Radiation Facility recherche  
Faculté, institut, centre: DUBBLE / bm26b / Contratado por el Dutch Polymer Institute  
Ville: Grenoble, Rhône-Alpes, France  
Début-Fin: 01/01/2013 - 31/07/2015  
Durée: 2 ans  
**Objectif du séjour: Post-doctoral**  
Tâches vérifiables: Projet DPI(598) Application of time resolved X-ray diffraction techniques for study on structural and morphological changes during polymerization and processing. • Contact scientifique entre les groupes de polymères néerlandais et DUBBLE pour l'application des rayons X en combinaison avec d'autres techniques pour étude des changements structuraux et morphologiques lors de la polymérisation et du traitement des polymères. Le rôle consistait à: - Attirer de nouveaux groupes DPI sur la ligne lumineuse et demander le temps d'éclairage pour de nouvelles expériences. - Contact local lors d'expériences DUBBLE. - Développement d'un environnement d'échantillonnage pour les besoins spécifiques de combinaison de différentes techniques en combinaison avec des techniques de rayons X. - Modélisation de la morphologie polymérique.
2. Etablissement où la formation a été réalisée: Type d'établissement: Organisme public de European Synchrotron Radiation Facility recherche  
Faculté, institut, centre: DUBBLE / bm26b / Contratado por el Dutch Polymer Institute  
Ville: Grenoble, Rhône-Alpes, France  
Début-Fin: 01/01/2011 - 31/12/2013 Durée: 2 ans  
**Objectif du séjour: Post-doctoral**  
Tâches vérifiables: Projet DPI(598) Application des techniques de diffraction des rayons X à résolution temporelle pour l'étude des changements structurels et morphologiques pendant la polymérisation et le traitement - Contact scientifique entre les groupes néerlandais de polymères et DUBBLE pour l'application des rayons X en combinaison avec d'autres techniques pour l'étude des changements structurels et morphologiques pendant la

polymérisation et le traitement. Le rôle impliqué : -Attracter de nouveaux groupes DPI à la ligne de lumière et demander le temps de lumière pour de nouvelles expériences - Contact local pendant les expériences de DUBBLE. Développement de l'environnement de l'échantillon pour les besoins spécifiques de la combinaison de différentes techniques en combinaison avec les techniques à rayons X. - Modélisation de la morphologie des polymères.

3. Établissement où la formation a été réalisée :  
Type d'établissement: Université Eindhoven university of technology  
Faculté, institut, centre: Department of Chemical Engineering and Chemistry  
Ville: Eindhoven, Pays-Bas  
Début-Fin: 01/03/2012 - 01/05/2012  
Durée: 3 mois Objectif du séjour: Invité  
Établissement où la formation a été réalisée:  
Type d'établissement: Université  
Wageningen University  
Faculté, institut, centre: Physical Chemistry & Soft Matter  
Ville: Wageningen, Pays-Bas  
Début-Fin: 01/02/2012 - 01/03/2012      Durée: 1 mois  
Objectif du séjour: Invité  
Tâches vérifiables: • Préparation d'expériences en dehors de la ligne synchrotron avec une nouvelle cellule conçue pour mesurer de SAXS en sc-CO<sub>2</sub>
4. Établissement où la formation a été réalisée:      Type d'établissement: Université Eindhoven university of technology  
Faculté, institut, centre: Department of Chemical Engineering and Chemistry  
Ville: Grenoble, Rhône-Alpes, France  
Début-Fin: 15/04/2010 - 31/12/2010      Durée: 8 mois - 15 jours  
Objectif du séjour: Post-doctoral  
Tâches vérifiables: • L'aide à l'application des propositions pour mener des expériences dans le cadre de l'ESRF.- Aide à la réduction des données et à la poursuite de l'analyse. Préparation d'expériences sur l'étude structurale in situ de l'étirage des films polymères.  
Établissement où la formation a été réalisée:  
Type d'établissement: University of Reading  
Faculté, institut, centre: School of Chemistry  
Ville: Reading, Berkshire, Buckinghamshire and Oxfordshire, Royaume-Uni  
Début-Fin: 01/09/2006 - 14/04/2010      Durée: 3 ans - 6 mois
5. Objectif du séjour: Tâches vérifiables: Achèvement du doctorat intitulé "Polyuréthanes supramoléculaires thermosensibles auto-assemblés". Le doctorat a étudié;- la conception et la caractérisation de nouveaux polymères supramoléculaires pour comprendre la relation structure-propriété des matériaux polymères fonctionnels intelligents  
Etablissement où la formation a été réalisée:: Université de Lorraine  
Laboratoire Matériaux Optiques, Photonique et Systèmes (LMOPS - EA 4423) Ville: Metz, Lorraine, France  
Date de début: 09/12/2019      Durée: 1 mois  
Objectif du séjour: Invité en tant que chercheur
6. Établissement où la formation a été réalisée: Université de Lorraine  
Laboratoire Matériaux Optiques, Photonique et Systèmes (LMOPS - EA 4423) Ville: Metz, Lorraine, France  
Date de début: 07/06/2018      Durée: 1 mois

Objectif du séjour: Invité en tant que chercheur  
Établissement où la formation a été réalisée: Universidad de Castilla-La Mancha  
Faculté, institut, centre: Farmacia/ Departamento Quimica Fisica  
Ville: Albacete, Castille-La Manche, Espagne  
Date de début: 29/05/2017      Durée: 1 mois  
Objectif du séjour: Invitation en tant que chercheur senior

7. Établissement où la formation a été réalisée: Universidad de Castilla-La Mancha  
Faculté, institut, centre: Farmacia Ville: Albacete, Castille-La Manche, Espagne  
Date de début: 18/05/2016      Durée: 1 mois  
Objectif du séjour: Invité en tant que jeune chercheur obtenu par concours en concours et  
doté d'une contribution financière de c.a. 2600

## Aides et bourses obtenues

1. Dénomination de la bourse ou de l'aide: L'objectif principal du séjour est un transfert de connaissances sur les GIWAXS de BM26b (ESRF) à NCD-SWEET beamline (ALBA), motivé par la grande expérience du personnel de ligne de Daniel Hermida Merino et de son équipe dédiée à cette technique.  
Objectif: El objetivo principal de la estancia es una transferencia de conocimiento sobre GIWAXS desde BM26b (ESRF) a NCD-SWEET beamline (ALBA), motivado por la alta experiencia del personal de la línea de Daniel Hermida Merino y su equipo dedicado a esta técnica.  
Organisme subventionnaire: Calipso PlusType d'établissement: Associations et groupements  
Date de délivrance: 01/11/2018      Durée de l'aide économique: 5 jours  
Date de fin: 28/12/2018  
Nom de l'entité: European Synchrotron Radiation Facility (ESRF)
2. Dénomination de la bourse ou de l'aide: Inhouse-Beamtime  
Objectif: Pendant la période où j'ai travaillé chez DUBBLE, j'ai effectué des dizaines de faisceaux en interne pour améliorer ou concevoir de nouvelles cellules, concevoir et installer de nouveaux éléments optiques sur la ligne et préparer de nouvelles expériences.  
Organisme subventionnaire: DUBBLE      Type d'établissement: Organisme public de recherche  
Date de délivrance: 25/08/2010  
Date de fin: 05/12/2018
3. Dénomination de la bourse ou de l'aide: CALIPSOplus (Grant 730872) funding/ synchrotron ;Crystallization behaviour of novel PLA derivatives for drug release applications  
Objectif: Grâce au projet CALIPSOplus, son expérience a été récompensée avec deux utilisateurs financés d'institutions européennes non espagnoles. Ma proposition a été retenue comme première par le comité scientifique et c'est pourquoi ils m'ont octroyé une subvention financière de 1800 euros pour aider à la réalisation des expériences.  
Organisme subventionnaire: Calipso PlusType d'établissement: Associations et groupements  
Date de délivrance: 22/06/2017      Durée de l'aide économique: 3 jours  
Date de fin: 07/07/2017  
Nom de l'entité: Alba sincrotrón Faculté, institut, centre: bl11-ncd-sweet

## Résumé des autres titres

1. Description: Reproduction de l'article: Enrique Niza, Cristina Nieto-Jiménez, María del Mar Noblejas-López, Iván Bravo, José Antonio Castro-Osma, Felipe de la Cruz-Martínez, Marc

Martínez de Sarasa Buchaca, Daniel Hermida-Merino, Eduardo Solano, Alberto Ocaña, Carlos Alonso-Moreno.

Poly(Cyclohexene Phthalate) Nanoparticles for Controlled Dasatinib Delivery in Breast Cancer Therapy. *Nanomaterials* 2019, 9, 1208. DOI: 10.3390/nano9091208 , dans la presse pour avoir été choisi pour son importance dans la recherche fondamentale et dans l'application des rayons X par le synchrotron ALBA.

<https://www.sincrotronalba.es/es/actualidad/noticias/nuevas-nanoparticulas-biocompatibles-contra-el-cancer-demama>

2. Organisme qui vous a décerné le titre: Alba synchrotron  
Ville: Cerdanyola del Valles, Catalogne, Espagne  
Date de délivrance: 20/11/2019
3. Description: Évaluation internationale jugée excellente, sur la production scientifique de Bm 26 b au sein de l'ESRF au cours de la période 2013-2018.  
Organisme qui vous a décerné le titre : ESRF  
Ville: Grenoble, Rhône-Alpes, France  
Date de délivrance: 07/11/2018
4. Description: Évaluation binationale jugée excellente, sur la production scientifique de Bm 26 b au cours de la période 2013-2018.  
Organisme qui vous a décerné le titre ou la récomp: NWO/FWO  
Ville: Grenoble, Rhône-Alpes, France  
Date de délivrance: 26/10/2018